



# THE UNIVERSITY *of* EDINBURGH

This thesis has been submitted in fulfilment of the requirements for a postgraduate degree (e.g. PhD, MPhil, DClinPsychol) at the University of Edinburgh. Please note the following terms and conditions of use:

This work is protected by copyright and other intellectual property rights, which are retained by the thesis author, unless otherwise stated.

A copy can be downloaded for personal non-commercial research or study, without prior permission or charge.

This thesis cannot be reproduced or quoted extensively from without first obtaining permission in writing from the author.

The content must not be changed in any way or sold commercially in any format or medium without the formal permission of the author.

When referring to this work, full bibliographic details including the author, title, awarding institution and date of the thesis must be given.



# THE UNIVERSITY *of* EDINBURGH

MicroRNAs as biomarkers in anti-tuberculosis drug-  
induced liver injury: a translational study from zebrafish  
to humans

---

**Sarah Ann Elisabeth Ruppachter**

Thesis presented for the degree of Doctor of Philosophy

College of Medicine and Veterinary Medicine

University of Edinburgh

August 2020

## Declaration:

I hereby declare that this thesis and the work presented in it are my own and have been generated by me as a result of my own original research, with the following exceptions:

- Chapter 2: The standard curve used for absolute quantification of miR-122 was generated by Emma Morrison. Clinical samples in the SAEFRIF trial were collected by the trial team at the Infectious Diseases Institute, Uganda. Healthy volunteer samples were collected by Kathleen Scullion. ALT activity in healthy volunteer samples was measured by Forbes Howie.
- Chapter 3: Jorge del Pozo assisted with the zebrafish histology and scoring. The collection and extraction of RNA for the triptolide small RNA sequencing experiment was performed by Bastiaan Vliegthart. Al Ivens was contracted to carry out the bioinformatic analysis of the small RNA sequencing data.
- Chapter 4: The concept of the toehold switch for miR-122 was jointly developed with Xinyi Wang. Plasmids and *E. coli* Top10 cells used in this work were supplied by Xinyi Wang.

No part of this thesis has been submitted for any other degree or professional qualification.

Sarah Rupprechter

University of Edinburgh

## Table of contents:

Declaration:.....	i
Table of contents: .....	ii
Abstract:.....	x
Lay abstract:.....	xii
Acknowledgements:.....	xiv
List of tables:.....	xv
List of figures:.....	xvi
Abbreviations:.....	xviii
1 Introduction .....	1
1.1 Drug-induced liver injury: .....	2
1.1.1 Pathology of drug-induced liver injury: .....	3
1.1.2 Histopathology of drug-induced liver injury: .....	4
1.2 Tuberculosis: .....	6
1.2.1 The global problem of tuberculosis: .....	6
1.2.2 Treatment for tuberculosis: .....	7
1.2.3 HIV and tuberculosis: .....	9
1.2.4 Nontuberculous mycobacterial infections:.....	10
1.3 Anti-tuberculosis drug-induced liver injury: .....	11
1.3.1 Isoniazid hepatotoxicity: .....	11
1.3.2 Rifampicin hepatotoxicity: .....	13
1.3.3 Pyrazinamide hepatotoxicity: .....	14
1.3.4 Other anti-tuberculosis drugs and hepatotoxicity:.....	15
1.3.5 Multi-drug hepatotoxicity:.....	16
1.3.6 Risk factors for developing anti-tuberculosis drug-induced liver injury:.....	16
1.4 Diagnosis of drug-induced liver injury: .....	17
1.4.1 Liver function tests:.....	17
1.4.2 Management of anti-tuberculosis drug-induced liver injury:.....	17
1.4.3 Causality assessment: .....	18
1.5 The need for novel biomarkers:.....	19
1.5.1 Limitations of alanine aminotransferase: .....	19
1.5.2 Features of a novel biomarker: .....	20
1.6 Novel biomarkers of drug-induced liver injury: .....	23
1.6.1 Case study – Paracetamol-induced liver injury:.....	23

1.6.2	MicroRNAs: .....	24
1.6.3	MiR-122:.....	26
1.6.4	MiR-122 as a biomarker:.....	28
1.6.5	Cytokeratin-18: .....	30
1.6.6	Cytokeratin-18 as a biomarker:.....	30
1.7	Zebrafish as models of drug-induced liver injury: .....	32
1.7.1	Models of drug-induced liver injury:.....	32
1.7.2	Advantages and limitations of zebrafish:.....	33
1.7.3	The zebrafish liver:.....	36
1.7.4	Assessing liver toxicity in zebrafish:.....	38
1.8	Diagnostic tests for miRNAs:.....	39
1.8.1	Current technologies: .....	39
1.8.2	Synthetic gene networks:.....	42
1.8.3	Riboregulators and toehold switches: .....	42
1.8.4	Advantages of toehold switches: .....	45
1.8.5	Challenges and limitations of toehold switches: .....	46
1.9	Hypotheses and aims:.....	47
1.9.1	Hypotheses: .....	47
1.9.2	Research aims: .....	47
2	Biomarkers of anti-tuberculosis drug-induced liver injury .....	48
2.1	Introduction: .....	49
2.1.1	Background: .....	49
2.1.2	Aims: .....	50
2.2	Methods:.....	51
2.2.1	ALISTER clinical study:.....	51
2.2.1.1	Research governance and ethics: .....	51
2.2.1.2	Patient population: .....	51
2.2.1.3	Calculation of sample size:.....	51
2.2.1.4	Identification and recruitment of participants: .....	52
2.2.1.5	Consenting process: .....	52
2.2.1.6	Study protocol:.....	53
2.2.1.7	Sample and data collection:.....	53
2.2.1.8	Sample and data anonymisation: .....	54
2.2.1.9	Sample handling:.....	54
2.2.1.10	Patient groupings for analysis:.....	54

2.2.2	SAEFRIF clinical trial: .....	54
2.2.2.1	Research governance and ethics: .....	55
2.2.2.2	Study design:.....	55
2.2.2.3	Patient population: .....	56
2.2.2.4	Study protocol:.....	56
2.2.2.5	Sample handling:.....	57
2.2.3	Healthy volunteers:.....	57
2.2.4	Quantification of miR-122:.....	57
2.2.4.1	RNA isolation:.....	57
2.2.4.2	Reverse transcription:.....	58
2.2.4.3	Quantitative real time analysis: .....	58
2.2.4.4	Standard curve for miR-122:.....	60
2.2.4.5	MiR-122 data analysis: .....	60
2.2.5	Quantification of K18: .....	60
2.2.5.1	M65 ELISA: .....	60
2.2.5.2	K18 data analysis:.....	61
2.2.6	Quantification of ALT: .....	61
2.2.7	Assessment of causality: .....	62
2.2.8	Statistical analysis: .....	62
2.3	Results:.....	63
2.3.1	Patient demographics: .....	63
2.3.1.1	ALISTER study:.....	63
2.3.1.2	SAEFRIF trial: .....	65
2.3.1.3	Healthy volunteers:.....	65
2.3.2	Circulating biomarkers in different populations:.....	66
2.3.3	Circulating biomarkers in treatment:.....	68
2.3.3.1	Commencing treatment:.....	68
2.3.3.2	Anti-tuberculosis drug treatments: .....	71
2.3.3.3	HIV treatment: .....	74
2.3.3.4	Time spent on treatment: .....	76
2.3.4	Circulating biomarkers correlate with ALT: .....	78
2.3.5	Circulating biomarkers in anti-tuberculosis drug-induced liver injury: .....	82
2.4	Discussion: .....	85
2.4.1	Main findings: .....	85
2.4.2	The concentration of circulating miR-122 and K18 in healthy volunteers in this study differs to that previously described: .....	85

2.4.3	Mycobacterial infection does not affect circulating miR-122 and K18:.....	86
2.4.4	Commencing treatment and the drug treatment taken does not affect circulating miR-122 and K18: .....	87
2.4.5	The circulating biomarkers miR-122 and K18 rise with elevated ALT and in anti-tuberculosis drug-induced liver injury:.....	88
2.4.6	Limitations:.....	90
2.4.7	Further work: .....	91
2.4.8	Summary: .....	92
3	Zebrafish as models of anti-tuberculosis drug-induced liver injury .....	93
3.1	Introduction: .....	94
3.1.1	Background: .....	94
3.1.2	Aims: .....	96
3.2	Materials & Methods:.....	97
3.2.1	Zebrafish lines: .....	97
3.2.2	Drug exposure:.....	97
3.2.2.1	Triptolide solution:.....	97
3.2.2.2	Anti-tuberculosis drug solutions:.....	97
3.2.2.3	Drug exposure experiments:.....	97
3.2.3	Anti-tuberculosis drug survival experiments: .....	98
3.2.4	Microscopy:.....	98
3.2.4.1	Morphological assessment: .....	98
3.2.4.2	Liver assessment: .....	98
3.2.5	Histology: .....	99
3.2.6	MiRNA quantification:.....	100
3.2.6.1	RNA extraction: .....	100
3.2.6.2	Reverse transcription:.....	101
3.2.6.3	Quantitative real time analysis: .....	101
3.2.6.4	Relative quantification: .....	102
3.2.7	Copies of miR-122 per fish experiment: .....	103
3.2.8	Small RNA sequencing: .....	103
3.2.8.1	Triptolide small RNA sequencing: .....	103
3.2.8.2	Anti-tuberculosis small RNA sequencing: .....	104
3.2.8.3	Small RNA sequencing data analysis:.....	105
3.2.8.4	MiRNA target prediction and function annotation:.....	105
3.2.9	Fluorescence Activated Cell Sorting:.....	106
3.2.9.1	Zebrafish larvae digest: .....	106

3.2.9.2	Cell sorting: .....	106
3.2.9.3	Sample collection and storage:.....	107
3.2.9.4	MiRNA extraction and quantification: .....	107
3.2.10	Translation of miRNA targets into human samples: .....	107
3.3	Results:.....	108
3.3.1	Anti-tuberculosis drug-induced liver injury model: .....	108
3.3.1.1	Survival:.....	108
3.3.1.2	Morphology:.....	109
3.3.1.3	Fluorescence microscopy:.....	115
3.3.1.4	Histology: .....	118
3.3.1.5	Copies of miR-122 per larvae:.....	122
3.3.2	MiRNA changes and associated pathways in drug-induced liver injury: ....	123
3.3.2.1	Isoniazid induced liver injury: .....	123
3.3.2.2	Pyrazinamide induced liver injury:.....	124
3.3.2.3	Pyrazinamide compared to isoniazid induced liver injury: .....	124
3.3.2.4	Triptolide induced liver injury:.....	125
3.3.3	MiRNA changes in specific cell populations:.....	142
3.3.4	Novel miRNA biomarkers of drug-induced liver injury: .....	148
3.3.4.1	Identification of novel miRNA biomarkers from small RNA sequencing: 148	
3.3.4.2	Translation of novel miRNA biomarkers of liver injury into humans:.....	151
3.4	Discussion: .....	153
3.4.1	Main findings: .....	153
3.4.2	Isoniazid and pyrazinamide cause liver injury in zebrafish larvae: .....	153
3.4.3	Changes in miRNA expression in anti-tuberculosis drug-induced liver injury are associated with the metabolism of drugs in the liver: .....	154
3.4.4	Changes in miRNA expression in anti-tuberculosis drug-induced liver injury are associated with further pathways: .....	155
3.4.5	Triptolide-induced liver injury causes miRNA down-regulation:.....	158
3.4.6	FACS can be used to investigate miRNA changes specific to different cell populations: .....	159
3.4.7	Zebrafish larvae models of liver injury can be used to identify novel biomarkers of liver injury:.....	160
3.4.8	Limitations of this study:.....	160
3.4.9	Further work: .....	162
3.4.10	Summary: .....	163
4	Development of a novel diagnostic test for miR-122 .....	164



4.1	Introduction: .....	165
4.1.1	Background: .....	165
4.1.2	Aims: .....	168
4.2	Materials and methods:.....	170
4.2.1	Toehold switch assembly overview: .....	170
4.2.1.1	Circular polymerase extension cloning:.....	172
4.2.1.2	Mutagenic primers:.....	174
4.2.1.3	pJET cloning vector: .....	175
4.2.2	Molecular biology and microbiology techniques:.....	176
4.2.2.1	Phusion PCR: .....	176
4.2.2.2	Gel analysis: .....	177
4.2.2.3	Gel and PCR purification of DNA:.....	177
4.2.2.4	Transformation procedure:.....	178
4.2.2.5	E. coli Top10 cells:.....	178
4.2.2.6	Miniprep of plasmid DNA:.....	178
4.2.2.7	Colony screening:.....	179
4.2.2.8	Sequencing:.....	179
4.2.2.9	Glycerol stocks: .....	180
4.2.3	Materials: .....	180
4.2.3.1	Antibiotic stock solutions:.....	180
4.2.3.2	Chlorophenol red-beta-D-galactopyranoside solution: .....	180
4.2.3.3	LB agar and LB broth: .....	180
4.2.3.4	MicroRNA solutions: .....	180
4.2.3.5	Plasmids: .....	180
4.2.3.6	Primers:.....	181
4.2.4	Testing of the switches: .....	181
4.2.4.1	GFP switches - cell-free reaction solutions:.....	181
4.2.4.2	GFP switches - analysis: .....	182
4.2.4.3	LacZ switches - cell free reaction solutions:.....	182
4.2.4.4	LacZ switches - analysis:.....	183
4.3	Results:.....	185
4.3.1	NUPACK assessment of switches:.....	185
4.3.2	GFP switches: .....	187
4.3.2.1	Optimisation of test conditions: .....	187
4.3.2.2	Sensitivity:.....	190

4.3.2.3	Specificity: .....	193
4.3.2.4	Further optimisation of test conditions: .....	195
4.3.3	LacZ switches: .....	198
4.3.3.1	Sensitivity: .....	198
4.3.3.2	Paper test of lacZ positive control: .....	201
4.4	Discussion: .....	202
4.4.1	Main findings: .....	202
4.4.2	Toehold switches can detect miRNAs: .....	202
4.4.3	GFP and lacZ switches exhibit different reaction kinetics: .....	202
4.4.4	Structural changes to toehold switches impact their functionality: .....	203
4.4.5	Limitations: .....	205
4.4.6	Further work: .....	206
4.4.7	Summary: .....	208
5	Conclusions .....	209
5.1	Summary of findings: .....	210
5.2	The possible role of miR-122 in liver injury beyond acting as a biomarker: .....	211
5.3	The expanding field of biomarkers of drug-induced liver injury: .....	212
5.4	Point of care tests are needed for biomarkers of drug-induced liver injury: .....	213
5.5	MiRNAs can be used as therapeutics: .....	214
5.6	Bioinformatics approaches for miRNA research: .....	215
5.7	Zebrafish larvae have substantial benefits as models of liver injury: .....	215
5.8	Zebrafish have the ability to regenerate tissues: .....	217
5.9	Conclusion: .....	218
Appendix	.....	219
Chapter 2 Appendices: .....	.....	220
i	RUCAM causality assessment: .....	220
ii	ALISTER: Protocol: .....	222
iii	ALISTER: Patient Information Sheet: .....	233
iv	ALISTER: Patient Consent Form: .....	236
v	ALISTER: GP Letter: .....	237
Chapter 3 Appendices: .....	.....	238
i	FACS gating strategy: .....	238
ii	Histology of other organs: .....	239
iii	Data normalisation for qRT-PCR: .....	241
iv	GO analysis: Isoniazid relative to control (up-regulated miRNAs): .....	242

v	GO analysis: Isoniazid relative to control (down-regulated miRNAs):.....	242
vi	GO analysis: Pyrazinamide relative to control (up-regulated miRNAs):.....	243
vii	GO analysis: Pyrazinamide relative to control (down-regulated miRNAs):.....	244
viii	GO analysis: Pyrazinamide relative to isoniazid (up-regulated miRNAs):.....	245
ix	GO analysis: Pyrazinamide relative to isoniazid (down-regulated miRNAs):.....	245
x	GO analysis: Rifampin relative to vehicle control:.....	246
	Chapter 4 Appendices:.....	247
i	Primer Sequences: .....	247
ii	Oligonucleotide sequences for THS2, 7 & 10:.....	248
iii	Primer sequences for THS5 and THS9:.....	249
iv	Toehold switch diagrams: .....	250
v	GFP switches time course data: Sensitivity: .....	255
vi	GFP switches time course data: Specificity:.....	257
vii	GFP switches time course data: Further optimisation:.....	258
viii	LacZ switches time course data: .....	260
	Bibliography .....	261

## Abstract:

Drug-induced liver injury is one of the leading causes of acute liver failure and is a serious barrier to drug development. Furthermore, it is a frequent adverse reaction to the antimicrobials used to treat tuberculosis, resulting in reduced treatment effectiveness, incomplete treatment, relapse and the development of antimicrobial resistance.

The aim of the studies in this thesis were threefold, to investigate biomarkers of liver injury in patients receiving anti-tuberculosis medication, to investigate miRNA changes in zebrafish larvae due to drug-induced liver injury, and to develop a novel point of care diagnostic test for miR-122, a miRNA biomarker of liver injury.

The novel biomarkers, microRNA-122 (miR-122) and cytokeratin-18 (K18) have been found to be diagnostic and prognostic in patients who overdose on paracetamol. A key question is, do these biomarkers retain their efficacy in the presence of infection? The circulating concentrations of miR-122 and K18 were defined in the following populations: healthy volunteers, active tuberculosis patients, latent tuberculosis patients, patients with non-tuberculous mycobacterial infection and HIV-tuberculosis coinfecting patients. Circulating concentrations of miR-122 and K18 were not significantly different across these groups, indicating infection does not affect concentrations of miR-122 and K18. Furthermore, concentrations of miR-122 and K18 did not rise upon starting treatment. There was a significant correlation between the gold standard marker alanine aminotransferase (ALT) and both miR-122 and K18 demonstrating these biomarkers rise with elevations in ALT. In two individuals who developed drug-induced liver injury, miR-122 and K18 rose with ALT, suggesting these biomarkers have diagnostic potential for anti-tuberculosis drug-induced liver injury.

To reduce the need for rodent studies a zebrafish larvae model of liver injury was developed. Reducing the number of rodent studies carried out reduces experimental costs and the use of zebrafish larvae enables rapid high-throughput experiments. Furthermore, using zebrafish larvae is in line with the “3Rs” (reduce, refine, replace) approach of animal use in science, with the replacement of rodents, a higher-order mammal, with the lower-order

zebrafish larvae. Zebrafish larvae exposed to isoniazid and pyrazinamide developed liver toxicity as determined by mortality, fluorescent imaging and histology. In order to investigate pathways altered in anti-tuberculosis drug-induced liver injury and identify potential novel biomarkers small RNA sequencing was undertaken. Pathways were altered in anti-tuberculosis drug induced liver injury, including those associated with the metabolism of xenobiotics. Building on previous work by my group, zebrafish larvae were exposed to triptolide, a Chinese herbal medicine which induces liver injury. A method was developed to collect specific cell populations, hepatocytes and immune cells, from transgenic zebrafish larvae using fluorescence activated cell sorting (FACS). The miRNA changes in isolated cells populations were determined using qRT-PCR, and in whole fish using small RNA sequencing. Novel miRNA biomarkers of liver injury were identified from the small RNA sequencing data and translated in plasma samples from patients with anti-tuberculosis drug-induced liver injury. Two of these miRNAs rose with ALT in liver injury.

A point of care test is needed for drug-induced liver injury, suitable for use in resource poor settings. A novel RNA toehold switch sensor was combined with a fluorescent and colorimetric outputs to provide a quantitative response to miR-122 concentrations. Toehold switches with a range of structures were developed and tested. Switches demonstrated varying levels of sensitivity and specificity for miR-122.

## Lay abstract:

Drugs which cause damage to the liver are not uncommon. The drugs used to treat the infectious disease tuberculosis can cause damage to the liver. As a result, some patients are unable to complete treatment, making them more likely to develop tuberculosis again in the future or develop tuberculosis which is more difficult to treat.

There were three main aims of these studies. Firstly, to measure the levels of molecules in the blood of individuals who are being treated for tuberculosis. These molecules, miR-122 and cytokeratin-18, increase in the blood of patients who have liver damage because they have overdosed on paracetamol. However, we do not know if someone with a disease, such as tuberculosis, has different levels of miR-122 and cytokeratin-18 to a healthy person without a disease. MiR-122 and cytokeratin-18 were measured in different patient groups with tuberculosis and also in people who were healthy. Levels of miR-122 and cytokeratin-18 were similar across the patient groups and healthy people. Patients who had high ALT, the current marker of liver damage, also had high miR-122 and cytokeratin-18. There were two patients who had liver damage during their tuberculosis treatment. In these patients, miR-122 and cytokeratin-18 rose when they had liver damage.

Often rodents are used in science to understand how drugs cause liver damage. However, zebrafish larvae are now being used more frequently as they are cheap and can rapidly provide information on liver damage. In this study, zebrafish larvae were exposed to isoniazid and pyrazinamide, drugs used to treat tuberculosis. These drugs caused liver damage in zebrafish larvae. This liver damage was shown through a reduction in the size of zebrafish larvae livers. In addition, using histology, liver damage was identified through changes in liver cells and liver cell death. Isoniazid and pyrazinamide also caused changes in the levels of microRNAs. Several microRNAs were identified as possible markers of liver damage. In order to investigate the specific microRNA changes occurring in different cell populations, flow cytometry was used to sort green fluorescent liver cells and red fluorescent immune cells from the other cells in zebrafish larvae.

A cheap diagnostic test for liver damage is needed for places without lab facilities. In this study, a diagnostic test was developed for the liver damage marker miR-122. A range of

different variations of this diagnostic test were developed. The result of this diagnostic test could be read by either fluorescence production or a colour change. This diagnostic test could identify different levels of miR-122. In addition, the diagnostic test did not activate for other types of microRNA.

## Acknowledgements:

I would like to thank my family, friends, colleagues and supervisors, who have supported and encouraged me throughout my studies. I would specifically like to thank:

- The Medical Research Council and University of Edinburgh for their generous funding
- Professor Adam Hill and all the staff at the TB clinic, particularly Ceri and Susan, for their help recruiting patients into the ALISTER study
- Dr Wilna Oosthuizen for all her help with qRT-PCR, FACS and data analysis
- Dr Carl Tucker and the staff in the Zebrafish facility
- Dr Xinyi Wang, for aiding in the development of the toehold switch system and for all her help in designing primers and troubleshooting assembly issues
- My colleagues, Dr Johannes Brennecke, Dr Charles Metcalf, Aishwarya Saxena, Olivia Matthews, Kathleen Scullion and John Tranter for their support and encouragement
- My supervisors, Professor Till Bachmann, Dr Kate Templeton and Dr Baojun Wang for their guidance throughout my PhD
- And finally, Professor James Dear, my primary supervisor, for his advice, enthusiasm, patience and continual optimism

I would like to dedicate this work to my husband Sam, thank you for your understanding, patience and support.



## List of tables:

Table 1-1: Overview of drugs used for TB treatment. ....	8
Table 1-2: Features of a novel biomarker for ATDILI. ....	22
Table 1-3: Healthy reference interval for miR-122. ....	29
Table 1-4: Healthy reference interval for CC-K18 and total K18 ....	32
Table 1-5: Advantages and limitations to the use of zebrafish larvae as models of DILI. ....	34
Table 1-6: MiRNA quantification techniques. ....	41
Table 2-1: SAEFRIF clinical trial arms. ....	55
Table 2-2: miScript SYBR Green PCR reaction cycling conditions. ....	58
Table 2-3: Demographic data for ALISTER clinical study patients. ....	64
Table 2-4: Demographic data for SAEFRIF trial patients. ....	65
Table 2-5: Circulating concentrations of ALT, miR-122 and K18 in the different patient groups. ....	66
Table 2-6: Correlation of the biomarkers with time on treatment. ....	76
Table 2-7: Correlation between the biomarkers. ....	79
Table 2-8: RUCAM causality assessment of ATDILI cases. ....	84
Table 3-1: RT reaction mixture components. ....	101
Table 3-2: qRT-PCR reaction mixture components. ....	102
Table 3-3: Statistically significantly changed miRNAs: INH relative to control. ....	132
Table 3-4: Statistically significantly changed miRNAs: PYR relative to control. ....	133
Table 3-5: Statistically significantly changed miRNAs: PYR relative to INH. ....	134
Table 3-6: Statistically significantly changed miRNAs: TP relative to vehicle control. ....	135
Table 3-7: KEGG pathways: INH relative to control (up-regulated miRNAs). ....	136
Table 3-8: KEGG Pathways: INH relative to control (down-regulated miRNAs). ....	137
Table 3-9: KEGG pathways: PYR relative to control (up-regulated miRNAs). ....	138
Table 3-10: KEGG pathways: PYR relative to control (down-regulated miRNAs). ....	139
Table 3-11: KEGG pathways: PYR relative INH (up-regulated miRNAs). ....	140
Table 3-12: KEGG pathways: PYR relative to INH (down-regulated miRNAs). ....	141
Table 3-13: KEGG pathways: TP relative to vehicle control. ....	141
Table 3-14: Novel miRNA biomarkers identified from small RNA sequencing. ....	149
Table 4-1: Panel of toehold switches. ....	169
Table 4-2: Overview of the different techniques used for the assembly of each switch. ...	170
Table 4-3: CPEC reaction mixture components. ....	172
Table 4-4: CPEC reaction cycling conditions. ....	173
Table 4-5: Phusion PCR reaction mixture components. ....	177
Table 4-6: Phusion PCR cycling conditions. ....	177
Table 4-7: GoTaq PCR reaction mixture components. ....	179
Table 4-8: GoTaq PCR cycling conditions. ....	179
Table 4-9: Cell-free reaction solution components for GFP switch tests. ....	181
Table 4-10: Cell-free reaction solution components for lacZ switch tests. ....	183
Table 4-11: Free energy of switches in the presence and absence of miR-122 at 37 °C ...	186
Table 4-12: MicroRNA sequences of miR-122, miR-39 and miR-3591. ....	193

## List of figures:

Figure 1-1: Metabolism of isoniazid in the liver. ....	13
Figure 1-2: Metabolism of pyrazinamide in the liver.....	15
Figure 1-3: Receiver-operating characteristic curve.....	21
Figure 1-4: MiRNA biogenesis.....	25
Figure 1-5: Riboregulators and toehold switches.....	44
Figure 2-1: Example dissociation curve for miR-122 and miR-39.....	59
Figure 2-2: Circulating concentrations of ALT, miR-22 and K18 in the different patient groups. .....	67
Figure 2-3: Circulating concentration of biomarkers in paired samples from patients in ALISTER study at baseline and on treatment.....	69
Figure 2-4: Circulating concentration of biomarkers in SAEFRIF trial patients.....	71
Figure 2-5: Circulating concentrations of ALT, miR-122 and K18 in the different drug treatment groups.....	73
Figure 2-6: Circulating concentration of ALT and K18 in SAEFRIF patients grouped by ART treatment.....	74
Figure 2-7: Circulating concentration of ALT and K18 in SAEFRIF patients grouped by ART status at baseline.....	75
Figure 2-8: Circulating biomarkers correlated with time on treatment.....	77
Figure 2-9: Correlation between circulating biomarkers.....	80
Figure 2-10: Diagnostic power of the circulating biomarkers miR-122 and K18.....	81
Figure 2-11: Circulating concentration of ALT, miR-122 and K18 in ALISTER ATDILI cases. .	83
Figure 3-1: Example dissociation curve for SNORD95.....	102
Figure 3-2: Survival of larvae after exposure to anti-TB drugs.....	108
Figure 3-3: Larvae morphology: representative images following INH exposure.....	111
Figure 3-4: Morphology of larvae exposed to 10 mM INH.....	112
Figure 3-5: Larvae morphology: representative images following PYR exposure.....	113
Figure 3-6: Morphology of larvae exposed to 6 mM PYR.....	114
Figure 3-7: Fluorescence imaging of larvae exposed to 10 mM INH.....	116
Figure 3-8: Fluorescence imaging of larvae exposed to 6 mM PYR.....	117
Figure 3-9: Histology of larvae.....	119
Figure 3-10: Histology of larvae exposed to 10 mM INH.....	120
Figure 3-11: Histology of larvae exposed to 6 mM PYR.....	121
Figure 3-12: Copies of miR-122 per larvae following anti-TB drug exposure.....	122
Figure 3-13: Small RNA sequencing volcano plots and pie charts.....	126
Figure 3-14: Heatmap of INH relative to control.....	128
Figure 3-15: Heatmap of PYR relative to control.....	129
Figure 3-16: Heatmap of TP relative to vehicle control.....	131
Figure 3-17: FACS data analysis.....	144
Figure 3-18: Relative gene expression of miRNAs in TP-exposed larvae and cell populations after 6 hrs.....	145
Figure 3-19: Relative gene expression of miRNAs in TP-exposed larvae and cell populations after 24 hrs.....	146
Figure 3-20: Fold change in miRNA expression in whole fish small RNA sequencing vs qRT- PCR of whole fish and specific cell populations.....	147
Figure 3-21: Heatmap of novel miRNA biomarkers of DILI.....	150
Figure 3-22: Translation of novel miRNA biomarkers of DILI into human ATDILI samples.	152

Figure 4-1: Schematic for toehold switch 1. ....	166
Figure 4-2: Schematic of the different assembly techniques used for the assembly of the toehold switches into plasmid backbones. ....	171
Figure 4-3: Optimisation of conditions for GFP switch tests. ....	188
Figure 4-4: Test of panel of switches. ....	191
Figure 4-5: Sensitivity test of a subset of switches. ....	192
Figure 4-6: Specificity test of switches. ....	194
Figure 4-7: Test of switches using different DNA concentrations: Fluorescence. ....	196
Figure 4-8: Test of switches using different DNA concentrations: Fold induction. ....	197
Figure 4-9: Test of lacZ switches: 1 hour. ....	199
Figure 4-10: Test of lacZ switches: 2.5 hrs. ....	200
Figure 4-11: Paper test with lacZ positive control. ....	201

## Abbreviations:

5-OH-PA	5-hydroxy pyrazinoic acid
a.u.	Arbitrary units
AGO2	Argonaute-2
AIDS	Acquired immunodeficiency syndrome
ALISTER	Assessing Antibiotic-Induced Liver Injury for the Stratification of Tuberculosis Patients
ALP	Alkaline phosphatase
ALT	Alanine aminotransferase
AMK	Amikacin
ART	Antiretroviral therapy
AST	Aspartate aminotransferase
ATDILI	Anti-tuberculosis drug-induced liver injury
ATP	Adenosine triphosphate
AZI	Azithromycin
CC-K18	Caspase-cleaved cytokeratin-18
cDNA	Complementary deoxyribonucleic acid
CLA	Clarithromycin
CPEC	Circular polymerase extension cloning
CPRG	Chlorophenol-red- $\beta$ -D-galactopyranoside
Cq	Cycle quantification
CV	Coefficient of variation
CYP	Cytochrome P450
DCL	Dynamic chemical labelling
DILI	Drug-induced liver injury
DILIN	Drug-Induced Liver Injury Network
DMEM	Dulbecco's Modified Eagle Medium
DMSO	Dimethyl sulfoxide
DNA	Deoxyribonucleic acid
dpf	Days post-fertilisation
DTG	Dolutegravir
ECM	Extracellular matrix
EFV	Efavirenz
ELISA	Enzyme-linked immunosorbent assay
EMB	Ethambutol
FACS	Fluorescent activated cell sorting
FL-K18	Full length cytokeratin-18
GFP	Green fluorescent protein
GLDH	Glutamate dehydrogenase
GO	Gene Ontology
GSH	Glutathione

GST	Glutathione S-transferase
HCV	Hepatitis C virus
HIV	Human immunodeficiency virus
HMGB1	High mobility group box 1
hpf	Hours post-fertilisation
HRP	Horseradish peroxidase
hrs	Hours
IDI	Infectious Diseases Institute
IGRA	Interferon-gamma release assay
INH	Isoniazid
INR	International normalised ratio
IQR	Interquartile range
K18	Cytokeratin-18
KEGG	Kyoto Encyclopaedia of Genes and Genomes
LFABP	Liver fatty acid binding protein
LFT	Liver function test
LLN	Lower limit of normal
MAC	Mycobacterium avium complex
MDA	Malondialdehyde
MDR	Multi-drug resistant
MFE	Minimum free energy
MGST	Microsomal glutathione S-transferase
min	Minute
miR-122	MicroRNA-122
miRNA	MicroRNA
MOX	Moxifloxacin
MPEG1	Macrophage-expressed gene 1
MPX	Myeloperoxidase
MRE	MiRNA response element
MS-222	Tricaine methanesulfonate
NAC	N-acetyl cysteine
NAPQI	N-acetyl-p-benzoquinone imine
NASBA	Nucleic acid sequence-based amplification
NASH	Non-alcoholic steatohepatitis
NAT2	N-acetyl transferase 2
NSAID	Non-steroidal anti-inflammatory drug
NTM	Nontuberculous mycobacterium
nts	Nucleotides
OD	Optical density
PCR	Polymerase chain reaction
PNA	Peptide nucleic acid
PPAR- $\alpha$	Peroxisome proliferator-activated receptor $\alpha$
PSTC	Predictive Safety Testing Consortium

PT	Prothrombin time
PXR	Pregnane X receptor
PYR	Pyrazinamide
qRT-PCR	Quantitative real-time polymerase chain reaction
RBS	Ribosome binding site
RIE	Royal Infirmary Edinburgh
RIN	RNA integrity number
RMP	Rifampicin
RNA	Ribonucleic acid
ROC-AUC	Receiver operating characteristic - area under the curve
ROS	Reactive oxygen species
RT	Reverse-transcription
RT-LAMP	Reverse-transcription loop-mediated isothermal amplification
RUCAM	Roussel Uclaf Causality Assessment Method
SAEFRIF	Safety and Efficacy of High Dose Rifampicin in Tuberculosis (TB)- HIV Co-infected Patients on Efavirenz- or Dolutegravir-based Antiretroviral Therapy
SAFE-T	Safer and Faster Evidence-Based Translation consortium
sec	Second
SOD1	Superoxide dismutase 1
SPIM	Selective plane illumination microscopy
TB	Tuberculosis
TFIIH	Transcription factor II human complex
TGF- $\beta$	Transforming growth factor $\beta$
THS	Toehold switch
TMB	3,3',5,5'-Tetramethylbenzidine
TNF- $\alpha$	Tumour necrosis factor $\alpha$
TP	Triptolide
TST	Tuberculin skin test
ULN	Upper limit of normal
VC	Vehicle control

## Publications:

Rupprechter SAE, Sloan DJ, Oosthuizen W, Bachmann TT, Hill AT, Dhaliwal K, Templeton K, Matovu J, Sekaggya-Wiltshire C, Dear JW. MicroRNA-122 and cytokeratin-18 have potential as a biomarkers of drug-induced liver injury in European and African patients on treatment for mycobacterial infection. *Br J Clin Pharmacol*. 2021 Jan 11. doi: 10.1111/bcp.14736. Epub ahead of print. PMID: 33432705.

# 1 Introduction



### 1.1 Drug-induced liver injury:

Drug-induced liver injury (DILI) is one of the leading causes of acute liver failure in the US [1] and continues to be a serious barrier to drug development and drug marketing. Given the unpredictable nature of idiosyncratic liver injury often the hepatotoxic nature of drugs is not apparent until a large number of people have been exposed to them. DILI is the most common cause of safety-related marketing withdrawals over the last 50 years [2]. For example, the antibiotic, telithromycin, gained popularity as a replacement for macrolide antibiotics because of its spectrum of activity. However, telithromycin had its approval revised due to the identification of several instances of acute liver failure in the 3 years after its approval [1]. The resulting revised approval meant that telithromycin had more limited indications and a black box warning from the Food and Drug Administration [1].

Drugs which cause liver injury can be classified into either intrinsic, with dose-dependent and predictable side-effects, or idiosyncratic, where hepatotoxicity is unpredictable and occurs at therapeutic doses [3]. Idiosyncratic DILI is a substantial global problem, with an estimated 19 cases of DILI per 100,000 individuals each year [4]. DILI can be grouped according to the type of damage to the liver, with hepatocellular liver injury typified by the infiltration of immune cells and hepatocyte necrosis, and cholestatic liver injury typified by the impairment of bile flow. The latent period for the development of idiosyncratic DILI is highly variable, ranging from several days to several months. Furthermore, DILI can cause a range of levels of liver injury; (a) mild and reversible, with asymptomatic rises in serum aminotransferases, (b) early impairment of liver function, (c) serious clinical illness with obvious jaundice and disabling symptoms, (d) acute liver failure with secondary loss of other organ function such as brain or kidney, (e) death of the patient or need for liver transplantation [5].

In the Drug-Induced Liver Injury Network (DILIN) study, of the 899 patients with confirmed DILI, 10% died or underwent liver transplantation and 17% developed chronic liver injury [6]. Idiosyncratic DILI is a relatively rare event and so its pathogenesis is not fully understood. As a result, it is hard to predict in the early stages of drug development and may not be identified during clinical trials, only coming to light after market approval and significant numbers of patients have been exposed.

The leading cause of DILI, as determined in the DILIN study, was anti-microbials, being the cause of DILI in 408 out of the 899 patients and equating to 45% of all cases [6]. The anti-microbial isoniazid was the second most common drug responsible for DILI, causing 48 (5.3%) of all the DILI cases [6]. The DILIN study was conducted in the US which has a relatively low incidence of tuberculosis (TB), therefore, the rates of anti-TB DILI (ATDILI) in countries with a higher incidence of TB is likely higher. One estimate suggests that ATDILI affects 3-25% of individuals receiving anti-TB treatment [7]. Although isoniazid is the anti-TB drug most frequently associated with DILI the first-line drugs rifampicin and pyrazinamide are also associated with hepatotoxicity, along with several of the second-line drugs to a lesser extent. ATDILI prevents the effective treatment of TB, resulting in incomplete cure, relapse and the development of antimicrobial resistance.

#### 1.1.1 Pathology of drug-induced liver injury:

The pathology of DILI is complex, involving multiple pathways. However the mechanisms of DILI can typically be classified as either immune-mediated hypersensitivity or nonimmune reactions [8]. Initial injury to hepatocytes can begin with either the drug itself, a drug metabolite or a drug-protein adduct [9]. These molecules can result in the activation of oxidative stress and endoplasmic reticulum stress pathways and inhibition of both mitochondrial function and bile salt export pump [8]. Reactive metabolites, oxidative stress and bile salt effects lead to the activation of further responses which can either be adaptive and protective, or cause further injury to the cell [8]. In immune-mediated DILI the major theory is the hapten hypothesis, whereby the drug is converted into a reactive metabolite in hepatocytes and undergoes covalent binding to form a drug-protein adduct [8]. This drug-protein adduct is taken up by antigen-presenting cells, leading to downstream activation of the adaptive immune system and production of hapten-specific antibodies and autoantibodies [8]. Another theory is the “pharmacological interaction” hypothesis which suggests that certain drugs can act like small molecules and directly form non-covalent interactions with major histocompatibility complex (MHC) molecules, leading to immune system activation [3]. This initial interaction allows T cell receptor interaction resulting in T cell activation [3]. Immune-mediated DILI is not fully understood and different patterns of immune mechanisms have been identified for different drugs. Furthermore, it is possible

that there are multiple risk factors for DILI, such as age, gender, pre-existing conditions and genetic polymorphisms, which overlap and combine to induce DILI [3].

Cell death in the DILI can be either apoptotic or necrotic depending on which signalling pathways are activated [9]. The mechanisms of cell death and the pathways involved are dependent on the drug, the magnitude of liver injury and the initiating mechanism of cell death [3]. Hepatocytes can undergo apoptosis by either the intrinsic or extrinsic pathways. The extrinsic pathway is initiated by death receptors whereas the intrinsic pathway is initiated by mitochondrial pathways. In both cases, the executioner caspases 3 and 7 are activated resulting in proteolysis, chromatin condensation and nuclear fragmentation [3]. The extrinsic pathway of apoptosis is activated when death receptors are engaged by their ligands resulting in caspase 8 activation. Activation of caspase 8 leads to the activation of the executioner caspases 3 and 7 [3]. The activation of cytotoxic T lymphocytes and cytokine release leads to the immune-mediated killing of hepatocytes. Caspase 8 initiates a further pathway within hepatocytes, causing mitochondrial outer membrane permeabilisation, leading to the release of cytochrome c from mitochondria and activation of the apoptosome, resulting in cell apoptosis [3]. Apoptosis is an organised process involving caspases, chromatin condensation and the phagocytosis of cell bodies, thus minimising inflammation [3]. The necrosis of hepatocytes also involves the activation of cellular signalling pathways resulting in mitochondrial permeability transition [3]. Necrosis is characterised by cell swelling and rupture of the plasma membrane. The release of intracellular components during necrosis cause ion imbalance, mitochondrial dysfunction, ATP release and results in an inflammatory response [3].

#### 1.1.2 Histopathology of drug-induced liver injury:

Histopathological changes in DILI are varied and reflect the range and complexity of the pathways associated with DILI. The different histopathological patterns of DILI can be broadly categorised as necroinflammatory, cholestatic, steatotic and vascular.

In acute hepatocellular liver injury early stages are characterised by portal and parenchymal inflammation, hepatocyte injury and in some cases hepatocyte necrosis [10]. There is evidence of liver regeneration, as shown by binucleate hepatocytes and thick cell plates [10].

In addition, hepatocyte rosette formation can also be seen [11]. The progression of acute hepatitis is identified through necrosis affecting single hepatocytes or groups of hepatocytes [10]. Further liver injury progression is characterised by zonal necrosis, which when extensive can lead to acute hepatic failure [10]. Zonal necrosis is characterised by inflammation around the central vein and destruction of hepatocytes [11]. Apoptotic cells and steatosis are also associated with this zonal necrosis, related to mitochondrial injury [11]. In some instances, if a biopsy is performed later on there may be evidence of resolving hepatitis, as demonstrated by minimal hepatocellular injury and inflammation along with high numbers of macrophages present in the sinusoids [10]. Chronic hepatitis is less common than acute hepatitis in DILI but is associated with inflammation in the portal regions and moderate inflammation within the parenchyma [11]. Granulomatous hepatitis and mononucleosis-like hepatitis are inflammatory patterns related to chronic liver injury [11]. Granulomatous hepatitis is demonstrated in the liver through granulomas in the portal tracts or the parenchyma [10]. These granulomas lack necrosis and can occur alongside other patterns of liver injury [10].

Cholestasis occurs when there is an impedance of bile flow at any step from transport across the canalicular membrane to flow from the liver through the major ducts [11]. Toxic compounds arriving in the bile may cause direct inflammation to the interlobular ducts, with severe duct injury potentially leading to ductopenia [11]. Acute cholestatic liver injury can be divided histologically into two forms, pure or bland cholestasis, or cholestatic hepatitis, associated with inflammation and hepatocellular injury [11]. In pure cholestasis bile plugs are seen in hepatocytes or canaliculi, most prominently in zone 3, however inflammation and hepatocellular inflammation are not seen [10]. Chronic cholestatic changes are less frequent than bile accumulation and include microvacuolation of periportal hepatocytes, or cholate-stasis [11]. Chronic cholestasis, is associated with duct loss, periportal cholate-stasis, portal-based fibrosis and copper accumulation [11].

Steatosis is a common component of DILI and is not only a direct consequence of hepatocellular injury, but also may result from secondary drug effects [11]. The pathology of steatosis is associated with the accumulation of lipid vacuoles within hepatocytes [10]. There are three main patterns of steatotic liver injury, macrovesicular, microvesicular and

steatohepatitis. In macrovesicular steatosis large and small fat droplets are present in hepatocyte cytoplasm [10]. Microvesicular steatosis typically occurs as a result of mitochondrial injury with hepatocytes having a foamy appearance, due to the many tiny microvesicles present [11]. Steatohepatitis is characterised by steatosis, lobular inflammation and hepatocellular injury or pericellular fibrosis [10].

There are several patterns of vascular injury which can be due to DILI, including sinusoidal obstruction syndrome, sinusoidal dilation and peliosis hepatis, hepatoportal sclerosis and nodular regenerative hyperplasia [11].

## 1.2 Tuberculosis:

### 1.2.1 The global problem of tuberculosis:

Tuberculosis is one of the top 10 global causes of death [12]. In 2018, there were an estimated 10 million new cases of TB, with an estimated 1.2 million deaths among HIV-negative individuals and 251,000 deaths among HIV-positive individuals [13]. Although the incidence of TB has been falling in recent years, antimicrobial resistance in TB is a rising issue, with an estimated half a million new cases of rifampicin-resistant TB in 2018, with 78% of these cases presenting with multi-drug resistant (MDR) TB [13]. Treatment of TB occurs over several months and aims to provide complete cure for individuals. This reduces the risk of relapse, prevents disease spread and reduces the development of antimicrobial resistance. However, one of the barriers to optimal treatment of TB is the adverse side effects experienced by patients on anti-TB medications, with one of the most frequent side effects being hepatotoxicity. Given the long period of treatment, the risk of hepatotoxicity developing during treatment is likely, thus increasing the potential for incomplete treatment and the development of drug-resistant tuberculosis.

TB is caused by the bacterium *Mycobacterium tuberculosis* and can cause either active or latent disease. Active TB infection comes in 2 main forms, pulmonary, where the mycobacterium resides and replicates in the lungs, and extrapulmonary, where infection is at other sites around the body, including pleura, central nervous system, spine, bones, joints, genitourinary system, gastrointestinal system, lymph nodes, pericardia and as disseminated or miliary disease. Latent TB is the presence of *M. tuberculosis* infection in the absence of

active disease and affects one quarter of the world's population [13]. Individuals infected with *Mycobacterium tuberculosis* have a 5-10% chance of developing the disease throughout their lifetime [13], with this chance rising in individuals with comorbidities which suppress their immune system. As a result, HIV-positive individuals are at a much higher risk of developing active disease. Further risk factors for TB include overcrowding, malnutrition, chronic lung disease, smoking, alcoholism and diabetes. As a result, the burden of TB largely falls on developing countries.

### 1.2.2 Treatment for tuberculosis:

Treatment of active TB relies on antimicrobial therapy, with a combination of antibiotics taken over 6-12 months. The standard combination of antibiotics taken by an individual with susceptible active pulmonary TB is isoniazid, rifampicin, ethambutol and pyrazinamide for two months followed by isoniazid and rifampicin for a further four months [14]. The current groupings of anti-TB drugs, as proposed by the 2016 update on WHO treatment guidelines for drug-resistant TB, can be found in Table 1-1. Individuals with latent TB are typically treated with isoniazid alone for 6-9 months or 3 months of a combination of isoniazid and rifampicin [15]. However, in individuals where hepatotoxicity is a concern treatment is offered depending on the risk of developing active TB, usually depending on the immune status of the individual. For both active TB and latent TB cases where resistance to specific antibiotics has developed, individuals are treated with a regime tailored to the resistance pattern of the mycobacterium.

Group	Role	Drugs	
<b>1<sup>st</sup> line</b>	Susceptible TB	Isoniazid Rifampicin Ethambutol Pyrazinamide	
<b>Group A</b>	Multi-drug resistant/ rifampicin-resistant TB	Fluoroquinolones Eg. Levofloxacin, Moxifloxacin, Gatifloxacin	
<b>Group B</b>	2 <sup>nd</sup> line injectable agents	Amikacin Capreomycin Kanamycin Streptomycin	
<b>Group C</b>	Other core 2 <sup>nd</sup> line agents	Ethionamide/ Prothionamide Cycloserine/ Terizidone Linezolid Clofazimine	
<b>Group D</b>	Add on treatments which are not part of the core regime	D1 – Added on to core 2 <sup>nd</sup> line agents unless confirmed resistance, pill burden, intolerance or drug-drug interactions prevent use	Pyrazinamide Ethambutol High-dose isoniazid
		D2 – Use yet to be fully defined as still in phase II trials	Bedaquiline Delamanid
		D3 – Only to be used when a multi-drug resistant TB regime with at least 5 effective drugs cannot otherwise be composed	p-aminosalicylic acid Imipenem-cilastatin Meropenem Amoxicillin-clavulanate Thioacetazone

**Table 1-1: Overview of drugs used for TB treatment.**

Table adapted from [14].

### 1.2.3 HIV and tuberculosis:

Worldwide, in 2018, there were 1.7 million individuals newly infected with human immunodeficiency virus (HIV), with 39.7 million individuals living with HIV and 0.8 million deaths due to HIV and acquired immunodeficiency syndrome (AIDS) related causes [16]. The human immunodeficiency virus infects T cells, specifically CD4+ T cells, as well as macrophages and dendritic cells. HIV infection results in a decline in the CD4+ T cell population through cell death of infected T cells, apoptosis of uninfected bystander cells and direct killing via CD8+ cytotoxic lymphocytes which recognise infected CD4+ T cells [17], [18]. This decline in CD4+ T cells leads to AIDS, the progressive failure of the immune system, and results in individuals becoming susceptible to opportunistic infections and cancers. Treatment for HIV relies on antiretroviral drugs which prevent viral replication, stop the progression of disease and prevent onward transmission. Antiretroviral therapy (ART) typically consists of a combination of antiretroviral drugs. Antiretroviral drugs fall into the following broad classes; entry inhibitors, nucleoside/nucleotide reverse-transcriptase inhibitors, non-nucleoside reverse-transcriptase inhibitors, protease inhibitors and integrase inhibitors.

TB coinfection is one of the leading causes of sickness and death in HIV-infected individuals, being present in one third of all HIV-infected individuals and causing one quarter of HIV-related deaths globally [19]. Individuals with latent TB typically have a 5-10% chance of developing active TB over the course of their life, however, in HIV-infected individuals this risk rises to 10% annually [20]. HIV-infected individuals are also at higher risk of developing extrapulmonary TB, disseminated disease and more rapidly deteriorating [20]. Individuals with early stage HIV infection tend to develop pulmonary TB with similar clinical symptoms to a HIV-negative individual, whereas, individuals at later stages of HIV infection are more likely to have extrapulmonary TB and have more rapid disease progression [21]. Not only does HIV infection accelerate TB progression but there is evidence the opposite is also true, with TB infection accelerating HIV infection and the progression to AIDS [22].

In individuals presenting with HIV infection, screening for TB is recommended, with HIV screening also recommended for those presenting with active TB [19]. HIV-positive individuals with a positive tuberculin skin test (TST) are recommended to receive



preventative treatment for TB [21], with evidence that this provides protection from the development of active disease [23]. The diagnosis of active TB in HIV-infected individuals is challenging for several reasons; frequent negative sputum smears, atypical radiographic findings, higher prevalence of extrapulmonary TB particularly at inaccessible sites and resemblance to other opportunistic infections [21].

The management of patients with HIV-TB coinfection relies on the treatment of both the HIV and TB infections. Treatment of TB infection always takes precedence over HIV infection due to the more acute nature of TB infections [21]. HIV-positive individuals already taking ART should continue treatment, with appropriate modifications in ART and TB treatment regimens [21]. Individuals who have yet to initiate ART should start ART, with timing and treatment depending on HIV disease progression (CD4+ cell count) and TB type [21]. However, there are substantial pharmacokinetic interactions between the rifamycin component of TB treatment and ART, especially the protease inhibitors and non-nucleoside reverse transcriptase inhibitors which are metabolised by the cytochrome P450 enzymes [24]. Furthermore, antiretroviral drugs are associated with their own side effects, including hepatotoxicity.

#### 1.2.4 Nontuberculous mycobacterial infections:

Nontuberculous mycobacterial infections also known as atypical or environmental mycobacterial infections are due to nontuberculous mycobacterium (NTM). NTM are all the mycobacterial species which do not belong to *M. tuberculosis* complex. The main disease-causing species are the slow growing *M. avium* complex (MAC) (consisting of *M. avium*, *M. intracellulare* and *M. chimaera*), *M. kansasii*, *M. malmoense* and *M. xenopii*, and the fast growing *M. abscessus*, *M. chelonae* and *M. fortuitum* [25]. Similar to *M. tuberculosis*, NTM can cause both pulmonary and extrapulmonary disease, with pulmonary disease having either a fibro-cavitary or nodular bronchiectatic pattern [25]. The recommended treatment for MAC infection is rifampicin, ethambutol and clarithromycin, typically for 2 years [25]. Dependent on the NTM species, disease severity, resistance profile of the infection and tolerance of the individual, drugs may be replaced or added to a regimen, including isoniazid, moxifloxacin, azithromycin and amikacin [25], [26].

### 1.3 Anti-tuberculosis drug-induced liver injury:

#### 1.3.1 Isoniazid hepatotoxicity:

Isoniazid is one of the most widely used anti-TB drugs, being part of the first-line therapy for active TB and as one of the main options for the treatment of latent TB. However, isoniazid is associated with idiosyncratic DILI. Elevations in alanine aminotransferase (ALT) are not uncommon in patients receiving isoniazid, typically occurring in 20% of patients [27] but severe liver injury is much less common and is seen in up to 1% of patients [28].

Although the pathology of isoniazid-induced liver injury can vary, typically a hepatocellular pattern of injury is seen, with necrosis and inflammation the main features, closely resembling viral hepatitis [29]. However, when isoniazid is given in combination with other anti-TB drugs there have been cases of steatosis and cholestatic liver injury as well as autoimmune reactions [28]. Isoniazid-induced liver injury normally has a delayed onset of at least one week but presentation can occur anytime during treatment. In one study of patients with isoniazid-induced liver injury nearly half of all patients developed DILI within two months, however, some patients developed DILI up to 11 months after starting treatment [29]. For the majority of patients with isoniazid-induced liver injury, liver injury resolves despite continued treatment whereas in some it progresses even after the drug is stopped [27]. Similarly, for those who restart TB treatment, for some it does not lead to immediate recurrence of injury, for others it does [28].

The hepatotoxicity mechanisms of isoniazid are proposed to have two main components, the production of toxic metabolites leading to hepatocyte necrosis, and an immune response to drug-protein adducts which form in hepatocytes. Some cases of isoniazid-induced hepatotoxicity are thought to involve an immune mechanism while others do not [27]. Limitations in understanding isoniazid hepatotoxicity are due to the difficulties in replicating human liver injury in a mammalian model with both rat and mouse models having different characteristics of isoniazid-induced liver injury compared to humans [30]. The metabolism of isoniazid in the liver, resulting in the production of toxic metabolites has been identified as another mechanism of liver injury (Figure 1-1). The metabolism of isoniazid leads to the formation of hydrazine and acetyl-hydrazine, both toxic metabolites which induce the production of reactive oxygen and reactive nitrogen species [27]. The metabolite

acetyl-diazine can also break down to give reactive acetyl onium ions, acetyl radicals and ketene [27]. In addition to causing the production of reactive oxygen and reactive nitrogen species, toxic metabolites can bind to liver macromolecules resulting in liver injury [31]. Toxic metabolites of isoniazid also induce mitochondrial dysfunction, through disruption of the mitochondrial membrane potential, decreased adenosine triphosphate production and production of reactive oxygen species [27]. Mitochondrial dysfunction results in DNA strand breaks leading to the induction of apoptosis [32]. Oxidative stress is also thought to have a role in isoniazid-induced liver injury, with isoniazid an effective inhibitor of antioxidant response elements activity [27], [33]. Isoniazid and its metabolites are also able to stimulate lipid peroxidation, resulting in the downstream effects of impaired membrane integrity and mitochondrial dysfunction, leading to cell death and liver necrosis [27]. The production of toxic metabolites from isoniazid would suggest an acute pattern of liver injury, however, liver injury with a delayed onset is also seen with isoniazid exposure, potentially due to an immune mechanism of liver injury [30]. Isoniazid has been shown to be bioactivated by cytochrome P450 (CYP) enzymes and covalently bound to liver macromolecules [31]. Evidence suggests that an immune response develops against these modified proteins, resulting in liver injury, with T-cells from patients with isoniazid-induced liver injury proliferating when incubated with isoniazid [34]. More recent work has found evidence of anti-isoniazid and anti-CYP antibodies in the sera of patients who developed isoniazid-induced liver injury [35]. Most cases resolve with immune tolerance, however, serious liver injury develops in some individuals, thought to be associated with immune response developing against the parent drug, and formation of anti-isoniazid antibodies [28]. The development of an immune response against isoniazid fits with a delayed onset of liver injury seen in some individuals.

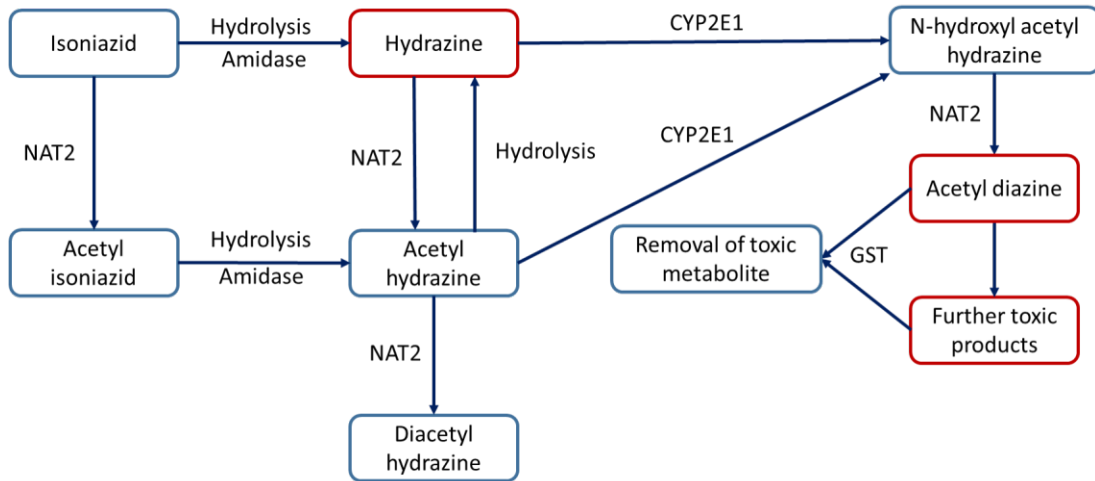


**Figure 1-1: Metabolism of isoniazid in the liver.**

Overview of the pathways by which isoniazid is metabolised in the liver. NAT2 is responsible for the metabolism of isoniazid to acetyl-isoniazid, which is then hydrolysed to acetyl-hydrazine. Isoniazid can also be directly hydrolysed to produce hydrazine. Both hydrazine and acetyl-hydrazine are toxic metabolites, inducing the production of reactive oxygen and reactive nitrogen species [27]. Acetyl-hydrazine can be further oxidised by CYP2E1 to N-hydroxyl-acetyl-hydrazine, which is then dehydrated to give acetyl-diazine. Acetyl-diazine may be a toxic metabolite, but it also has the potential to break down to give reactive acetyl onium ions, acetyl radicals and ketene [27]. N-acetyl transferase 2 (NAT2), cytochrome P450 2E1 (CYP2E1), glutathione S-transferase (GST).

### 1.3.2 Rifampicin hepatotoxicity:

Rifampicin is considered to be fairly well tolerated with a low risk of DILI, [36], but it is difficult to be certain of the hepatotoxicity of rifampicin as it is widely used as part of multidrug regimes for the treatment of TB. However, rifampicin is used as a monotherapy in the treatment of pruritis, with one study reporting 3 cases (7.3%) of rifampicin-induced hepatotoxicity, with two patients developing significant impairment of liver function and one requiring liver transplantation [37].

Rifampicin itself inhibits the bile salt export pump resulting in an increase in serum conjugated bilirubin levels [38], [39]. However, rifampicin's main role in contributing to DILI lies in its use in multi-drug regimens. Rifampicin is a potent inducer of metabolic pathways in the liver, including the CYP enzymes via the pregnane X receptor and isoniazid hydrolases

[36], [40], [41]. It is this effect on metabolism in the liver that means rifampicin can potentiate the hepatotoxicity effects of other drugs and affect the levels of drugs present in the body, with the induction of isoniazid hydrolases [36], resulting in increased hydrazine production and an increase in hepatotoxicity. Another effect of rifampicin is to lower plasma concentrations of other anti-TB drugs as defined in a study which showed that coadministration of moxifloxacin with isoniazid and rifampicin demonstrated a reduction in plasma concentrations of moxifloxacin [42]. Rifampicin's ability to cause alterations in liver function impacts individuals with pre-existing liver conditions and those who are more susceptible to hepatotoxicity such as the elderly. Patients particularly at risk include HIV-positive patients on ART and individuals with NTM infections [26]. However, rifampicin is still the recommended rifamycin used in the treatment of NTM infections, as rifabutin affects clarithromycin metabolism and is less well-tolerated in the elderly population [26]. On the other hand, rifabutin is better tolerated in the young, and so has been used in HIV-positive patients who are also taking antiretrovirals, as rifampicin has more severe drug-interactions [26].

### 1.3.3 Pyrazinamide hepatotoxicity:

Pyrazinamide is associated with transient and asymptomatic elevations in ALT, along with DILI. Early studies in the 1950s reported that the use of pyrazinamide was associated with hepatotoxicity in high numbers of patients, although these studies were using a relatively high dose of pyrazinamide (40-50 mg/kg) [43]. In studies using a lower dose of pyrazinamide (25-35 mg/kg) hepatotoxicity was much rarer [43], indicating that there is potentially a direct DILI effect associated with pyrazinamide. However, a recent review found that high dose pyrazinamide is not significantly associated with increased hepatotoxicity and further suggested that the previous reports of hepatotoxicity relied on liver function tests with poor clinical predictive value [44]. Therefore, there may be both direct and idiosyncratic mechanisms involved in the hepatotoxicity of pyrazinamide. Furthermore, pyrazinamide is usually only ever used in combination with other anti-TB medications, so its contribution to hepatotoxicity is unclear. In pyrazinamide-induced liver injury, onset is typically 4-8 weeks, but also may only become apparent after pyrazinamide is stopped. The pattern of liver injury is typically hepatocellular and resembles viral hepatitis, similar to isoniazid [45], [46].

There is a limited understanding of the mechanisms of pyrazinamide hepatotoxicity, with studies reporting on the formation of toxic metabolites and the potential for an immune response to be involved. The metabolism of pyrazinamide in the liver occurs via two pathways (Figure 1-2), both of which end up with the production of 5-hydroxy pyrazinoic acid (5-OH-PA). The metabolite 5-OH-PA is reported to be toxic, inducing inflammation and oxidative stress, as demonstrated in a mouse model [47], [48]. Further work found pyrazinamide also led to the up-regulation of inflammatory cytokines and increased oxidative stress in a zebrafish model [49], a mouse model [48] and a rat model [50].

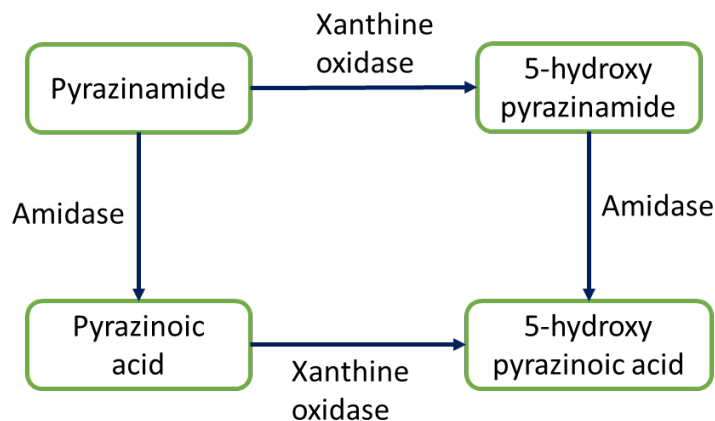


**Figure 1-2: Metabolism of pyrazinamide in the liver.**

The metabolism of pyrazinamide occurs via two pathways. Pyrazinamide is metabolised by microsomal amidases to generate pyrazinoic acid, an active inhibitor of *M. tuberculosis*, which is then hydroxylated by xanthine oxidase to produce 5-hydroxy pyrazinoic acid (5-OH-PA). The second pathway involves the hydroxylation of pyrazinamide by xanthine oxidase to generate 5-hydroxy pyrazinamide and this is then metabolised by microsomal amidases to generate 5-OH-PA [47], [48].

#### 1.3.4 Other anti-tuberculosis drugs and hepatotoxicity:

Isoniazid, pyrazinamide and rifampicin are the most widely used anti-TB drugs and are most frequently associated with DILI. However, some of the other drugs used for TB treatment are associated with DILI. Fluoroquinolones are associated with reversible elevations in ALT in approximately 2-3% of patients [51]. Despite this, fluoroquinolones are widely used in cases of multi-drug resistant (MDR)-TB, NTM infection and in those unable to tolerate first-

line therapy. Furthermore, they are often used to treat patients with active TB whilst awaiting the resolution of elevated liver enzymes. In addition to the fluoroquinolones, several second-line drugs are associated with hepatotoxicity including ethionamide, prothionamide, para-aminosalicylic acid and cycloserine [52]. The macrolides clarithromycin and azithromycin used in the treatment of NTM infections are known to cause elevations in ALT, especially in the more susceptible elderly population [26].

#### 1.3.5 Multi-drug hepatotoxicity:

Incidence of hepatotoxicity is higher in those receiving combination therapy than monotherapy. The co-administration of pyrazinamide with rifampicin and isoniazid is reported to increase the risk of hepatotoxicity [53]. Furthermore, experiments with cell lines indicate that isoniazid and its toxic metabolite hydrazine increase *in vitro* pyrazinamide toxicity [54]. However, it is difficult to assess the contribution of individual drugs to hepatotoxicity as they are largely used in combination therapies and not as monotherapies. Furthermore, different studies use different criteria for DILI, have different monitoring policies and are in different populations.

#### 1.3.6 Risk factors for developing anti-tuberculosis drug-induced liver injury:

The risk of developing ATDILI increases with a range of factors, including, age, female sex, alcohol intake, pre-existing liver conditions (hepatitis B & C), chronic viral infection, HIV infection, disseminated TB disease, concomitant use of other hepatotoxic drugs and malnutrition [27], [55]. Alcohol increases the hepatotoxicity of isoniazid, through inducing the oxidation of mono-acetyl hydrazine into hepatotoxins [56]. Individuals with extrapulmonary TB, most commonly abdominal TB, have been associated with increased risk of DILI, likely due to subclinical liver involvement in abdominal TB patients [39].

Pharmacogenomic risk factors for DILI include polymorphisms in genes encoding drug metabolising enzymes, for example NAT2, CYP2E1 and GST1 [55], [57]. NAT2 slow acetylators were shown to be at increased risk of isoniazid-induced liver injury, with accumulation of hydrazine proposed to be the reason for increased hepatotoxicity [58]. In addition, polymorphisms in genes encoding enzymes for drug clearance, such as ABCC1, can result in the accumulation of toxic products [55]. Human leukocyte antigens genotypes have

been associated with ATDILI, due to the role that major histocompatibility complex play in presenting drug-metabolite adducts and their interaction with the immune system [55]. These pharmacogenomic risk factors mean that different ethnic groups potentially have differing susceptibilities to developing ATDILI.

#### 1.4 Diagnosis of drug-induced liver injury:

##### 1.4.1 Liver function tests:

Currently, routine liver function tests (LFTs) measure a panel of biomarkers including, the serum aminotransferases, alanine aminotransferase (ALT) and aspartate aminotransferase (AST), prothrombin time (PT), international normalised ratio (INR), alkaline phosphatase (ALP), albumin and bilirubin. This panel gives a range of information on the health of a patient's liver and can help differentiate different mechanisms and patterns of liver injury. Patterns of liver injury can be divided into hepatocellular, cholestatic and mixed. Hepatocellular liver injury is due to the necrosis of hepatocytes often with infiltration of inflammatory cells and is typified by a rise in ALT, whereas cholestatic liver injury is caused by an impairment of bile flow and is identified by an initial ALP rise [59]. Using ALT and ALP measurements the R ratio (ALT/ULN : ALP/ULN) can be determined, with  $\geq 5$  indicating hepatocellular injury,  $\leq 2$  indicating cholestatic injury and mixed injury indicated by a ratio of 2-5 (ULN = Upper limit of normal) [59].

##### 1.4.2 Management of anti-tuberculosis drug-induced liver injury:

The serum aminotransferase ALT is the mostly commonly used measure for determining the presence of ATDILI. Typically, a baseline measurement of liver function is taken before an individual commences treatment. Periodic monitoring is usually only done in individuals with a higher risk of liver injury, such as those with abnormal LFTs, those who consume alcohol, who are HIV or hepatitis positive, or take any other hepatotoxic drugs [52]. Individuals who develop liver dysfunction during treatment also have LFTs monitored [60].

The guidelines from the American Thoracic Society for halting treatment in cases of liver injury suggests that treatment should be interrupted and a modified or alternative regimen used for those with ALT elevation more than three times the ULN in the presence of hepatitis symptoms and/or jaundice, or five times the ULN in the absence of symptoms [52]. Usually



all hepatotoxic drugs are stopped and in individuals with active TB this period is covered with second-line drugs. For most individuals upon stopping anti-TB drugs, liver injury resolves and the drugs can be reintroduced. Typically anti-TB drugs can be reintroduced once ALT levels have fallen below x2 the ULN, bilirubin levels have returned to the normal range and hepatotoxic symptoms have resolved [61]. The guidelines for reintroducing TB medications differs between countries, with the British Thoracic Society recommending all TB drugs be introduced at the same time but at lower doses [62], and the American Thoracic Society recommending that the full dose of rifampicin is started with or without ethambutol, followed by isoniazid one week later, and pyrazinamide a week after that, provided ALT levels are within normal range [52]. If reintroducing a drug causes a reaction of similar or greater severity, that drug is removed from future regimens. In instances of recurrence of hepatotoxicity, the drug responsible is stopped and therapy is continued with second-line drugs in its place.

Although these guidelines are useful in preventing DILI developing into acute liver failure, they rely on patients undergoing LFTs. In some countries, patients do not undergo frequent monitoring and so elevations in ALT are not detected, rather individuals develop DILI and present with symptoms such as jaundice. Furthermore, there is no way of detecting DILI before it has developed. Consequently, DILI is a common side effect of TB treatment, resulting in interruptions in treatment, increasing the potential for incomplete cure, relapse and the development of antimicrobial resistance.

#### 1.4.3 Causality assessment:

Although elevation of liver enzyme levels indicates injury, it does not provide a definitive diagnosis that the drug a patient is taking is causing their liver injury. Therefore, a causality assessment is required to determine a link between the drug and liver toxicity. Systems have been developed to standardise causality assessment of DILI. One of the frequently used systems for DILI is the Roussel Uclaf Causality Assessment Method (RUCAM) [63]. The first step in using the RUCAM system is to define the pattern of liver injury using the R ratio, as described in section 1.4.1. The RUCAM system then awards points for seven different components:

1. Time to onset of the injury following start of the drug

2. Subsequent course of the injury after stopping the drug
3. Specific risk factors (age, alcohol use, pregnancy)
4. Use of other medications with a potential for liver injury
5. Exclusion of other causes of liver disease
6. Known potential for hepatotoxicity of the implicated drug
7. Response to rechallenge

The individual points awarded for each component range from -3 to +3. Total scores range from -9 to 14, although scores at the extremes of this range are rare. A total score of <3 indicating unlikely, 4-5 possible, 6-8 probable, and >8 highly probable hepatotoxicity. Using the RUCAM system with patients who experience ATDILI has limitations. Anti-TB regimens are multi-drug, and disentangling which drug was the causative agent of DILI is challenging. Either anti-TB drugs can be identified as a single entity, or an experienced clinician may be able to determine which anti-TB drug was the causative agent of DILI from its pattern of injury.

## 1.5 The need for novel biomarkers:

### 1.5.1 Limitations of alanine aminotransferase:

ALT is considered the gold standard biomarker for the diagnosis of liver injury, with its use being qualified by decades of clinical experience [64]. In addition, it has a central role in most assessment frameworks used to determine the presence of DILI, such as RUCAM. However, there are several issues with the use of ALT. Firstly, ALT is not specific to the liver but is also present in kidney, heart, skeletal muscle and pancreas. Increased serum ALT can result from muscular damage following exercise [65] or subsequent to a myocardial infarction [66]. Changes in ALT activity not only occur in DILI but also in a wide range of other liver pathologies such as fatty liver disease, viral hepatitis, acute alcoholic liver disease, autoimmune hepatitis and liver cancer [64]. Furthermore, enzymatic induction of the ALT gene is shown to occur during metabolic perturbations such as starvation and diabetes mellitus [67], [68], or during treatment with drugs which alter the metabolism [69]. Therefore, serum ALT may be elevated as a result of increased hepatocyte turnover, resulting in false positive signals for conditions separate from liver injury. In addition to elevations due to other causes, ALT has been shown to be variable within a single individual, with rises and falls in ALT seen during a single day [5]. This indicates the need for serial

measurements which are not achievable in an outpatient visit or resource poor settings. ALT has limitations as a diagnostic marker, as low-level insults to the liver may not affect ALT, on the other hand even fairly high elevations in ALT do not reliably indicate or predict DILI, with some patients able to adapt and recover completely even when exposure to the causative agent is continued [5]. There is a delay period between insult to the liver and rise in ALT, as demonstrated in paracetamol overdose where this slow ALT rise can occur up to 24 hrs or later after overdose [70], meaning ALT cannot be used as an early biomarker of DILI in this context. Finally, the method for determining ALT activity has not been standardised, varying between laboratories and resulting in a “normal” range not being completely defined [64].

#### 1.5.2 Features of a novel biomarker:

A biomarker is an indicator of the presence or severity of a disease state. In order to be able to use a biomarker for diagnostic purposes the biomarker needs to be accurately and rapidly detected from an easy to access sample such as saliva, urine or blood. The accuracy of a biomarker depends on its sensitivity and specificity. Sensitivity measures the proportion of positive or diseased individuals who are correctly identified, whereas specificity measures the proportion of negative or healthy individuals who are correctly identified. Biomarkers have an associated sensitivity and specificity, with the balance between these two variables contributing to the effectiveness of the biomarker. Individuals who test positive but who do not have the disease are false positives, these individuals may undergo interventions despite not having a disease. Similarly, individuals who test negative but do have the disease are false negatives, these individuals may not have a disease identified and thus may not be treated despite requiring treatment. In the case of ATDILI, false positive cases of DILI would halt TB treatment or change treatment regimens despite not having DILI and therefore hindering the effective treatment of their TB. Individuals who are false negatives, and therefore who have ATDILI, would continue anti-TB treatment, with progression of their liver injury. Therefore, a higher sensitivity and specificity is required in a biomarker so as to accurately identify individuals who have the disease state of interest. One of the methods used to assess this is through the use of a receiver operating characteristic (ROC) curve. This graph plots the sensitivity or true positive rate against 1-specificity or the false positive rate. From this curve the area under the ROC curve, or AUC, can be calculated. The AUC is the average sensitivity of a biomarker over the range of specificities. Comparing the AUC of a

biomarker with an AUC of 0.5, or chance, is used to determine the effectiveness of a biomarker.

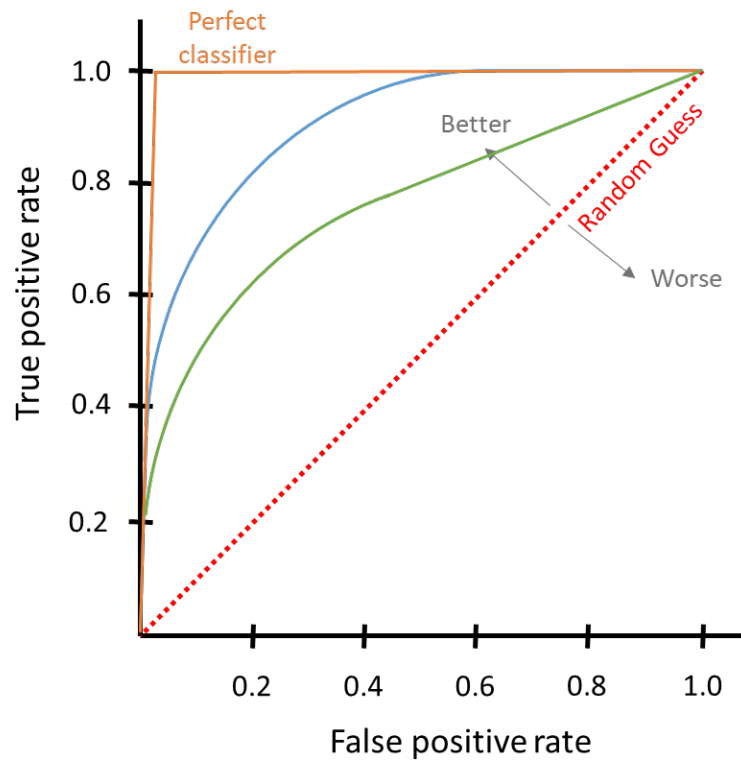


**Figure 1-3: Receiver-operating characteristic curve.**

The receiver-operating characteristic (ROC) curve describes the sensitivity and specificity of a biomarker. The true positive rate or sensitivity is plotted against the true negative rate or 1-specificity. The dotted red line describes the line of no-discrimination, or a random guess. Curves above this line represent good classification results, better than random. Curves below this line represent poor classification results. The perfect classifier can be described by the orange line. The area under the ROC curve, or AUC, is the average sensitivity of a biomarker over the range of specificities.

In DILI ALT is widely used as the gold standard biomarker of liver injury. However, there are issues with its use, as highlighted in the section above. It is hoped that novel biomarkers will enable diagnosis of DILI earlier than traditional biomarkers and will predict the development of DILI before it occurs. Not only will this contribute to better management of TB therapy but also has the potential to contribute to the earlier detection of liver injury signals during

clinical trials and drug development, facilitating easier and more rapid drug development and marketing. In order to be an effective biomarker for ATDILI the biomarker needs to have high sensitivity and specificity, ideally with a ROC-AUC of >0.9. Elevations in the novel biomarker would ideally be predictive of serious liver injury, rather than rising with benign increases in ALT. Furthermore, biomarkers should be easily quantified, in resource poor settings and in easy to access samples. The desired and acceptable attributes for a novel biomarker, specifically for ATDILI, are described further in Table 1-2.

<b>Attribute</b>	<b>Desired</b>	<b>Acceptable</b>
<b>Specific for ATDILI</b>	Exclusively elevated in ATDILI over other forms of liver injury	Specific for liver injury
<b>Sensitivity for ruling out injury</b>	ROC-AUC >0.9	ROC-AUC >0.8
<b>Distinguish benign and clinically relevant increase in ALT</b>	Predicts liver failure	Predicts ALT rise
<b>Predictive for ATDILI</b>	Elevated before the development of ATDILI injury in order to enable change in TB treatment management	Diagnostic for ATDILI
<b>Quantitative relationship with disease severity</b>	Quantitative	Qualitative
<b>Rapidly assayed</b>	At point of care or home monitoring <30-minute turnaround time	<60-minute turnaround time
<b>Feasibility of assay</b>	Feasible in resource poor settings, eg. the developing world	Feasible in a standard clinical laboratory
<b>Invasiveness/sample preparation time</b>	Whole blood or fingerprick	Serum or plasma
<b>Translational across species and models</b>	Full conserved across <i>in vitro</i> and <i>in vivo</i> models	Conserved in humans and rodents
<b>Signal to noise</b>	Single measurement required to differentiate between healthy reference value and disease	Requires measurement at two time points
<b>Mediator of liver injury</b>	Provide mechanistic understanding of liver injury and has existing therapeutic intervention	Potential drug target

**Table 1-2: Features of a novel biomarker for ATDILI.**

Table adapted from [71]. Receiver operator characteristic – area under the curve (ROC-AUC).

## 1.6 Novel biomarkers of drug-induced liver injury:

### 1.6.1 Case study – Paracetamol-induced liver injury:

One of the main examples where novel biomarkers of DILI have been identified and demonstrated to benefit clinical care is in paracetamol-induced acute liver injury. Paracetamol is a safe analgesic drug when taken at therapeutic doses, but in overdose it results in predictable and dose-dependent hepatotoxicity [72]. Paracetamol overdose is the commonest cause of acute liver failure in the USA and Europe [2]. Hepatic injury occurs due to the toxic metabolite of paracetamol, N-acetyl-p-benzoquinone imine (NAPQI), which is generated in excess leading to the depletion of glutathione (GSH) and results in NAPQI covalently binding to sulfhydryl groups in structural proteins, forming protein adducts [73]. This results in oxidative stress, mitochondrial injury and hepatocyte death via apoptosis and necrosis [73]. The current antidote, N-acetylcysteine (NAC), prevents liver injury by replenishing GSH if administered within a few hrs of overdose, but if treatment is delayed its efficacy is significantly reduced. The currently used biomarkers, ALT and a timed blood paracetamol concentration, lack sensitivity and specificity when measured soon after overdose [70]. Therefore, there is a need for biomarkers which can accurately stratify patients, predicting which individuals will go on to develop acute liver injury if not treated with NAC, and those who require no further treatment and can be sent home, at initial presentation to the hospital. Accurate stratification of patients should reduce the number of individuals who go on to develop acute liver injury as well as reducing the burden on the hospital and individual, as those not requiring treatment do not take up hospital resources and are not exposed to the potential side-effects of NAC treatment. Recent work in this area has identified the novel biomarkers microRNA-122 (miR-122), cytokeratin-18 (K18), glutamate dehydrogenase (GLDH) and high mobility group box 1 (HMGB1) [74]. Additional biomarkers, all highlighted by a recent paper by Church and colleagues as being potential biomarkers of DILI include alpha-fetoprotein, arginase-1, cadherin-5, fatty acid binding protein-1, glutathione S-transferase A, macrophage colony-stimulating factor receptor, osteopontin, leukocyte cell-derived chemotaxin 2, paraoxonase-1 and sorbitol dehydrogenase [75].

However, there are limited data on the use of these biomarkers in different populations and in DILI caused by different drugs.

### 1.6.2 MicroRNAs:

MicroRNAs are a class of short non-protein coding RNA species, approximately 22 nucleotides in length. They were first discovered in *C. elegans* in 1993 [76]. MicroRNAs are involved in RNA silencing and post-transcriptional regulation of gene expression, either through the degradation of mRNA sequences resulting in reduced gene expression, or by binding promoter regions leading to activation of gene expression [77]. The biological functions of miRNAs include stress resistance, metabolism, defence against infection by pathogens, cell proliferation, cell death and tumorigenesis [78].

Roughly 30% of miRNAs are processed from the introns of protein-coding genes, with most other miRNAs being expressed from a dedicated miRNA loci [79]. MiRNAs which are found in a dedicated miRNA loci are called miRNA clusters. A miRNA cluster is a series of more than one miRNAs which are transcribed from physically adjacent genes, are transcribed in the same orientation and are not separated by another gene or miRNA in the opposite orientation [80]. MiRNA clusters typically regulate multiple cellular targets. MicroRNAs are transcribed as primary transcripts consisting of a hairpin loop. When two mature miRNAs originate from the opposite arms of the same pre-miRNA hairpin they are denoted by the suffix -3p or -5p to denote their position in the hairpin [81]. On occasion, the primary transcript contains multiple hairpins, and these multiple hairpins give rise to different miRNAs. The hairpins generated from these polycistronic miRNA transcripts have their own unique name [81]. The function of miRNAs depends on complementary binding of the miRNA with its mRNA target. The seed region is a 6-8 nucleotide sequence at the 5' end of the miRNA which recognises its target miRNA, this region must be perfectly complementary even if the base pairing throughout the rest of the miRNA and its target mRNA is not perfectly matched. A miRNA family consists of miRNAs which share complete sequence identity in the seed regions and therefore can regulate the same targets [82]. Mature miRNAs which are completely identical in sequence but originate from different genomic locations are indicated with an additional dash-number suffix. MiRNAs with near identical sequences are annotated with an additional lower case letter in their names. MiRNAs are produced by two main pathways, the canonical pathway and the non-canonical pathway. The canonical pathway of miRNA biogenesis is shown in Figure 1-4, whereby miRNAs are transcribed in the nucleus, processed and then exported to the cytoplasm where they bind

with protein complexes before causing translational repression and mRNA decay. Although the canonical pathway is the main route by which miRNAs are produced multiple non-canonical miRNA biogenesis pathways have been elucidated. These pathways make use of different combinations of the proteins involved in the canonical pathways and can be classed into DROSHA/DGCR8-independent and DICER-independent pathways [79].

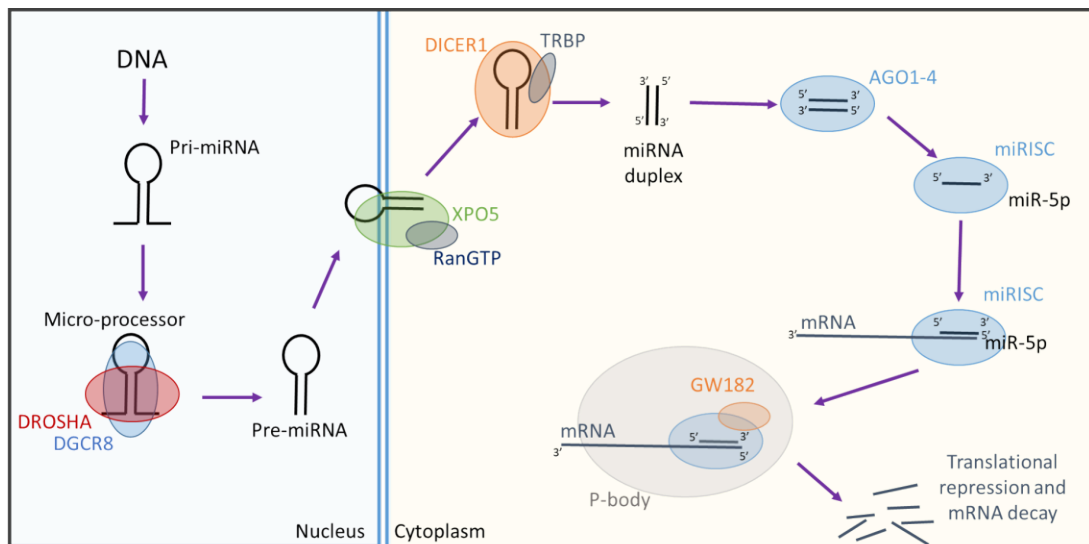


**Figure 1-4: MiRNA biogenesis.**

MiRNAs are transcribed by RNA polymerase II in the nucleus, forming primary miRNAs (pri-miRNAs). The pri-miRNAs are then capped, spliced and polyadenylated before being cleaved by microprocessor, consisting of the double-strand RNase III enzyme DROSHA and its co-factor, the double-stranded RNA-binding protein DiGeorge syndrome critical region 8 (DGCR8). DROSHA, a class 2 ribonuclease III enzyme, cleaves both strands of the dsRNA complex near the hairpin loop structure to produce a 60-70 nucleotide sequence containing the hairpin, this is a precursor miRNA (pre-miRNA). Pre-miRNAs are exported from the nucleus via the exportin 5 (XPO5)/RanGTP complex to the cytoplasm. Further processing is done by DICER in association with transactivation-responsive RNA-binding protein (TRBP). DICER1 is an RNase III enzyme which cleaves the pre-miRNA to produce a mature 22-nucleotide miRNA duplex. One strand of the mature miRNA (the guide strand) is loaded into the miRNA-induced silencing complex (miRISC). miRISC consists of DICER1 and AGO1-4 proteins. The miRISC, when associated with members of the GW182 family of proteins, uses the guide miRNA strand to target complementary mRNAs for post-transcriptional gene silencing. Diagram adapted from [79].



MiRNAs main role is to regulate gene expression, mainly through translational repression and gene silencing. The miRISC is the main mechanism of gene silencing, with the guide miRNA strand providing target specificity by binding complementary miRNA response elements (MREs) at the 3' UTR of mRNAs. In the presence of a fully complementary miRNA-MRE interaction argonaute-2 (AGO2) endonuclease activity is induced and mRNA cleavage occurs. When the miRNA-MRE interaction is not fully complementary the miRISC causes mRNA deadenylation and decapping resulting in mRNA degradation [77]. Further mechanisms of translational repression by miRNA include via binding to the 5' UTR or coding sequences, although these mechanisms are less well understood. In addition to translational repression, miRNA binding to promoters has been demonstrated to induce transcription. Furthermore, nuclear-localised miRISC can regulate transcriptional rates and post-transcriptional levels of mRNA [77].

Although the main mechanism of action of miRNAs occurs within cells, miRNAs are also released into extracellular fluids and have been found in bodily fluids including serum/plasma, cerebrospinal fluid and urine [77]. They can be delivered to target cells to modulate cellular activities and can act in a paracrine, autocrine or endocrine manner [83]. Extracellular miRNAs tend to exist in one of two forms, either in vesicles such as exosomes, microvesicles and apoptotic bodies [84], or associated with proteins such as AGO2, RNA binding complexes and high-density lipoproteins [85]. The form which extracellular miRNAs exist seems to depend on the miRNA, the cell they originate from and other factors affecting their release from cells. The release of miRNAs from cells is a regulated process but miRNAs can also be released in an unregulated way after cell injury and death. Extracellular miRNAs are highly stable, resisting degradation at room temperature for up to 4 days and surviving tough conditions including low/high pH, boiling, extended storage and freeze-thaw cycles [86]. The stability of miRNAs in extracellular fluids, along with their potential to differ in disease states makes miRNAs potentially good biomarkers of disease.

### 1.6.3 MiR-122:

MiR-122 is a 22-nucleotide microRNA which is highly expressed in, and highly specific for, the liver, with little to no expression in other tissues, making up 70% of the miRNA content in hepatocytes [87]. It is highly conserved across many species including *Homo sapiens*, *Bos*

*Taurus*, *Sus scrofa*, *Mus musculus* and *Rattus norvegicus*, with sequences of miR-122 being clustered in the same clade [78]. In humans miR-122 is encoded at a single genomic locus on chromosome 18, as in mice, however, in zebrafish miR-122 is found on chromosome 21. MiR-122 is expressed as a unique miRNA within a single transcript [88]. During embryogenesis miR-122 levels in the liver increase, reaching approximately 135,000 copies per cell in human hepatocytes and 66,000 copies per cell in the adult mouse liver [88]. Transcription of the primary miR-122 transcript is regulated by four liver-enriched transcription factors which bind to the miR-122 promoter and lead to miR-122 expression [89]. These transcription factors include hepatocyte nuclear factor (HNF) 1 $\alpha$ , HNF3 $\beta$ , HNF4 $\alpha$  and CCAAT/enhancer-binding protein [89]. As the miR-122 promoter is under the regulation of hepatocyte specific transcription factors this drives miR-122's specificity for hepatocytes and low levels of expression seen in other organs. HNF4 $\alpha$  controls the expression of HNF1 $\alpha$ , a transcription factor which controls the expression of several hepatic genes. Furthermore, miR-122 stimulates HNF6, establishing a positive feedback loop directing hepatocyte differentiation and liver development [89]. The high expression of miR-122 in the liver, and the targets that miR-122 regulates, suggests that miR-122 plays a role in hepatocyte differentiation and liver development. Furthermore, miR-122 helps maintain the phenotype of adult hepatocytes through suppressing the expression of non-liver genes [78]. In addition to maintaining hepatocyte phenotype, miR-122 has a role in lipid metabolism, cholesterol accumulation and fatty acid metabolism [89]. In disease, miR-122 stimulates hepatitis C virus (HCV) replication, inhibits hepatitis B virus (HBV) replication and suppresses hepatocarcinogenesis [89]. MiR-122 is down-regulated in hepatocellular carcinoma [78]. Evidence suggests that miR-122 inhibits cyclin G1 and the ADAM17, genes commonly associated with tumorigenesis [88]. In addition, miR-122 acts as a tumour suppressor gene, with overexpression of miR-122 reducing tumour formation in hepatocellular carcinoma cell lines [88]. MiR-122 is essential for hepatitis C viral replication. Within the viral RNA there are two miR-122 binding sites in the non-coding region at the 5' end. MiR-122 can bind to these regions, protecting the viral RNA from degradation [89]. In contrast, miR-122 binds to the hepatitis B virus RNA, causing its degradation and thus inhibiting the replication of the virus [89].

#### 1.6.4 MiR-122 as a biomarker:

In liver injury miR-122 is released from necrotic hepatocytes, resulting in elevated miR-122 concentrations in the bloodstream, as first demonstrated by Wang and colleagues in a mouse model of paracetamol overdose [90]. Further work reported miR-122 as a biomarker of acute liver injury in rats [91], zebrafish [92], chimpanzees [93] and dogs [94]. In humans, miR-122 has been demonstrated to be a biomarker of different liver diseases including DILI [95], hepatitis C [96] and ethanol consumption [97]. Patients who developed acute liver injury following paracetamol overdose had an approximately 100-fold increase in circulating miR-122 concentrations [95], [98]. For paracetamol overdose induced acute liver injury miR-122 has demonstrated superior sensitivity and specificity than ALT [99]. In 129 paracetamol overdose patients in Newcastle and Edinburgh miR-122 correlated with peak ALT and INR. In addition, in patients presenting with normal ALT or INR, miR-122 identified the development of liver injury with a high degree of accuracy, and out-performed ALT, INR and plasma paracetamol concentration for the prediction of subsequent acute liver injury compared with no injury in patients presenting within 8 hrs of overdose [99]. A large multi-centre study on patients who overdosed on paracetamol has demonstrated that miR-122 can predict acute liver injury at hospital presentation and has superior sensitivity compared with ALT [74]. This study included a total of 1187 patients, 985 in the derivation cohort (MAPP) and 202 in the validation cohort (BIOPARR). Acute liver injury was predicted at hospital presentation by miR-122 in the derivation cohort (ROC-AUC 0.97 [95% CI 0.95-0.98]) and in the validation cohort (ROC-AUC 0.97 [95% CI 0.95-0.99]) [74]. A recent study investigating biomarkers of DILI across a range of drug classes had a lower ROC-AUC value for the diagnosis of DILI with miR-122, (ROC-AUC 0.83 [95% CI 0.78-0.88]) [75]. This may be due to miR-122 being less sensitive and specific for DILI from causes other than paracetamol. However, there are limitations to this study, as some samples were stored for extended periods and due to the difference in miR-122 quantification methods. All of this evidence has led to miR-122 receiving regulatory support for further qualification as a biomarker of DILI from the US Food and Drug Administration and the European Medicines Agency [100], [101].

A consortium recently determined the healthy reference intervals of a range of DILI biomarkers, including miR-122 [75]. Healthy volunteers were recruited in the Predictive

Safety Testing Consortium (PSTC) and Safer and Faster Evidence-Based Translation consortium (SAFE-T). A healthy reference interval, the lower and upper limits of normal, was defined from each dataset by the 5<sup>th</sup> and 95<sup>th</sup> percentile (Table 1-3). Values for miR-122 demonstrated a high inter-subject variation. In individuals within the PSTC three serial measurements were taken in order to determine intra-subject variation. Interestingly, intra-subject variation was higher in black participants compared to white participants.

MiR-122 is reported to be highly liver specific, however there is the potential for other diseases or factors to influence the circulating levels of miR-122 in a similar manner to ALT. A study has shown that ethanol does affect miR-122 concentrations, with a 2.2-fold increase in circulating miR-122 concentrations seen after alcohol consumption, and no significant change in ALT identified [97]. Another study showed that extreme exercise can significantly lower miR-122 concentrations, along with a significant elevation in ALT [102].

	<b>PSTC (n=81)</b>	<b>SAFE-T (n=192)</b>
<b>Mean (copies/μl)</b>	2153	3174
<b>LLN (copies/μl)</b>	347	368
<b>ULN (copies/μl)</b>	13,357	27,368
<b>Inter-subject variation (CV %)</b>	90.89	93.56
<b>Intra-subject variation (CV %)</b>	213.5	-

**Table 1-3: Healthy reference interval for miR-122.**

*Data from [75]. Predictive Safety Testing Consortium (PSTC), Safer and Faster Evidence-Based Translation (SAFE-T), lower limit of normal (LLN), upper limit of normal (ULN).*

MiR-122 fulfils many of the criteria of an ideal biomarker with enhanced sensitivity and specificity for DILI, along with a prognostic capability. Furthermore, miR-122 has been shown to be translational across several species, requires only serum/plasma as a sample and can be easily quantified by qRT-PCR. Consequently, miR-122 has the potential to greatly aid the process of preclinical and clinical drug development. However, further qualification is needed to determine miR-122's potential for use as a biomarker of DILI from causes other than paracetamol.

### 1.6.5 Cytokeratin-18:

Keratins are epithelial-specific intermediate filament proteins that are responsible for cell structure, differentiation, mitosis and apoptosis. Cytokeratin-18 (K18) is an intermediate filament responsible for maintaining the cytoskeletal structure in the liver and other epithelial cells and is reported to make up 5% of the liver's total protein content [103]. K18 is a mechanistic biomarker of liver injury, providing information on the pattern of cell death occurring in the liver. In apoptosis, the release of a caspase-cleaved form of K18 (CC-K18) is an early event during cellular structural rearrangement [104]. Cleavage of K18 by caspases 3, 6 and 7 generates fragments of 30 kDa and 45 kDa [105]. Whereas in necrosis the full-length form of K18 (FL-K18) is passively released upon cell death [104]. The quantification of total K18 and CC-K18 is possible through the M65 and M30 ELISAs. Quantification of total K18 is possible with the M65 ELISA, with the M5 antibody detecting a common epitope present in the full-length protein as well as the caspase-cleaved form. The M65 ELISA measures total K18, that which is released from both necrosis and apoptosis. Quantification of CC-K18 is possible with the M30 ELISA, where the M30 antibody binds the neoepitope mapped to positions 387 to 396 of a 21-kDa fragment of K18 which is only revealed after caspase cleavage [106].

### 1.6.6 Cytokeratin-18 as a biomarker:

Early work identified that K18 was released from apoptotic cells into the supernatants of cell cultures [107]. Further work identified increases in FL-K18 and CC-K18 in a mouse model of paracetamol overdose, demonstrating correlation with serum ALT and histology and providing insight into the mechanisms of hepatocyte death occurring [108]. In humans the measurement of FL-K18 and CC-K18 has been undertaken in chemotherapeutic studies to determine tumour cell death and anti-tumour activity of drugs [109]. Furthermore, FL-K18 and CC-K18 have been used to quantify the pattern of hepatocyte death in non-alcoholic steatohepatitis (NASH) [110] and hepatitis C [111]. Much of the most recent work has focussed on K18 as a biomarker of paracetamol overdose induced acute liver injury. A study of patients with paracetamol overdose induced acute liver injury and abnormal ALT (n=78) demonstrated a 200-fold increase in FL-K18 compared to healthy volunteers (n=31), (median [IQR]: healthy volunteers 169 [130-191]; liver injury 34176 [11225-86205] U/L) [112]. A 14.6-fold increase in CC-K18 was also seen, (median [IQR]: healthy volunteers 193 [160-257]; liver

injury 2813 [1026-7510] U/L) [112]. For paracetamol overdose induced acute liver injury both forms of K18 demonstrated an ability to both diagnose and predict acute liver injury, with significant correlation with peak ALT and INR in a study of 129 paracetamol overdose patients in Newcastle and Edinburgh [99]. In addition, FL-K18 identified the development of liver injury or not with a high degree of accuracy, and out-performed ALT, INR and plasma acetaminophen concentration for the prediction of subsequent acute liver injury compared with no injury in patients presenting within 8 hrs of overdose [99]. CC-K18 was less accurate at diagnosing acute liver injury, which is consistent with necrosis being more dominant in paracetamol overdose induced liver injury than apoptosis [71]. A large multi-centre study has shown that FL-K18 can predict acute liver injury at hospital presentation and has superior sensitivity compared with ALT [74]. This study included a total of 1187 patients, 985 in the derivation cohort (MAPP) and 202 in the validation cohort (BIOPARR). In the derivation cohort, acute liver injury was predicted at hospital presentation by FL-K18 (ROC-AUC 0.95 [95% CI 0.92-0.97]) and the validation cohort (ROC-AUC 0.93 [95% CI 0.86-0.99]). A combined model of miR-122, HMGB1 and FL-K18 predicted acute liver injury better than ALT alone [74]. A recent paper assessing the diagnostic value of a range of biomarkers, across DILI due to a range of different drugs, found both total K18 and CC-K18 had high sensitivity and specificity for the identification of DILI, (ROC-AUC: total K18 0.95 [95% CI 0.93-0.97]; CC-K18 0.91 [95% CI 0.89-0.93]) [75]. In addition, total K18 and CC-K18 had some prognostic power for patients who died or needed liver transplant 6 months after the onset of DILI, (ROC-AUC: total K18 0.83 [95% CI 0.74-0.93]; CC-K18 0.78 [95% CI 0.68-0.88]) [75]. Furthermore, the ratio of CC-K18 to total K18, a measure of the pattern of cell death, indicated necrosis was higher in patients who died or required transplant [75]. As a consequence K18 has received regulatory support for further qualification as a biomarker of DILI from the US Food and Drug Administration and the European Medicines Agency [100], [101].

Healthy reference intervals have been described for CC-K18 and total K18, similar to miR-122 (Table 1-4) [75]. Calculation of the reference intervals was limited due to the assays used, with a substantial number of CC-K18 values, and approximately 90% of total K18 measurements falling below the lower limit of quantification. Therefore, the LLN cannot be quantified for total K18, nor a measurement of the variation within and between subjects.

In comparison to miR-122, the inter-subject variation is lower at approximately 70% compared to 90% for miR-122. Similarly, the intra-subject variation is much lower, at 35% compared to 213% for miR-122.

	CC-K18		Total K18	
	PSTC (n=81)	SAFE-T (n=192)	PSTC (n=81)	SAFE-T (n=192)
<b>Mean (U/L)</b>	91	140	-	-
<b>LLN (U/L)</b>	32	53	-	-
<b>ULN (U/L)</b>	260	374	121	151
<b>Inter-subject variation (CV %)</b>	70.79	65.39	-	-
<b>Intra-subject variation (CV %)</b>	34.76	-	-	-

**Table 1-4: Healthy reference interval for CC-K18 and total K18**

Data from [75]. Predictive Safety Testing Consortium (PSTC), Safer and Faster Evidence-Based Translation (SAFE-T), lower limit of normal (LLN), upper limit of normal (ULN).

Cytokeratin-18 has potential as a biomarker of DILI, with good sensitivity and specificity along with a prognostic power. K18 can be easily assayed from serum/plasma using the M30 and M65 ELISAs. Furthermore, the two forms of K18 provide mechanistic understanding of the type of cell death occurring. However, there is limited evidence for K18 ability to translate across species, only being shown to translate into the mouse model so far [108].

## 1.7 Zebrafish as models of drug-induced liver injury:

### 1.7.1 Models of drug-induced liver injury:

Our understanding of DILI relies on models of liver injury, including *in vitro* and *in vivo* systems. Ideally a model of DILI should develop liver injury with a clinical resemblance to humans, with similar mechanisms to human liver injury and should be convenient for experiments.

*In vitro* models of liver toxicity include liver tissue slices, isolated liver microsomes, perfused livers, immortalised cell lines (HepG2 and HepaRG) and primary isolated hepatocytes [113]. In comparison to animal models, *in vitro* models have a reduced cost and complexity. They reduce the use of animals in research according to the 3R's principle (reduction, replacement

and refinement) and can be high throughput, with the potential to test many different compounds. Primary isolated hepatocytes and immortalised cell lines are the commonest models used, however, issues with their use include, a loss of viability, a reduction in liver specific functions and alterations in gene expression [113]. Developments in the field of *in vitro* models include the introduction of 3D systems, regenerating stem cell systems and the use of co-cultures [113].

Although *in vitro* approaches have some advantages, for a fuller understanding of hepatotoxicity an *in vivo* approach is required to model the dose-dependent toxicity of a drug within the complex physiology of a whole organism. One of the main components missing with *in vitro* models is the immune response. Traditionally, histopathology and clinical chemistry have been used to report liver toxicity in established animal models, including rodents (rats, mice, rabbits and guinea pigs) and other animals such as pigs, sheep and monkeys. Most preclinical research relies on rats and mice as model organisms for liver toxicity. In comparison to *in vitro* models, mice have advantages as models of DILI, having a full complement of mammalian organs and physiological similarities to humans along with similar metabolic pathways. Although rodents are typically used in liver toxicity studies, evidence suggests that smaller, lower order vertebrates, such as zebrafish, can accurately model human physiology.

#### 1.7.2 Advantages and limitations of zebrafish:

Zebrafish, *Danio rerio*, began to be used as a model vertebrate organism for developmental biology and embryology from the 1930s due to their optical clarity and ease of embryo manipulation [114]. They are widely used as a model organism, with well-established assays for the measurement of the function of the cardiac system, central nervous system and gastrointestinal system [115], [116]. In addition, they are used as high-throughput screening tools for novel drugs and toxicity, especially developmental toxicity and hepatotoxicity [117]. The optimum breeding and maintenance conditions for zebrafish have been well defined [118]. The use of zebrafish instead of other higher organisms in animal research follows the 3Rs, reduction, replacement and refinement, with replacement of higher order mammals with zebrafish embryos. In addition, the zebrafish genome has been sequenced and annotated providing a wealth of genetic information available [119]. Furthermore, ~70% of



human genes have a zebrafish orthologue and ~82% of potential human disease-related genes have at least one obvious zebrafish orthologue [119]. The genetic modification of zebrafish is possible and enables the formation of modified zebrafish containing tagged cell lines. Zebrafish have an advantage over *in vitro* and *ex vivo* studies in that they are still high throughput but in the context of a whole organism. The advantages and limitations in the use of zebrafish larvae are summarised in Table 1-5.

<b>Advantages</b>	<b>Limitations</b>
High throughput and numbers per experiment	Differences in liver structure to mammals
High fecundity (~200 eggs per week)	Difficult to quantify drug uptake from system water
Short generation time and rapid development compared to mammalian models	Unable to draw blood from larvae to assess liver injury biomarkers and drug pharmacokinetics
Larvae can be grown at a high density in multi-well plates	Genome duplication in zebrafish results in multiple copies of genes
Cost for feeding and housing zebrafish is low	Differential gene expression with age
Develop outside of the uterus and are optically transparent	
Possible to study embryonic lethal phenotypes	
Possible to deliver drugs by dissolving in the system water	
Similarities in metabolism and enzyme pathways	
Transgenic zebrafish enable visual assessment of liver injury	

**Table 1-5: Advantages and limitations to the use of zebrafish larvae as models of DILI.**

Although there are a significant number of advantages of using zebrafish as a model of liver injury, there are several challenges. The delivery of drugs to zebrafish embryos is achieved by dissolving the drug in system water. This is useful for high-throughput phenotypic screening. However, it is difficult to determine exactly how much of the drug is taken up by the zebrafish larvae, as demonstrated in a study where the uptake of nine different compounds by larvae indicated a large variability in the bioavailability of different compounds [120]. This limits the study of toxicokinetics. Absorption of different compounds into the larvae, via gills and intestine, depends on their physiochemical properties and not

just their concentration in solution. A method of quantifying the amount of administered drug is by injecting the drug into the yolk sac of the embryo [115], but this process is time-consuming and reduces the advantage of dissolving the drug in system water for a high throughput experiment. Further methods of determining how much drug has been absorbed by larvae include using radio-labelled compounds, liquid scintillation, radio high-performance liquid chromatography and lysing of embryos followed by liquid chromatography-tandem mass spectrometry [121]. Another method to measure the uptake of compounds would be through determining the levels of the compound in the blood of the zebrafish. However, this is not possible for zebrafish larvae, and for adults low blood volumes are typically acquired from adult fish, requiring the pooling of 10-20 fish [92].

The second challenge associated with the use of zebrafish is their differential gene expression. The expression of genes in zebrafish larvae differs throughout their development, with 66 of the 88 studied CYP genes in zebrafish embryos having a differential level of expression between 3-48 hpf (hrs post-fertilisation) [122]. This differential gene expression indicates that zebrafish larvae should only be used for liver toxicity studies from 3 dpf (days post-fertilisation). Furthermore, circadian rhythms can affect an organism's response and susceptibility to drugs. In mice it has been reported that some transporters, which affect bioavailability, metabolism and drug excretion, may be under circadian transcriptional regulation [123]. This may also be true for zebrafish. Therefore, as age and circadian related gene expression profiles can impact on drug susceptibility the standardisation of protocols is needed for using zebrafish embryos in liver toxicity and high throughput studies.

A further challenge when working with zebrafish is measuring circulating biomarkers of liver injury. Measurement of circulating biomarkers is possible in mouse models of liver injury, although the volume of blood collected can be low. In a zebrafish model of liver toxicity, adult zebrafish are needed to measure circulating biomarkers of liver toxicity as it is not possible to bleed zebrafish larvae. Using the standard method of blood collection (lateral incision) one can collect approximately 2.8  $\mu\text{l}$  of blood from a single fish and even using a new retro-orbital technique, the average amount of blood collected is 5.3  $\mu\text{l}$  [92]. Despite the increase in blood volume collected using the retro-orbital technique several samples

need to be pooled in order to quantify circulating biomarkers using assays. Studies have used pooled blood samples from adult zebrafish to measure circulating biomarkers including ALT, ALP and total bilirubin [124]. In addition, research has shown changes in circulating biomarkers similar to changes observed in humans. For example, in a paracetamol liver injury model in adult zebrafish ALT rose in a dose- and time-dependent manner [125]. Although this suggests that changes in biomarker levels are translational between humans and zebrafish, being unable to quantify circulating biomarkers in zebrafish larvae is a limitation to their use.

### 1.7.3 The zebrafish liver:

The process of liver development in the zebrafish is similar to higher vertebrates. In zebrafish larvae liver budding begins at 28 hpf, with liver-specific markers occurring at 16 hpf [126]. Primary liver morphogenesis is completed by 48 hpf and by 72 hpf the larvae have a fully formed and functioning liver [127]. At 5 dpf the heart, liver, brain, pancreas and other organs are developed. At 6 dpf, the zebrafish yolk sac is depleted, and the zebrafish is actively seeking food. In comparison, in mice embryos the primary liver bud begins developing at day 8.5-9 and is mature at day 18.5, just before birth [128]. During the process of liver development in zebrafish the growth factors and gene expression patterns are like those of humans [126].

The main difference between the zebrafish and mammalian liver is the liver structure, with hepatocytes in the zebrafish arranged in tubules compared to plates in mammals. Instead of having bile ducts, portal veins and hepatic arteries arranged in portal tracts, the zebrafish liver has these randomly arranged throughout the liver parenchyma. Zebrafish hepatocytes are arranged as tubules that enclose small bile ducts rather than as bilayered hepatocytes plates as seen in mammals [126]. The intrahepatic bile ducts are derived from the bile canaliculi and form a network of biliary channels, with bile collected in the gallbladder through large ducts and an extra-hepatic biliary system [126]. The lack of lobular arrangement of hepatocytes impairs morphological differentiation between venules from the portal and hepatic veins, as these vessels are histologically identical [129]. All the different cell types are present in zebrafish livers, with the exception of Kupffer cells, which are replaced by macrophages [130].

The cellular and physiological processes in zebrafish and human livers are similar, including processing of lipids, vitamins, proteins, carbohydrates and the synthesis of serum proteins [131]. Zebrafish have the ability to perform phase I (oxidation, N-demethylation, O-demethylation) and phase II (sulfation and glucuronidation) metabolism reactions [132]. The metabolic enzymes responsible for these reactions are highly conserved across mammals and zebrafish [133], [134]. In mammals, phase I enzymes largely consist of five CYP gene families, CYP1, CYP2, CYP3, CYP4 and CYP7, which play a crucial role in the metabolism and eliminations of xenobiotics and drugs, with CYP families 1-4 considered to be mainly responsible for xenobiotic metabolism [135]. The importance of CYP enzymes in mammals for metabolism, and especially in drug metabolism, means they are required in a model organism. A full range of CYP enzymes have been identified in zebrafish and annotated regarding their phylogenetic relationship to human CYP enzymes. Zebrafish express a total of 94 CYP genes across 18 gene families also found in mammals, as determined by homologous amino-acid sequences [122]. In CYP families 1-4, responsible for the metabolism of exogenous compounds, gene sequences were more diverse in zebrafish than in humans [122]. In CYP families 5-51 there were 32 genes present with high homology to human sequences [122]. In addition, the CYP enzymes are regulated by similar pathways in zebrafish as in humans and other mammals, with one example of this being induction of CYP enzymes in zebrafish via the pregnane X receptor pathway, which plays an important role in DILI [134]. As overviewed by Vliegenthart and colleagues [129], drugs metabolised by zebrafish typically undergo a similar process of metabolism to humans, including both phase I and II reactions. Metabolism of verapamil by zebrafish results in the formation of metabolites by N-dealkylation and hydroxylation [132]. Furthermore, three major metabolites of chlorpromazine, found in human urine, are also excreted by zebrafish; these metabolites are formed by hydroxylation, oxidation, N-demethylation, glucuronidation and sulfation [132]. In addition, zebrafish embryos can de-ethylate phenacetin, demethylate dextromethorphan and hydroxylate bupropion [132]. Further evidence of similarities with mammals is through the metabolism and excretion of ibuprofen, which occurs in a CYP-dependent manner (hydroxylation) in zebrafish [136]. Zebrafish larvae exposed to paracetamol form the product NAPQI [134], the same product produced by CYP3A4 and CYP2E1 in humans exposed to high-dose paracetamol [137], [138]. In zebrafish the

formation of NAPQI is due to the bioactivation of APAP by CYP3A65, an orthologue of human CYP3A4 [134]. Furthermore, zebrafish CYP3A65 also contributes to the hydroxylation of testosterone, the same as in humans [134]. However, there are some cases where the metabolism of mammals and zebrafish differ. One such example is the metabolism of cisapride, where phase I (N-alkylation and oxidation) and phase II (glucuronidation) reactions were not observed [132]. Currently there is limited understanding of the metabolism of anti-TB drugs by zebrafish larvae, with studies focussing on pathways involved in DILI.

There are many similarities between the zebrafish and mammalian immune systems. Most, if not all of the cells of the human immune system can be found in zebrafish [139] but there is a variation in the chemokine receptors found in the different species [140]. However, the expression and function of orthologous chemokine receptors in lower and higher vertebrates are highly similar [140]. In humans, inflammation is common in DILI and can lead to the productions of damage associated molecular patterns, release of cytokine and chemokines and infiltration of immune cells into the liver [141]. While zebrafish metabolise drugs using similar pathways to humans, there is limited evidence whether a similar immune response takes place with DILI in zebrafish.

MiRNAs play an important role in regulating mRNA expression and have shown potential as biomarkers of disease. The high levels of conservation across species [142] means that miRNAs are translational biomarkers. For the liver injury specific biomarker miR-122 the sequence in humans and zebrafish is identical [143]. In humans the gene for miR-122 is found on chromosome 18, whereas in zebrafish it is found on chromosome 21. Not only is the sequence of miR-122 conserved, its liver-specific pattern of expression is also conserved [144]. Furthermore, work by Vliegenthart and colleagues have demonstrated that miR-122 is also a biomarker of triptolide [145] and paracetamol [92] DILI in zebrafish.

#### 1.7.4 Assessing liver toxicity in zebrafish:

Liver toxicity in zebrafish larvae can be assessed using a range of different methods including visual assessment, the use of transgenic lines, histology and measurement of markers of injury. The transparent properties of zebrafish larvae enable the visual assessment of phenotypic changes in a high-throughput manner. Commonly used liver-specific phenotypic

endpoints, assessed under a light microscope, include change in liver size and shape, liver morphology, abdominal oedema and yolk-sac retention [127], [146]. Liver morphological changes in liver injury include smaller, darker livers, indicating necrosis [146]. Phenotypic changes in zebrafish larvae exposed to non-steroidal anti-inflammatory drugs (NSAIDs) correlated with the toxicity seen in rat hepatocytes and mitochondria [147]. Building on the commonly used endpoints, transgenic lines have enabled more quantitative, high-throughput analysis of liver toxicity. Zhang and colleagues developed a transgenic zebrafish line which expresses a red fluorescent protein specific to the liver, tagged to liver fatty acid binding protein (LFABP) [148]. When exposed to the hepatotoxic drugs, paracetamol, aspirin, isoniazid and phenylbutazone, dose-dependent changes in liver red fluorescence and liver size were demonstrated [148]. A reduction in liver volume and changes in liver shape, as determined using selective plane illumination microscopy (SPIM) technology, in transgenic larvae with green fluorescent protein (GFP) tagged LFABP, after triptolide exposure has also been demonstrated [145].

Assessment of liver injury can also be undertaken in zebrafish larvae using histology. Zebrafish larvae can be arrayed in an agar mould to enable high-throughput histology [149]. Exposure of zebrafish larvae to hepatotoxins can induce histological changes that accompany different liver pathologies, such as steatosis, apoptosis and necrosis [150]. Examples of histological changes seen include hepatocyte vacuolation, disarray and oncotic necrosis upon exposure to triptolide [145], hepatic necrosis and areas of focal haemorrhage upon exposure to paracetamol [125], formation of hepatic macrovesicular triglyceride droplets, glycogen depletion and the presence of club-shaped mitochondria upon exposure to hexachlorocyclohexane [115], apoptosis and accumulation of fatty droplets in hepatocytes upon exposure to thioacetamide [151], and steatosis upon exposure to ethanol [152]. The range of histological changes identified after exposure to hepatotoxins highlights the potential for zebrafish larvae to model a whole variety of different types of DILI.

## 1.8 Diagnostic tests for miRNAs:

### 1.8.1 Current technologies:

As highlighted in previous sections miR-122 is a biomarker of DILI with greater diagnostic and prognostic potential than ALT in paracetamol overdose induced liver injury. The current

gold standard method for quantifying circulating miRNAs is using qRT-PCR. However, there are limitations to qRT-PCR as a diagnostic test, including the time taken for analysis and the need for specialist equipment and lab technicians. These factors mean that currently miRNA quantification happens within a laboratory setting, therefore limiting the utility of miRNAs as diagnostic biomarkers in a range of point of care settings. Point of care diagnostic tests need to occur as close to the bedside of the patient as possible and include settings such as patient homes, ambulances, acute care settings, clinical trials, rural settings and the developing world [153]. Furthermore, point of care diagnostic tests should provide a rapid diagnosis which is able to contribute to the optimisation of patient care. In the case of miR-122, a point of care diagnostic test could be used to monitor for hepatotoxic side effects of drugs across a wide range of settings, providing early warning of the development of hepatotoxicity in patient homes, acute care settings and in drug development within clinical trials. This early warning system could be used to prevent the development of acute liver injury, enable the alteration of drug regimens and provide information on novel drugs under development.

Recent advances into new technologies for miRNA detection take a range of different approaches. These approaches include isothermal amplification, lateral flow assays, nanobead-based systems and electrochemical signalling-based systems [153]. The methods involved in these techniques, along with their advantages and limitations are outlined in Table 1-6. These technologies have largely focussed on miRNA biomarkers of disease other than miR-122. However, one new technique has demonstrated high sensitivity and specificity for detecting miR-122 [154]. This recently published work describes an extraction- and amplification-free method for quantifying miR-122 using single molecule dynamic chemical labelling (DCL) assay [154]. The assay is based on a miR-122 hybridisation to an abasic peptide nucleic acid (PNA) probe, containing a reactive amine instead of nucleotide at a specific position in the sequence, attached to superparamagnetic beads. Binding of a target molecule, with an exact match in sequence to the PNA probe, results in a biotinylated reactive nucleobase covalently binding to the PNA probe [155]. These biotinylated probes are then labelled with streptavidin- $\beta$ -galactosidase, resuspended in a fluorogenic enzyme substrate, and fluorescence imaged to quantify which beads are associated with single enzymes.

	Method	Advantages	Limitations
qRT-PCR (Current gold standard)	RNA extraction is followed by reverse transcription to generate cDNA. The resulting cDNA is quantified using qPCR. In qRT-PCR specific primers bind to the miRNA sequence and polymerases amplify the sequence. In SYBR green PCR the fluorescent SYBR green binds to double stranded DNA products. The timepoint at which the fluorescence passes a threshold enables quantification.	High sensitivity High specificity Absolute quantification Can be automated Small reagent quantities required	Time consuming Medium throughput Requirement for laboratory facilities Multiple steps, increasing the risk of error Requires extraction of RNA prior to quantification Variation in miRNA extraction from samples Lack of single standardised method for quantification and normalisation
Isothermal amplification-based assays	Relies on the amplification of target miRNA at an isothermal temperature. For example, reverse-transcription loop-mediated isothermal amplification (RT-LAMP), whereby several sets of primers and a polymerase carry out amplification at a constant temperature. The resulting amplified product can be detected visually or through intercalating fluorescent dyes.	Simple conditions Rapid Could be used at point of care No precise temperature cycling required	Potential need for miRNA extraction step Limited specificity (poor sequence discrimination) RT-LAMP is limited by primer design and target sequence Multiple primer sets are costly and complex to design
Lateral flow-based assays	The sample containing the target miRNA is added at one end of the strip and flows along the strip. Probes present on the strip capture the target miRNA. The captured miRNA can then be visualised with a label, either pre-labelled miRNA, biotin labelled miRNA or through the addition of a label.	Simple conditions Rapid Could be used at point of care Low cost	Potential need for miRNA extraction step Potential need for amplification prior to addition of sample to paper
Nano-bead based systems	The target miRNA hybridises with a capture probe coupled to a nanobead. These nanobeads can then be extracted and the miRNA hybridised to their surface quantified by labelling.	Rapid Could be used at point of care No amplification needed No extraction needed	Requires a reader to measure output
Electrochemical based systems	The target miRNA hybridises with a capture probe coupled to the surface of an electrode. This hybridisation leads to a measurable change in current or charge, enabling quantification of the bound miRNA.	Rapid Can be used at point of care Low cost	Potential need for miRNA extraction step Requires a reader to measure output

**Table 1-6: MiRNA quantification techniques.**

*Summary of recent new advances in detection techniques for miRNAs. Table highlights the methods involved for each technique, along with their advantages and limitations.*



### 1.8.2 Synthetic gene networks:

Synthetic biology is a new and expanding area which uses the fact that cells are complex systems, takes components of cells (DNA, RNA and proteins), and generates synthetic networks which have a particular function. One of these particular functions is an ability to sense and report the presence of specific molecules. Much of the work so far on synthetic networks relies on these networks functioning inside cells. However, this has limitations, including biosafety concerns and the practicality of using cells. Pardee and colleagues have developed a novel method for embedding cell-free synthetic gene networks onto paper and other materials [156]. Cell-free systems can be freeze-dried onto paper and other porous substrates to create materials with the fundamental transcription and translation properties of a cell but which are sterile and abiotic [156]. These materials are stable at room temperature and can be readily stored and distributed, with rehydration of the paper or other material activating the cell-free system. The paper-based diagnostic developed as part of this PhD project relies on synthetic biology.

### 1.8.3 Riboregulators and toehold switches:

One of the most easily adaptable cell components is RNA, which has the potential to be rationally designed to carry out different functions and enable the production of specific outputs. There are a range of RNA regulatory elements in nature, including riboregulators, which control translation and transcription in response to cognate RNAs. Riboregulators are typically composed of two RNAs, a switch RNA which contains the reporter gene for the output of the system, and a trigger RNA which modulates the output of the system. The switch consists of a repressed reporter gene with a hairpin loop upstream containing a sequestered ribosome binding site (RBS). Conventional riboregulators are found in nature and have been used in synthetic biology, however, an adapted version of a riboregulator, a toehold switch, has been recently developed (Figure 1-5) [156], [157]. Although the basic principle is the same, toehold switches are more adaptable for the detection of a wide range of target sequences. Conventional riboregulators work by repressing translation through the sequestration of the RBS within a hairpin. Upon binding of the trigger RNA, the hairpin unwinds to reveal the RBS, resulting in translation of the previously repressed reporter gene. Base-pairing is used to sequester the RBS, therefore, trigger RNAs must contain an RBS sequence to displace the repressing sequence, thus reducing the sequence potential of

trigger RNA sequences. Toehold switch systems are an adapted version of traditional riboregulators, with alterations in the structure of the switch enabling the use of virtually any sequence for trigger RNA. In toehold switches the RBS is moved to the loop of the hairpin and repression of translation is controlled by the sequestration of the region around the start codon. Toehold switches also contain a single-stranded domain, the toehold region, at the 5' end which provides the initial binding site between the trigger and switch RNAs, and initiates RNA-RNA strand displacement interactions. Once binding is initiated in the single-stranded region further binding of the trigger RNA causes unwinding of the hairpin, exposing the RBS and start codon and leading to translation of the previously repressed gene. Conventional riboregulators rely on loop-linear interactions between the switch and trigger RNA whereas toehold switches utilise linear-linear interactions. These linear-linear interactions are more amenable to rational engineering and exhibit more favourable reaction kinetics and thermodynamics, factors which can be exploited to increase switch dynamic range [156], [157].

Riboregulators and toehold switches can be designed to have virtually any gene as an output, however, for diagnostic tests a fluorescent, luminescent or colorimetric output is typically used. Fluorescent outputs include GFP, mCherry, venus and cerulean. Colorimetric outputs usually rely on the production of an enzyme which catalyses the conversion of a substrate into a different coloured product. Examples of enzymes which produce a colorimetric output include uidA, a  $\beta$ -glucuronidase and lacZ, a  $\beta$ -galactosidase. Detection of these outputs can be determined using a plate reader or a specifically designed hand-held reader, or can be read by eye.

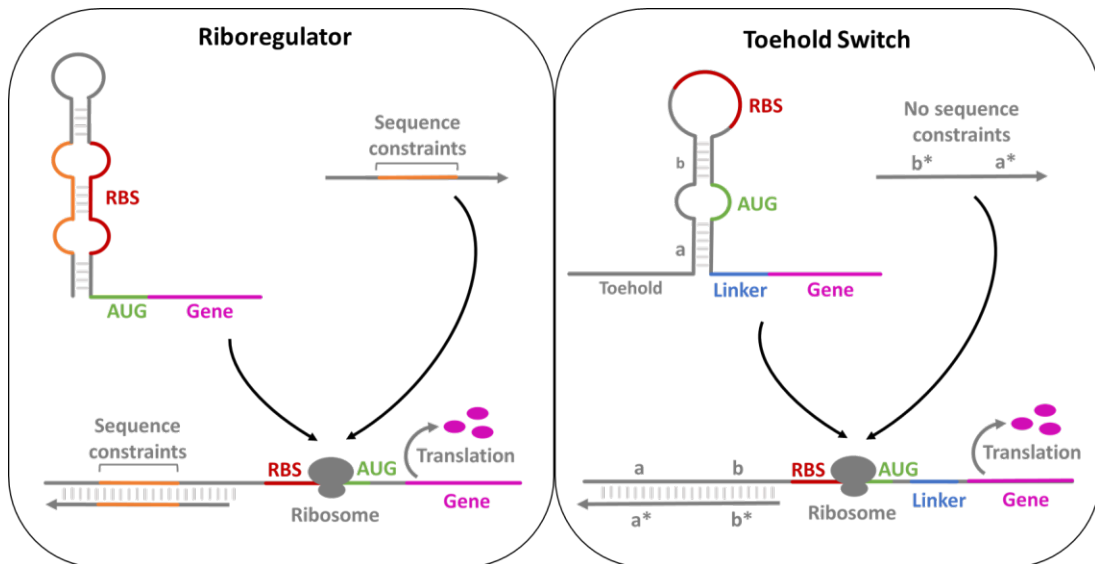


**Figure 1-5: Riboregulators and toehold switches.**

Left: Conventional Riboregulator; Right: Toehold Switch. A conventional riboregulator consists of a hairpin loop containing the sequestered RBS (red). The RBS is sequestered through base-pairing to the repressing sequence (orange). Downstream of the hairpin loop is the start codon, AUG (green) and the repressed gene (pink). The trigger for the conventional riboregulator contains a sequence complementary to the RBS (orange), thus constricting the sequence of the trigger. Upon binding of the trigger RNA to the switch RNA, the hairpin loop in the conventional riboregulator is unwound via loop-linear interactions resulting in the RBS becoming accessible. The ribosome binds to the RBS and initiates translation of a previously repressed gene, leading to an output. The toehold switch consists of a linear toehold domain and hairpin loop containing a sequestered RBS (red) and AUG start codon (green). Downstream of the hairpin loop is a linker sequence (blue) followed by a repressed gene (pink). The trigger RNA for contains no sequence constraints but is complementary to the toehold domain and hairpin loop regions a & b. Upon binding of the trigger RNA to the switch the hairpin loop unwinds allowing the ribosome to bind and resulting in translation of the previously repressed gene. Figure adapted from [157].

#### 1.8.4 Advantages of toehold switches:

Synthetic biology and toehold switches are relatively recent technology, with papers on toehold switches starting to be published in 2014. Toehold switches have been developed for a range of clinical applications, including the detection of outbreak viruses Ebola and Zika [158], norovirus [159], species-specific bacterial 16S ribosomal RNA [160], host biomarker mRNAs [160] and endogenous and exogenous miRNAs [161]. Pardee and colleagues were the first to show that toehold switches can be used as a diagnostic test, using a cell-free paper-based system with toehold switches designed to be complementary to regions of the Zika and Ebola viral genome [158]. The rationally designed switches were able to detect 30 nM of viral target [158]. Furthermore, the switches were shown to be highly specific, not reacting to dengue virus genome [158]. A diagnostic test for norovirus was able to demonstrate higher sensitivity, detecting 270 aM of norovirus RNA [159]. More recent work by Takahashi and colleagues, has demonstrated further that these switches can be highly specific by developing toehold switches to target the V3 hypervariable region of the 16S ribosomal RNA [160]. This enabled the detection and differentiation of 10 different bacterial species from clinical stool samples, with no/low reaction of the designed switches to other bacterial species RNA [160]. Furthermore, the toehold switch system was capable of identifying and quantifying levels of RNA present in complex RNA samples, including RNA extracted from clinical stool samples and in the presence of yeast RNA [160]. Finally, miRNAs, both endogenous and exogenously expressed, have been detected in mammalian cells by novel toehold switches [161].

As well as having high sensitivity and specificity, toehold switches have a range of other advantages. Firstly, by freeze-drying cell free systems and toehold switches onto paper and using a colorimetric output, the diagnostic test could be used at point of care. Limited training and equipment would be required to undertake the diagnostic test, with the colorimetric output easily read by eye or with a hand-held reader. Furthermore, the freeze-dried paper-based switches have a high stability, with evidence suggesting they are stable over 1 year [158]. In addition, the freeze-dried paper-based switches are low cost, with an estimated cost of \$0.1-1 per test for Zika virus [158]. The freeze-dried paper-based switches are easily transportable and do not require refrigeration.

As diagnostics for certain diseases and situations toehold switches have advantages over conventional methods of diagnosis. In the case of diagnostics for Zika virus, standard serological approaches are limited due to cross-reactivity in patients who have previously been infected with other flaviviruses [158]. Therefore, accurate diagnosis relies on nucleic acid-based detection methods, such as qRT-PCR and isothermal nucleic acid amplification. These techniques are relatively expensive, require technological expertise to run and interpret, use equipment which is incompatible with use in remote and low-resource locations where surveillance and containment are critically needed. [158]. In addition, in the context of emerging pathogens, the freeze-dried paper-based switches can be rapidly developed and deployed for the diagnosis. The development of a novel toehold switch for the Zika virus was undertaken in approximately 5 days, with 4 days of design and synthesis, 7 hrs of screening and 1 day of manufacturing [158]. Furthermore, it is easy to adapt sensors as the virus mutates over time [158].

#### 1.8.5 Challenges and limitations of toehold switches:

The main limitation with the use of toehold switches as a diagnostic test is their low sensitivity, with many of the diagnostic test systems using toehold switches so far developed utilising a pre-amplification step before adding the RNA trigger to the toehold switch system. For example, the diagnostic test for Zika virus was able to detect 30 fM of viral RNA, however the clinically relevant levels of Zika viral target are 1.2 fM in serum and 300 fM in saliva [158]. Therefore, a nucleic acid sequence-based amplification (NASBA) step was included, resulting in the detection of 3 fM of trigger RNA after amplification [158]. The NASBA step is also used in the diagnostic tests developed for the detection of Zika virus [158], norovirus [159] and bacterial ribosomal RNA [160].

The concentration of RNA before addition to the toehold switch system was another technique which has been utilised. Ma and colleagues used synbodies to capture and enrich concentrations of norovirus before further amplification of the viral RNA by NASBA and detection by the toehold switch system [159]. The virus particles within faecal samples or dilute samples were captured by synbodies (biotin-labelled synthetic peptide affinity ligands) and concentrated using streptavidin-coated magnetic beads [159]. The norovirus RNA was released by heating and then amplified using NASBA and then detected using the

toehold switch system [159]. Despite these limitations, toehold switches appear to have promise as novel diagnostic tests for a range of different targets.

### 1.9 Hypotheses and aims:

This introduction highlights the global problem of ATDILI and introduces the novel biomarkers which have been discovered, and which have the potential to help improve the management of TB treatment. In addition, it describes the model organism, zebrafish larvae, and their use in understanding liver toxicity and defining new miRNA biomarkers. Finally, this introduction covers toehold switches, a novel diagnostic test which has potential as point of care diagnostic for miRNAs.

#### 1.9.1 Hypotheses:

The hypotheses investigated in this study are:

- MiR-122 and K18 can be used as biomarkers of ATDILI
- Zebrafish larvae can be used to develop models of ATDILI and identify changes in miRNA expression in ATDILI
- The novel toehold switch system can be used to detect miR-122

#### 1.9.2 Research aims:

Given the above hypotheses, the aims of this thesis are:

- Determine the circulating concentrations of miR-122 and K18 activity in patients receiving anti-TB treatment. Investigate if miR-122 and K18 rise upon starting treatment, in patients with elevated levels of ALT and in cases of ATDILI.
- Develop a model of ATDILI and investigate miRNA expression changes in ATDILI.
- Develop a novel toehold switch based diagnostic test for the liver injury biomarker miR-122.

## 2 Biomarkers of anti-tuberculosis drug-induced liver injury

## 2.1 Introduction:

### 2.1.1 Background:

A panel of highly sensitive circulating biomarkers for acute liver injury have been identified and demonstrated to identify liver injury on first presentation to hospital before standard liver function tests are elevated in patients with paracetamol overdose [74], [75]. Furthermore, some of this panel of biomarkers can identify which patients will develop clinically important liver failure once liver injury has started [74]. There is a need for novel biomarkers as current biomarkers of liver injury lack sensitivity and specificity. The novel biomarkers focussed on in this study are miR-122 and K18, having either enhanced liver specificity (miR-122) or providing mechanistic insights into cell death (K18). A key question is: do these biomarkers retain their efficacy in the presence of infection?

Tuberculosis is a serious global disease, with an estimated 10 million new cases of active TB in 2018 and latent TB affecting one quarter of the world's population [13]. HIV infection increases the risk of patients developing TB, leading to a situation where patients are experiencing two difficult to treat diseases. In addition to TB, caused by *M. tuberculosis*, there are other species of mycobacterium, the non-tuberculous mycobacterium, which can cause pulmonary disease like TB but more commonly found in the elderly and infirm. Treatment for all these mycobacterial infections rely on antimicrobials. However, these antimicrobials are associated with side-effects, frequently DILI.

Currently, the diagnosis of ATDILI relies on the gold standard marker ALT, with guidelines suggesting treatment is halted if ALT rises more than three times the ULN in the presence of symptoms or five times the ULN in the absence of symptoms [52]. In local clinical practice the ULN for ALT is 50 IU/L. Frequently, patients present with symptoms of liver injury and elevated ALT, and so have already developed liver injury resulting in the need to halt medication for the liver to recover. However, breaks in treatment increase the potential for drug-resistance to develop and can mean that patients may not complete treatment. Therefore, there is a need for novel biomarkers, able to more accurately diagnose ATDILI. Furthermore, novel biomarkers may also be able to predict the early onset of liver injury, resulting in treatment being adapted before the further development of liver injury.



These experiments defined the circulating concentration of miR-122 and K18 in healthy volunteers and patients with active TB, latent TB, NTM infection and HIV-TB coinfection. For this work the ALISTER clinical study was set up at the Royal Infirmary Edinburgh (RIE) and 143 patients undergoing treatment for active TB, latent TB and NTM infection were recruited. 64 HIV-TB coinfecting patients were recruited into the SAEFRIF clinical trial in Uganda. Healthy volunteer samples used in this work were from the MicroRNA signatures of disease activity in the ANCA-associated vasculitis study in Edinburgh. The biomarkers miR-122 and K18 were quantified by qRT-PCR and ELISA respectively. Circulating concentrations of miR-122, K18 and ALT were compared between patient groups. Further analysis determined if there was any change in these biomarkers upon starting treatment and investigated whether the biomarkers correlated with ALT. The cases of ATDILI in the ALISTER study and SAEFRIF trial are described.

#### 2.1.2 Aims:

The hypothesis of this chapter is that circulating miR-122 and K18 can be used as biomarkers of ATDILI. The research aims of this chapter are:

1. Determine the circulating concentration of the biomarkers miR-122 and K18 in healthy volunteers and in patients with active TB, latent TB, NTM infection and HIV-TB coinfection
2. Determine if commencing treatment alters the circulating concentrations of miR-122 and K18
3. Determine if the biomarkers miR-122 and K18 rise from baseline levels in patients with elevated ALT compared to those with no rise in ALT
4. Determine if the biomarkers miR-122 and K18 rise from baseline levels in patients with ATDILI

## 2.2 Methods:

### 2.2.1 ALISTER clinical study:

#### 2.2.1.1 Research governance and ethics:

The “Assessing Antibiotic-Induced Liver Injury for the Stratification of Tuberculosis Patients” (ALISTER) clinical study was approved by the local Research Ethics Committee (West of Scotland (WoSREC5)) and ran for 3 years from March 2017 to March 2020 (REC number – 17/WS/0017). The protocol for the study can be found in Appendix 2.ii.

#### 2.2.1.2 Patient population:

The ALISTER clinical study was set up at the Royal Infirmary Edinburgh (RIE) to prospectively recruit patients who were receiving anti-TB drugs. The TB clinic at the RIE typically sees 60-90 new cases of active TB, 150-200 new cases of latent TB and 20 new cases of environmental TB every year. The primary patient cohort for the ALISTER clinical study was patients at RIE outpatient clinics, with additional patients recruited from in-patient wards.

The inclusion criteria for the study was adults (aged 16-85 years) who were receiving anti-TB drugs for the treatment of active TB, latent TB or NTM infection, and who had the capacity to consent. The exclusion criteria were HIV positive patients and those who were unable or unwilling to give informed consent.

#### 2.2.1.3 Calculation of sample size:

The primary aim of the study was to determine if the biomarkers miR-122 and K18 can accurately identify patients with ATDILI in active TB, latent TB and NTM infection. Therefore, the study had a nested case control design. Patients with ATDILI (cases) would be age, sex and treatment matched with patients who did not developed ATDILI (controls). The difference in biomarkers from baseline (pre or at starting TB medication) to time of established DILI would be compared with controls. The sample size required was calculated using fold-change from baseline data from Antoine and colleagues [112]. In this study, at baseline K18 was at 170 U/L and this rose to 34,000 U/L in DILI [112]. This 200-fold increase had a standard deviation of 150 across subjects. Therefore, with a 2 sided-significance level, 0.8 power, 20 patients (10 cases and 10 controls) are required for each group, (active TB, latent TB and NTM infection). For the primary aim of this clinical study a total of 60 patients

(10 case and 10 control for separate active TB, latent TB and NTM infection groups) would be needed.

#### 2.2.1.4 Identification and recruitment of participants:

Eligible patients were identified from clinic lists each week or by the clinical staff at out-patient clinics and in-patient wards at the RIE. A broad recruitment approach was taken to recruit all eligible patients with a high likelihood of starting TB treatment or already on treatment. This included some eligible patients who did not have a definitive diagnosis of TB at time of recruitment due to the long-time taken to culture *Mycobacterium* and definitively diagnose active TB. In addition, some patients who did not have a definite diagnosis of active TB were included, if they had commenced on anti-TB drugs. Furthermore, not all patients with a latent TB diagnosis underwent treatment. For those patients who were recruited and did not receive anti-TB treatment basic data was retained, along with any collected blood samples, but further patient progress was not monitored, and no further blood samples were collected. Although most patients were recruited from out-patient clinics at the RIE, additional patients were recruited from in-patient wards and during appointments with the TB nurses outside the times of dedicated out-patient clinics.

#### 2.2.1.5 Consenting process:

Patients were approached for consent by myself, after I completed Good Clinical Practice (GCP) training. Patients were given information, including the Patient Information Sheet and Patient Consent Form, (Appendices 2.iii & 2.iv). They were allowed time to assimilate the information and to ask any questions. Although 24 hrs is the recommended time for patients to consider whether to take part in a clinical study, in this setting of a short hospital appointment/admission this was too long to be possible. If the patient did not wish to consent, then no further action was taken. If the patient was willing to consent, then written informed consent was taken using the consent form. Three copies of the completed consent form were made, one of which was placed in the patient records, one given to the patient and the other was stored in the site file. Following recruitment into the study the patient's GP was informed through a letter (Appendix 2.v).

#### 2.2.1.6 Study protocol:

The aim was to collect samples from patients at every clinic visit. However, research blood samples could only be collected when blood samples were requested by the clinician. The number of visits a patient makes to the TB outpatient clinic depended on which treatment regime they are on, as well as whether they experienced any issues with their treatment. However, all patients, after starting treatment, would return 2 weeks later to check for any side-effects from treatment. For active TB patients on a typical 6-month treatment programme, clinic visits would occur at 2 weeks, 2 months, 4 months and 6 months. For latent TB patients, after the check-up at two weeks, they had a single clinic visit at the end of their treatment. And finally, for patients with NTM infection, clinic visits usually occurred every 3 months.

#### 2.2.1.7 Sample and data collection:

After patients had consented to take part in the study, research blood samples were collected at that clinic visit and every following visit to the TB clinic. Research specific samples collected were one serum gel (S-Monovette Z-Gel, Sarstedt, Nümbrecht, Germany) and one plasma (S-Monovette K3EDTA, Sarstedt, Nümbrecht, Germany). Patient progress was monitored remotely through the review of electronic medical records on TRAK. Patients with abnormal blood results were sometimes further monitored at their GPs. In these cases, additional blood samples taken at the GPs were requested. The patient's GP was asked to take one extra 9 ml serum sample when routine blood sampling was taking place. This was communicated by letter (GP letter) and by telephoning the patient's GP. The extra blood sample was then sent for 'virology storage' at the RIE. The laboratory at RIE processed and stored these samples until they could be collected.

Demographic and clinical data was also recorded from the patient's medical files on TRAK. The following demographics were recorded: CHI number, date of birth, sex, and ethnicity. Clinical data were recorded for; type of infection, mycobacterial species causing the infection, resistance of mycobacterium, drug treatment (start and end date, drugs, any changes to treatment regime), other diseases/health factors and concomitant drugs. ALT measurements were recorded from TRAK for each clinical blood sample collected.

#### 2.2.1.8 Sample and data anonymisation:

Samples were stored in a linked anonymised form, with each patient assigned a 4-digit code. The link between the code and patient, along with other patient identifiable data was stored on a secure NHS server. All identifiable data were removed when the data was entered into a database for analysis and transferred out of NHS server space to the University of Edinburgh. Paper copies of the anonymised patient data and consent forms were kept in a locked drawer in a locked office.

#### 2.2.1.9 Sample handling:

After collection, blood samples were processed within 4 hrs. Blood tubes were centrifuged at 2,300 x *g* for 5 min. The resulting supernatant was then isolated and stored as three approximately 500 µl aliquots. Samples were then labelled with the date and patient ID and stored at -80 °C. Plasma samples were used for the quantification of miR-122 and K18.

#### 2.2.1.10 Patient groupings for analysis:

Patients within the ALISTER study were classified into one of three groups, active TB, latent TB and NTM infection. Patients were classified as having active TB either if they had culture confirmation of *M. tuberculosis* and presence of active disease, or if a clinician decided there was sufficient evidence of active disease to start them on treatment. Latent TB patients had a positive interferon-gamma release assay (IGRA) and no evidence of active disease as demonstrated by a clear chest X-ray and no symptoms such as coughing, weight loss and night sweats. Patients with NTM infection had grown at least two cultures with non-tuberculous mycobacterium, had clinical signs of pulmonary disease and an exclusion of other relevant diagnoses [25], [26].

#### 2.2.2 SAEFRIF clinical trial:

The SAEFRIF trial is running at the Infectious Disease Institute (IDI) at Makerere University in Uganda. I went out to Uganda in February 2020 to set up the K18 assay in the lab at the IDI and to perform the analysis of the samples already collected in the study.

## 2.2.2.1 Research governance and ethics:

The SAEFRIF “Safety and Efficacy of High Dose Rifampicin in Tuberculosis (TB)-HIV Co-infected Patients on Efavirenz- or Dolutegravir-based Antiretroviral Therapy” clinical trial (NCT03982277) is running at the Infectious Disease Institute (IDI) at Makerere University, Uganda. This trial was approved by a local research and ethics committee, the National Drug Authority and the Uganda National Council for Science and Technology. The study was performed in accordance with the general principles in the International Ethical Guidelines for Biomedical Research Involving Human Subjects and the Declaration of Helsinki. The SAEFRIF trial began recruitment April 2019 and at the time samples were analysed in February 2020 there were 64 patients recruited.

## 2.2.2.2 Study design:

Suboptimal levels of rifampicin are common in TB patients, reducing the effectiveness of treatment [162], [163]. Increasing the dose of rifampicin to 20-35 mg/kg has been demonstrated to be safe and lead to accelerated clearance of mycobacteria from sputum [164], [165]. However, there is limited data on the safety of high dose rifampicin in patients coinfecting with HIV, who are more at risk of drug-drug interactions and drug-related toxicity. Therefore, the SAEFRIF trial aims to recruit 120 TB-HIV coinfecting patients initiating TB treatment. There are four arms to the trial, defining the initiation phase of TB treatment (Table 2-1). Following completion of the initiation phase all patients received the standard dose of isoniazid and rifampicin.

Arm		Therapy
1	A	High dose rifampicin (35 mg/kg) Standard doses of isoniazid, pyrazinamide & ethambutol Dolutegravir (DTG)-based ART therapy
	B	Standard dose rifampicin (10 mg/kg) Standard doses of isoniazid, pyrazinamide & ethambutol Dolutegravir (DTG)-based ART therapy
2	A	High dose rifampicin (35 mg/kg) Standard doses of isoniazid, pyrazinamide & ethambutol Efavirenz (EFV)-based ART therapy
	B	Standard dose rifampicin (10 mg/kg) Standard doses of isoniazid, pyrazinamide & ethambutol Efavirenz (EFV)-based ART therapy

**Table 2-1: SAEFRIF clinical trial arms.**

Previous work has indicated that higher doses of rifampicin are safe in African populations, however, these studies largely excluded HIV infected patients with low CD4+ cell counts who were on ART [164], [165]. Risk factors for hepatotoxicity include advanced immunosuppression, co-administration of multiple potentially hepatotoxic drugs and comorbidities that may involve the liver [166]. Whether there is a relationship between rifampicin concentrations and hepatotoxicity in heavily immunosuppressed individuals is unknown. Therefore, one of the outcomes of the SAEFRIF trial was to determine whether individuals receiving higher doses of rifampicin were at higher risk of experiencing hepatotoxicity.

#### 2.2.2.3 Patient population:

Patients were recruited from the IDI TB clinic at Makerere University, Uganda, where over 300 HIV-TB coinfecting patients are initiated on TB treatment each year. Inclusion criteria were patients aged 18 years and older who had confirmed HIV-1 infection, were already on efavirenz (EFV) or dolutegravir (DTG)-based ART or planning to start ART and were diagnosed with TB and due to initiate rifampicin-containing therapy. Further inclusion criteria included providing informed consent and complying with scheduled trial visits, treatment, laboratory tests and other study procedures. Exclusion criteria were patients who have rifampicin resistant TB, pregnant women or those planning on getting pregnant during treatment, women of reproductive age on DTG who decline the use of effective contraceptive, patients with liver disease, ALT > x5 ULN or glomerular filtration rate < 50 ml/min.

#### 2.2.2.4 Study protocol:

The protocol for this study is published [167]. Patients who went to the IDI TB clinic were screened, and if eligible and willing, were recruited into the study on the same visit. TB was diagnosed using chest X-ray, sputum fluorescent microscopy or Xpert MTB/RIF and clinical history which included any one of the following symptoms: cough, fever, weight loss and drenching night sweats. Only individuals with confirmed TB were included in the study. Patients were randomised to one of the four arms of the trial. Patients who were not on ART at baseline were started on EFV or DTG-based ART following 2 weeks of TB treatment. EFV and DTG were given in combination with tenofovir, zidovudine, or abacavir plus either lamivudine or emtricitabine. DTG was given at double the standard dose due to the induction

of UDP-glucuronosyltransferase 1A (UGT1A1) and CYP3A4 by rifampicin, which results in reduced blood concentrations of DTG. Patients underwent study visits every two weeks for the initiation phase of treatment. At each visit adherence to treatment was confirmed with pill counts, patients were asked about adverse reactions and vital signs and clinical samples were collected. For the purposes of the work in this thesis, baseline blood samples (serum) were collected before commencing treatment and further blood samples were collected at weeks 2, 4, 6, and 8 of treatment.

#### 2.2.2.5 Sample handling:

After collection blood tubes were centrifuged and the resulting supernatant was then isolated and stored as aliquots. Samples were then labelled and stored at -80 °C. Serum samples were used for the quantification of K18.

#### 2.2.3 Healthy volunteers:

Healthy blood samples were used from the “MicroRNA signatures of disease activity in ANCA-associated vasculitis” study. After collection blood samples were immediately centrifuged at 4°C for 15 min at 1,100 x *g*. The resulting supernatant was isolated and stored as aliquots at -80°C.

#### 2.2.4 Quantification of miR-122:

##### 2.2.4.1 RNA isolation:

Plasma samples were stored at -80 °C before analysis. Freeze thawing was avoided in order to preserve sample integrity. MiRNA was extracted using the miRNeasy Serum/Plasma kit (Qiagen, Venlo, Netherlands) following the manufacturer’s instructions. Total RNA was extracted from 50 µl of plasma diluted in 150 µl nuclease free water. 1 ml of QIAzol lysis reagent was added and the reaction mixture vortexed briefly and then incubated at room temperature for 5 min. To monitor extraction efficiency 3.5 µl ( $5.6 \times 10^8$  copies) of synthetic *C. elegans* miR-39 spike-in control (Qiagen, Venlo, Netherlands) were added which was made up following the manufacturer’s instructions. Following the addition of the spike-in control 200 µl of chloroform was added and the reaction mixture shaken for 15 sec and then incubated at room temperature for 2-3 min. The reaction mixture was then centrifuged at 12,000 x *g* for 15 min at 4 °C. 600 µl of the aqueous phase was then transferred to a new



tube with 900  $\mu$ l absolute ethanol. This solution was mixed thoroughly and then 750  $\mu$ l was added to the RNeasy MinElute spin column and centrifuged at  $\geq 8000 \times g$  for 15 s. This process was repeated with the remaining 750  $\mu$ l. The spin column was then washed with the following buffers: 700  $\mu$ l RWT and 500  $\mu$ l RPE, with centrifugation at  $\geq 8000 \times g$  for 15 s between. A final wash was undertaken with 500  $\mu$ l 80% ethanol, followed by centrifugation at  $\geq 8000 \times g$  for 2 min. The spin column was then placed in a new 2 ml collection tube and centrifuged at  $\geq 8000 \times g$  for 5 min to dry the membrane. For the elution step, the spin column was placed in a new 1.5 ml collection tube, 15  $\mu$ l of RNase free water was added to the membrane and then centrifuged at 8,000  $\times g$  for 1 min. The resulting RNA was stored at  $-80 \text{ }^\circ\text{C}$ .

#### 2.2.4.2 Reverse transcription:

The miScript II Reverse Transcription kit (Qiagen, Venlo, Netherlands) was used to prepare cDNA according to the manufacturer's instructions. 2.5  $\mu$ l of RNA was added to a master mix of 2  $\mu$ l 5x HiSpec buffer, 1  $\mu$ l 10x nucleics mix, 1  $\mu$ l reverse transcriptase and 3.5  $\mu$ l RNase-free water. The reaction mixture was then incubated at  $37 \text{ }^\circ\text{C}$  for 60 min,  $95 \text{ }^\circ\text{C}$  for 5 min, followed by a hold of  $4 \text{ }^\circ\text{C}$ . The resulting cDNA was then diluted with 90  $\mu$ l of RNase-free water and stored at  $-20 \text{ }^\circ\text{C}$ .

#### 2.2.4.3 Quantitative real time analysis:

Real-time quantification of miRNAs was performed using the miScript SYBR Green PCR kit (Qiagen, Venlo, Netherlands) and the miR-122 and miR-39 specific miScript assays (Qiagen, Venlo, Netherlands). 2  $\mu$ l cDNA was added to a master mix of 5  $\mu$ l SYBR Green PCR mix, 1  $\mu$ l miScript Universal primer, 1  $\mu$ l miScript primer assay and 1  $\mu$ l RNase-free water. For each patient sample miR-122 and miR-39 were measured in duplicate. qRT-PCR was performed on a Light Cycler 480 (Roche, Burgess Hill, UK) using the recommended miScript cycling parameters (Table 2-2).

Step	Time	Temperature ( $^\circ\text{C}$ )	Cycles
PCR initial activation step	15 min	95	X1
Denaturation	15 sec	94	X40
Annealing	30 sec	55	X40
Extension	30 sec	70	X40

**Table 2-2: miScript SYBR Green PCR reaction cycling conditions.**

Three controls were used for each qRT-PCR plate. Firstly, a plate control (a previously run cDNA sample) with known Cq value. Secondly, a no enzyme control, omitting the reverse transcriptase enzyme during reverse transcription. Thirdly, a no template control (RNase-free water) omitting the cDNA. The no enzyme and no template controls should have Cq values of >35. Cq values less than 35 were regarded as positive amplification signals.

Following the PCR reaction cycling dissociation curve analysis was performed by increasing the temperature slowly from 65 °C to 95 °C. At low temperatures PCR products are double-stranded, so SYBR Green dye is bound to them and fluorescence is high. As the temperature increases, PCR products are denatured, resulting in a rapid decrease in fluorescence. Dissociation curves plot the derivatives of the curves generated, with peaks at the melting temperature of the double-stranded product. A single peak at the melting temperature of the double-stranded product is indicative of the production of a single specific product. The presence of multiple peaks indicates the formation of primer-dimers, whilst multiple different peaks or plateaus suggest the production of non-specific products. Dissociation curves were generated for each plate and assessed for the specificity of the product and to determine the absence of primer-dimers, see Figure 2-1 for an example.

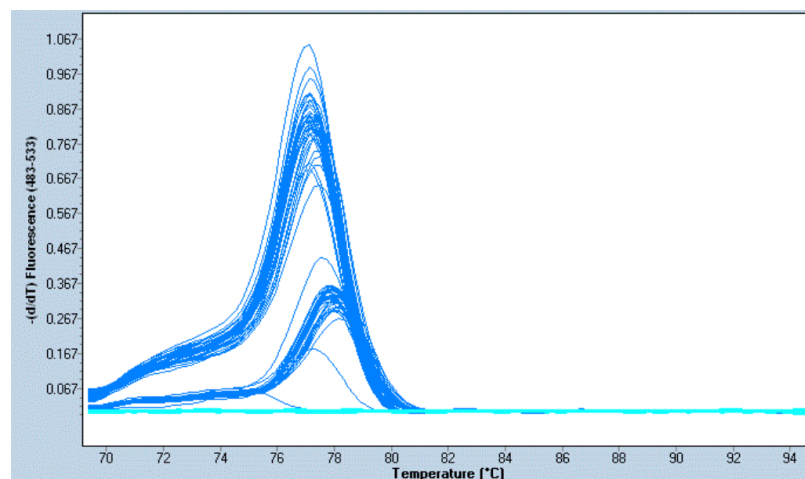


**Figure 2-1: Example dissociation curve for miR-122 and miR-39.**

*Example dissociation of a plate with ALISTER RNA samples and the primers miR-122 and miR-39. Specificity of the primers is demonstrated by a single peak for each miRNA primer.*

#### 2.2.4.4 Standard curve for miR-122:

Serial dilutions of known standard were made using miR-122 mimic (syn hsa-miR-122-5p) (Qiagen, Venlo, Netherlands). The dilutions were prepared in triplicate, using the same RT and qRT-PCR protocol described above. The Cq values were plotted against the logarithm of the concentration, demonstrating a clear linear relationship between Cq value and Log (conc.). The resultant regression line was used to ascertain the concentration of miR-122 present in the plasma samples.

#### 2.2.4.5 MiR-122 data analysis:

Samples were run in duplicate for both miR-122 and miR-39. The duplicate Cq values were averaged and the difference, standard deviation and coefficient of variance of the duplicate values were calculated. Samples with an absolute difference of greater than 0.5 for miR-122 or miR-39 Cq were repeated. MiR-39 Cq values were assessed for each extraction run to determine if there was variation in extraction efficiency. Absolute quantification of miR-122 concentration was undertaken using the standard curve for miR-122 described in the section above. Log (conc.) was calculated using the formula,  $\log (fM) = (Cq-30.87)/-3.387$ .

Repeatability was determined by assessing the intra-assay variability in miR-122 Cq duplicates (CV median [IQR]: 0.25 [0.11-0.49] %). The intra-assay variation in miR-39 Cq values was assessed (CV median [IQR]: 3.04 [2.50-3.64] %). Reproducibility was determined by measuring the inter-assay variation across plates and days of reference samples (plate controls). All ALISTER samples were stored for a maximum of one year (median [IQR]: 16.3 [7.6-33.3] weeks). This is less time in storage than previously published studies which have demonstrated miRNA stability [168], [169].

#### 2.2.5 Quantification of K18:

##### 2.2.5.1 M65 ELISA:

Serum (SAEFRIF) and plasma (ALISTER and healthy volunteers) samples were stored at -80 °C before analysis. Total K18 was quantified using the Peviva M65 classic ELISA (Bioaxxes, Tewkesbury, UK). The M65 classic ELISA is a solid-phase sandwich enzymes immunoassay. The wells are coated with the capture antibody M6 directed against K18. Horseradish peroxidase (HRP) is conjugated to the M5 antibody which is directed against a different

epitope of K18. The addition of the substrate TMB (3,3',5,5'-Tetramethylbenzidine) results in a colour change by HRP. The addition of the stop solution (sulfuric acid) halts the reaction so that absorbance can be measured. Samples were measured in duplicate according to the manufacturer's instructions. Briefly, 25 µl of standards, controls or samples was pipetted into each well. 75 µl of diluted M65 HRP conjugate was added per well and the ELISA plate incubated for 2 hrs at room temperature and 600 rpm. The plate was then washed with 5 x 400 µl wash buffer using a plate washer (Edinburgh: Biotek, Swindon, UK; Uganda: Biotek, Swindon, UK). 200 µl TMB substrate was added and the plate incubated in darkness for 20 min. 50 µl of stop solution was then added per well and the plate shaken briefly. Finally, the absorbance was read on a plate reader (Edinburgh: Tecan, Switzerland; Uganda: Biotek, Swindon, UK) at 450 nm.

#### 2.2.5.2 K18 data analysis:

Samples were run in duplicate, then values were averaged, and coefficient of variation calculated. Samples with a coefficient of variation >15% were repeated. Results were calculated using the standards which came with the ELISA kit and fitting this data with a cubic spline fitting algorithm, (x-axis: U/L, y-axis: absorbance 450 nm). The low and high controls provided by the kit were used to check the functioning of the kit.

All ALISTER samples had a coefficient of variation of (median [IQR]: 3.5 [1.8-6.5] %) and were stored for a maximum of just over 2 years (113 weeks), (median [IQR]: 48.4 [28.7-77.8] weeks). All SAEFRIF samples analysed for K18 had a coefficient of variation of (median [IQR]: 2.3 [1.1-4.9] %) and were stored for a maximum of 1 year (median [IQR]: 19.1 [11.1-26.2] weeks).

#### 2.2.6 Quantification of ALT:

For ALISTER study samples and SAEFRIF trial samples ALT was measured in hospital facilities. ALT activity was then recorded from patient medical records or from trial datasets. For samples collected from healthy volunteers ALT activity was measured by Forbes Howie using a commercial serum ALT kit (Alpha Laboratories Ltd., Eastleigh, UK).

### 2.2.7 Assessment of causality:

The Roussel Uclaf Causality Assessment Method (RUCAM) was used to determine formal causality between anti-TB medication and liver injury. The pattern of liver injury was determined using the R ratio, considering ALT and ALP activity. Further factors considered include time to onset, course of injury, risk factors (age and alcohol), concomitant drugs, the exclusion of non-drug causes of injury and previous information on drug hepatotoxicity [63]. The outline used for RUCAM causality assessment can be found in Appendix 2.i.

### 2.2.8 Statistical analysis:

Data were summarised as median (IQR) or n (%) for summary statistics of the study participants. A one-way Kruskal-Wallis ANOVA was used to determine the presence of a significant difference between patient groups and between drug treatment groups. Wilcoxon matched-pairs signed-rank test was used to determine if the circulating biomarkers significantly changed after starting treatment compared to baseline in ALISTER and SAEFRIF samples. The Mann-Whitney t-test was used to determine if the circulating biomarkers differed significantly between ART treatment groups, and between naïve compared to established ART patients. Correlation between the circulating biomarkers, and between the circulating biomarkers and time on treatment was determined using Spearman rank correlation. ROC-AUC analysis was undertaken on samples grouped by normal ( $\leq 50$  IU/L) and elevated ALT ( $> 50$  IU/L). Statistical analyses were performed using GraphPad Prism (GraphPad Software, La Jolla, California). A P-value of  $< 0.05$  was considered significant.

## 2.3 Results:

### 2.3.1 Patient demographics:

#### 2.3.1.1 ALISTER study:

A total of 194 patients were recruited into the ALISTER clinical study. However, of these, 51 patients were not eligible for analysis for reasons including having no research samples collected, not receiving treatment and results indicating the patient did not have active TB. As a result, a total of 143 patients were included in the analysis, 30 with active TB, 88 with latent TB and 25 with NTM infection. The demographics for these 143 patients are shown in Table 2-3.

		Active (n=30)	TB (n=88)	NTM infection (n=25)
Age (yrs)		41 (33-56)	40 (23-63)	66 (57-74)
Gender	Male	20 (67%)	23 (26%)	10 (40%)
	Female	10 (33%)	65 (74%)	15 (60%)
Ethnicity	African	2 (7%)	7 (8%)	0 (0%)
	Arab	0 (0%)	1 (1%)	0 (0%)
	Bangladeshi	1 (3%)	2 (2%)	0 (0%)
	Indian	7 (23%)	3 (3%)	0 (0%)
	Iraqi	1 (3%)	0 (0%)	0 (0%)
	Pakistani	5 (17%)	3 (3%)	1 (4%)
	South East Asian	2 (7%)	1 (1%)	0 (0%)
	White	12 (40%)	66 (75%)	24 (96%)
	Unknown	0 (0%)	5 (6%)	0 (0%)
Location of infection	Pulmonary	11 (37%)	-	-
	Pulmonary and lymph node	3 (10%)	-	-
	Lymph node	8 (27%)	-	-
	Lymph node and ocular	1 (3%)	-	-
	Lymph node and joint	1 (3%)	-	-
	Abdominal/Gastrointestinal	4 (13%)	-	-
	Ocular	1 (3%)	-	-
	Spinal	1 (3%)	-	-
Culture confirmed	Yes	20 (67%)	-	-
	No	10 (33%)	-	-
Resistance	None	26 (87%)	-	-
	Isoniazid	1 (3%)	-	-
	Pyrazinamide	2 (7%)	-	-
	Rifampicin	0 (0%)	-	-
	Multi-drug	1 (3%)	-	-
NTM species	<i>M. avium</i> complex	-	-	22 (88%)
	<i>M. abscessus</i>	-	-	2 (8%)
	<i>M. malmoense</i>	-	-	1 (4%)
Baseline ALT (IU/L)		18 (14-35)	15 (12-21)	15 (12-22)
Treatment	Isoniazid, Rifampicin	-	43 (48%)	-
	Isoniazid	-	26 (30%)	-
	Rifampicin	-	18 (20%)	-
	Moxifloxacin	-	1 (1%)	-
	Rifampicin, Azithromycin	-	-	1 (4%)
	Rifampicin, Clarithromycin	-	-	3 (12%)
	Rifampicin, Clarithromycin, Amikacin	-	-	1 (4%)
	Rifampicin, Ethambutol	-	-	1 (4%)
	Rifampicin, Ethambutol, Amikacin	-	-	1 (4%)
	Rifampicin, Ethambutol, Clarithromycin	-	-	15 (60%)
	Rifampicin, Ethambutol, Moxifloxacin	-	-	1 (4%)
	Rifabutin, Clarithromycin, Moxifloxacin	-	-	1 (4%)
	Clarithromycin, Clofazimine, Azithromycin	-	-	1 (4%)
Initiation phase	Isoniazid, Rifampicin, Pyrazinamide, Ethambutol	22 (73%)	-	-
	Isoniazid, Rifampicin, Pyrazinamide, Moxifloxacin	1 (3%)	-	-
	Isoniazid, Rifampicin, Pyrazinamide, Ethambutol, Moxifloxacin	1 (3%)	-	-
	Isoniazid, Rifabutin, Pyrazinamide, Ethambutol	1 (3%)	-	-
	Isoniazid, Rifampicin, Ethambutol, Moxifloxacin	3 (10%)	-	-
	Rifampicin, Ethambutol, Moxifloxacin	1 (3%)	-	-
	Bedaquiline, Clofazimine, Cycloserine	1 (3%)	-	-
Continuation phase	Isoniazid, Rifampicin	20 (67%)	-	-
	Isoniazid, Rifampicin, Moxifloxacin	2 (7%)	-	-
	Isoniazid, Rifampicin, Ethambutol	2 (7%)	-	-
	Isoniazid, Rifabutin, Moxifloxacin	1 (3%)	-	-
	Isoniazid, Ethambutol, Moxifloxacin	1 (3%)	-	-
	Isoniazid, Rifampicin, Pyrazinamide, Ethambutol	1 (3%)	-	-
	Rifampicin, Ethambutol, Moxifloxacin	2 (7%)	-	-
	Bedaquiline, Clofazimine, Cycloserine	1 (3%)	-	-

**Table 2-3: Demographic data for ALISTER clinical study patients.**

Data shown as median (IQR) or number (%).

## 2.3.1.2 SAEFRIF trial:

There were 64 patients recruited into the SAEFRIF trial at the time sample analysis was undertaken in February 2020. All participants were Ugandan. Patient demographics are shown in Table 2-4. As the trial is still underway the treatment arms are still blinded for the dose of rifampicin.

		<b>HIV-TB coinfection (n=64)</b>
<b>Age (yrs)</b>		38 (32-44)
<b>Gender</b>	Male	40 (62%)
	Female	24 (38%)
<b>Location of infection</b>	Pulmonary	51 (80%)
	Extrapulmonary	9 (14%)
	Both	1 (1%)
	Unknown	3 (5%)
<b>Naïve to ART at start of treatment</b>	Yes	14 (22%)
	No	50 (78%)
<b>Therapy</b>	TB therapy plus DTG-based ART	36 (56%)
	TB therapy plus EFV-based ART	24 (38%)
	TB therapy (ART therapy unknown)	4 (6%)
<b>Baseline ALT (IU/L)</b>		20 (14-30)

**Table 2-4: Demographic data for SAEFRIF trial patients.**

*Data shown as median (IQR) or number (%).*

## 2.3.1.3 Healthy volunteers:

Healthy volunteers were recruited into the “MicroRNA signatures of disease activity in ANCA-associated vasculitis” study in Edinburgh. Demographics were not recorded for all participants. For the participants who had data recorded, participants were predominantly white, with a median age of 27 [IQR: 24-30] years.



## 2.3.2 Circulating biomarkers in different populations:

The novel biomarkers miR-122 and K18, along with the gold standard measure ALT, were quantified in healthy volunteers, the first samples taken from ALISTER study patients and the baseline samples taken prior to commencing treatment for SAEFRIF trial patients. For all healthy volunteers ALT fell within the normal range ( $\leq 50$  IU/L). For individuals with normal ALT ( $\leq 50$  IU/L), ALT, miR-122 and K18 measurements are detailed in Figure 2-2 and the mean and interquartile data for each group is summarised in Table 2-5. There was no significant difference in ALT ( $P=0.2$ ) and miR-122 ( $P=0.09$ ) between the groups. There was a statistically significant difference in K18 between groups ( $P=0.03$ ). Inter-patient variation within each group for each biomarker was calculated (Table 2-5). Inter-patient variation was higher for both miR-122 and K18 than ALT.

		Healthy volunteers (n=28)	Active TB (n=26)	Latent TB (n=87)	NTM infection (n=25)	HIV-TB coinfection (n=59)
<b>ALT (IU/L)</b>	Median [IQR]	18 [12-22]	22 [14-27]	16 [12-23]	16 [13-25]	18 [14-27]
	CV (%)	44.0	40.7	48.4	54.3	50.3
<b>MiR-122 (fM)</b>	Median [IQR]	2.88 [1.75-3.96]	4.14 [1.34-7.56]	2.92 [1.46-4.54]	1.57 [0.91-3.72]	-
	CV (%)	65.8	183.4	120.6	168.5	-
<b>K18 (U/L)</b>	Median [IQR]	210 [134-259]	145 [92-220]	152 [105-215]	163 [138-263]	172 [132-276]
	CV (%)	45.9	62.2	207.8	69.2	79.4

**Table 2-5: Circulating concentrations of ALT, miR-122 and K18 in the different patient groups.**

*The median, IQR and CV of circulating concentrations of ALT, miR-122 and K18 in the different patient groups. Data included from the first samples from ALISTER study patients and baseline samples prior to commencing treatment from patients in the SAEFRIF trial. Only participants with normal ALT ( $\leq 50$  IU/L) were included.*

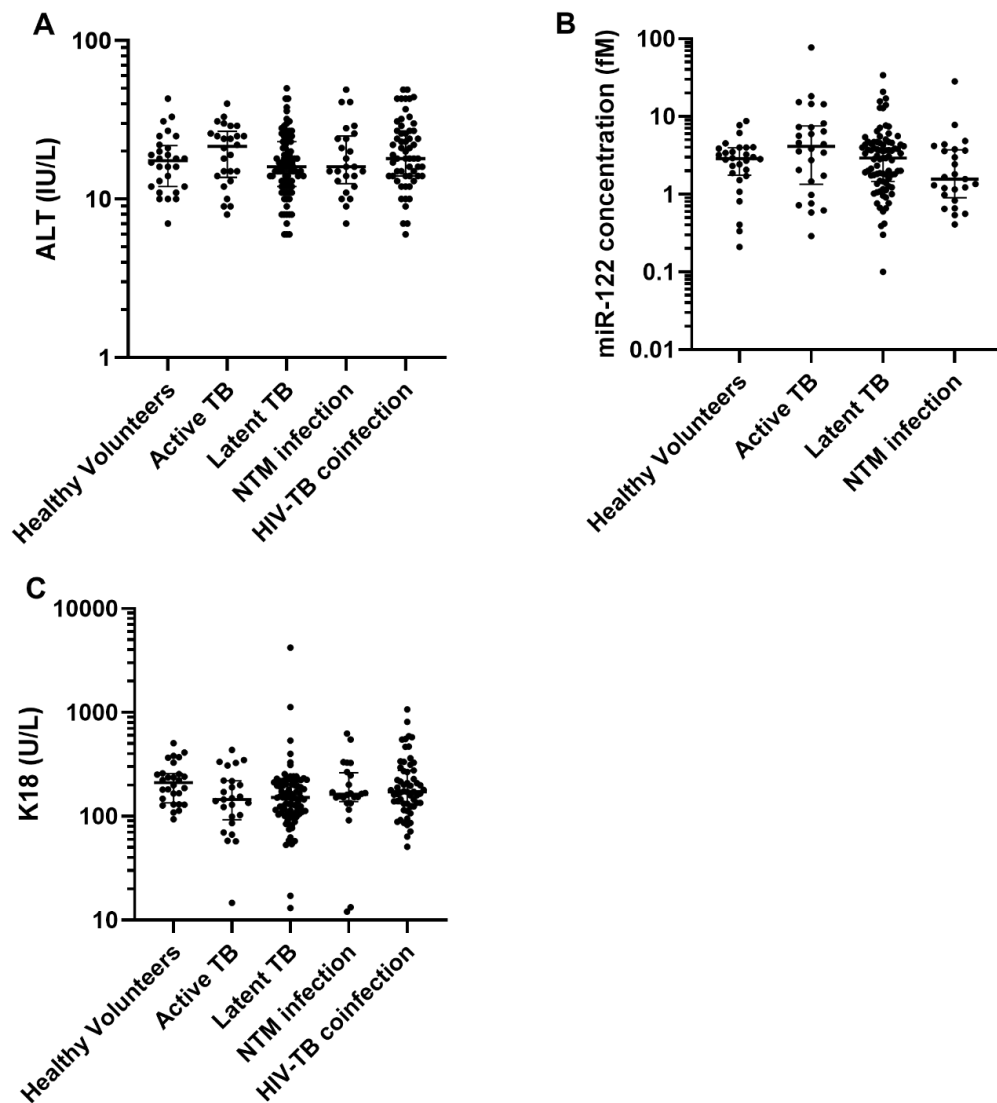


**Figure 2-2: Circulating concentrations of ALT, miR-22 and K18 in the different patient groups.**

Circulating concentrations of; (A) ALT (IU/L); (B) miR-122 (fM); (C) K18 (U/L) in healthy volunteers ( $n=28$ ), active TB patients ( $n=26$ ), latent TB patients ( $n=87$ ), NTM infection patients ( $n=25$ ), HIV-TB coinfecting patients ( $n=59$ ). Data included from the first samples from ALISTER study patients and baseline samples prior to commencing treatment from patients in the SAEFRIF trial. Only participants with normal ALT ( $\leq 50$  IU/L) were included. Data shown as dot plots. Line represents median and bars represent interquartile range. The significance of differences between groups were determined by one-way Kruskal-Wallis ANOVA, (ALT  $P=0.2$ ; miR-122  $P=0.09$ ; K18  $P=0.03$ ).

### 2.3.3 Circulating biomarkers in treatment:

#### 2.3.3.1 Commencing treatment:

To investigate if commencing treatment alters the circulating concentration of the biomarkers, miR-122 and K18 were measured in sequential samples from patients at baseline and on treatment in the ALISTER study. In addition, sequential samples were analysed from patients in the SAEFRIF trial.

A total of 65 patients in the ALISTER had samples collected at baseline and whilst on treatment (active TB n=9; latent TB n=46; NTM infection n=10), (Figure 2-3). The time patients had spent on treatment was (median [IQR]: active TB 3.0 [2.4-6.9]; latent TB 3.9 [2.4-12.2]; NTM infection 4.0 [2.2-6.9] weeks). Across all 65 patients there was a significant difference in ALT (median [IQR]: baseline 15 [12-24]; on treatment 17 [13-27] IU/L; P=0.03) and miR-122 (median [IQR]: baseline 3.12 [1.20-5.63]; on treatment 3.95 [1.75-7.98] fM; P=0.01) upon commencing treatment. There was no significant difference in K18 (median [IQR]: baseline 150 [103-224]; on treatment 167 [110-246] U/L; P=0.4).

Of these 65 patients, two patients had elevated ALT at baseline which resolved upon starting treatment, and there were five patients who experienced elevations in ALT upon starting treatment but did not reach the pre-defined criteria for a case of DILI. Of the patients with elevated ALT upon starting treatment, all experienced an increase in miR-122 concentration, with two experiencing a substantial increase to 51 fM and 68 fM respectively. Furthermore, four out of five of these patients had an increase in K18.

In the 58 patients who had normal ALT at baseline and on treatment (active TB n=5; latent TB n=44; NTM infection n=9), with a time on treatment of median [IQR]: 4.0 [2.5-8.9] weeks, there was a statistically significant, but small, increase in miR-122 concentration upon starting treatment (median [IQR]: 2.63 [1.13-5.16]; on treatment 3.55 [1.51-6.05] fM; P=0.03). There was no significant change in K18 (median [IQR]: baseline 148 [99-220]; on treatment 162 [107-233] U/L; P=0.6). In the absence of DILI, commencing treatment does not result in substantial elevations in miR-122 and K18.

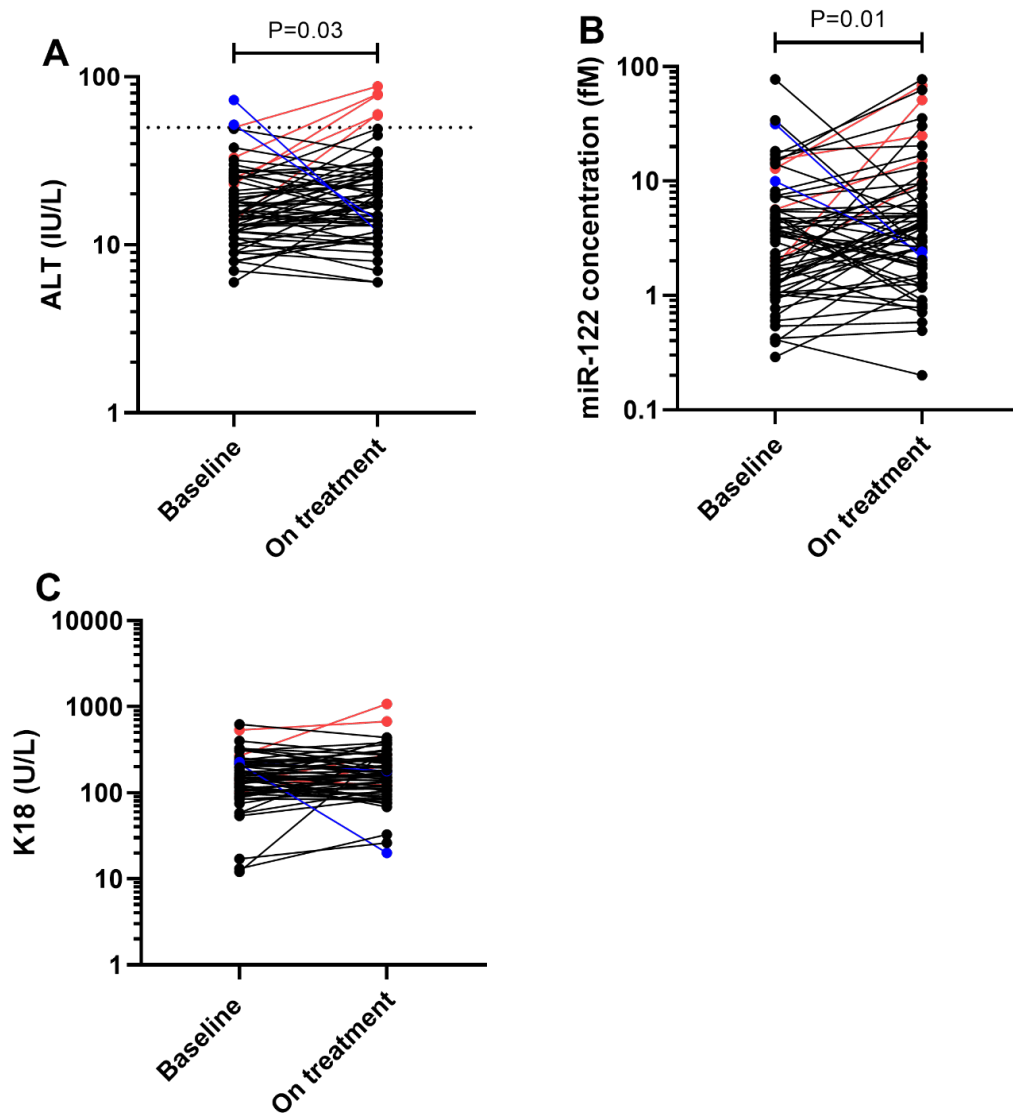


**Figure 2-3: Circulating concentration of biomarkers in paired samples from patients in ALISTER study at baseline and on treatment.**

Circulating concentrations of; (A) ALT (IU/L); (B) miR-122 (fM); (C) K18 (U/L). ALISTER paired patient samples ( $n=65$ : active TB ( $n=9$ ); latent TB ( $n=46$ ); NTM infection ( $n=10$ )). Data shown as dot plots. Black points are those with normal ALT ( $\leq 50$  IU/L) at baseline and on treatment. Blue points are patients whose ALT falls from  $>50$  IU/L on starting treatment. Red points are patients whose ALT rises  $>50$  IU/L upon starting treatment. Dotted line on (A) ALT = 50 IU/L. The significance of differences between baseline and on treatment concentrations of biomarkers was determined by Wilcoxon matched-pairs signed rank test, (ALT  $P=0.03$ ; miR-122  $P=0.01$ ; K18  $P=0.4$ ).

Patients in the SAEFRIF trial had samples collected at baseline and at weeks 2, 4, 6 and 8 after starting TB treatment (Figure 2-4). Out of the total of 64 patients, 10 experienced elevations in ALT >50 IU/L during their treatment without reaching the criteria for DILI.

There were 50 patients who had a sample collected at baseline and two weeks into treatment. In these 50 patients there was no significant difference in ALT (median [IQR]: baseline 22 [14-31]; week 2 24 [14-32] IU/L;  $P=0.62$ ) or K18 (median [IQR]: baseline 204 [130-344]; week 2 169 [117-262] U/L;  $P=0.3$ ) upon commencing treatment. Of these patients 4 experienced an elevation in ALT >50 IU/L and 4 patients ALT fell from >50 IU/L. Of the patients who experienced an elevation in ALT, three out of four had increased K18. Two out of four patients whose ALT fell upon commencing treatment experienced a fall in K18.

In the patients who had normal ALT at baseline and 2 weeks into treatment, there was no significant change in K18 (median [IQR]: baseline 184 [122-299]; week 2 158 [113-220] U/L;  $n=42$ ;  $P=0.09$ ). As demonstrated in the ALISTER patients, in the absence of DILI, commencing treatment does not elevate K18.

In the SAEFRIF trial, there were 50 patients whose ALT remained within the normal healthy range throughout treatment. Of these patients, there were 35 with 3 or more samples collected. The intra-patient coefficient of variation was calculated for these patients, (median [IQR]: ALT 23.7 [16.6-36.1] %; K18 35.4 [24.9-41.9] %;  $P=0.02$ ). The coefficient of variation of intra-patient ALT measurements was lower than that demonstrated by K18.

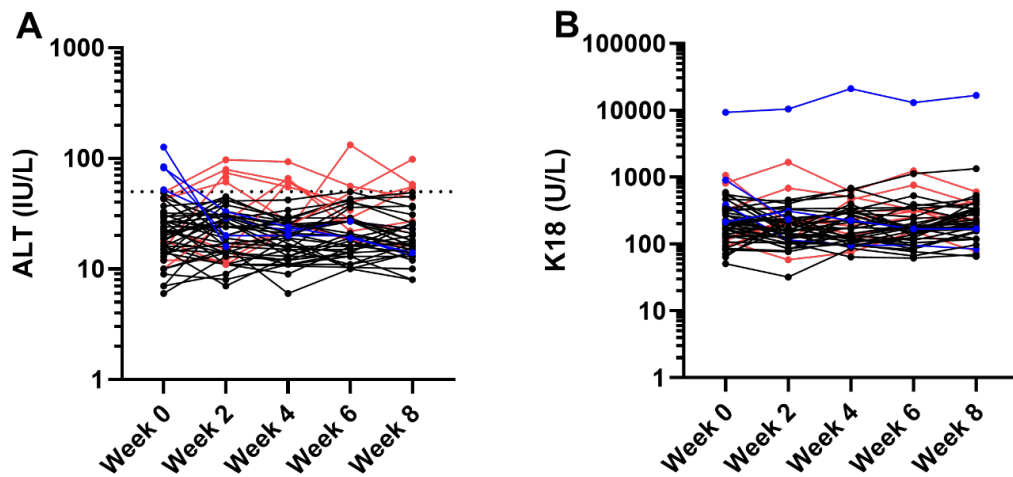


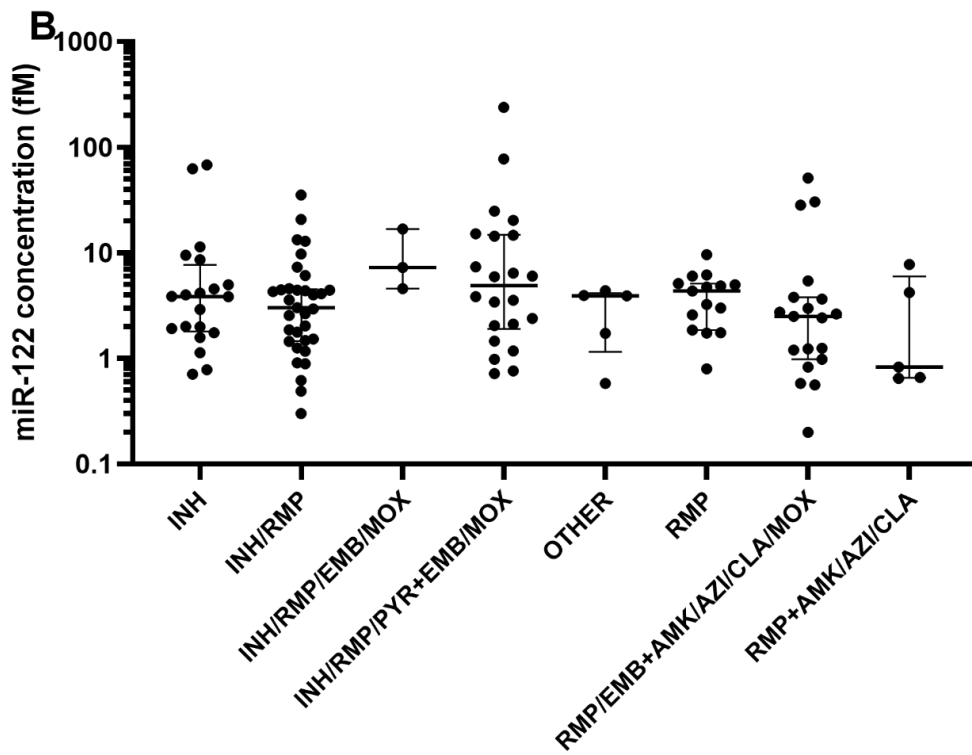
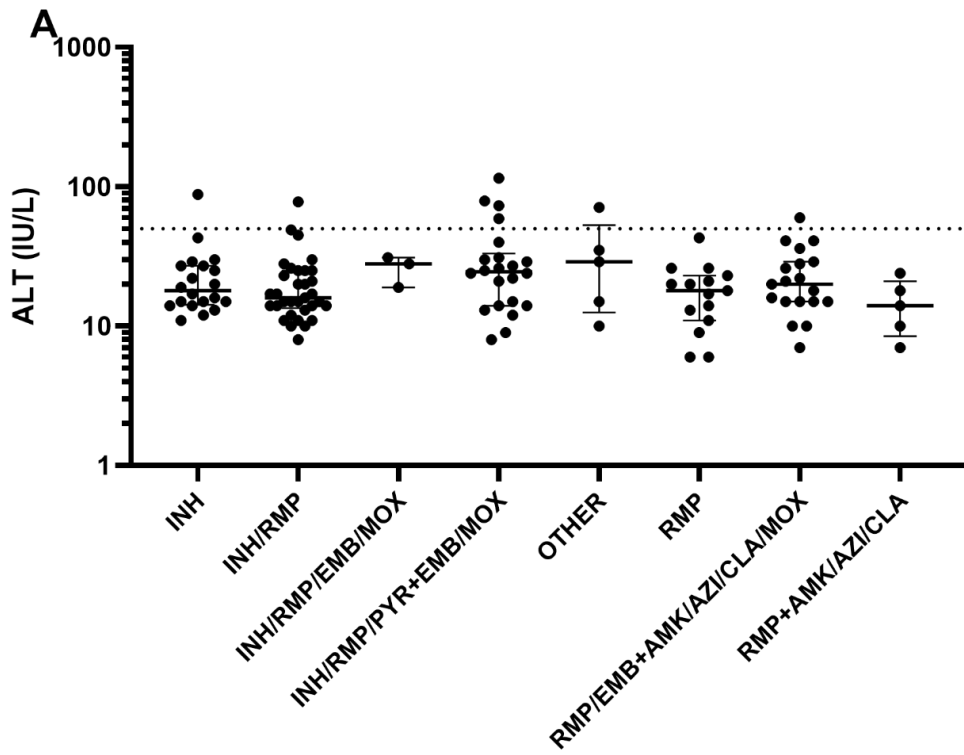
**Figure 2-4: Circulating concentration of biomarkers in SAEFRIF trial patients.**

Circulating concentrations of; (A) ALT (IU/L) and (B) K18 (U/L). SAEFRIF patient samples ( $n=64$ ). Data shown as dot plots. Black points are those with normal ALT ( $\leq 50$  IU/L) throughout treatment. Blue points are patients whose ALT falls from  $>50$  IU/L upon starting treatment. Red points are patients whose ALT rises  $>50$  IU/L during treatment. Dotted line on (A) ALT = 50 IU/L.

#### 2.3.3.2 Anti-tuberculosis drug treatments:

To determine if different drugs affected ALT and the circulating miR-122 and K18 concentration, patients in the ALISTER study were grouped according to their drug treatment. Samples were included if the patient was receiving anti-TB treatment when the sample was collected.

There was a total of 122 patients in the ALISTER study who had a sample collected whilst they were on treatment, (active TB  $n=30$ ; latent TB  $n=67$ ; NTM infection  $n=25$ ) (Figure 2-5). There were 20 different drug combinations taken by these patients, these treatments were combined into 8 categories. There was no significant difference in ALT ( $P=0.2$ ) and miR-122 ( $P=0.2$ ) between the different drug treatment groups. There was a slight statistically significant difference in K18 between the drug treatment groups ( $P=0.05$ ).



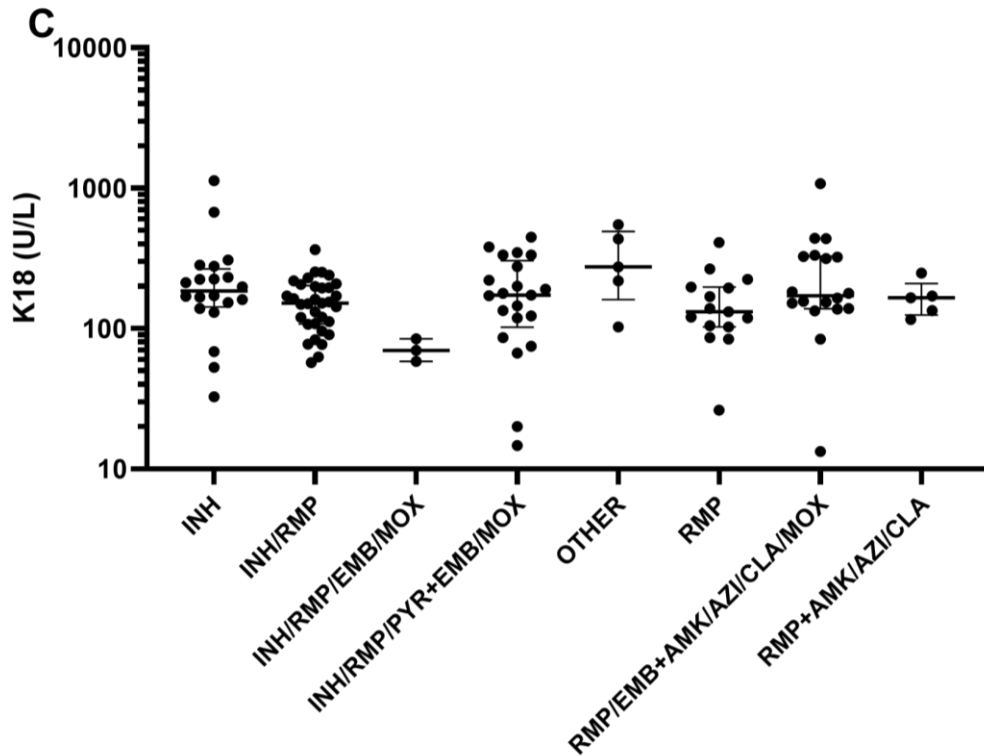


**Figure 2-5: Circulating concentrations of ALT, miR-122 and K18 in the different drug treatment groups.**

Circulating concentrations of; (A) ALT (IU/L); (B) miR-122 concentration (fM); (C) K18 (U/L). ALISTER patient samples ( $n=122$ : active TB  $n=30$ ; latent TB  $n=67$ ; NTM infection  $n=25$ ). Data shown as dot plot. Lines show median and interquartile range. INH (isoniazid); RMP (rifampicin); PYR (pyrazinamide); EMB (ethambutol); MOX (moxifloxacin); AMK (amikacin); AZI (azithromycin); CLA (clarithromycin). INH/RMP/PYR+EMB/MOX (isoniazid, rifampicin, pyrazinamide plus one or more of ethambutol and moxifloxacin); RMP/EMB+AMK/AZI/CLA/MOX (rifampicin and ethambutol plus one or more of amikacin, azithromycin, clarithromycin and moxifloxacin); RMP+AMK/AZI/CLA (rifampicin plus one or more of amikacin, azithromycin and clarithromycin); OTHER (includes 1 patient on each of; moxifloxacin alone, isoniazid/rifabutin/moxifloxacin, clarithromycin/clofazimine/amikacin, rifabutin/clarithromycin/moxifloxacin, bedaquiline/clofazimine/cycloserine). Statistical significance of the difference between the groups was determined with one-way Kruskal-Wallis ANOVA, (ALT  $P=0.2$ ; miR-122  $P=0.2$ ; K18  $P=0.05$ ).



## 2.3.3.3 HIV treatment:

Patients in the SAEFRIF trial received standard TB treatment, (isoniazid, rifampicin, pyrazinamide and ethambutol) along with either dolutegravir or efavirenz-based ART. Although patients also received high and standard doses of rifampicin, as the trial is ongoing, this information is not available. There were 28 patients receiving DTG-based ART and 22 patients receiving EFV-based ART (Figure 2-6). Samples were included from week 2 onwards. Between the drug treatment groups there was no significant difference in ALT, (median [IQR]: DTG-based 20 [15-27]; EFV-based 25 [14-42] IU/L;  $P=0.1$ ) or K18, (median [IQR]: DTG-based 185 [128-320]; EFV-based 180 [120-303] U/L;  $P=0.5$ ).

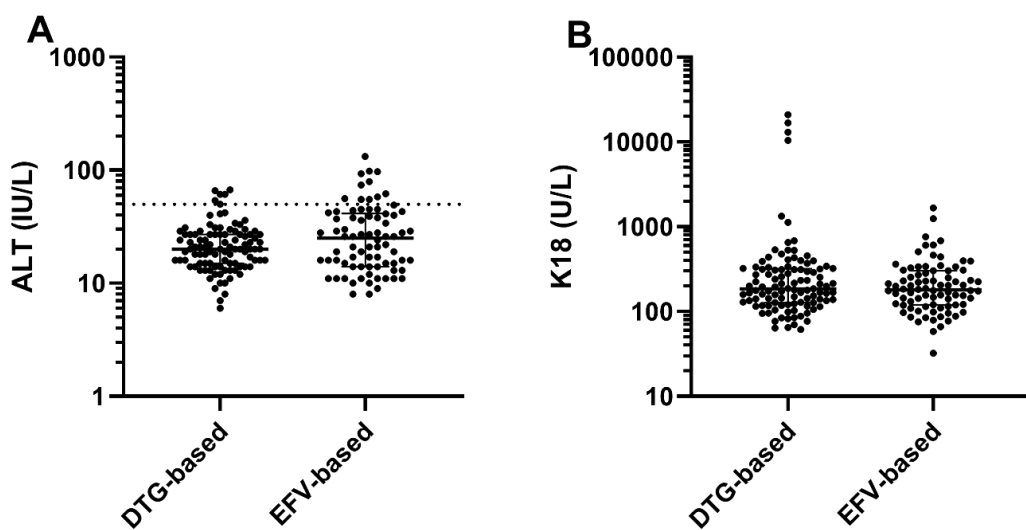


**Figure 2-6: Circulating concentration of ALT and K18 in SAEFRIF patients grouped by ART treatment.**

Circulating concentration of; (A) ALT (IU/L) and (B) K18 (U/L). Samples from SAEFRIF patients taken from week 2 onwards whilst on ART treatment, repeated measurements in some patients during the course of treatment. Patients were treated with the standard TB treatment of isoniazid, rifampicin, pyrazinamide and ethambutol along with either dolutegravir (DTG) ( $n=28$ ) or efavirenz (EFV)-based ( $n=22$ ) ART. Data shown as dot plots. Line represents median and bars represent interquartile range. Dotted line on (A) ALT = 50 IU/L. Statistical significance of the difference between groups was determined with Mann-Whitney  $t$ -test, (ALT  $P=0.1$ ; K18  $P=0.5$ ).

In the SAEFRIF trial most patients had already started on ART therapy prior to developing TB, however, there were some patients who commenced on ART 2 weeks into the trial (naïve to ART n=14; established on ART n=50) (Figure 2-7). There was no significant difference in ALT, (median [IQR]: naïve 21 [14-32]; established 21 [14-31] IU/L; P=0.9) or K18, (median [IQR]: naïve 193 [138-337]; established 179 [130-305] U/L; P=0.8) in patients naïve to ART and those already established on ART.

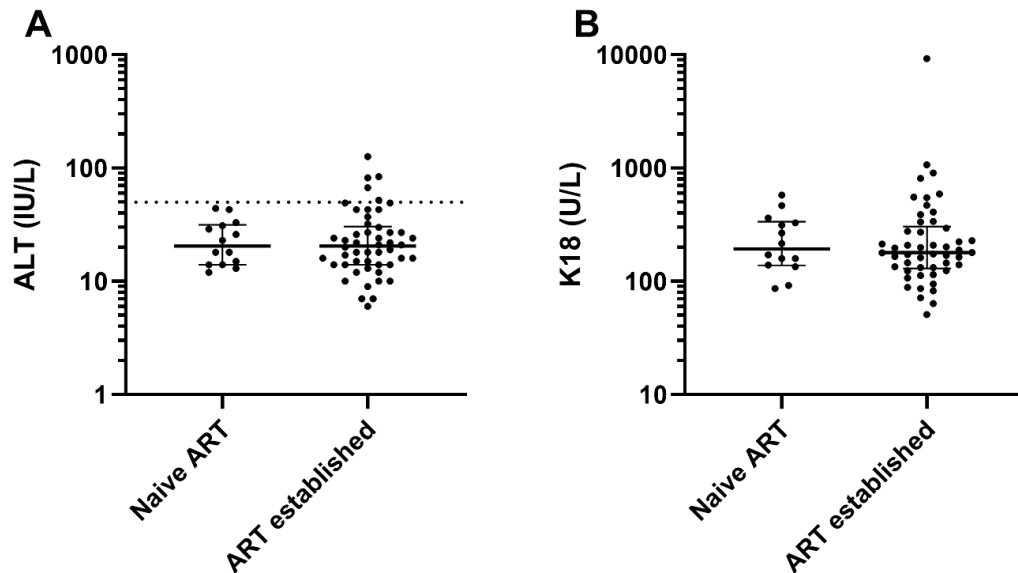


**Figure 2-7: Circulating concentration of ALT and K18 in SAEFRIF patients grouped by ART status at baseline.**

Circulating concentration of; (A) ALT (IU/L) and (B) K18 (U/L). Samples from SAEFRIF patients naïve to ART (n=14) and patients already established on ART (n=50). Data shown as dot plots. Line represents median and bars represent interquartile range. Dotted line on (A) ALT = 50 IU/L. Statistical significance between the groups determined using Mann-Whitney t-test, (ALT P=0.9; K18 P=0.8).

## 2.3.3.4 Time spent on treatment:

To investigate if the time a patient spent on treatment affected ALT, miR-122 and K18 the biomarkers were correlated against time spent on treatment, (Figure 2-8 & Table 2-6). Overall there was no significant correlation between miR-122 and time spent on treatment (P=0.9) or K18 and time on treatment (P=0.1). There was a significant slight positive correlation between ALT and time on treatment (P=0.02). In the latent TB patient group, ALT showed a significant positive correlation with time spent on treatment (P=0.005). In active TB patients miR-122 demonstrated a significant negative correlation with time on treatment (P=0.02).

		<b>ALT (IU/L)</b>	<b>miR-122 (fM)</b>	<b>K18 (U/L)</b>
<b>Active TB (n=44)</b>	P-value	0.6	0.02	0.8
	Spearman r [95% CI]	-0.08 [-0.4-0.2]	-0.4 [-0.6- -0.05]	0.03 [-0.3-0.3]
<b>Latent TB (n=142)</b>	P-value	0.005	0.2	0.1
	Spearman r [95% CI]	0.2 [0.07-0.4]	0.1 [-0.06-0.3]	0.1 [-0.04-0.3]
<b>NTM infection (n=39)</b>	P-value	0.8	1.0	0.3
	Spearman r [95% CI]	0.04 [-0.3-0.4]	-0.003 [-0.3-0.3]	-0.2 [-0.5-0.2]
<b>HIV-TB coinfection (n=241)</b>	P-value	0.9	-	0.4
	Spearman r [95% CI]	0.005 [-0.1-0.1]	-	0.06 [-0.07-0.2]
<b>Overall</b>	P-value	0.02 (n=459)	0.9 (n=219)	0.1 (n=466)
	Spearman r [95% CI]	0.1 [0.01-0.2]	0.009 [-0.1-0.1]	0.073 [-0.02-0.2]

**Table 2-6: Correlation of the biomarkers with time on treatment.**

*Circulating concentration of ALT, miR-122 and K18 correlated with time on treatment (weeks). Statistical significance of the correlation determined with Spearman's rank correlation coefficient. Data shows n, P-values, Spearman's rank correlation coefficient and 95% confidence intervals.*

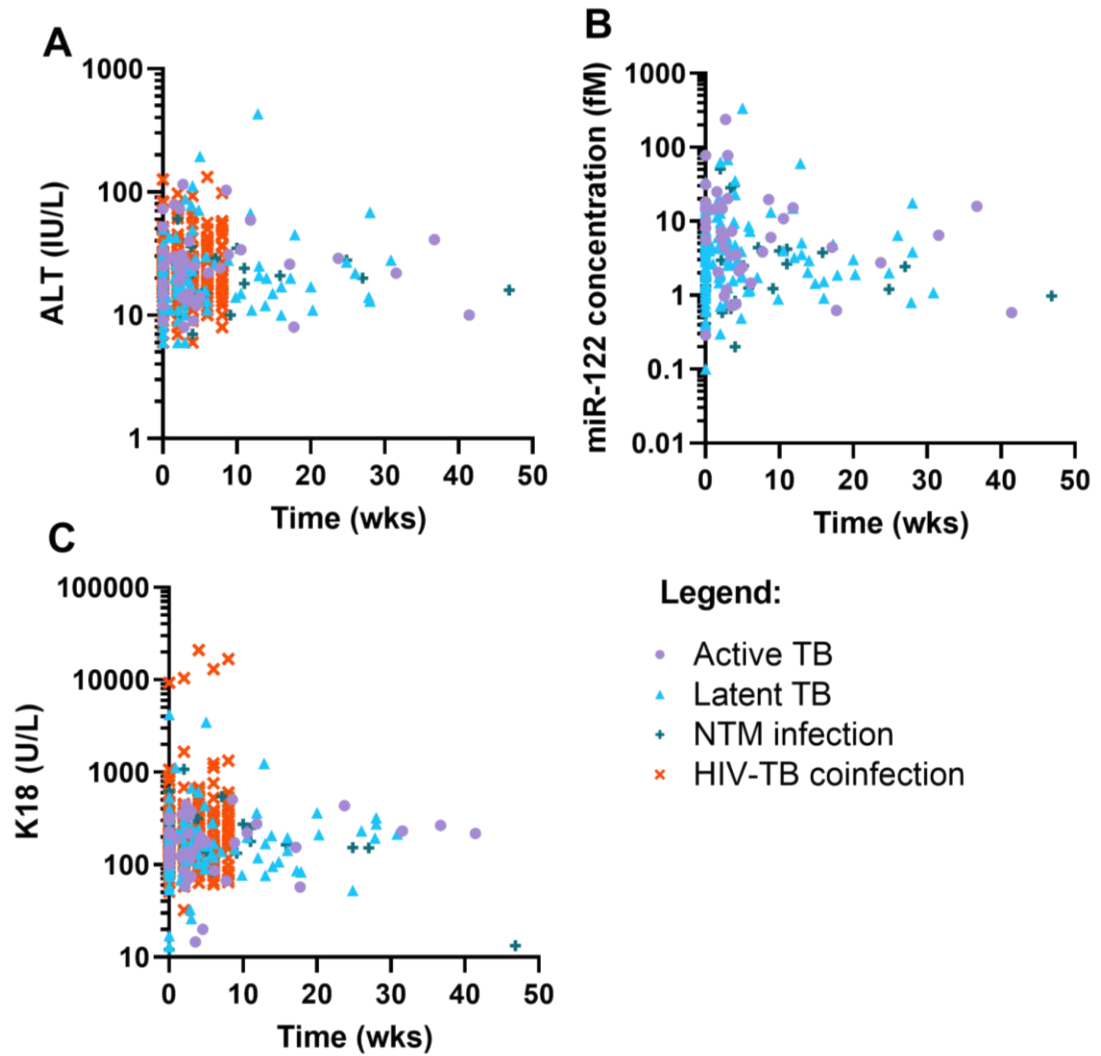


**Figure 2-8: Circulating biomarkers correlated with time on treatment.**

Circulating concentrations of; (A) ALT (IU/L); (B) miR-122 concentration (fM); (C) K18 (U/L). Time on treatment (weeks). Patients samples included: active TB n=44; latent TB n=142; NTM infection n=39; HIV-TB coinfection n=241. Repeated measurements in some patients during the course of treatment are included. Statistical analysis of the significance of the correlation calculated using Spearman's rank correlation coefficient, data shown in Table 2-6.

#### 2.3.4 Circulating biomarkers correlate with ALT:

To investigate the diagnostic capability of the novel biomarkers, miR-122 and K18 were correlated against the gold standard ALT and against each other. Healthy volunteers and ALISTER study samples were included in all comparisons, SAEFRIF samples were included only in the ALT-K18 comparison, (Table 2-7 & Figure 2-9). A significant correlation was seen between miR-122 and ALT ( $P < 0.0001$ ), and K18 and ALT ( $P < 0.0001$ ). This significant correlation was seen across all patient groups except for the healthy volunteers. Furthermore, miR-122 significantly correlated with K18 ( $P < 0.0001$ ).

All patient samples were grouped by normal ALT ( $\leq 50$  IU/L) and elevated ALT ( $> 50$  IU/L) (Figure 2-10). MiR-122 was increased 8.0-fold in samples with elevated ALT ( $> 50$  IU/L) compared with normal ALT ( $\leq 50$  IU/L) (median [IQR]: normal ALT 3.00 [1.31-4.82]; elevated ALT 23.9 [11.5-60.4] fM;  $P < 0.0001$ ) (Figure 2-10A). K18 was increased 2.3-fold in those samples with elevated ALT ( $> 50$  IU/L) compared to samples with normal ALT ( $\leq 50$  IU/L) (median [IQR]: normal ALT 170 [120-250]; elevated ALT 395 [217-683] U/L;  $P < 0.0001$ ) (Figure 2-10B). ROC analysis was performed on these grouped samples. MiR-122 identified elevated ALT ( $> 50$  IU/L) with high accuracy, (ROC-AUC 0.93; 95% CI 0.88-0.98) (Figure 2-10C). K18 identified elevated ALT ( $> 50$  IU/L) with a slightly lower accuracy (ROC-AUC 0.80; 95% CI: 0.72-0.87) (Figure 2-10D).

		ALT (IU/L) vs miR-122 (fM)	ALT (IU/L) vs K18 (U/L)	miR-122 (fM) vs K18 (U/L)
<b>Healthy volunteers (n=28)</b>	P-value	0.6	0.6	0.7
	Spearman r [95% CI]	0.09 [-0.3-0.5]	0.1 [-0.3-0.5]	0.07 [-0.3-0.4]
<b>Active TB (n=44)</b>	P-value	<0.0001	0.006	0.05
	Spearman r [95% CI]	0.7 [0.5-0.8]	0.4 [0.1-0.6]	0.3 [-0.003-0.6]
<b>Latent TB (n=142)</b>	P-value	<0.0001	<0.0001	<0.0001
	Spearman r [95% CI]	0.5 [0.3-0.8]	0.3 [0.2-0.5]	0.4 [0.3-0.6]
<b>NTM infection (n=39)</b>	P-value	<0.0001	0.0007	0.04
	Spearman r [95% CI]	0.6 [0.3-0.8]	0.5 [0.2-0.7]	0.3 [0.01-0.6]
<b>HIV-TB coinfection (n=241)</b>	P-value	-	<0.0001	-
	Spearman r [95% CI]	-	0.5 [0.3-0.5]	-
<b>Overall</b>	P-value	<0.0001 (n=251)	<0.0001 (n=491)	<0.0001 (n=252)
	Spearman r [95% CI]	0.5 [0.4-0.6]	0.4 [0.3-0.5]	0.3 [0.2-0.4]

**Table 2-7: Correlation between the biomarkers.**

Circulating concentration of ALT, miR-122 and K18 correlated with each other. Statistical significance of the correlation determined with Spearman's rank correlation coefficient. Data shows n, P-values, Spearman's rank correlation coefficient and 95% confidence intervals.

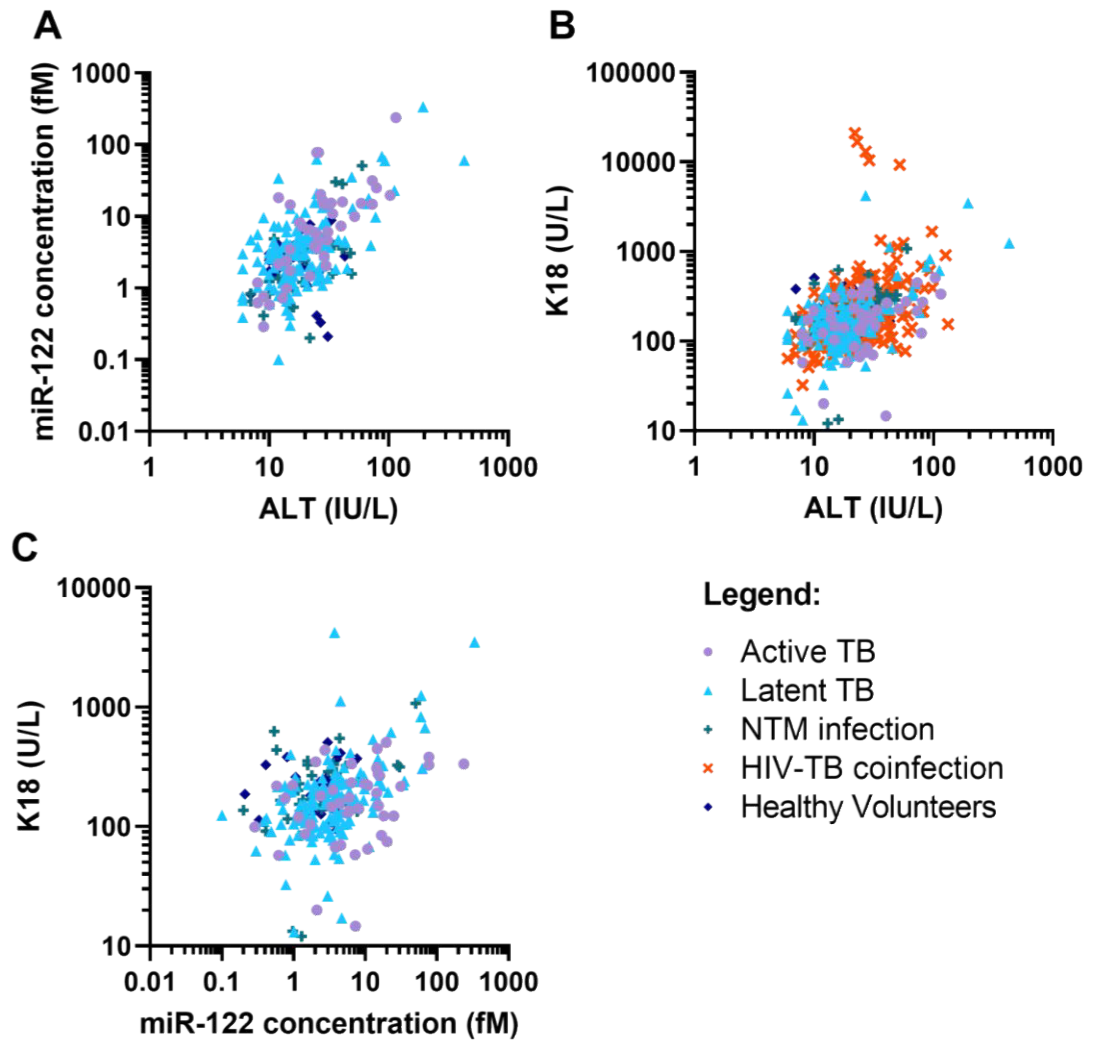


**Figure 2-9: Correlation between circulating biomarkers.**

Circulating concentrations of; (A) ALT (IU/L) & miR-122 (fM); (B) ALT (IU/L) & K18 (U/L); (C) miR-122 (fM) & K18 (U/L). Patients samples included: healthy volunteers  $n=28$ ; active TB  $n=44$ ; latent TB  $n=142$ ; NTM infection  $n=39$ ; HIV-TB coinfection  $n=241$ . Repeated measurements in some patients during the course of treatment are included. Statistical analysis of the significance of the correlation calculated using Spearman's rank correlation coefficient, data shown in Table 2-7.

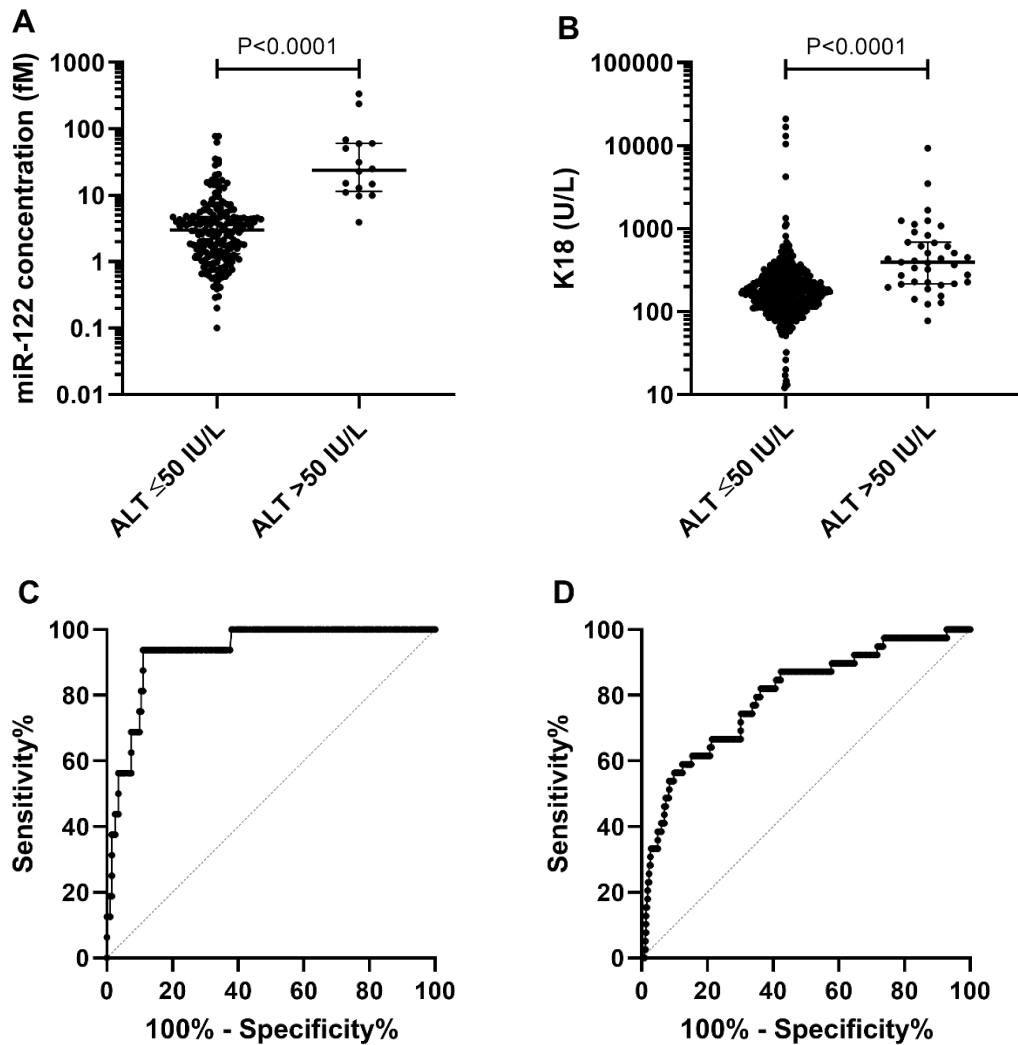


**Figure 2-10: Diagnostic power of the circulating biomarkers miR-122 and K18.**

(A & B) Circulating concentrations of; (A) miR-122 concentration (fM) and (B) K18 (U/L) grouped by normal ALT ( $\leq 50$  IU/L) and elevated ALT ( $> 50$  IU/L). Patients samples included: healthy volunteers  $n=28$ ; active TB  $n=44$ ; latent TB  $n=142$ ; NTM infection  $n=39$ ; HIV-TB coinfection  $n=241$ . Repeated measurements in some patients during the course of treatment are included. Data shown as dot plots. Line represents median and bars represent interquartile range. Statistical analysis of the significance of the difference between the groups calculated with the Mann-Whitney t-test (miR-122  $P<0.0001$ ; K18  $P<0.0001$ ). (C & D) ROC analysis of patient samples grouped by normal ALT ( $\leq 50$  IU/L) and elevated ALT ( $> 50$  IU/L). Circulating biomarkers (C) miR-122; (D) K18. ROC-AUC analysis (miR-122: ROC-AUC 0.93; 95 % CI 0.88-0.98;  $P<0.001$ ) (K18: ROC-AUC 0.80; 95% CI 0.72-0.87;  $P<0.0001$ ). (ROC) receiver operator characteristic; (AUC) area under the curve.



### 2.3.5 Circulating biomarkers in anti-tuberculosis drug-induced liver injury:

In the ALISTER study there were 2 patients who developed ATDILI. Both cases were patients receiving isoniazid alone for the treatment of latent TB. The first case was of a 51-year-old white Scottish male patient. The pattern of liver injury was hepatocellular, as described by an R ratio of 9.0, calculated from a peak ALT of 431 IU/L and peak ALP of 110 IU/L. Formal causality between isoniazid and liver injury was determined using the RUCAM scale and was identified as probable (RUCAM scale = 6) (Table 2-8). Before starting treatment, he had normal ALT (18 IU/L). MiR-122 concentration was 4 fM and K18 was 58 U/L (Figure 2-11 A, C & E). 3 months into treatment his ALT had risen to 431 IU/L. Upon discontinuing treatment, ALT returned to normal (28 IU/L). The circulating concentration of miR-122 increased to 60 fM, and K18 rose to 1248 U/L at the time of peak ALT. Drug treatment was halted when DILI was determined from the elevated ALT. Upon halting treatment, ALT had returned to within normal limits 18 weeks later. The concentration of miR-122 had also fallen to 1 fM and K18 to 215 U/L. This patient showed no symptoms of liver injury other than elevated ALT. However, he did have a high alcohol consumption. Patient did not recommence treatment and was lost to further follow up.

The second case was of a 71-year-old white British female patient. The pattern of liver injury was identified as hepatocellular, with a peak ALT of 194 IU/L and peak ALP of 89 IU/L, giving an R ratio of 5.1. The RUCAM causality assessment indicated isoniazid was the probable cause of liver injury (RUCAM = 7) (Table 2-8). At baseline her ALT was 28 IU/L, miR-122 concentration was 17 fM and K18 was 219 U/L. 2 weeks into treatment her ALT was still within normal range at 25 IU/L and K18 had risen slightly to 307 U/L. However, miR-122 concentration had risen to 63 fM. 5 weeks into treatment DILI was determined with the presence of a drug rash, nausea and elevated ALT at 194 IU/L. The concentration of miR-122 had risen further to 336 fM and K18 had risen to 3490 U/L (Figure 2-11 B, D & F). Drug treatment was halted, and the patient was discharged as it was determined that the risk of developing liver toxicity again was greater than the risk of developing active TB.

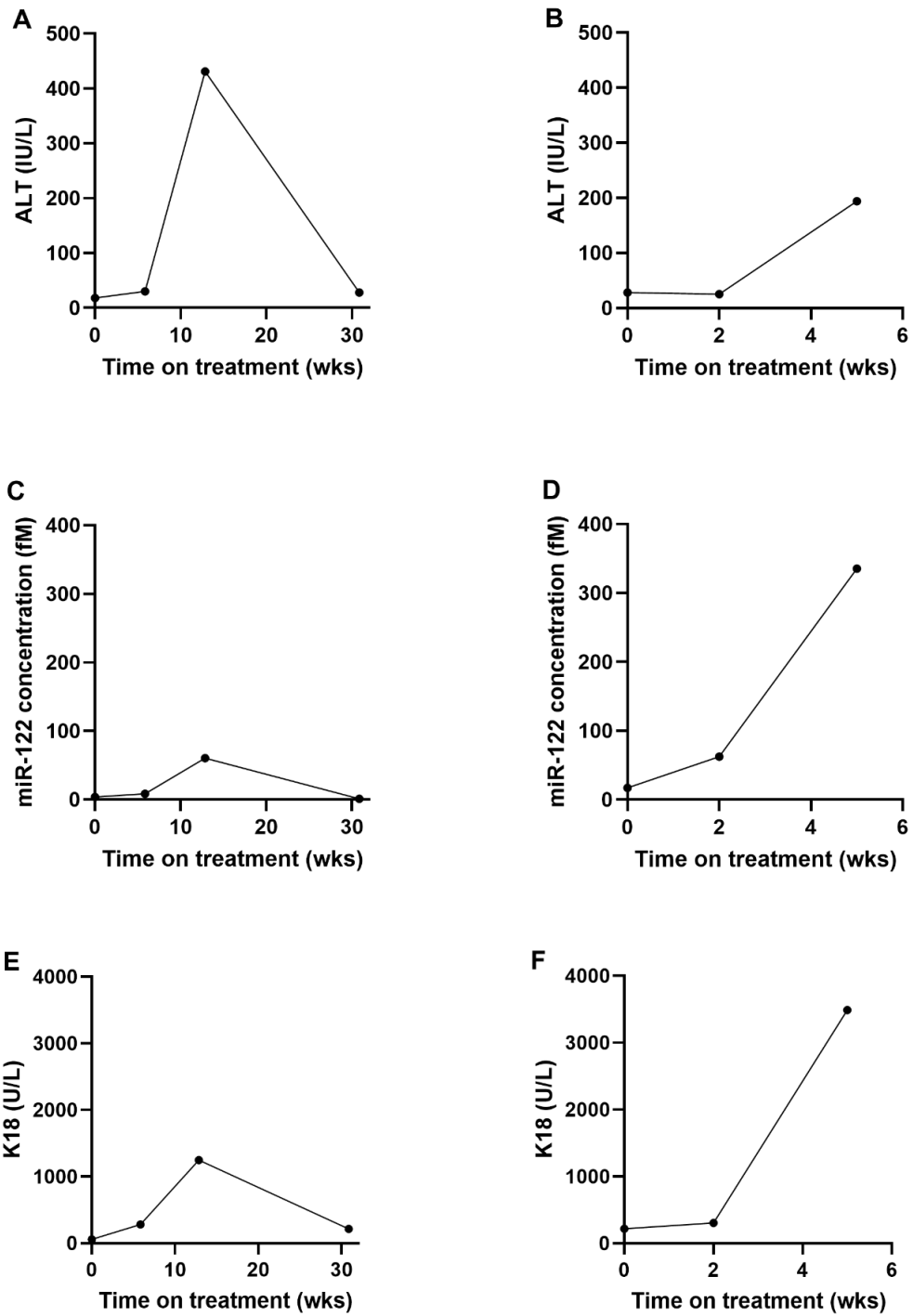


**Figure 2-11: Circulating concentration of ALT, miR-122 and K18 in ALISTER ATDILI cases.**  
 Circulating concentrations of; (A & B) ALT (IU/L); (C & D) miR-122 concentration (fM); (E & F) K18 (U/L) during treatment (weeks). (A, C & E) 1<sup>st</sup> case. (B, D & F) 2<sup>nd</sup> case.

	Case 1		Case 2	
	Assessment	Score	Assessment	Score
1. Time to onset (days)	90	+2	35	+2
2. Course	Inconclusive	0	Unknown	0
3. Risk factors	Age >55 yrs Alcohol	+2	Age >55 yrs	+1
4. Concomitant drugs	None	0	None	0
5. Exclusion of other causes	Alcohol consumption	0	All ruled out	+2
6. Previous information on drug	Reaction labelled in product	+2	Reaction labelled in product	+2
7. Re-administration	Not done	0	Not done	0
<b>Total</b>		<b>+6</b>		<b>+7</b>

**Table 2-8: RUCAM causality assessment of ATDILI cases.**

Data shows ATDILI cases 1 and 2 from ALISTER study. Both patients had a hepatocellular pattern of liver injury. Case 1 had a peak ALT of 431 IU/L and peak ALP of 110 IU/L giving an R ratio of 9.0. Case 2 had a peak ALT of 194 IU/L and peak ALP of 89 IU/L giving an R ratio of 5.1. (ALT ULN = 50 IU/L; ALP ULN = 115 IU/L).

Within the SAEFRIF trial there were 2 patients who had to stop treatment due to DILI. The first case was of a 50-year-old male. At baseline his ALT was 31 IU/L and K18 was 466 U/L. Two weeks into treatment his ALT had fallen slightly to 20 IU/L and K18 to 439 U/L. Between the second study visit at week 2 and third visit at week 4 he developed DILI. The patient reported to a private clinic and so there is no sample for when he was experiencing DILI. After stopping treatment between week 2 and 4 he returned to clinic for the week 4 study visit. At the week 4 clinic visit, his ALT was 30 IU/L and K18 was 531 U/L.

The second case of DILI was in a 45-year-old female. Upon starting treatment ALT rose from a baseline of 29 IU/L to 45 IU/L and K18 rose from 313 U/L to 363 U/L. However, the biomarker which had risen significantly at week 2, resulting in the patient needing to stop treatment, was bilirubin.

## 2.4 Discussion:

### 2.4.1 Main findings:

- There is no significant difference in the circulating concentration of miR-122 in healthy volunteers and patients with active TB, latent TB and NTM infection. Furthermore, there is no significant difference in the circulating concentration of K18 between healthy volunteers and patients with active TB, latent TB, NTM infection and HIV-TB coinfection. Therefore, indicating that mycobacterial infection itself does not affect circulating concentrations of miR-122 and K18.
- In the absence of DILI, commencing anti-TB treatment had no substantial effect on the circulating concentrations of miR-122 and K18 in both ALISTER and SAEFRIF patients.
- Patients who developed mildly elevated ALT upon commencing treatment also experienced elevations in miR-122 and K18. MiR-122 and K18 significantly correlate with ALT.
- In two cases of ATDILI in this study both miR-122 and K18 rose with peak ALT.

### 2.4.2 The concentration of circulating miR-122 and K18 in healthy volunteers in this study differs to that previously described:

The circulating concentration of miR-122 in healthy volunteers in this study fell between 0.21-8.75 fM. This is considerably lower than the published ULN of 45 fM which was generated from the SAFE-T dataset, and 22 fM from the PSTC dataset which had fewer participants [75]. However, the healthy reference defined by Church et al was determined using different quantification and normalisation methods, therefore a direct comparison is challenging. For this work the healthy volunteer data provides a comparison to the other patient groups. However, a much larger sample size is needed to accurately define a reference interval.

This study used the M65 classic ELISA to quantify total K18, however, the published reference interval described by Church and colleagues uses a different ELISA, the M65 Epideath, to quantify total K18. The M65 Epideath ELISA is an adapted version of the M65 classic ELISA designed for use with samples with high K18. As the two ELISAs differ, they have different quantitative ranges, with the classic ELISA having a range of 0-2,000 U/L and a

minimum of 11 U/L, and the Epideath ELISA having a range of 0-5,000 U/L and a minimum of 25 U/L. The reference range described by the ELISA manufacturers also differs, with the classic ELISA having a median of 264 U/L and 95<sup>th</sup> percentile of 413 U/L, and the Epideath ELISA having a median of 62 U/L and 95<sup>th</sup> percentile of 266 U/L, as determined in 222 Swedish blood donors. An earlier study containing healthy volunteers quantified both FL-K18 and CC-K18 (median [IQR]: FL-K18 169 [130-191]; CC-K18 193 [160-257] U/L) [112]. This study by Antoine and colleagues calculated FL-K18 by subtracting the M30 ELISA values (CC-K18) from the M65 classic ELISA, therefore, a value for total-K18 can be back-calculated, giving a median of 362 U/L. The healthy volunteers included in this study had total K18 values of 93-506 U/L, therefore, likely falling in a similar range to the K18 values of the healthy volunteers in the Antoine et al study [112] and also the range described by the manufacturers.

#### 2.4.3 Mycobacterial infection does not affect circulating miR-122 and K18:

This work provides evidence that mycobacterial infection itself does not affect the circulating concentrations of miR-122 and K18. In patients without DILI, the circulating concentrations of miR-122 and K18 did not differ significantly from the healthy volunteers. Furthermore, in patients with normal ALT, circulating concentrations of miR-122 largely fell within the published healthy reference interval of 45 fM [75]. However, there were two patients who had miR-122 concentrations outside of the healthy reference interval of 45 fM, both of 77 fM, with a normal ALT of 25 and 26 IU/L. Neither of these patients went on to develop DILI. This elevated miR-122 in the absence of DILI, and the absence of DILI developing, could be described as false positives. However, although these miR-122 values fall outside of the healthy reference interval, they do not reach the 100-fold increase in miR-122 typically seen in patients with paracetamol overdose induced acute liver injury and abnormal ALT [95], [98].

For patients with normal ALT, their K18 values largely fell below 500 U/L. Within ALISTER, there was one patient with elevated K18, at 4207 U/L, with an ALT of 43 IU/L. Although this patient had K18 significantly elevated over the expected healthy range of 93-506 U/L, K18 did not reach the values indicative of liver injury. In a study of paracetamol overdose patients who exhibited abnormal ALT FL-K18 had a median of 34,176 U/L and CC-K18 a median value

of 2813 U/L [112]. In the SAEFRIF trial there was a single patient whose K18 was elevated throughout treatment, ranging from 10,000-20,000 U/L, however, their ALT was 22-52 IU/L. A measurement of K18 of 10,000-20,000 U/L would likely be considered as DILI. Whether these patients had comorbidities which were causing these elevations in K18 is unknown. However, if these elevations are false positive signals, this highlights a potential issue with the use of K18 alone in the diagnosis of ATDILI.

In comparison to ALT, the inter-patient variation of both miR-122 and K18 is higher, however not to the extent that this would be expected to limit clinical utility. Inter-patient variation of miR-122 within the healthy volunteers in this study was 66%, lower than the approximately 90% described in the Church paper [75], although this study used a smaller population. However, inter-patient miR-122 variation was higher in the different patient groups, ranging from 121-183%. It wasn't possible to determine the intra-patient variation in this study, due to the limited samples collected from ALISTER patients and miR-122 not being quantified in the SAEFRIF samples. A high miR-122 intra-patient variation, 214%, has been described in healthy volunteers, with higher intra-patient variation seen in black individuals than white individuals [75]. This would be interesting to explore in future studies, especially in African populations.

The inter-patient variation of K18 within the healthy volunteers in this study was 46%, with variation ranging from 62-208% for the different patient groups. As the Church study used a different ELISA there is no direct comparison, however they described an inter-patient variation of CC-K18 of 65-70% [75]. In this study intra-patient variation in K18 was measured in HIV-TB coinfecting patients in the SAEFRIF trial. The intra-patient variation was 35%, which is the same as the intra-patient variation described for CC-K18 of 35% [75]. The lower intra-patient variation demonstrated by K18 compared to miR-122 may mean K18 is a better biomarker.

#### 2.4.4 Commencing treatment and the drug treatment taken does not affect circulating miR-122 and K18:

There was no substantial change in miR-122 and K18 in patients who commenced treatment, indicating that drug treatment itself does not cause elevations in miR-122 and K18. In the

absence of DILI, patients who commenced treatment did not experience significant elevations in K18 in both ALISTER and SAEFRIF patient cohorts. Patients in the ALISTER study experienced a slight elevation in miR-122 although this is not clinically significant, with most miR-122 values still falling within the range of 0.21-8.75 fM described for the healthy volunteers in this study.

There was no significant difference demonstrated in miR-122 and K18 across the different drug treatment groups included in the ALISTER study. This indicates that different drugs and drug combinations do not cause substantial elevations in miR-122 and K18 in the absence of DILI. However, these results are limited by the number of patients included, the inclusion of only one sample per patient and the varying periods of time patients were on treatment prior to sample collection. Patients within the SAEFRIF trial were receiving HIV medication alongside their TB treatment. For these patients, neither the type of ART they received (DTG- or EFV-based), nor whether the patient was naïve or established on ART affected ALT or K18. As HIV-TB coinfection is common in low- and middle-income countries with a high burden of TB it is important to determine whether ART itself can affect miR-122 and K18.

Although there were significant correlations identified between the time a patient spends on treatment and the biomarkers, these correlations were slight. Therefore, suggesting that the biomarkers are not substantially affected by the length of time a patient spends on treatment.

#### 2.4.5 The circulating biomarkers miR-122 and K18 rise with elevated ALT and in anti-tuberculosis drug-induced liver injury:

Elevations in ALT between 50-150 IU/L were not uncommon in both the ALISTER and SAEFRIF studies. Often these elevations in ALT were associated with increases in the novel biomarkers miR-122 and K18. As demonstrated in sequential samples in the ALISTER study, four out of five patients who experienced an elevation in ALT also showed an increase in both miR-122 and K18. Within the SAEFRIF study, of the four patients who experienced an elevation in ALT >50 IU/L upon starting treatment three experienced an increase in K18. Both miR-122 and K18 were shown to significantly correlate with ALT. When samples were grouped according to normal ( $\leq 50$  IU/L) ALT and elevated ( $> 50$  IU/L) ALT, K18 was 2.3-fold,

and miR-122 increased 8-fold in the samples with elevated ALT. Further evidence of the diagnostic potential of miR-122 and K18 is demonstrated through the ROC-AUC analysis. MiR-122 had a ROC-AUC of 0.93, indicating its sensitivity for determining elevations in ALT. Furthermore, K18 also demonstrates sensitivity for elevations in ALT, although less so than miR-122, with a ROC-AUC of 0.80. This provides evidence of the diagnostic potential of circulating miR-122 and K18 in patients with mycobacterial infections.

There were limited cases of ATDILI in the ALISTER clinical study, less than anticipated. In the first patient ALT rose from 18 to 431 IU/L, with this elevation in ALT associated with a 16-fold increase in miR-122 and 21-fold increase in K18. In the second patient ALT rose from 28 to 194 IU/L, with a 20-fold increase in miR-122 and 16-fold increase in K18. These elevations in miR-122 and K18, although outside of what could be considered the normal, are not as large as the increases seen in patients with abnormal ALT experiencing paracetamol overdose induced acute liver injury. These paracetamol overdose patients have been shown to have an approximately 100-fold increase in miR-122 concentrations [95], [98], a 200-fold increase in FL-K18 and 14.6-fold increase in CC-K18 [112]. However, in paracetamol overdose the insult to the liver is acute, resulting in the rapid onset of liver injury and release of biomarkers into the circulation. Therefore, it is not surprising that patients who experience ATDILI have lower concentrations of miR-122 and K18 as the insult to the liver is more chronic in nature, likely resulting in a more prolonged release of miR-122 and K18 into the bloodstream.

Both ATDILI cases in the ALISTER study provide evidence that the biomarkers rise in ATDILI. The second case in ALISTER however is more interesting. This patient had an elevation in circulating miR-122 concentration of 63 fM at week 2 when ALT was within the normal range. This elevation in miR-122 is outside Church and colleagues reference interval of 45 fM, and substantially outside the healthy volunteer range of 0.21-8.75 fM described in this study, suggesting the presence or early development of liver injury. In clinical practice identifying the development of liver injury at week 2, rather than week 5, would have been beneficial to the patient. Early identification of the development of liver injury would have enabled treatment to be halted or changed, limiting liver injury and its associated symptoms. This would be especially beneficial in the management of active TB patients, where side-effects



can prevent completion of treatment regimens, resulting in disease relapse and the development of antimicrobial resistance.

Although there were cases of ATDILI within the SAEFRIF trial these are less informative, with no samples collected at peak ALT for the first case. However, the second case indicates that DILI associated with elevated bilirubin is not linked to elevations in K18. Patients with elevated bilirubin are likely to have a cholestatic pattern of liver injury which is caused by obstruction of the bile ducts. However, the release of K18 into the bloodstream is associated with hepatocyte death [104], and not the obstruction of bile ducts. This highlights a potential limitation in the use of K18 as a biomarker of ATDILI, in that it may be unable to detect cholestatic patterns of liver injury. However, it is worth noting that ALT was not elevated in this patient either. Additional tests were taken when the patient presented with jaundice and nausea, resulting in the detection of liver injury via the elevation of bilirubin.

#### 2.4.6 Limitations:

The number of patients and healthy volunteers recruited into the studies limits the outcomes of this work. Firstly, a limited number of healthy volunteers were recruited meaning that it was not possible to calculate a healthy reference interval for miR-122 and K18. Typically, a sample size of 120 is required to set up a reference interval for a population when developing a novel biomarker [170]. Secondly, there was a limited number of patients available for recruitment into ALISTER, and of these patients a lower number than expected developed ATDILI. The RIE can expect to see 2-5% of patients develop ATDILI during their treatment. However, only 2 out of 143 patients (1.4%) developed ATDILI in ALISTER. In addition, the limited number of patients and number who developed ATDILI meant that we were unable to analyse our main study outcome, as this required a sample size of 30 patients with ATDILI, 10 active TB, 10 latent TB and 10 NTM infection. Similarly, the SAEFRIF trial, although having recruited a sizeable number of patients, had limited cases of ATIDILI, and in these cases there were few samples at peak ALT.

Another factor which limits this study is the lack of an accurate reference interval for the biomarkers miR-122 and K18. The recent paper by Church and colleagues described the circulating concentrations of these biomarkers in healthy controls and patients with DILI.

However, the methods used in this study makes it difficult to compare with other work. The method used to quantify miR-122 is poorly described and normalisation technique used to determine copies/ $\mu$ l differs from our own technique. As a result, it is difficult to compare the data collected in this study to the published healthy reference interval. The concentration of miR-122 in healthy volunteers in this study ranged from 0.21-8.75 fM, demonstrating a much smaller range than the published ULN of 45 fM [75]. In addition, the ELISA used to perform the K18 analysis is different to the one used in this study. This makes further comparison of the K18 data collected in this study to the published reference interval also difficult. Not only is the Church study limited by its methods but also by the population used for the study. Most individuals included were Caucasian. Therefore, there is limited evidence of how these biomarkers perform in other populations.

#### 2.4.7 Further work:

Future work should focus on collecting enough samples to determine the reference intervals for the different patient groups with mycobacterial infection. Typically, a sample size of 120 is required to set up a reference interval for a population when developing a novel biomarker [170]. From this sample size the 5<sup>th</sup> and 95<sup>th</sup> percentile can be calculated, generating the reference interval. In the UK this could be achieved by expanding ALISTER to be a multi-site study, focussing on regions with a high incidence of TB. The addition of a Manchester as a site to the ALISTER clinical study was achieved at a late stage of this PhD, however, they only managed to recruit one patient. There is a need not only for reference intervals to be developed in Caucasian populations but across different population groups, with a focus on Asian and African populations where TB is more of an issue. A high intra-patient variation has been identified in healthy black individuals compared to Caucasians [75]. Further work is needed to investigate whether this is the case in a larger population, as high intra-patient variability may limit the clinical utility of a biomarker. In this study, the SAEFRIF clinical trial enabled the inclusion of Ugandan patients with both TB and HIV. Future work should determine reference intervals for different disease groups in an African population. This work should include healthy volunteers and HIV positive, TB negative individuals, to help isolate if any changes in biomarker levels are due to HIV or TB.

In addition to determining reference intervals across different populations, a standardised method is needed for biomarker quantification and normalisation. Although the biomarkers miR-122 and K18 have a previously defined healthy reference interval [75], the lack of standardisation of methods for quantification and normalisation limits the potential for comparison and thus the utility of these data. This is particularly true for miR-122, where different qRT-PCR systems can be used, along with different normalisation techniques, and different units of measurement are used.

The biomarkers miR-122 and K18 are not the only novel biomarkers which have been identified in DILI. Other novel biomarkers such as the protein biomarkers HMGB1 and GLDH have been demonstrated to be elevated in paracetamol overdose [74]. In addition, a wide panel of novel biomarkers have been identified and tested for sensitivity and specificity in the context of DILI diagnosis [75]. Future work should assess the diagnostic and prognostic potential of a broader range of biomarkers in the context of ATDILI as it is possible one of these biomarkers is better than miR-122 or K18. In addition, although there are plenty of biomarkers already described in the literature there is also the possibility that there are novel biomarkers yet to be discovered which have greater diagnostic or prognostic power. Ideally, these biomarkers would also be specific for ATDILI over other forms of liver injury.

#### 2.4.8 Summary:

To summarise, this study demonstrates that mycobacterial infection itself does not affect circulating miR-122 and K18. Furthermore, this work provides preliminary evidence that miR-122 and K18 can diagnose DILI in patients receiving anti-TB treatment. This study is the first to describe K18 concentrations in a HIV-TB coinfecting African population. Due to the limitations of the patient cohort size, further work should determine miR-122, K18 and other novel biomarkers diagnostic and prognostic power in this population.

### 3 Zebrafish as models of anti-tuberculosis drug-induced liver injury

### 3.1 Introduction:

#### 3.1.1 Background:

Zebrafish larvae have potential as models of DILI, being low cost and high throughput, yet able to model toxicity within the context of a whole organism. Zebrafish larvae livers have similarities to mammalian livers in terms of cellular and physiological functions. Furthermore, many of the enzymes involved in metabolism in the liver are conserved across zebrafish and mammals. Zebrafish larvae have been previously used to understand mechanisms of liver injury due to a wide range of drugs. In addition, transgenic zebrafish allow visual assessment of changes in the liver with DILI. The work described in this chapter investigates DILI caused by the anti-TB drugs isoniazid (INH) and pyrazinamide (PYR), and the Chinese herbal medicine triptolide (TP).

MicroRNAs play a role in the regulation of gene expression, with the ability to both down-regulate and up-regulate gene expression [77]. MiRNA expression patterns give an insight into gene regulation, enabling an understanding of the mechanisms involved in disease. Furthermore, miRNAs can be used as biomarkers for disease. They are highly conserved across species [142] and so miRNA biomarkers identified in animal models can be translated into human studies. The microRNA miR-122, a biomarker of paracetamol-induced liver injury [95], is an example of a miRNA which translates across humans and animal models. In zebrafish miR-122 has an identical sequence and a liver-specific pattern of expression, the same as humans [144]. In addition, miR-122 has been demonstrated as a biomarker of triptolide [145] and paracetamol [92] DILI in zebrafish.

Previous work on zebrafish and anti-TB drugs has shown that both INH and PYR induce dose- and time-dependent hepatotoxicity, as well as developmental toxicity. In recently published work, larvae exposed to INH and PYR exhibited spinal curvature, yolk sac retention, lack of swim bladder, tail bending and shorter body lengths [49], [171]. Furthermore, in larvae exposed to PYR pericardial oedema and liver degeneration was also observed [49], and in larvae exposed to INH a reduced locomotor capacity was identified [171]. Liver histology of larvae exposed to INH and PYR indicated hepatotoxicity with the presence of loose cell-to-cell contact and large vacuoles in hepatocytes [49], [171]. Previous work utilising transgenic zebrafish larvae with fluorescent protein (DsRed or eGFP) expression under the *fabp10a*

promoter demonstrated reduced liver size and fluorescence intensity when exposed to INH or PYR [49], [148]. Elevations in the liver transaminases ALT and AST have been shown in homogenised whole larvae following exposure to INH and PYR [172]–[174]. In addition, recent work demonstrated that the exposure of zebrafish larvae to 6 mM INH for 48 hrs led to a significant reduction in miR-122 at the gene expression level [173]. Mechanisms of hepatotoxicity in INH and PYR exposed larvae include the induction of oxidative stress and reduced antioxidant capacity in larvae, with elevations in reactive oxygen species (ROS) leading to endoplasmic reticulum stress and hepatocyte apoptosis [49], [172], [173]. Previous work has identified the down-regulation of liver fatty acid binding protein (LFABP) and superoxide dismutase 1 (SOD1), along with up-regulation of ROS and malondialdehyde (MDA) in INH-exposed larvae [171]. These pathways are associated with the induction of oxidative stress and reduced anti-oxidant capacity [171]. A more recent study identified up-regulation of endoplasmic reticulum stress and apoptosis, along with the stress compensation pathway Nrf2 in larvae exposed to INH [173]. Furthermore, larvae exposed to INH have been shown to have altered metabolism of xenobiotics, with the up-regulation of the phase I enzyme CYP3A and phase II enzyme GSTP2 [171]. Larvae exposed to PYR demonstrated a similar pattern of liver injury, with down-regulation of LFABP and SOD1 and up-regulation of ROS and MDA [49]. In larvae exposed to PYR pathways of liver injury are associated with the down-regulation of LFABP and its target gene peroxisome proliferator-activated receptor  $\alpha$  (PPAR- $\alpha$ ), resulting in oxidative stress and the release of inflammatory cytokines such as tumour necrosis factor  $\alpha$  (TNF- $\alpha$ ) and transforming growth factor  $\beta$  (TGF- $\beta$ ) [49].

An example of a widely used herbal supplement is the traditional Chinese medicine *Tripterygium wilfordii* Hook F or “thunder duke vine” which contains the major active compound triptolide (TP) [175]. TP is a diterpene tri-epoxide which is reported to have neuroprotective, anti-inflammatory and contraceptive effects [176]–[179]. However, TP is associated with relatively high toxicity, including hepatotoxicity. TP’s mechanism of toxicity is due to its ability to bind to cellular macromolecules through its three epoxide groups [180]. TP is reported to covalently bind to a subunit of the transcription factor II human complex (TFIIH) and lead to inhibition of its DNA-dependent ATPase activity, resulting in the inhibition of RNA polymerase II mediated transcription [181]. Our group has previously developed a

model of TP-induced liver injury, with a dose-response relationship in the micromolar range, and histological examination showing that TP induced highly reproducible hepatic necrosis without affecting other organs [145]. TP can be easily administered through dissolving in water and produces reproducible and tractable liver injury. The concentrations of TP used were in the micromolar range, similar to the plasma concentrations reported in humans of 0.15-0.4  $\mu\text{M}$  [182].

The work described in this chapter can be divided into four sections. Firstly, an anti-TB drug induced liver injury model in zebrafish larvae was developed using histology, microscopy and fluorescent imaging. Secondly, small RNA sequencing identified miRNA changes in larvae exposed to anti-TB drugs and TP to investigate the pathways these miRNAs regulate. Thirdly, using a TP-induced liver injury model, miRNA expression in different cell populations was investigated. Finally, novel biomarkers of DILI were identified from the small RNA sequencing data and translated back into humans.

### 3.1.2 Aims:

The hypothesis of this chapter is that zebrafish larvae can be used to develop models of ATDILI and identify changes in miRNA expression in ATDILI.

The aims of this work were:

- Develop a model of anti-TB DILI in zebrafish larvae
- Investigate miRNA changes in DILI
- Develop a method to investigate miRNA changes in specific cell populations
- Identify novel biomarkers of DILI and translate these biomarkers back into humans

## 3.2 Materials & Methods:

### 3.2.1 Zebrafish lines:

Wild-type (*WIK*) zebrafish and three established transgenic zebrafish lines were used for experiments. Transgenic fish lines were sourced from Professor Stephen Renshaw at the University of Sheffield. The transgenic lines used for experiments were:

- *Tg(-2.8fabp10a:eGFP)*
- *Tg(-2.8fabp10a:eGFP;mpx:mCherry)*
- *Tg(-2.8fabp10a:eGFP;mpeg1:mCherry)*

Where eGFP is enhanced green fluorescence protein and mCherry is red fluorescent protein. FABP is liver fatty acid binding protein (liver specific), MPX is myeloid-specific peroxidase (neutrophil specific) and MPEG1 is macrophage-expressed gene 1 (macrophage specific).

### 3.2.2 Drug exposure:

#### 3.2.2.1 Triptolide solution:

Stock solutions of TP (10 mM) were produced by dissolving TP (Cayman Chemicals, Michigan, USA) in DMSO. Stock solutions were diluted in system water to the required concentrations.

#### 3.2.2.2 Anti-tuberculosis drug solutions:

Solutions of PYR (Sigma-Aldrich, Gillingham, UK) and INH (Sigma-Aldrich, Gillingham, UK) were made by dissolving the drug in system water and diluting to the required concentrations.

#### 3.2.2.3 Drug exposure experiments:

Experiments were conducted in accordance with the United Kingdom Animals (Scientific Procedures) Act 1986 in a United Kingdom Home Office approved establishment. Zebrafish (*Danio rerio*) were maintained at 28.5 °C as previously described by Westerfield [118]. For experiments both the wild-type *WIK* line and transgenic fish lines were used. 30 larvae per petri dish were maintained at 28.5 °C in 20 mL of system water. The drug, concentration and exposure period for each experiment are detailed with each method for each experiment. All experiments finished when larvae reached 5 dpf. Larvae were then anaesthetised with MS-222 (tricaine methanesulfonate – 40 µg/mL) dissolved in system water.



### 3.2.3 Anti-tuberculosis drug survival experiments:

Wild-type (*WIK*) zebrafish larvae were exposed to anti-TB drugs for 48 hrs from 3-5 dpf and mortality determined at 5 dpf. Death was determined by the absence of a heartbeat. 30 larvae were treated per petri dish with 3 dishes at each concentration.

### 3.2.4 Microscopy:

Transgenic larvae were exposed to INH or PYR. At 5 dpf larvae were anaesthetised and fixed on their side in agar for imaging. Larvae were then imaged using a fluorescent microscope (Leica M165 FC, Leica-Microsystems, Milton-Keynes, UK), with images taken of each fish using no filter and of the liver using the GFP filter. Images were taken at the same magnification and exposure. Images were assessed for larvae morphology and liver size and fluorescence intensity.

#### 3.2.4.1 Morphological assessment:

Toxicity was assessed visually via morphological assessment of a range of features. Early stages of toxicity are indicated by swimming bladder deficiency and yolk retention [117], [183]. In the later stages of toxicity, the swim bladder is absent, there is severe yolk retention, liver degeneration can be observed by a loss of transparency in the liver tissue and larvae may have pericardial oedema [117], [183]. For this study, images were analysed using the ImageJ software (US National Institute of Health, Bethesda, USA) to determine larvae area, swim bladder area, yolk sac area and area of pericardial oedema. Individual features from each larvae were manually drawn around using ImageJ and quantified using the analysis feature of ImageJ software. Data for swim bladder area, yolk sac area and area of pericardial oedema are presented as a percentage of the total larvae area. Statistical analysis of the differences between groups were performed using GraphPad Prism (GraphPad software, La Jolla, California) and a one-way Kruskal-Wallis ANOVA and Dunn's multiple comparison tests between the control and each timepoint.

#### 3.2.4.2 Liver assessment:

Images were analysed using the ImageJ software (US National Institute of Health, Bethesda, USA) to determine the liver area and fluorescence intensity of the liver. The analysis features

of ImageJ were used to select the fluorescent areas in each image. The area of fluorescence was then quantified using ImageJ. Fluorescence intensity was quantified using the analysis tools within ImageJ, quantifying the fluorescence of the pixels within the area of fluorescence and comparing to the background. This quantified fluorescence was expressed over the area of fluorescence, giving a value for fluorescence intensity. Liver area was presented as a percentage of the total larvae area. Liver fluorescence intensity was presented as a percentage of the controls. Statistical analysis of the differences between groups were performed using GraphPad Prism (GraphPad software, La Jolla, California) and a one-way Kruskal-Wallis ANOVA and Dunn's multiple comparison tests between the control and each timepoint.

### 3.2.5 Histology:

For the histology experiments, wild-type (*WIK*) larvae were exposed to INH or PYR. At 5 dpf larvae were anaesthetised and prepared for histology. Larvae were submerged in neutral buffered formalin (10%) and left to fix overnight at 4 °C before processing. Larvae were prepared for histology as described by [149]. Larvae were embedded in agarose blocks, with 3 x 15 larvae per block. The agarose blocks were then embedded in paraffin blocks using a Thermo Electron Excelsior tissue processor (Thermo, UK). This was achieved through serial immersion in the following solutions: 70% ethanol (1 hr), 90% ethanol (1 hr), absolute ethanol (1 hr x4), xylene (1 hr x2), wax (1.3 hr x3). The blocks were sectioned at 4 µm and placed on a glass slide. The slides were then incubated at 52 °C for at least 1 hour. Tissue sections were then dewaxed and rehydrated using an autostainer (ST5010 Autostainer XL, Leica Microsystems, UK) through cycles of the following; xylene (5 min x3), 100% ethanol (3 min x2), 95% ethanol (2 min x1), distilled dH<sub>2</sub>O (5 min x1). The slides were left to stand in dH<sub>2</sub>O until the next procedure. After rehydration, the slides were stained for haematoxylin and eosin (H&E) in the autostainer by immersion in the following cycles; hematoxylin (5 min), dH<sub>2</sub>O (5 min), Scott's tap water (2 min), dH<sub>2</sub>O (5 min), and eosin (3 min). Stained slides were then dehydrated in the following cycles; dH<sub>2</sub>O wash (45 sec), 70% ethanol (30 sec), 95% ethanol (30 sec x2), 100% ethanol (1 min x2), ethanol/xylene (1 min), and xylene (1 min x3), and cover slipped using Pertex Mounting Medium (CellPath Ltd, UK). Fish were sectioned sagittally along the midline to facilitate examination of the liver.

Pathological changes in the liver were scored visually in a blinded manner. A semi-quantitative scoring system was used to grade the pathological changes noted in these livers. Briefly, each feature of interest was ranked as follows: 0 = absent, 1 = 1-25% of total area examined, 2 = 26-75%, 3 = 76-100% [145]. The features of interest were hepatocyte vacuolation and hepatocyte necrosis. Statistical analysis of the differences between groups were performed using GraphPad Prism (GraphPad software, La Jolla, California) and a one-way Kruskal-Wallis ANOVA and Dunn's multiple comparisons. Further assessment of other organs including brain, kidney, gut and heart were undertaken to determine if there was any other organ toxicity.

### 3.2.6 MiRNA quantification:

#### 3.2.6.1 RNA extraction:

The following method was used to extract RNA from homogenised whole fish samples to determine the number of miR-122 copies per larvae (section 3.2.7) and from cells collected via FACS (section 3.2.9). An adapted version of this RNA extraction protocol was used to collect the RNA used for small RNA sequencing (section 3.2.8).

Whole RNA was extracted with the miRNeasy extraction kit (Qiagen, Venlo, Netherlands) as per the manufacturer's instructions. Briefly, 140  $\mu$ l chloroform was added to the sorted cells and homogenised tissues suspended in Qiazol. The samples were then shaken vigorously and incubated at room temperature for 2-3 min. Samples were centrifuged at 12,000  $\times g$  for 15 min at 4 °C. The upper aqueous phase (150  $\mu$ l  $\times 3$ ) was transferred to a 1.5 ml tube and 1.5 volumes of 100% ethanol (750  $\mu$ l) was added. After mixing thoroughly 700  $\mu$ l of the sample was placed on the RNeasy spin column, the spin column was centrifuged at  $>8,000 \times g$  and flow-through discarded. This process was repeated with the remainder of the sample. The spin column was then washed with the following buffers, 700  $\mu$ l RWT and 500  $\mu$ l RPE, with centrifugation at  $>8,000 \times g$  for 15 sec after each addition. A final wash was undertaken with 500  $\mu$ l RPE, followed by centrifugation at  $>8,000 \times g$  for 2 min. The spin column was placed in a new 2 ml collection tube and dried by centrifugation at  $>8,000 \times g$  for 5 min. Next, the spin column was placed in a new 1.5 ml tube and 30  $\mu$ l nuclease-free water was added to the column. The spin column was centrifuged at 8,000  $\times g$  for 1 min and RNA collected. The 30  $\mu$ l eluate was then placed back on the spin column and eluted again to get a higher

RNA concentration. The resulting RNA was analysed on the NanoDrop spectrophotometer (Thermo Fisher Scientific, Perth, UK) to determine RNA concentration and quality. RNA was stored at -80 °C. Freeze-thaw cycles were avoided to preserve RNA integrity.

#### 3.2.6.2 Reverse transcription:

Total extracted RNA was used in the RT reaction using the miScript II RT kit (Qiagen, Venlo, Netherlands) as per the manufacturer's instructions. The reaction mixture was assembled as shown in Table 3-1. Due to the low RNA yield from FACS cells the reaction mixture was adapted to contain a higher volume of RNA. Following assembly, the reaction mixture was incubated at 37 °C for 60 min, 95 °C for 5 min and then held at 4 °C. The cDNA from whole fish was diluted with 90 µl RNase free water and the cDNA from FACS cells was diluted 180 µl RNase free water. The cDNA was used as template for qRT-PCR reactions.

Component	Volume (µl) for whole fish RNA	Volume (µl) for FACS cell RNA
Hiflex buffer	2.0	4.0
Nucleics	1.0	2.0
RNase free water	4.0	0.0
Reverse transcriptase	1.0	2.0
RNA	2.0	12.0

**Table 3-1: RT reaction mixture components.**

#### 3.2.6.3 Quantitative real time analysis:

The synthesised cDNA template was used in combination with SYBR Green PCR kit (Qiagen, Venlo, Netherlands) and specific miScript primer assays (Qiagen, Venlo, Netherlands). The reaction mixture for a single 10 µl reaction is shown in Table 3-2. As the RNA yield was low for the FACS cells, resulting in a low cDNA yield, a higher volume of cDNA was used in the reaction mixture compared to whole fish.

Component	Volume ( $\mu$ l) for whole fish cDNA	Volume ( $\mu$ l) for FACS cells cDNA
SYBR Green buffer	5.0	5.0
Universal primer	1.0	1.0
miScript primer assay	1.0	1.0
RNase free water	1.0	0.0
cDNA	2.0	3.0

**Table 3-2: qRT-PCR reaction mixture components.**

qRT-PCR was performed on a Light Cycler 480 (Roche, Burgess Hill, UK) using the recommended cycling parameters, the same as for the clinical samples in the previous chapter (section 2.2.4.3). In addition, samples were measured in duplicate and three controls were included as described in the previous chapter (section 2.2.4.3). Dissociation curves were analysed for each plate as described in the previous chapter (section 2.2.4.3). An example dissociation curve is included below (Figure 3-1).

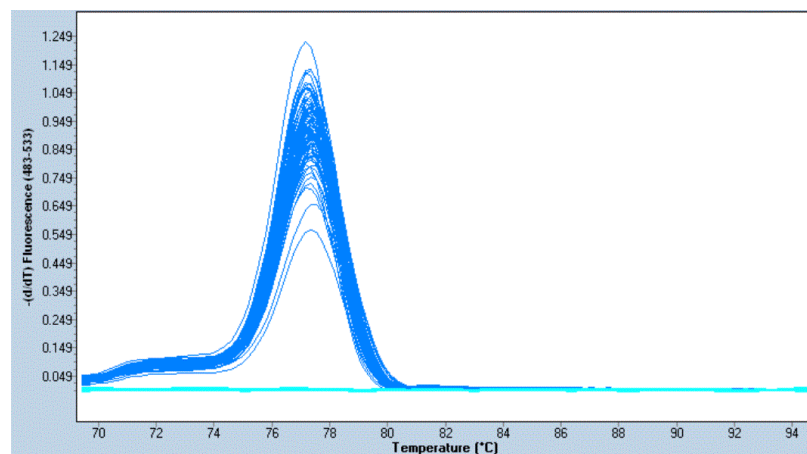


**Figure 3-1: Example dissociation curve for SNORD95.**

*Example dissociation curve for a plate with zebrafish RNA samples and the primer SNORD95. Specificity of the primers is demonstrated by a single peak.*

#### 3.2.6.4 Relative quantification:

For the experiments investigating the relative expression of miRNAs in treatment groups and different cell populations, relative quantification was undertaken with the  $2^{-\Delta\Delta Cq}$  method. The internal reference miRNA, small nucleolar RNA, C/D box 95 (SNORD95), was used to normalise miRNA data. SNORD95 was chosen as a reference miRNA as it correlated with both the number of cells collected by FACS (Spearman  $r=-0.75$ ,  $p<0.0001$ ) and RNA

concentration (Spearman  $r=-0.85$ ,  $p<0.0001$ ), see Appendix 3.iii. The average of the duplicate Cq measurements was taken. To quantify the relative expression of miRNAs,  $\Delta Cq$  values were calculated by subtracting the Cq value for SNORD95 from the Cq value of the miRNA of interest for each sample.  $\Delta\Delta Cq$  values were calculated by subtracting the  $\Delta Cq$  value of the experimental condition from the  $\Delta Cq$  value of the control. For all experiments untreated (not exposed to vehicle control or drug treatment) whole fish RNA was used as the control. Finally,  $2^{-\Delta\Delta Cq}$  was calculated, giving the relative gene expression.

### 3.2.7 Copies of miR-122 per fish experiment:

Wild-type (*WIK*) larvae were exposed to INH or PYR. At 5 dpf larvae were anaesthetised and as much water removed as possible from the tube. 700  $\mu$ l Qiazol was then added. Tissues were homogenised in a tissue homogeniser and then stored at  $-80\text{ }^{\circ}\text{C}$  until RNA extraction. RNA was extracted (section 3.2.6.1), cDNA was generated (section 3.2.6.2) and miRNAs quantified (section 3.2.6.3). Absolute quantification was undertaken using the method and standard curve described in the previous chapter (section 2.2.4.4). The final number of copies/ $\mu$ l was divided by the number of larvae used within the pooled sample to obtain the average miRNA copy number per larva. Statistical analysis of the differences between groups were performed using GraphPad Prism (GraphPad software, La Jolla, California) and a one-way Kruskal-Wallis ANOVA and Dunn's multiple comparison test to determine the difference between the control and each timepoint.

### 3.2.8 Small RNA sequencing:

For the small RNA-sequencing work Bastiaan Vliegthart, a previous PhD student in my group, had already undertaken the triptolide experiment, RNA extraction and sequencing work. I did the anti-TB drug experiments and RNA extraction. Bioinformatics was performed by Al Ivens.

#### 3.2.8.1 Triptolide small RNA sequencing:

For the small RNA sequencing experiment wild-type (*WIK*) zebrafish were exposed to TP (1.6  $\mu$ M) or vehicle control for 6 hrs. Each treatment group had 8 biological replicates, each replicate consisting of 30 pooled fish. For quality control RIN values were measured on Agilent Technologies 2100 Bioanalyzer using the Eukaryote Total RNA Nano kit (Agilent

Technologies, Stockport, UK). All samples had an RNA integrity number (RIN) of  $\geq 9.5$ . Sequencing was performed at the Wellcome Trust Clinical Research Facility at the Western General Hospital, Edinburgh.

#### 3.2.8.2 Anti-tuberculosis small RNA sequencing:

For the anti-TB small RNA sequencing experiment wild-type (*WIK*) zebrafish were exposed to INH (10 mM), PYR (6 mM) for 24 hrs. Control zebrafish larvae were maintained in system water. Each treatment group had 8 biological replicates, each replicate consisting of 30 pooled fish.

Whole RNA was extracted using an adapted version of the RNA extraction method described in section 3.2.6.1. An additional DNase digest step was included using the recommended protocol by Qiagen. Instead of adding 700  $\mu$ l of RWT buffer to the spin column the following steps were undertaken. 350  $\mu$ L RWT buffer (made up with isopropanol) was added to the spin column, the spin column was then centrifuged at 8,000  $\times g$  for 15 sec. Next, 80  $\mu$ L of DNase solution (Qiagen, Venlo, Netherlands) was added to the spin column and incubated for 15 min at room temperature. The spin column was then washed with 500  $\mu$ L of RWT buffer (made up with isopropanol) and centrifuged at 8,000  $\times g$  for 15 sec. The eluate was reapplied to the spin column and centrifuged again at 8,000  $\times g$  for 15 sec. After this step the RNA extraction protocol follows the protocol in section 3.2.6.1, with the next step a wash with 500  $\mu$ L RPE buffer. Following extraction, RNA was stored at  $-80^{\circ}\text{C}$  prior to sequencing. RNA quality was assessed on the LabChip GX24 (Perkin Elmer, UK) using the standard sensitivity RNA kit. All samples had a RIN of  $\geq 9.5$ . Sequencing was undertaken at the Wellcome Trust Clinical Research Facility at the Western General Hospital, Edinburgh. Libraries were prepared from total-RNA samples using the NEXTFLEX small RNA-seq Kit v3 (Bio Scientific, UK). To select for small RNA libraries only, a bead size selection was used to recover the final 150bp libraries. Libraries were quantified by fluorometry using the Qubit dsDNA HS assay (Thermo Fisher Scientific, Perth, UK) and assessed for quality and fragment size using the Agilent Bioanalyser with the DNA HS Kit (Agilent Technologies, Stockport, UK). Fragment size and quantity measurements were used to calculate molarity for each library pool. Sequencing was performed using the NextSeq 500/550 High-Output v2.5 (75 cycles) Kit on the NextSeq 550 platform (Illumina, California, USA). Libraries were combined in 1

equimolar pool based on the library quantification results and run across 1 High-Output Flow Cell v2.5. Following sequencing FASTQ files were generated using Bcl2fastq2.

#### 3.2.8.3 Small RNA sequencing data analysis:

Following small RNA sequencing both the TP and anti-TB data were analysed together following the same analysis method. The raw sequences were quality assessed using FASTQC software (Babraham Institute, Cambridge, UK). Based on the output of the FASTQC analysis further pre-processing was required using the cutadapt software (Massachusetts Institute of Technology, USA) to remove primers and low-quality regions. Cleaned sequences were collapsed within each sample to generate a non-redundant set of fasta sequences. Singletons were not included. Alignments (end-to-end, very sensitive settings) were performed using bowtie (v0.12.5) as part of the miRDEEP2 package [184] to the zebrafish genome (Danio rerio GRCz11, NCBI). Only sequences with full length perfect match to the genome were retained. MiRNA prediction was undertaken using miRDEEP2 software [184], with species-specific matures and precursors obtained from miRbase (v22). MiRNA tag counts were used directly by Bioconductor DESeq2 package (v3.10) [184], with normalisation as appropriate for the comparison being undertaken. Pairwise comparisons of sample groups were performed between groups, using the Bioconductor DESeq2 package [184]. LogFC values were not shrunk. A series of group-wise comparisons were undertaken to identify differences (fold changes). Each fold change is associated with significance statistics, but as the number of significance tests being done is equal to the rows of data, significance values are controlled for false discovery, yielding a more rigorous adjusted P-value. Statistical significance was set at adjusted  $P < 0.05$ .

#### 3.2.8.4 MiRNA target prediction and function annotation:

To predict miRNA targets and functional annotations in zebrafish the online open-source DIANA-miRPath (v6.0) software was used [185]. The miRPath server enables functional annotation of miRNAs with analyses with the Kyoto Encyclopaedia of Genes and Genomes (KEGG) molecular pathways and gene ontology (GO). Predicted targets are generated using the microT-CDS algorithms and experimentally validated miRNA interactions are derived from DIANA-TarBase (v8.0) [186]. For this work, miRNAs with a significant adjusted P-value



of <0.05 and a fold change of greater than 1.5 were included in the KEGG and GO analyses. The P-value was selected as <0.05 and the micro-T threshold of 0.8 for the analyses.

### 3.2.9 Fluorescence Activated Cell Sorting:

#### 3.2.9.1 Zebrafish larvae digest:

For the fluorescence activated cell sorting (FACS) experiments, approximately 100 larvae were used per experiment. Larvae were exposed to 1.6  $\mu$ M TP or vehicle control for 6 or 24 hrs. Transgenic larvae were used to generate GFP and mCherry cell populations via FACS. Wild-type (*WIK*) larvae were used as controls. Following drug exposure, at 5 dpf, zebrafish larvae were anaesthetised. Larvae were then pooled, with as much water removed as possible. Then the larvae were digested with 1 mL FACSmax Cell Dissociation solution (Genlantis, San Diego, USA) for approximately 45 min whilst pipetting solution every few min to break down tissues. Once the fishes were digested the cell suspension was pelleted at 600 x *g* for 1 min and then resuspended in 1.5 mL of FACSmax cell dissociation solution. The solution was then passed through a 40  $\mu$ m cell strainer (Sigma-Aldrich, Gillingham, UK) and the digestion stopped with the addition of 1:3 ratio of Dulbecco's Modified Eagle Medium (DMEM) supplemented with 10% Foetal Bovine Serum. The isolated cells were pelleted at 1200 x *g* for 5 min and resuspended in 1 mL DMEM. The above digest method was adapted from [187], [188].

#### 3.2.9.2 Cell sorting:

The single cell solution generated from the transgenic lines was run through the BD FACS Aria Fusion cell sorter (BD Biosciences, California, USA). Wild-type (*WIK*) cell solution was used as a negative control to set the gates for the sorting protocol. The gating strategy is shown in Appendix 3.i. GFP positive cells and mCherry positive cells were sorted into different tubes. During FACS data was collected on the percentage of live cells, the percentage of GFP positive cells and the fluorescence intensity of the GFP positive cells. FACS data analysis were performed using the FlowJo software (Ashland, USA). Statistical analysis of the differences between groups were performed using GraphPad Prism (GraphPad software, La Jolla, California) and a two-way ANOVA.

#### 3.2.9.3 Sample collection and storage:

The sorted cells were collected into 200  $\mu$ L DMEM, 700  $\mu$ L Qiazol was added and samples immediately frozen at -80 °C. The wild-type (*WIK*) single cell solutions were centrifuged at 1200  $\times g$  for 5 min and resuspended in 200  $\mu$ L DMEM. 700  $\mu$ L Qiazol was added and samples immediately frozen at -80 °C.

#### 3.2.9.4 MiRNA extraction and quantification:

RNA was extracted from the collected cells (section 3.2.6.1) and RNA then quantified (sections 3.2.6.2 - 3.2.6.4). For the experiment investigating miRNA expression in TP-treated whole fish and cell populations the statistical analysis of the differences between groups were performed using GraphPad Prism (GraphPad software, La Jolla, California) and a two-way ANOVA with Sidak's multiple comparisons.

#### 3.2.10 Translation of miRNA targets into human samples:

Validation of miRNA targets identified by small RNA sequencing was undertaken on the two ALISTER ATDILI cases described in the previous chapter. RNA was extracted as described in section 2.2.4.1, cDNA was generated as described in section 2.2.4.2 and miRNAs were quantified as described in section 2.2.4.3. Dissociation curves were analysed for each miRNA as described in the previous chapter (section 2.2.4.3). The following specific miScript assays were used; miR-122, miR-39, miR-21, miR-146a, miR-133b-3p, miR-205-3p, miR-132-3p, miR-365 and miR-193a-3p (Qiagen, Venlo, Netherlands). Relative quantification was undertaken using the  $2^{-\Delta\Delta Cq}$  method, with miR-39, the external spike-in control, for normalisation (section 3.2.6.4). Relative gene expression was determined as compared to baseline.

### 3.3 Results:

#### 3.3.1 Anti-tuberculosis drug-induced liver injury model:

##### 3.3.1.1 Survival:

Zebrafish larvae were exposed to a range of concentrations of INH and PYR from 3-5 dpf and mortality assessed by the absence of a heartbeat (Figure 3-2). Mortality was variable between experiments and larvae. Larvae exposed to INH appeared to have developmental changes, with curvature to the spine and a reduced size. Therefore, 10 mM INH was chosen for further experiments as higher doses appeared to affect larvae development. Larvae exposed to PYR had very variable mortality rates between experiments, with even slight differences in PYR concentration leading to large increases in mortality. Therefore, 6 mM PYR was chosen for future experiments as this concentration led to mortality in approximately 50% of larvae.

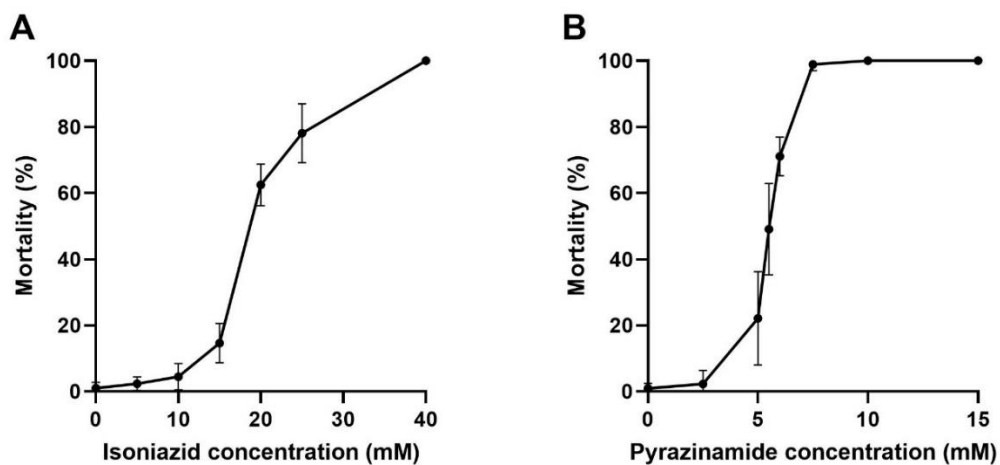


**Figure 3-2: Survival of larvae after exposure to anti-TB drugs.**

Larvae mortality (as determined by lack of heartbeat); (A) INH, (B) PYR. Wild-type (WIK) larvae were used. Exposure to the drug for 48 hrs. Data are the mean mortality of 3 dishes of 30 larvae. Bars shown standard deviation.

### 3.3.1.2 Morphology:

Zebrafish larvae were exposed to 10 mM INH, or 6 mM PYR, for 0, 6, 24 and 48 hrs. Images were taken (Figure 3-3 & Figure 3-5) and morphology was assessed (Figure 3-4 & Figure 3-6). Zebrafish larvae were assessed for early stages of toxicity, swimming bladder deficiency and yolk retention [117], [183], and later stages of toxicity, lack of swim bladder, severe yolk retention and pericardial oedema [117], [183].

Larvae exposed to 10 mM INH demonstrated a significant deficiency in swim bladder size after 6 hrs exposure, with a fall in the size of larvae swim bladder as a percentage of larvae area over increasing periods of exposure to INH, (Figure 3-4A) (mean [95% CI]: control 5.21 [5.03-5.39]; 6 hrs 4.43 [4.01-4.85]; 24 hrs 3.19 [2.43-3.95]; 48 hrs 1.77 [1.29-2.24] %). The size of the yolk sac was significantly larger in larvae exposed to INH at all timepoints, with an increase in yolk sac size demonstrated with increasing periods of exposure to INH, (Figure 3-4B) (mean [95% CI]: control 1.69 [1.26-2.13]; 6 hrs 4.53 [3.38-5.67]; 24 hrs 5.72 [4.85-6.60]; 48 hrs 8.34 [7.15-9.52] %). Pericardial oedema was present in two control larvae and four larvae after exposure to INH for 6 hrs (Figure 3-4C). In larvae exposed to INH for 24 and 48 hrs pericardial oedema was more common, with a mean size of oedema of 0.76% (95% CI: 0.41-1.10%) in larvae exposed to INH for 24 hrs, and a mean of 2.21% (95% CI: 1.15-3.27%) in larvae exposed for 48 hrs. There was a significant difference in larvae area at 24 hrs ( $P=0.0009$ ) and 48 hrs exposure ( $P=0.01$ ) compared to controls (Figure 3-4D), indicating INH hinders larval development and growth. A further morphological change identified in larvae exposed to INH was curvature of the spine (Figure 3-3).

For larvae exposed to 6 mM PYR there was a slight, but not statistically significant, fall in swim bladder size after exposure to PYR, (Figure 3-6A) (mean [95% CI]: control 5.21 [5.03-5.39]; 6 hrs 4.67 [3.97-5.16]; 24 hrs 3.80 [2.81-4.80]; 48 hrs 3.81 [2.67-4.95] %). The size of the yolk sac was significantly larger in larvae exposed to PYR at all timepoints, (Figure 3-6B) (mean [95% CI]: control 1.69 [1.26-2.13]; 6 hrs 4.07 [2.92-5.21]; 24 hrs 5.20 [3.72-6.68]; 48 hrs 4.75 [3.20-6.30] %). Pericardial oedema was not commonly seen in larvae exposed to PYR, however, several larvae exposed to PYR for 48 hrs had substantial oedemas (Figure 3-6C). There was no significant difference in larvae area between the control and drug exposed groups (Figure 3-6D). Curvature of the spine and significantly reduced larval development were not identified in larvae exposed to PYR (Figure 3-5).

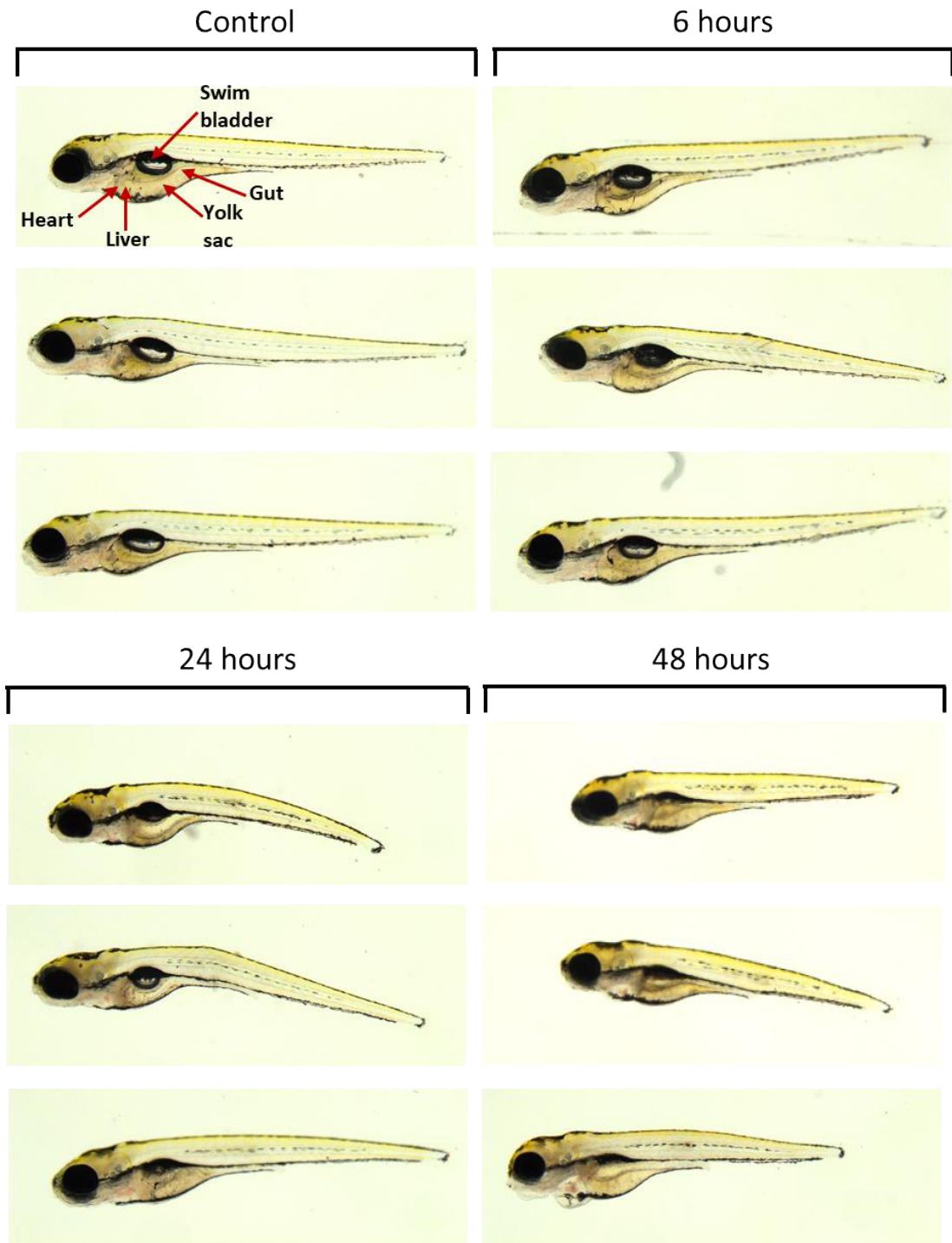


**Figure 3-3: Larvae morphology: representative images following INH exposure.**

Representative lateral images of zebrafish larvae exposed to 10 mM INH for 0, 6, 24 or 48 hrs. Transgenic larvae were used.

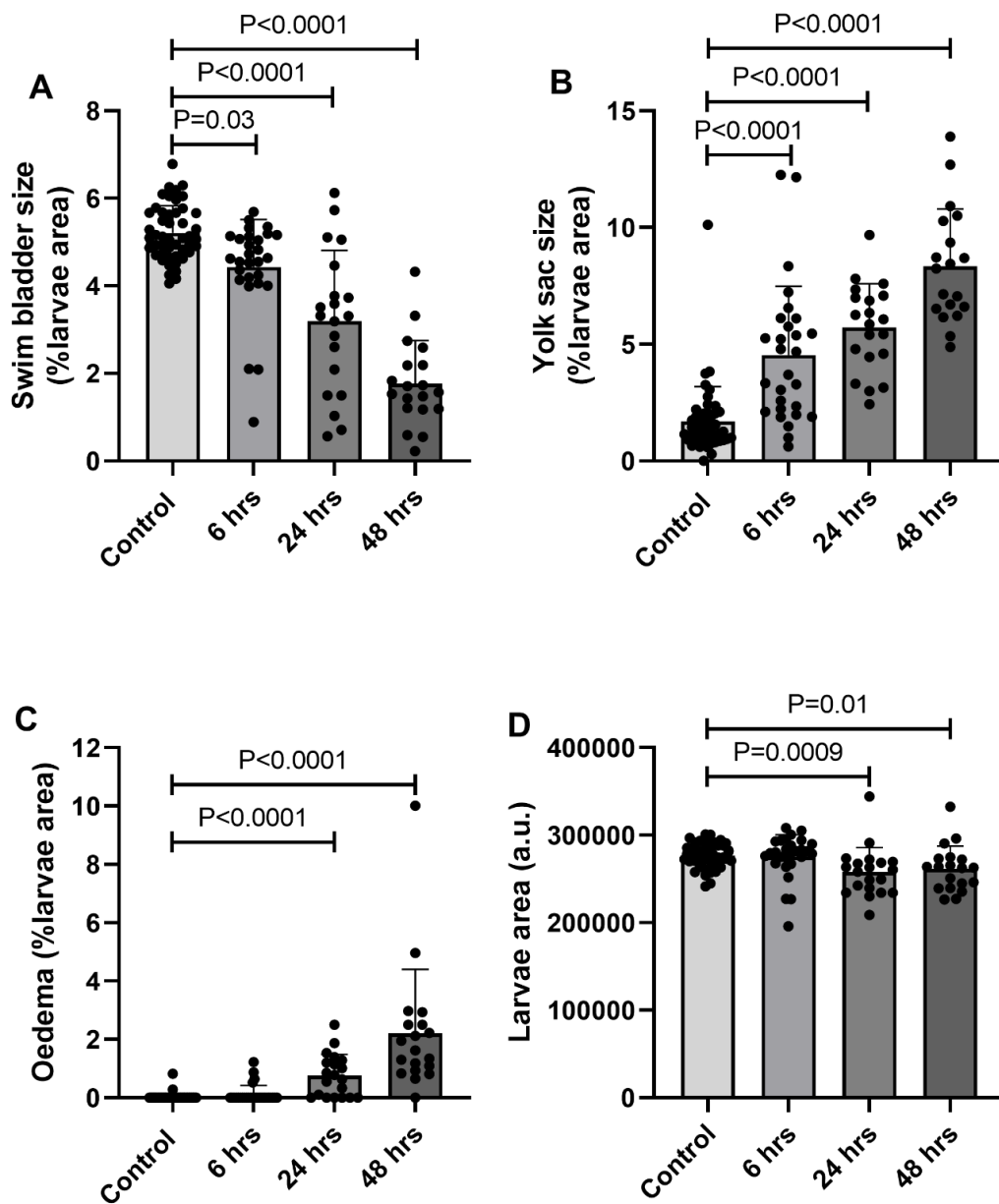


**Figure 3-4: Morphology of larvae exposed to 10 mM INH.**

(A) Swim bladder size; (B) Yolk sac size; (C) Pericardial oedema size; (D) Larvae area. Exposure to 10 mM INH for 0 hrs/controls n=48; 6 hrs n=28; 24 hrs n=20; 48 hrs n=19. Transgenic larvae were used. (A-C) Data presented as a percentage of total larvae area. (D) Larvae area expressed in arbitrary units. (A-D) Bars show mean and standard deviation, statistical significance was determined by Kruskal-Wallis test and Dunn's multiple comparison tests between the control and each timepoint.

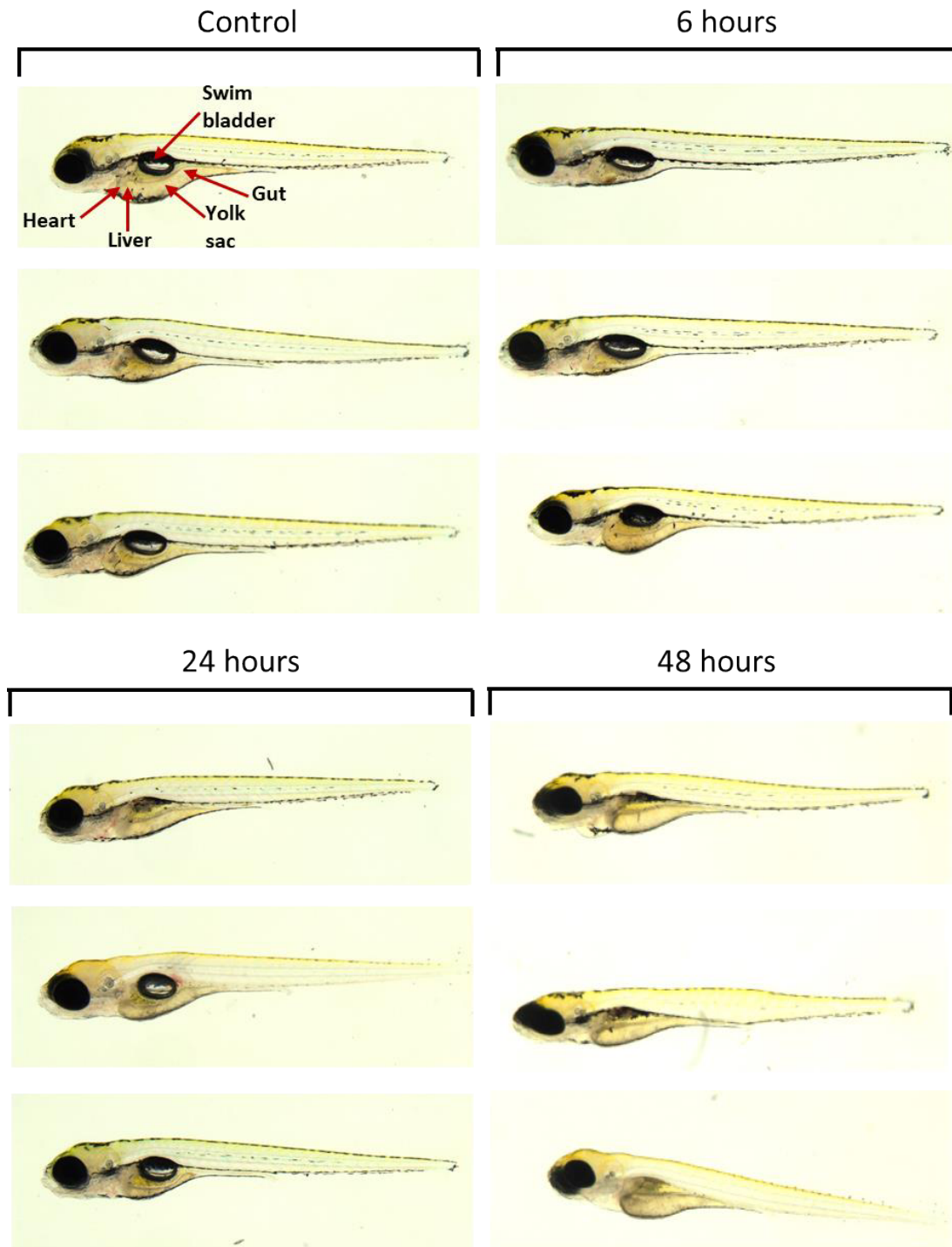


**Figure 3-5: Larvae morphology: representative images following PYR exposure.**

Representative lateral images of zebrafish larvae exposed to 6 mM PYR for 0, 6, 24 or 48 hrs.

Transgenic larvae were used.



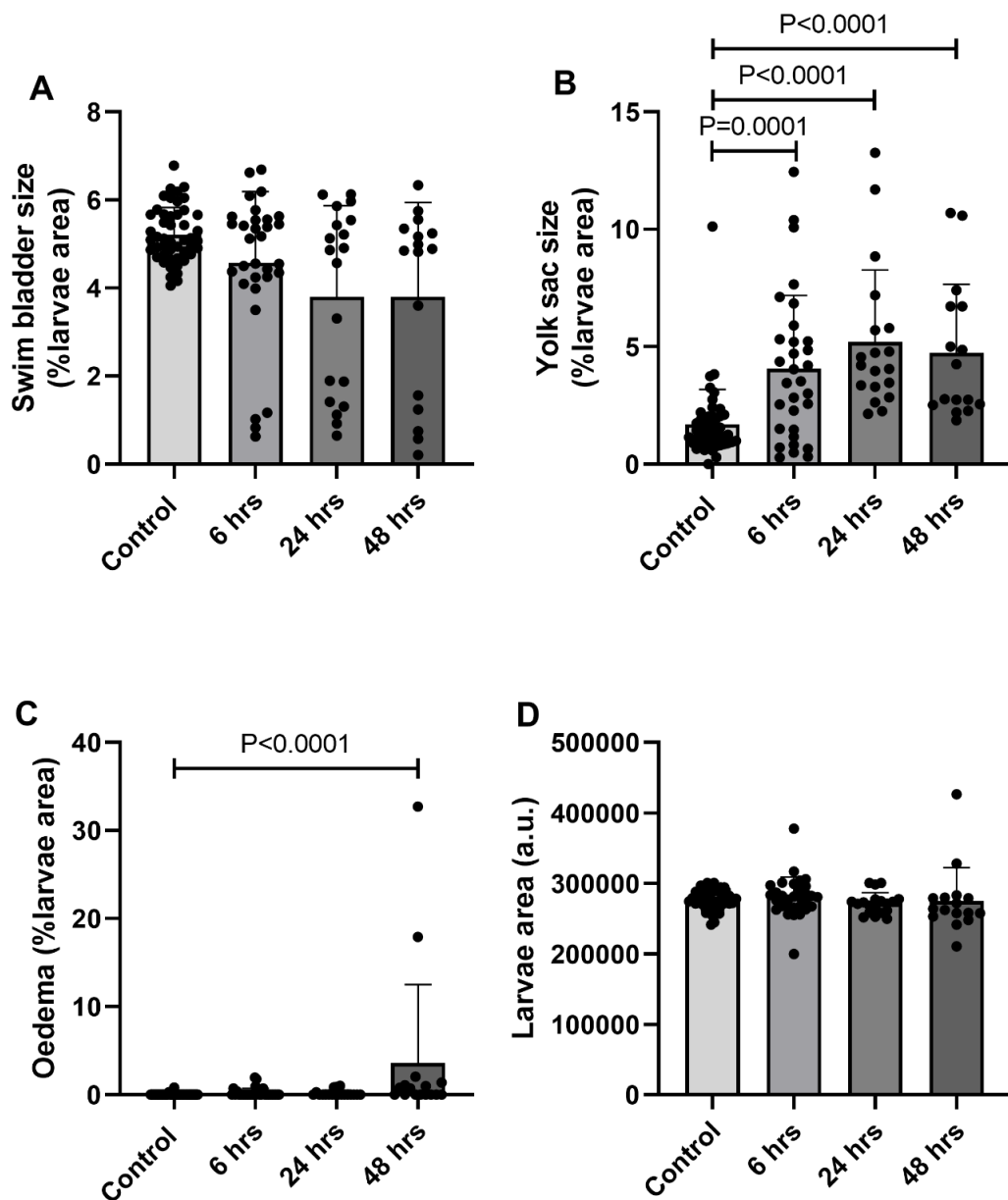


**Figure 3-6: Morphology of larvae exposed to 6 mM PYR.**

(A) Swim bladder size; (B) Yolk sac size; (C) Pericardial oedema size; (D) Larvae area. Exposure to 6 mM PYR for 0 hrs/control  $n=48$ ; 6 hrs  $n=31$ ; 24 hrs  $n=19$ ; 48 hrs  $n=16$ . Transgenic larvae were used. (A-C) Data presented as a percentage of total larvae area. (D) Larvae area expressed in arbitrary units. (A-D) Bars show mean and standard deviation, statistical significance was determined by Kruskal-Wallis test and Dunn's multiple comparison tests between the control and each timepoint.

### 3.3.1.3 Fluorescence microscopy:

Zebrafish larvae were exposed to 10 mM INH (Figure 3-7), or 6 mM PYR (Figure 3-8), for 0, 6, 24 and 48 hrs and images taken. Liver fluorescence intensity and liver area were determined.

Liver fluorescence intensity was decreased in larvae exposed to INH, (Figure 3-7B) (mean [95% CI]: control 100.0 [96.4-103.7]; 6 hrs 95.5 [88.7-102.3]; 24 hrs 83.4 [76.0-90.8]; 48 hrs 74.7 [68.5-80.9] %). Liver area as a percentage of the larvae area was reduced in larvae exposed to INH, (Figure 3-7C) (mean [95% CI]: control 2.56 [2.38-2.74]; 6 hrs 1.96 [1.67-2.25]; 24 hrs 2.22 [1.93-2.51]; 48 hrs 1.72 [1.38-2.07] %).

In larvae exposed to PYR a significant reduction in fluorescence intensity was only seen after 48 hrs exposure, (Figure 3-8B) (mean [95% CI]: control 100 [96.4-103.7]; 6 hrs 108.8 [101.8-115.9]; 24 hrs 99.9 [90.5-109.3]; 48 hrs 71.6 [55.7-87.5] %). Similarly, for liver area, a significant reduction was only seen after 48 hrs exposure to PYR, (Figure 3-8C) (mean [95% CI]: control 2.56 [2.38-2.74]; 6 hrs 2.31 [2.07-2.56]; 24 hrs 2.54 [2.29-2.79]; 48 hrs 1.47 [0.93-2.00] %).

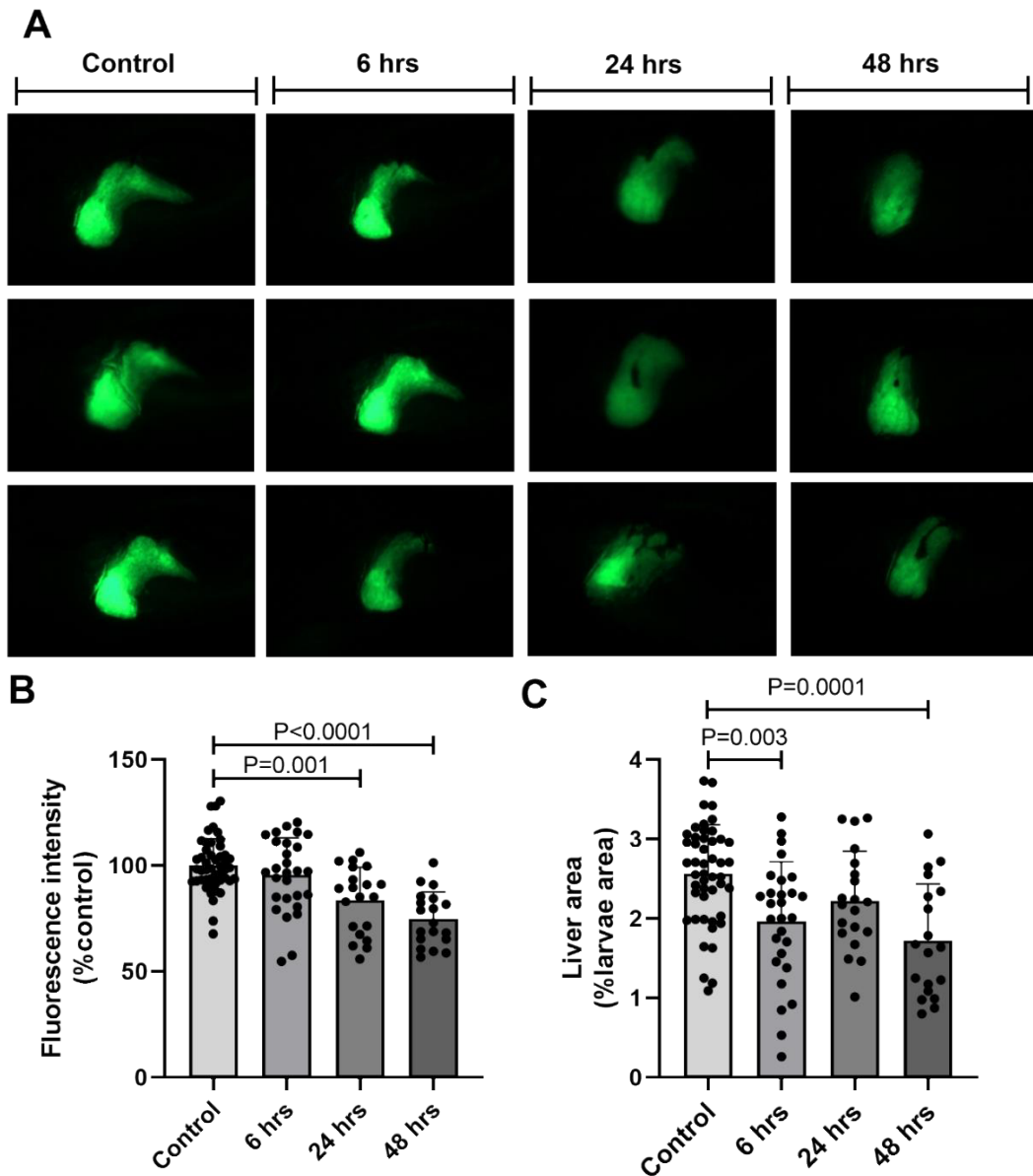


**Figure 3-7: Fluorescence imaging of larvae exposed to 10 mM INH.**

(A) Representative liver images; (B) Liver fluorescence intensity; (C) Liver area. Exposure for 0 hrs/controls  $n=48$ ; 6 hrs  $n=28$ ; 24 hrs  $n=20$ ; 48 hrs  $n=19$ . Transgenic larvae were used. (B) Data presented as a percentage of the control. (C) Data presented as a percentage of larvae area. (B & C) Data shows mean, bars show standard deviation. Statistical significance was determined by a one-way Kruskal-Wallis ANOVA and Dunn's multiple comparison tests between the control and each timepoint.

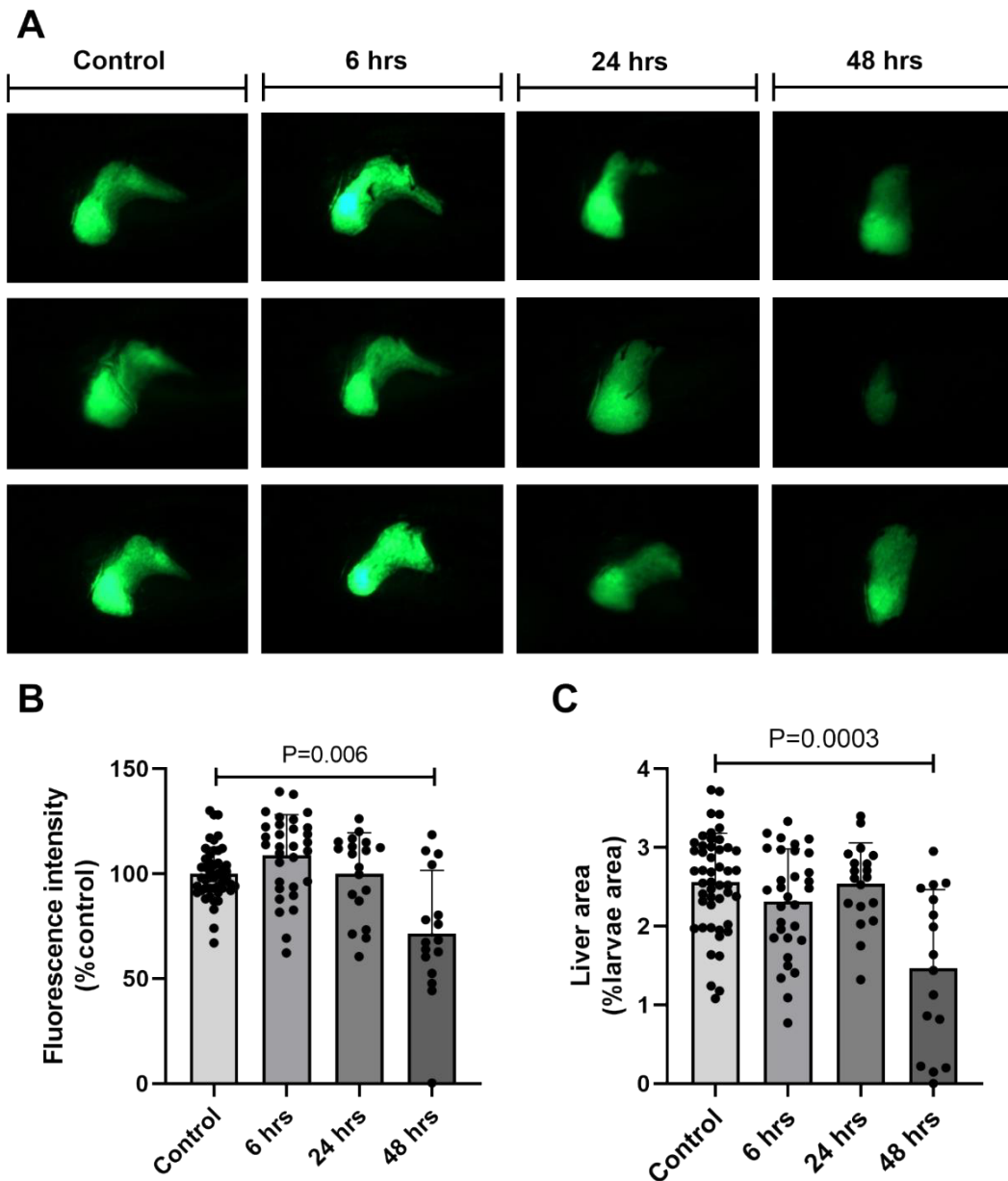


**Figure 3-8: Fluorescence imaging of larvae exposed to 6 mM PYR.**

(A) Representative liver images; (B) Liver fluorescence intensity; (C) Liver area. Exposure for 0 hrs/controls  $n=48$ ; 6 hrs  $n=31$ ; 24 hrs  $n=19$ ; 48 hrs  $n=16$ . Transgenic larvae were used. (B) Data presented as a percentage of the control. (C) Data presented as a percentage of larvae area. (B & C) Data shows mean, bars show standard deviation. Statistical significance was determined by a one-way Kruskal-Wallis ANOVA and Dunn's multiple comparison tests between the control and each timepoint.

#### 3.3.1.4 Histology:

Wild-type (WIK) zebrafish larvae were exposed to 10 mM INH and 6 mM PYR (Figure 3-8) for 0, 6, 24 and 48 hrs. Larvae then underwent histology and were scored for hepatic vacuolation and necrosis.

Liver histology of control larvae, which had not experienced drug exposure, indicated normal tissue and cell structure, with tight cell contacts and well delineated polygonal cells with well-preserved cytoplasm and a prominent nucleus. Exposure to PYR and INH resulted in hepatic vacuolation, as demonstrated by the presence of macrovacuoles within hepatocytes. In addition, hepatocyte necrosis was found, demonstrated by loose cell-to-cell contact, irregularly shaped cells and the presence of karyolytic and karyohectic nuclei.

In larvae exposed to 10 mM INH hepatocyte vacuolation was observed after 6 hrs, with a significant difference between the 6 hour and control groups ( $P=0.02$ ) (Figure 3-10A). The severity of hepatocyte vacuolation increased with increased periods of exposure to INH (Figure 3-10A). Hepatocyte necrosis was also observed, with some necrosis seen after 6 hrs and significant necrosis after 24 hrs ( $P<0.0001$ ) and 48 hrs ( $P<0.0001$ ) (Figure 3-10B).

Larvae exposed to 6 mM PYR developed hepatocyte vacuolation. This vacuolation was observed after exposure to PYR for 6 hrs (Figure 3-11A). There was a significant increase in hepatocyte vacuolation observed after 24 hrs ( $P=0.0002$ ) (Figure 3-11A). Hepatocyte necrosis was also observed, with a significant difference between exposed and control groups after 24 hrs ( $P=0.002$ ) (Figure 3-11B). There were only 2 images available for 48 hrs exposure as for this group of larvae many were dead and rapidly decomposing at the 5 dpf endpoint. This was sometimes seen, that different groups of larvae were more susceptible to drug exposure.

There was no other organ damage observed (Appendix 3.ii).

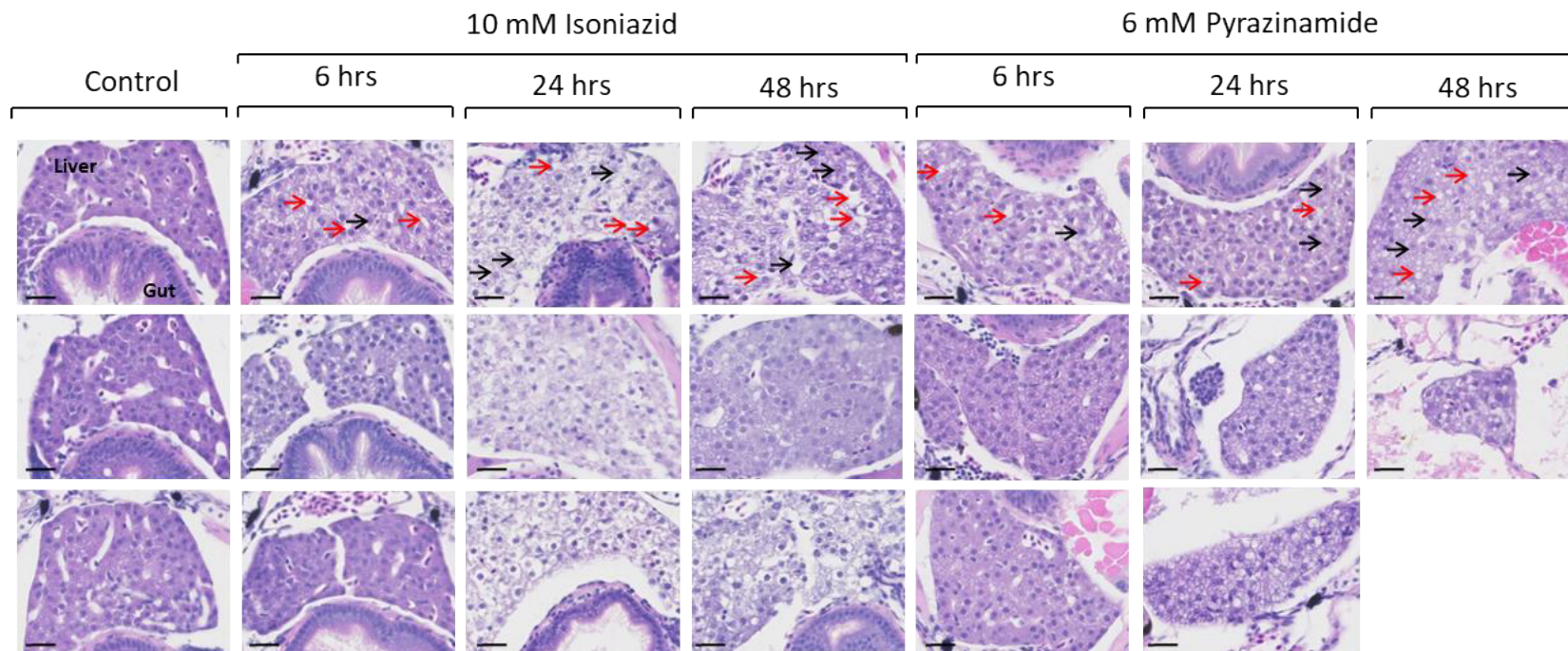


**Figure 3-9: Histology of larvae.**

Representative histology images zebrafish larvae livers. Control larvae and larvae exposed to 10 mM INH or 6 mM PYR for 6, 24 or 48 hours. Wild-type (WIK) larvae were used. Black arrows indicate karyolytic and karyohectic nuclei which are suggestive of apoptosis and necrosis. Red arrows indicate vacuoles. Scale bars are 20  $\mu$ m.

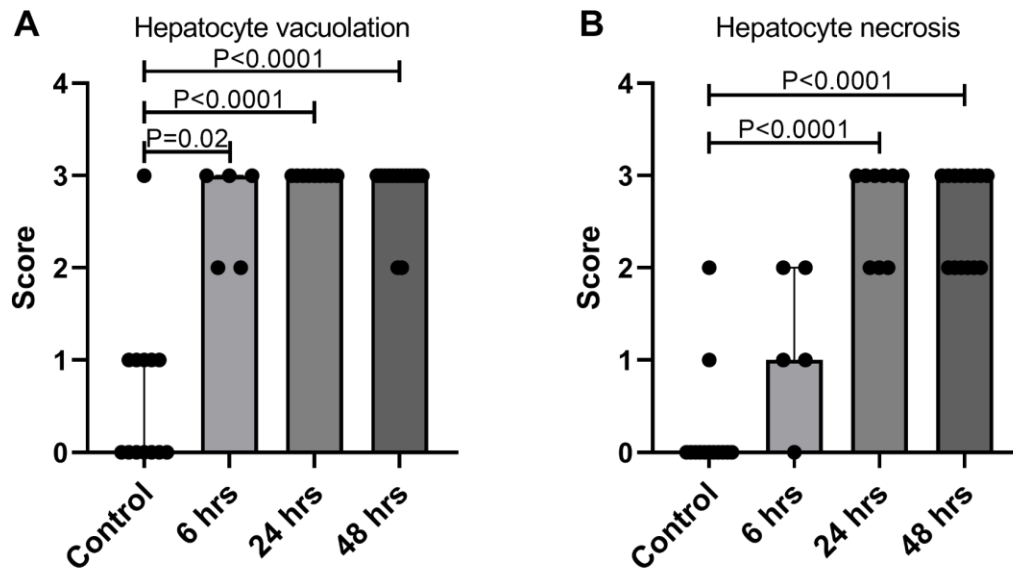


**Figure 3-10: Histology of larvae exposed to 10 mM INH.**

(A) Hepatocyte vacuolation; (B) Hepatocyte necrosis. Exposure for 0 hrs/controls  $n=13$ ; 6 hrs  $n=5$ ; 24 hrs  $n=9$ ; 48 hrs  $n=14$ . Wild-type (WIK) larvae were used. (B & C) Scoring system ranked each feature according to the percentage of total area examined; 0 = absent, 1 = 1-25% of total area examined, 2 = 26-75%, 3 = 76-100%. Bar charts show median and interquartile range. Statistical significance was determined by one-way Kruskal-Wallis ANOVA and Dunn's multiple comparison tests between the control and each timepoint.

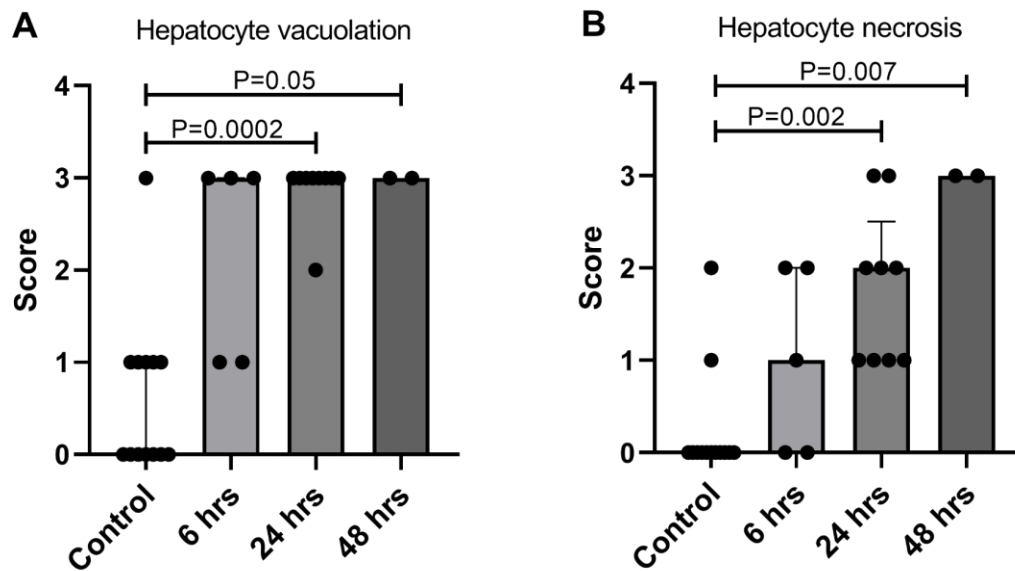


**Figure 3-11: Histology of larvae exposed to 6 mM PYR.**

(A) Hepatocyte vacuolation; (B) Hepatocyte necrosis. Exposure for 0 hrs/controls  $n=13$ ; 6 hrs  $n=5$ ; 24 hrs  $n=9$ ; 48 hrs  $n=2$ . Wild-type (WIK) larvae were used. (B & C) Scoring system ranked each feature according to the percentage of total area examined; 0 = absent, 1 = 1-25% of total area examined, 2 = 26-75%, 3 = 76-100%. Bar charts show median and interquartile range. Statistical significance was determined by one-way Kruskal-Wallis ANOVA and Dunn's multiple comparison tests between the control and each timepoint.



## 3.3.1.5 Copies of miR-122 per larvae:

Zebrafish larvae were exposed to 10 mM INH and 6 mM PYR for 0, 6, 24 and 48 hrs. Following exposure, larvae were homogenised, RNA extracted and miR-122 quantified using qRT-PCR and absolute quantification. Larvae exposed to 10 mM INH had no significant difference in copies of miR-122 per larvae after drug exposure (Figure 3-12A). For larvae exposed to 6 mM PYR there was a significant difference in the number of copies of miR-122 per larvae after 48 hrs of exposure compared to controls ( $P=0.0005$ ) (Figure 3-12B).

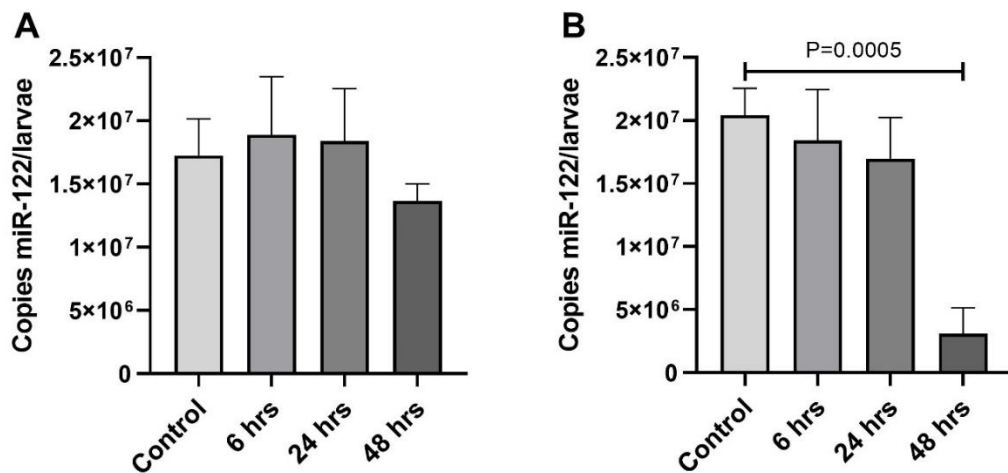


**Figure 3-12: Copies of miR-122 per larvae following anti-TB drug exposure.**

Larvae were exposed to (A) 10 mM INH and (B) 6 mM PYR for 0, 6, 24 or 48 hrs. Wild-type (WIK) larvae were used. Data shown as bar chart, with mean and bars showing standard deviation,  $n=6$  (with each plate consisting of 30 larvae). Statistical significance was determined by one-way Kruskal-Wallis ANOVA and Dunn's multiple comparison tests between the control and each timepoint.

### 3.3.2 MiRNA changes and associated pathways in drug-induced liver injury:

For the anti-TB small RNA sequencing experiment, wild-type (*WIK*) larvae were exposed to 10 mM INH or 6 mM PYR for 24 hrs. This timepoint was chosen as histology demonstrated significant evidence of liver necrosis after 24 hrs of exposure to the anti-TB drugs. Zebrafish larvae which had been maintained in system water were used as controls. A total of 24 sequencing experiments were performed (control N=8, INH N=8, PYR N=8). Each replicate consisted of 30 pooled larvae; therefore 720 larvae were included in total.

For the TP small RNA sequencing experiment larvae were exposed to 1.6  $\mu$ M TP for 6 hrs, an early time point identified by microscopy and histology as being before the onset of fulminant hepatocyte death [145]. The control larvae were exposed to DMSO vehicle control for 6 hrs. A total of 16 sequencing experiments were performed (control N=8, treatment N=8). Each replicate consisted of 30 pooled larvae; therefore 480 larvae were included in total.

Volcano plots were generated to describe the fold change in miRNA expression with drug treatment along with associated adjusted p-values. Pie charts demonstrate the total number of miRNAs up or down-regulated, irrespective of adjusted P-value. The significantly changed miRNAs (adjusted P-value <0.05) were used to generate the heatmaps. Significantly changed miRNAs (adjusted P-value <0.05) with a fold change of greater than 1.5 are listed. Significantly changed miRNAs, divided into up- and down-regulated miRNAs were used in KEGG and GO analyses to identify functional pathways associated with each drug treatment.

#### 3.3.2.1 Isoniazid induced liver injury:

One of the INH-treated samples generated only 9,000 reads, compared to the approximately 15 million reads generated for all other samples, despite passing quality control. Therefore, this sample was not included in the data analysis. In the comparison between the INH exposed and control larvae, there were 91 miRNAs which were statistically significantly differentially expressed (adjusted P-value <0.05), of which 46 miRNAs were up-regulated and 45 were down-regulated (Figure 3-13 A & B), with 18 miRNAs with greater than 1.5-fold change up-regulated and 23 down-regulated (Table 3-4). These significantly changed miRNAs with a greater the 1.5-fold change were used to create the heatmap, (Figure 3-14)

and identify predicted KEGG pathways and targets (Table 3-8 & Table 3-9). KEGG pathways identified included metabolism of xenobiotics by the microsomal enzymes MGST2 and MGST3. Further pathways identified included the biosynthesis of steroid hormones, mucin-type O-glycan and other type O-glycan synthesis and ECM-receptor interactions. GO analysis identified lipopolysaccharide biosynthetic processes as significantly altered (Appendix 3.iv & Appendix 3.v).

#### 3.3.2.2 Pyrazinamide induced liver injury:

There were 179 miRNAs which were statistically significantly differentially expressed with an adjusted p-value of 0.05 or less, 96 miRNAs were up-regulated and 83 were down-regulated (Figure 3-13 C & D). Of these miRNAs, 29 were more than 1.5-fold down-regulated and 28 more than 1.5-fold up-regulated (Table 3-5). KEGG analysis identified the metabolism of xenobiotics pathway, with the genes MGST2 and MGST3 again identified (Table 3-10 & Table 3-10). Other pathways identified by KEGG analysis included the biosynthesis of mucin type O-glycans, biosynthesis of unsaturated fatty acids, lysine degradation and valine, leucine and isoleucine degradation. GO analysis identified no significantly altered pathways (Appendix 3.vii & Appendix 3.vii).

#### 3.3.2.3 Pyrazinamide compared to isoniazid induced liver injury:

Directly comparing the small RNA sequencing data of PYR-treated larvae relative to INH-treated identified 104 miRNAs which were significantly altered, with 52 up-regulated and 52 down-regulated. Of these miRNAs, there were 19 with greater than 1.5-fold up-regulation and 25 with more than 1.5-fold down-regulation, (Figure 3-13 E & F). KEGG analysis identified the metabolism of xenobiotics pathway, along with several pathways involved in the production and metabolism of fatty acids. KEGG pathways also identified included, mucin type O-Glycan biosynthesis, steroid hormone biosynthesis, purine biosynthesis, biosynthesis of unsaturated fatty acids and other types of O-glycan biosynthesis (Table 3-12 & Table 3-13). GO analysis identified, lipopolysaccharide biosynthetic processes (Appendix 3.viii & Appendix 3.ix).

#### 3.3.2.4 Triptolide induced liver injury:

There were 56 miRNAs which were statistically significantly differentially expressed (adjusted p-value <0.05), 24 miRNAs were up-regulated and 32 were down-regulated (Figure 3-13 G & H). Of these miRNAs, there were 23 with greater than 1.5-fold down-regulation and none with more than 1.5-fold up-regulation (Table 3-7). These significantly changed miRNAs, with a greater 1.5-fold change, were used to create the heatmap, ( ) and identify predicted KEGG pathways and targets (Table 3-14). The biosynthesis pathways for unsaturated fatty acids and glycosaminoglycans were identified in the KEGG analysis, along with the glycan degradation pathways and ECM-receptor interactions. GO analysis did not identify any pathways (Appendix 3.x).

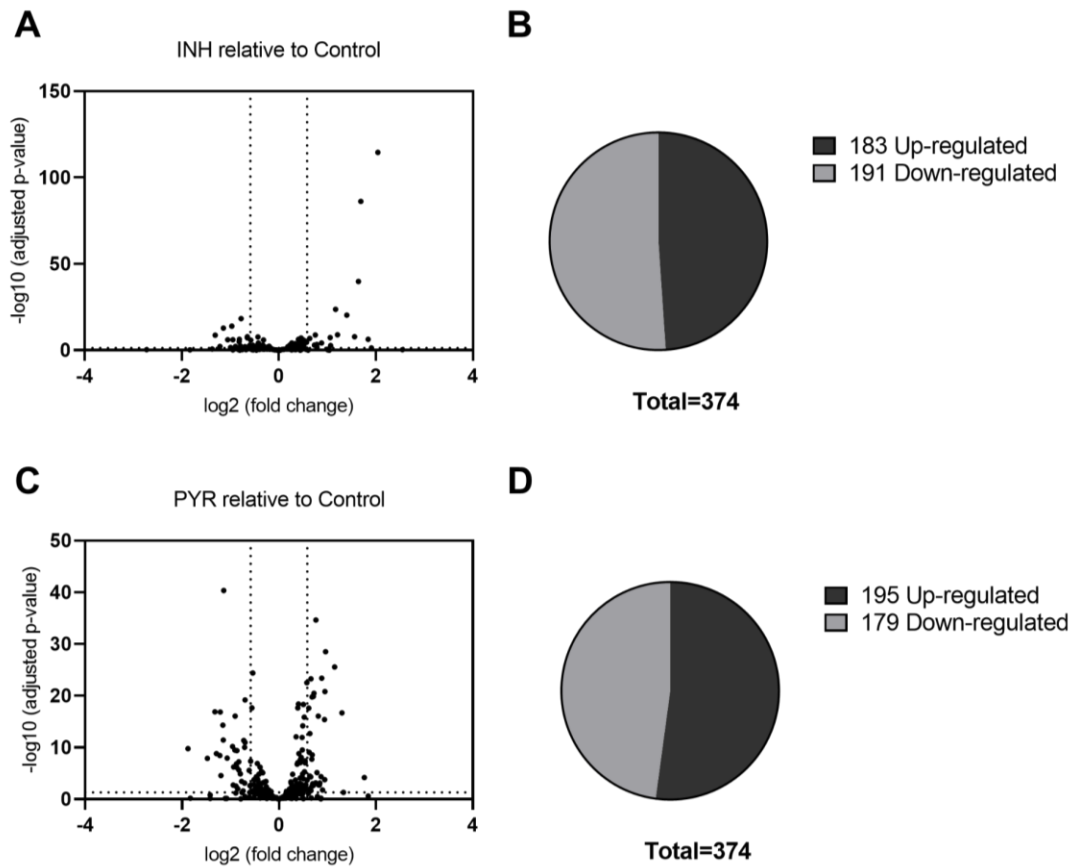


**Figure 3-13: Small RNA sequencing volcano plots and pie charts.**

Figures (A, C, E & G) show volcano plots with  $\log_2(\text{fold change})$  on the x-axis and  $-\log_{10}(\text{adjusted } p\text{-value})$  on the y-axis. Dotted lines indicate  $\pm 1.5$  fold change and adjusted  $p$ -value of  $< 0.05$ . Figures (B, D, F & H) show pie charts with total proportion of up- and down-regulated miRNAs, irrespective of significance. (A & B) INH relative to control; (C & D) PYR relative to control; (E & F) PYR relative to INH; (G & H) TP relative to TP control.

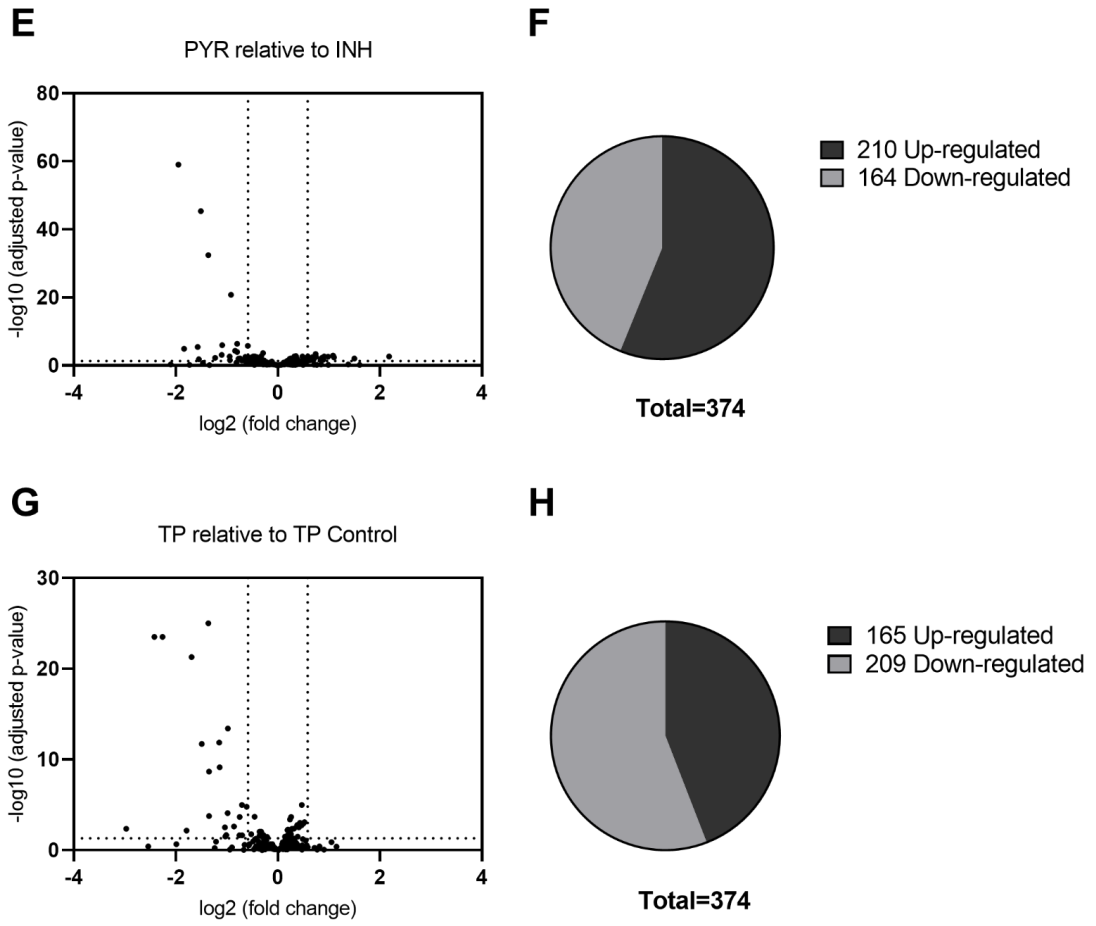
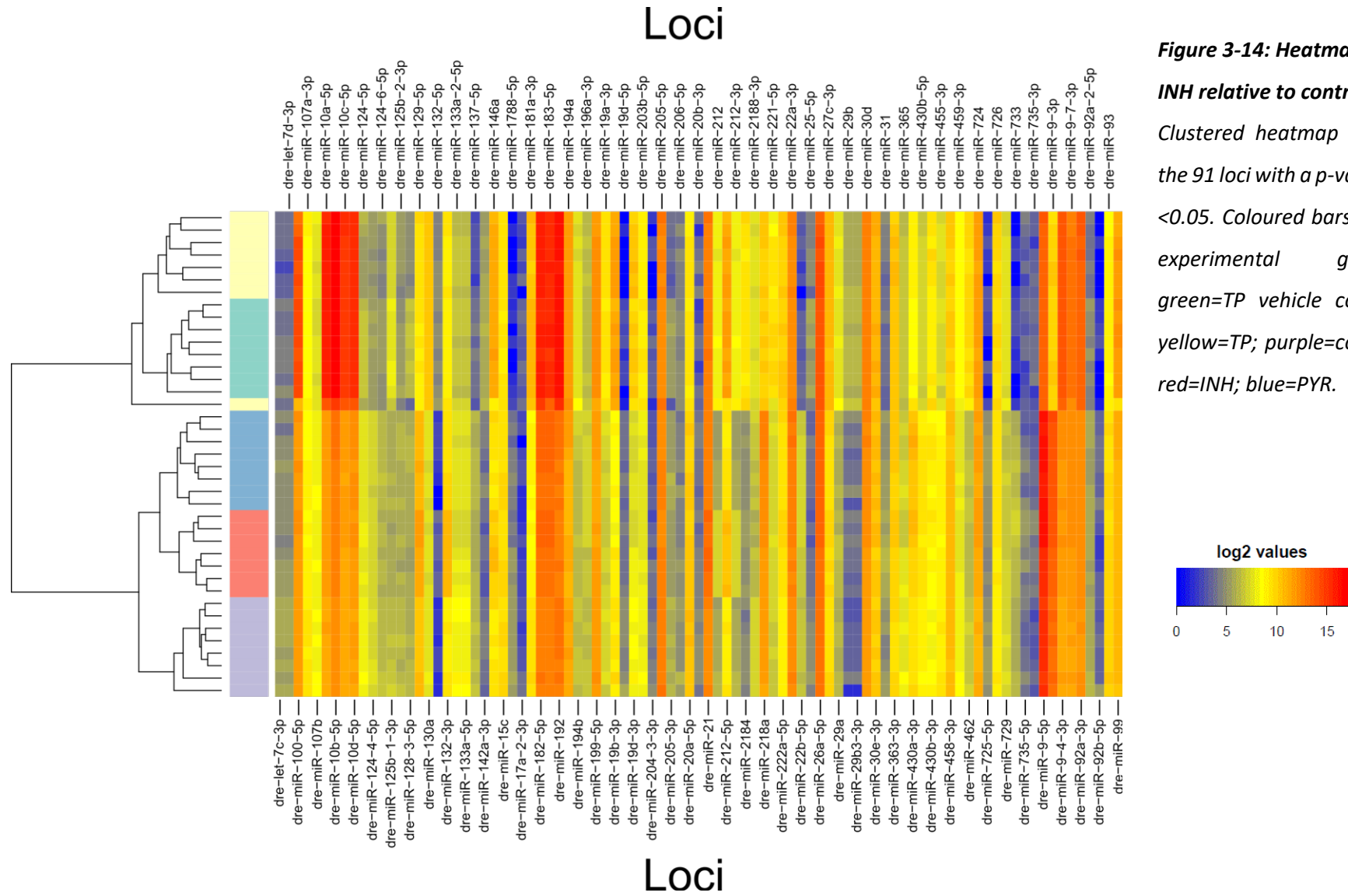
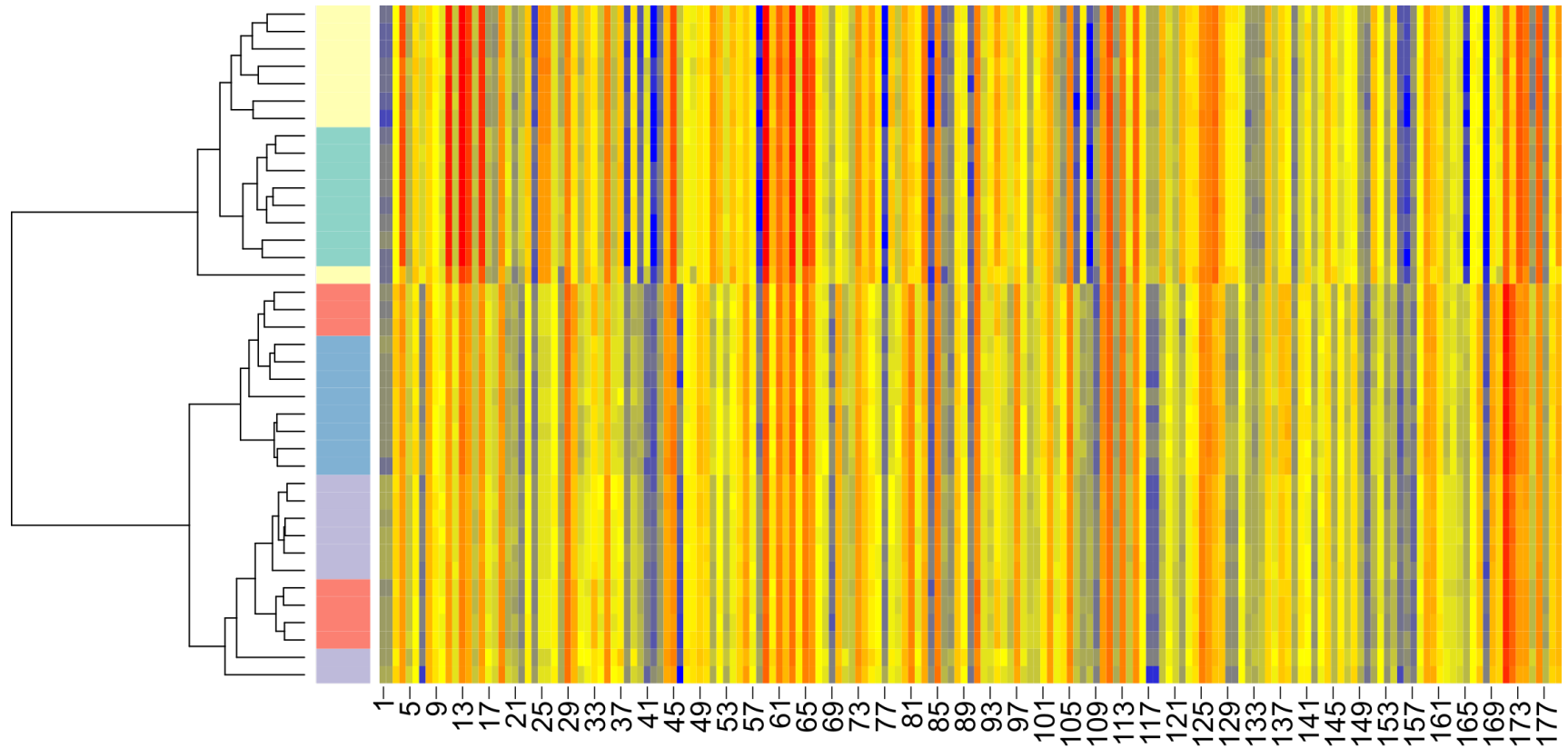


Figure 3-12: (cont.)



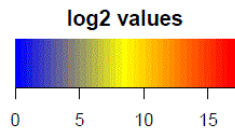
**Figure 3-14: Heatmap of INH relative to control.**  
 Clustered heatmap shows the 91 loci with a p-value of <0.05. Coloured bars show experimental groups: green=TP vehicle control; yellow=TP; purple=control; red=INH; blue=PYR.



## Loci Number

**Figure 3-15: Heatmap of PYR relative to control.**

Clustered heatmap shows the 179 loci with a  $p$ -value of  $<0.05$ . Coloured bars show experimental groups: green=TP vehicle control; yellow=TP; purple=control; red=INH; blue=PYR. Numbered loci are defined in Table 3-3.





No.	Loc	No.	Loc	No.	Loc	No.	Loc	No.	Loc	No.	Loc	No.	Loc	No.	Loc	No.	Loc
1	dre-let-7c-3p	21	dre-miR-125b-3-3p	41	dre-miR-1388-5p	61	dre-miR-181b-5p	81	dre-miR-200b-3p	101	dre-miR-222a-3p	121	dre-miR-301c-3p	141	dre-miR-430b-5p	161	dre-miR-726
2	dre-let-7d-3p	22	dre-miR-125b-5p	42	dre-miR-139-3p	62	dre-miR-181c-5p	82	dre-miR-203b-5p	102	dre-miR-222a-5p	122	dre-miR-301c-5p	142	dre-miR-430c-3p	162	dre-miR-727-3p
3	dre-let-7e	23	dre-miR-125c-3p	43	dre-miR-141-3p	63	dre-miR-182-3p	83	dre-miR-204-3-3p	103	dre-miR-223	123	dre-miR-30a-5p	143	dre-miR-451	163	dre-miR-727-5p
4	dre-miR-100-2-3p	24	dre-miR-125c-5p	44	dre-miR-141-5p	64	dre-miR-182-5p	84	dre-miR-204-5p	104	dre-miR-22a-3p	124	dre-miR-30b	144	dre-miR-454a	164	dre-miR-729
5	dre-miR-100-5p	25	dre-miR-126a-5p	45	dre-miR-143	65	dre-miR-183-5p	85	dre-miR-205-3p	105	dre-miR-22a-5p	125	dre-miR-30c-5p	145	dre-miR-455-2-5p	165	dre-miR-733
6	dre-miR-101a	26	dre-miR-126b-3p	46	dre-miR-144-3p	66	dre-miR-184	86	dre-miR-205-5p	106	dre-miR-22b-3p	126	dre-miR-30d	146	dre-miR-455-3p	166	dre-miR-734
7	dre-miR-101b	27	dre-miR-126b-5p	47	dre-miR-145-3p	67	dre-miR-187	87	dre-miR-206-5p	107	dre-miR-22b-5p	127	dre-miR-30e-3p	147	dre-miR-455-5p	167	dre-miR-737-3p
8	dre-miR-103	28	dre-miR-128-3p	48	dre-miR-145-5p	68	dre-miR-18a	88	dre-miR-20a-5p	108	dre-miR-23b-5p	128	dre-miR-30e-5p	148	dre-miR-456	168	dre-miR-737-5p
9	dre-miR-107a-3p	29	dre-miR-128-5p	49	dre-miR-148	69	dre-miR-18b-5p	89	dre-miR-20b-3p	109	dre-miR-25-3p	129	dre-miR-338	149	dre-miR-457b-3p	169	dre-miR-7a
10	dre-miR-107b	30	dre-miR-129-3p	50	dre-miR-152	70	dre-miR-18c	90	dre-miR-20b-5p	110	dre-miR-25-5p	130	dre-miR-338-3p	150	dre-miR-457b-5p	170	dre-miR-7b
11	dre-miR-10a-3p	31	dre-miR-129-5p	51	dre-miR-153a-3p	71	dre-miR-193b-3p	91	dre-miR-21	111	dre-miR-26a-3p	131	dre-miR-34a	151	dre-miR-459-3p	171	dre-miR-92a-2-5p
12	dre-miR-10a-5p	32	dre-miR-130b	52	dre-miR-153b-3p	72	dre-miR-196a-3p	92	dre-miR-210-3p	112	dre-miR-26a-5p	132	dre-miR-34c-3p	152	dre-miR-459-5p	172	dre-miR-92a-3p
13	dre-miR-10b-5p	33	dre-miR-132-3p	53	dre-miR-15a-5p	73	dre-miR-199-3-3p	93	dre-miR-210-5p	113	dre-miR-26b	133	dre-miR-34c-5p	153	dre-miR-460-5p	173	dre-miR-92a-5p
14	dre-miR-10c-3p	34	dre-miR-133a-2-5p	54	dre-miR-15b-5p	74	dre-miR-199-5p	94	dre-miR-212-5p	114	dre-miR-27b-3p	134	dre-miR-363-3p	154	dre-miR-462	174	dre-miR-93
15	dre-miR-10c-5p	35	dre-miR-133a-3p	55	dre-miR-15c	75	dre-miR-19b-3p	95	dre-miR-2188-3p	115	dre-miR-27b-5p	135	dre-miR-363-5p	155	dre-miR-7132-3p	175	dre-miR-9-3p
16	dre-miR-10d-5p	36	dre-miR-133a-5p	56	dre-miR-16b	76	dre-miR-19c-3p	96	dre-miR-2188-5p	116	dre-miR-27d	136	dre-miR-365	156	dre-miR-7132-5p	176	dre-miR-9-4-3p
17	dre-miR-124-4-5p	37	dre-miR-133b-3p	57	dre-miR-16c-3p	77	dre-miR-19d-3p	97	dre-miR-218a	117	dre-miR-29b	137	dre-miR-375	157	dre-miR-7148-5p	177	dre-miR-9-5p
18	dre-miR-124-5p	38	dre-miR-133c-3p	58	dre-miR-1788-5p	78	dre-miR-19d-5p	98	dre-miR-218b	118	dre-miR-29b3-3p	138	dre-miR-430a-3p	158	dre-miR-722	178	dre-miR-9-7-3p
19	dre-miR-125b-1-3p	39	dre-miR-133c-5p	59	dre-miR-181a-3p	79	dre-miR-200a-3p	99	dre-miR-2191	119	dre-miR-301a	139	dre-miR-430a-5p	159	dre-miR-724	179	dre-miR-99
20	dre-miR-125b-2-3p	40	dre-miR-137-5p	60	dre-miR-181a-5p	80	dre-miR-200a-5p	100	dre-miR-221-5p	120	dre-miR-301b-5p	140	dre-miR-430b-3p	160	dre-miR-725-3p		

**Table 3-3: Loci for heatmap of PYR relative to control.**

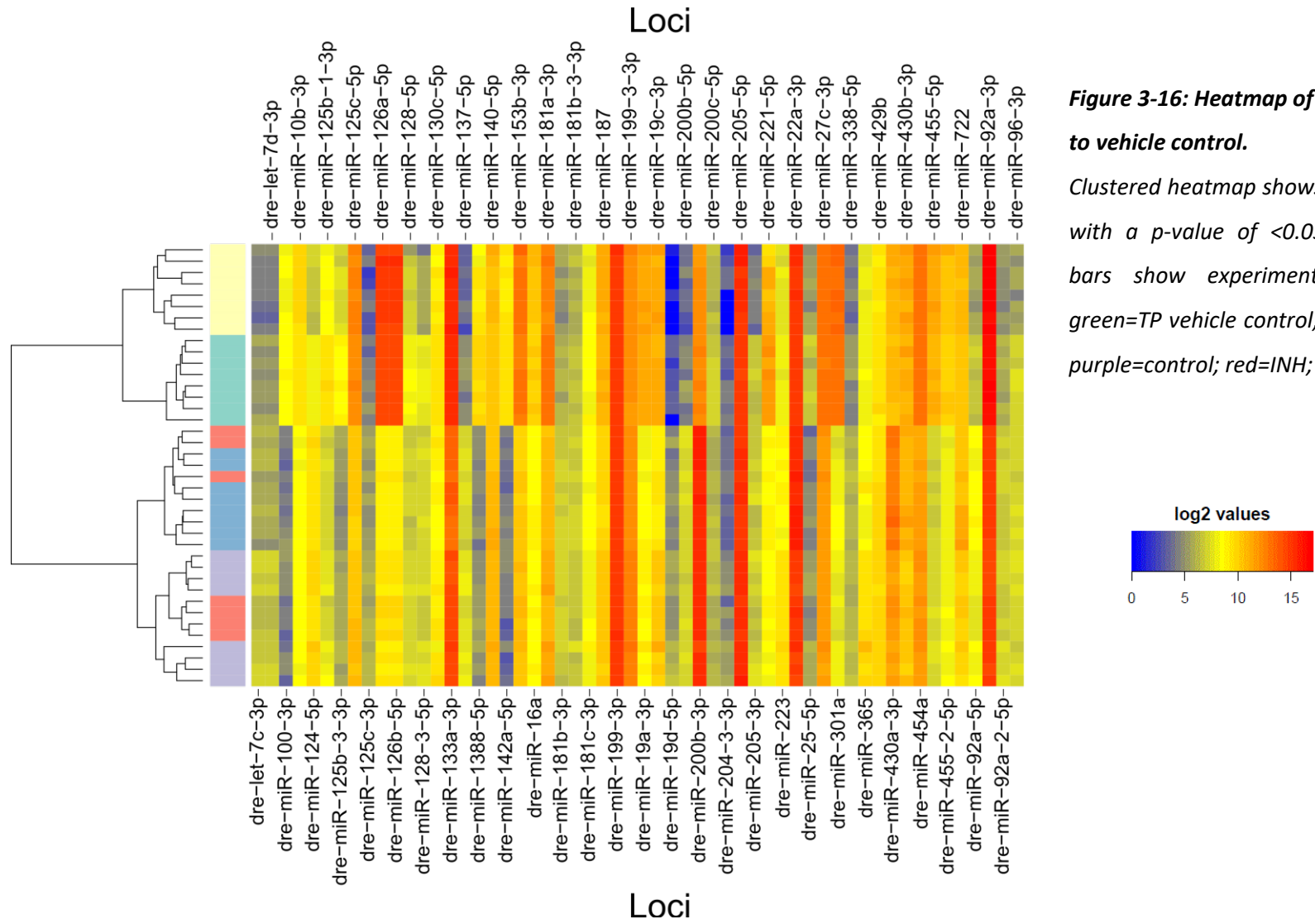


**Figure 3-16: Heatmap of TP relative to vehicle control.**

Clustered heatmap shows the 56 loci with a p-value of <0.05. Coloured bars show experimental groups: green=TP vehicle control; yellow=TP; purple=control; red=INH; blue=PYR.

MiRNA	Fold Change	Adjusted p-value
dre-miR-132-3p	4.11	$2.71 \times 10^{-115}$
dre-miR-132-5p	3.58	$5.35 \times 10^{-7}$
dre-miR-212-5p	3.23	$7.04 \times 10^{-87}$
dre-miR-212	3.12	$1.41 \times 10^{-40}$
dre-miR-212-3p	3.12	$1.41 \times 10^{-40}$
dre-miR-735-3p	2.95	$1.66 \times 10^{-8}$
dre-miR-129-5p	2.64	$5.61 \times 10^{-21}$
dre-miR-146a	2.31	$1.20 \times 10^{-9}$
dre-miR-21	2.25	$2.36 \times 10^{-24}$
dre-miR-735-5p	2.10	0.002
dre-miR-31	2.08	$4.97 \times 10^{-8}$
dre-miR-430a-3p	1.85	$6.00 \times 10^{-5}$
dre-miR-29b	1.73	0.029
dre-miR-29b3-3p	1.73	0.029
dre-miR-9-5p	1.72	$4.5 \times 10^{-4}$
dre-miR-183-5p	1.69	$1.67 \times 10^{-9}$
dre-miR-733	1.66	0.001
dre-miR-182-5p	1.56	$1.52 \times 10^{-7}$
dre-miR-25-5p	-2.48	$2.00 \times 10^{-9}$
dre-miR-92b-5p	-2.31	0.007
dre-miR-2188-3p	-2.20	$1.43 \times 10^{-13}$
dre-miR-19d-5p	-2.07	$9.22 \times 10^{-7}$
dre-miR-17a-2-3p	-1.99	0.030
dre-miR-125b-1-3p	-1.95	$1.16 \times 10^{-14}$
dre-miR-133a-2-5p	-1.92	$7.66 \times 10^{-7}$
dre-miR-133a-5p	-1.92	$7.66 \times 10^{-7}$
dre-miR-204-3-3p	-1.85	0.006
dre-let-7c-3p	-1.76	$1.24 \times 10^{-5}$
dre-let-7d-3p	-1.76	$1.24 \times 10^{-5}$
dre-miR-205-3p	-1.75	$4.9 \times 10^{-7}$
dre-miR-206-5p	-1.73	0.003
dre-miR-181a-3p	-1.71	$5.46 \times 10^{-19}$
dre-miR-19d-3p	-1.62	0.009
dre-miR-1788-5p	-1.61	0.011
dre-miR-142a-3p	-1.57	0.035
dre-miR-459-3p	-1.57	$1.45 \times 10^{-8}$
dre-miR-137-5p	-1.57	$5.98 \times 10^{-8}$
dre-miR-365	-1.56	0.036
dre-miR-725-5p	-1.52	0.002
dre-miR-19b-3p	-1.51	0.012
dre-miR-194a	-1.50	$2.99 \times 10^{-6}$

**Table 3-4: Statistically significantly changed miRNAs: INH relative to control.**

*MiRNAs with an adjusted p-value <0.05 with a 1.5-fold or greater change in expression are listed.*

MiRNA	Fold Change	Adjusted p-value	MiRNA	Fold Change	Adjusted p-value
dre-miR-144-3p	3.39	$6.71 \times 10^{-5}$	dre-miR-133b-3p	-3.68	$1.75 \times 10^{-10}$
dre-miR-430a-3p	2.46	$2.14 \times 10^{-17}$	dre-miR-204-3-3p	-2.79	$1.24 \times 10^{-8}$
dre-miR-9-5p	2.22	$2.66 \times 10^{-26}$	dre-miR-1788-5p	-2.50	$1.24 \times 10^{-17}$
dre-miR-183-5p	1.95	$3.01 \times 10^{-29}$	dre-miR-19d-5p	-2.45	$1.61 \times 10^{-9}$
dre-miR-182-5p	1.93	$1.57 \times 10^{-21}$	dre-miR-365	-2.33	$3.62 \times 10^{-9}$
dre-miR-153a-3p	1.93	$1.71 \times 10^{-4}$	dre-miR-19d-3p	-2.31	$1.42 \times 10^{-17}$
dre-miR-218a	1.92	$4.12 \times 10^{-16}$	dre-miR-129-3p	-2.30	$2.67 \times 10^{-5}$
dre-miR-29b	1.87	0.018	dre-miR-19c-3p	-2.23	$5.09 \times 10^{-15}$
dre-miR-29b3-3p	1.87	0.018	dre-let-7c-3p	-2.22	$3.69 \times 10^{-12}$
dre-miR-9-3p	1.84	$4.18 \times 10^{-24}$	dre-let-7d-3p	-2.22	$3.69 \times 10^{-12}$
dre-miR-722	1.83	$4.58 \times 10^{-5}$	dre-miR-133a-2-5p	-2.20	$4.49 \times 10^{-41}$
dre-miR-338	1.79	$8.06 \times 10^{-4}$	dre-miR-133a-5p	-2.20	$4.49 \times 10^{-41}$
dre-miR-338-3p	1.79	$8.06 \times 10^{-4}$	dre-miR-25-5p	-2.10	$1.21 \times 10^{-8}$
dre-miR-430c-3p	1.78	0.002	dre-miR-133a-3p	-1.95	$6.48 \times 10^{-11}$
dre-miR-30e-5p	1.76	0.002	dre-miR-206-5p	-1.93	0.002
dre-miR-196a-3p	1.75	$8.74 \times 10^{-17}$	dre-miR-34c-3p	-1.91	$5.65 \times 10^{-7}$
dre-miR-430b-3p	1.72	$6.91 \times 10^{-6}$	dre-miR-19b-3p	-1.88	$3.31 \times 10^{-10}$
dre-miR-9-4-3p	1.69	$2.33 \times 10^{-35}$	dre-miR-430a-5p	-1.87	$8.76 \times 10^{-17}$
dre-miR-459-5p	1.69	$6.93 \times 10^{-4}$	dre-miR-7132-5p	-1.85	0.003
dre-miR-30d	1.65	$3.20 \times 10^{-21}$	dre-miR-727-5p	-1.84	$1.48 \times 10^{-7}$
dre-miR-15a-5p	1.64	0.002	dre-miR-20b-3p	-1.83	$7.10 \times 10^{-7}$
dre-miR-10d-5p	1.63	$1.38 \times 10^{-20}$	dre-miR-223	-1.83	$3.95 \times 10^{-10}$
dre-miR-218b	1.62	0.001	dre-miR-193b-3p	-1.81	0.010
dre-miR-363-3p	1.61	$2.86 \times 10^{-9}$	dre-miR-729	-1.78	$6.08 \times 10^{-8}$
dre-miR-10b-5p	1.60	$1.72 \times 10^{-20}$	dre-miR-125c-3p	-1.78	$2.18 \times 10^{-6}$
dre-miR-22a-3p	1.60	$1.82 \times 10^{-8}$	dre-miR-125b-3-3p	-1.74	$1.22 \times 10^{-5}$
dre-miR-7148-5p	1.60	0.003	dre-miR-133c-3p	-1.71	$3.73 \times 10^{-4}$
dre-miR-9-7-3p	1.58	$5.12 \times 10^{-24}$	dre-miR-139-3p	-1.67	0.026
dre-miR-101b	1.58	0.023	dre-miR-125b-1-3p	-1.66	$4.49 \times 10^{-12}$
dre-miR-200a-5p	1.58	$5.07 \times 10^{-5}$	dre-miR-107a-3p	-1.63	$9.22 \times 10^{-11}$
dre-miR-222a-5p	1.55	$2.08 \times 10^{-13}$	dre-miR-145-5p	-1.63	$8.13 \times 10^{-4}$
dre-miR-101a	1.55	$3.19 \times 10^{-5}$	dre-miR-459-3p	-1.62	$1.03 \times 10^{-11}$
dre-miR-210-3p	1.54	$8.54 \times 10^{-10}$	dre-miR-181a-3p	-1.62	$6.52 \times 10^{-20}$
dre-miR-18b-5p	1.54	0.012	dre-miR-2188-3p	-1.53	$2.78 \times 10^{-6}$
dre-miR-129-5p	1.53	$2.56 \times 10^{-18}$	dre-miR-737-3p	-1.52	0.049
			dre-miR-23b-5p	-1.51	0.003
			dre-miR-30b	-1.50	$4.26 \times 10^{-8}$

**Table 3-5: Statistically significantly changed miRNAs: PYR relative to control.**

MiRNAs with an adjusted p-value <0.05 with a 1.5-fold or greater change in expression are listed.

MiRNA	Fold Change	Adjusted p-value
dre-miR-301b-3p	4.53	0.002
dre-miR-144-3p	2.83	0.009
dre-miR-92b-5p	2.14	0.005
dre-miR-459-5p	2.11	0.001
dre-miR-153a-3p	1.98	0.003
dre-miR-301c-3p	1.88	0.002
dre-miR-18b-5p	1.86	0.019
dre-miR-30e-5p	1.83	0.005
dre-miR-142a-3p	1.79	0.014
dre-miR-15a-5p	1.68	0.003
dre-miR-18a	1.67	$4.10 \times 10^{-4}$
dre-miR-338	1.62	0.030
dre-miR-338-3p	1.62	0.030
dre-miR-216b	1.62	0.039
dre-miR-301a	1.60	0.004
dre-miR-430c-3p	1.54	0.030
dre-miR-722	1.52	0.026
dre-miR-101a	1.50	0.003
dre-miR-216a	1.50	0.030
dre-miR-212	-3.86	$9.82 \times 10^{-60}$
dre-miR-212-3p	-3.86	$9.82 \times 10^{-60}$
dre-miR-132-5p	-3.58	$1.30 \times 10^{-5}$
dre-miR-129-3p	-2.97	$3.53 \times 10^{-6}$
dre-miR-738	-2.93	0.015
dre-miR-132-3p	-2.85	$4.24 \times 10^{-46}$
dre-miR-212-5p	-2.57	$3.81 \times 10^{-33}$
dre-miR-133b-3p	-2.35	0.006
dre-miR-735-3p	-2.14	$7.93 \times 10^{-4}$
dre-miR-146a	-2.13	$1.04 \times 10^{-6}$
dre-miR-23a-5p	-1.92	0.002
dre-miR-735-5p	-1.92	0.027
dre-miR-21	-1.89	$1.65 \times 10^{-21}$
dre-miR-31	-1.79	$4.71 \times 10^{-5}$
dre-miR-129-5p	-1.74	$4.01 \times 10^{-7}$
dre-miR-430a-5p	-1.74	$1.02 \times 10^{-4}$
dre-miR-34c-3p	-1.71	0.010
dre-miR-19c-3p	-1.67	0.009
dre-miR-7132-5p	-1.63	0.037
dre-miR-1388-5p	-1.56	0.024
dre-miR-223	-1.56	0.003
dre-miR-133a-3p	-1.55	0.011
dre-miR-22a-5p	-1.50	$1.78 \times 10^{-6}$
dre-miR-202-5p	-1.50	0.028
dre-miR-125b-3-3p	-1.50	0.004

**Table 3-6: Statistically significantly changed miRNAs: PYR relative to INH.**

MiRNAs with an adjusted p-value <0.05 with a 1.5-fold or greater change in expression are listed.

MiRNA	Fold Change	Adjusted p-value
dre-miR-19d-5p	-7.84	$4.22 \times 10^{-3}$
dre-miR-205-3p	-5.35	$3.11 \times 10^{-24}$
dre-miR-128-3-5p	-4.79	$3.11 \times 10^{-24}$
dre-miR-204-3-3p	-3.46	$6.73 \times 10^{-3}$
dre-miR-96-3p	-3.23	$5.28 \times 10^{-22}$
dre-miR-128-5p	-2.81	$1.89 \times 10^{-12}$
dre-miR-125b-3-3p	-2.57	$9.70 \times 10^{-26}$
dre-miR-25-5p	-2.55	$2.13 \times 10^{-9}$
dre-miR-137-5p	-2.55	$1.69 \times 10^{-4}$
dre-miR-124-5p	-2.22	$1.38 \times 10^{-12}$
dre-miR-92a-5p	-2.20	$7.32 \times 10^{-10}$
dre-miR-338-5p	-2.06	$2.99 \times 10^{-3}$
dre-miR-125c-3p	-2.04	$3.15 \times 10^{-2}$
dre-miR-200b-5p	-2.01	$2.23 \times 10^{-2}$
dre-miR-92a-2-5p	-1.98	$8.14 \times 10^{-5}$
dre-miR-125b-1-3p	-1.98	$3.88 \times 10^{-14}$
dre-miR-221-5p	-1.81	$2.42 \times 10^{-31}$
dre-let-7c-3p	-1.69	$2.35 \times 10^{-2}$
dre-let-7d-3p	-1.69	$2.35 \times 10^{-2}$
dre-miR-1388-5p	-1.68	$2.18 \times 10^{-4}$
dre-miR-200c-5p	-1.63	$1.03 \times 10^{-5}$
dre-miR-181b-3p	-1.63	$2.35 \times 10^{-2}$
dre-miR-181a-3p	-1.53	$1.65 \times 10^{-5}$

**Table 3-7: Statistically significantly changed miRNAs: TP relative to vehicle control.**

MiRNAs with an adjusted p-value <0.05 with a 1.5-fold or greater change in expression are listed.

KEGG pathway (associated miRNAs)	p-value	Gene symbol	Gene description
<b>ECM-receptor interaction</b> (dre-miR-735-3p, dre-miR-29b, dre-miR-183-5p)	<math>1 \times 10^{-325}</math>	COL4A5	Collagen, type IV, alpha 5
		COL1A2	Collagen, type I, alpha 2
		COL1A1B	Collagen, type I, alpha 1b
		COL5A2	Collagen, type V, alpha 2
		LAMC1	Laminin gamma 1
		COL2A1A	Collagen, type II, alpha 1
		COL1A1A	Collagen, type I, alpha 1a
<b>Mucin type O-Glycan biosynthesis</b> (dre-miR-146a, dre-miR-182-5p)	$2.22 \times 10^{-16}$	POC1B1	POC1 centrilobular protein homolog B
		GALNT2	Polypeptide N-acetylgalactosaminyltransferase 2
		GALNT8	Polypeptide N-acetylgalactosaminyltransferase 8b
		WBSCR17	Polypeptide N-acetylgalactosaminyltransferase 17
<b>Metabolism of xenobiotics by cytochrome P450</b> (dre-miR-735-5p)	$4.22 \times 10^{-7}$	MGST2	Microsomal glutathione S-transferase 2
<b>Glycosphingolipid biosynthesis - lacto and neolacto series</b> (dre-miR-182-5p)	0.008	B3GNT5A	UDP-GlcNAc:betaGal beta-1,3-N-acetylglucosaminyltransferase 5a
		FUT9A	Fucosyltransferase 9a
<b>Steroid hormone biosynthesis</b> (dre-miR-132-3p, dre-miR-212)	0.012	CYP19A1B	Cytochrome P450, family 19, subfamily A, polypeptide 1b
		CYP17A1	Cytochrome P450, family 17, subfamily A, polypeptide 1
<b>Other types of O-glycan biosynthesis</b> (dre-miR-132-3p, dre-miR-212)	0.030	POMT1	Protein-O-mannosyltransferase 1

**Table 3-8: KEGG pathways: INH relative to control (up-regulated miRNAs).**

KEGG pathways identified from up-regulated miRNAs (>+1.5-fold change), with an adjusted p-value <0.05.

KEGG pathway (associated miRNAs)	p-value	Gene symbol	Gene description
<b>Metabolism of xenobiotics by cytochrome P450</b> (dre-miR-133a-2-5p, dre-miR-133a-5p)	3.33 x 10 <sup>-16</sup>	MGST3	Microsomal glutathione S-transferase 3
<b>ECM-receptor interaction</b> (dre-let-7c-3p, dre-let-7d-3p, dre-miR-205-3p, dre-miR-206-5p, dre-miR-1788-5p)	2.75 x 10 <sup>-09</sup>	COL4A5	Collagen, type IV, alpha 5
		COL1A1B	Collagen, type I, alpha 1b
		COL11A2	Collagen, type XI, alpha 2
		COL6A2	Collagen, type VI, alpha 2
		COL1A1A	Collagen, type I, alpha 1a
<b>Tyrosine metabolism</b> (dre-miR-125b-1-3p, dre-miR-142a-3p, dre-miR-194a)	0.012	COMTA	Catechol-O-methyltransferase a
		ALDH3B1	Aldehyde dehydrogenase 3 family, member B1

**Table 3-9: KEGG Pathways: INH relative to control (down-regulated miRNAs).**

KEGG pathways identified from down-regulated miRNAs (<-1.5-fold change), with an adjusted p-value <0.05.



KEGG pathway (associated miRNAs)	p-value	Gene symbol	Gene description
<b>ECM-receptor interaction</b> (dre-miR-183-5p, dre-miR-153a-3p, dre-miR-29b, dre-miR-459-5p, dre-miR-7148-5p)	<1 x 10 <sup>-325</sup>	COL4A5	Collagen, type IV, alpha 5
		COL1A2	Collagen, type I, alpha 2
		COL1A1B	Collagen, type I, alpha 2b
		CHAD	Chondroadherin
		COL5A2	Collagen, type V, alpha 2
		LAMC1	Laminin gamma 1
		COL6A2	Collagen, type VI, alpha 2
		COL2A1A	Collagen, type II, alpha 1
		COL1A1A	Collagen, type I, alpha 1
<b>Mucin type O-Glycan biosynthesis</b> (dre-miR-182-5p, dre-miR-722, dre-miR-30e-5p, dre-miR-30d, dre-miR-22a-5p)	1.58 x 10 <sup>-14</sup>	C1GALT1C1	C1GALT1-specific chaperone 1
		GALNTL6	Polypeptide N-acetylgalactosaminyl-transferase like 6
		GALNT8	Polypeptide N-acetylgalactosaminyl-transferase 8
		GALNT1	Polypeptide N-acetylgalactosaminyl-transferase 1
		GALNT2	Polypeptide N-acetylgalactosaminyl-transferase 2
		GALNT7	Polypeptide N-acetylgalactosaminyl-transferase 7
		POC1B1	POC1 centrilobular protein homolog B
<b>Biosynthesis of unsaturated fatty acids</b> (dre-miR-722, dre-miR-15a-5p, dre-miR-7148-5p)	2.62 x 10 <sup>-9</sup>	PTP1B	3-hydroxylacyl-CoA dehydratase
		PECR	Peroxisomal trans-2-enoyl-CoA reductase
		ELOVL6	ELOVL fatty acid elongase 6
		HSD17B12A	Hydroxysteroid (17-beta) dehydrogenase 12a
		HSB17B12B	Hydroxysteroid (17-beta) dehydrogenase 12b
		SCDB	Stearoyl-CoA desaturase b
		TECRA	Trans-2,3-enoyl-CoA reductase a
		ELOVL2	ELOVL fatty acid elongase 2
<b>Lysine degradation</b> (dre-miR-430a-3p, dre-miR-153a-3p, dre-miR-29b, dre-miR-430c-3p, dre-miR-430b-3p, dre-miR-363-3p)	0.002	KMT2BB	Lysine (K)-specific methyltransferase 2Bb
		DOT1L	DOT1-like histone H3K79 methyltransferase
		HADHAB	Hydroxyacyl-CoA dehydrogenase trifunctional multienzyme complex subunit alpha b
		TMLHE	Trimethyllysine hydroxylase, epsilon
		SETD7	SET domain containing 7, histone lysine methyltransferase
		ALDH7A1	Aldehyde dehydrogenase 7 family, member A1
		KMT2A	Lysine (K)-specific methyltransferase 2A
		EHMT1B	Euchromatic histone-lysine N-methyltransferase 1b
<b>Valine, leucine and isoleucine degradation</b> (dre-miR-218a, dre-miR-459-5p, dre-miR-218b)	0.024	HSD17B10	Hydroxysteroid (17-beta) dehydrogenase 10
		ACAT1	Acetyl-CoA acetyltransferase 1
		ACAD8	Acyl-CoA dehydrogenase family, member 8
		BCAT2	Branched chain amino-acid transaminase 2, mitochondrial
		BCKDHA	Branched chain keto acid dehydrogenase E1 subunit alpha
		BCAT1	Branched chain amino-acid transaminase 1, cytosolic

**Table 3-10: KEGG pathways: PYR relative to control (up-regulated miRNAs).**

KEGG pathways identified from up-regulated miRNAs (>+1.5-fold change), with an adjusted p-value <0.05.

KEGG pathway (associated miRNAs)	p-value	Gene symbol	Gene description
<b>Metabolism of xenobiotics by cytochrome P450</b> (dre-miR-133a-2-5p, dre-miR-133a-5p, dre-miR-145-5p)	1.11 x 10 <sup>-16</sup>	MGST3	Microsomal glutathione S-transferase 3
		MGST2	Microsomal glutathione S-transferase 2
<b>Mucin type O-Glycan biosynthesis</b> (dre-miR-133b-3p, dre-miR-19c-3p, dre-miR-133a-3p, dre-miR-19b-3p, dre-miR-133c-3p, dre-miR-30b)	0.005	GALNT7	Polypeptide N-acetylgalactosaminyl-transferase 7
		POC1B1	POC1 centrilobular protein homolog B

**Table 3-11: KEGG pathways: PYR relative to control (down-regulated miRNAs).**

KEGG pathways identified from down-regulated miRNAs (<-1.5-fold change), with an adjusted p-value <0.05.

KEGG pathway (associated miRNAs)	p-value	Gene symbol	Gene description
<b>Biosynthesis of unsaturated fatty acids</b> (dre-miR-15a-5p, dre-miR-722)	2.16 x 10 <sup>-7</sup>	PTPN1	Protein tyrosine phosphatase non-receptor type 1
		ELOVL6	ELOVL fatty acid elongase 6
		HSD17B12A	Hydroxysteroid (17-beta) dehydrogenase 12a
		HSD17B12A	Hydroxysteroid (17-beta) dehydrogenase 12b
		SCDB	Stearoyl-CoA desaturase b
		TECRA	Trans-2,3-enoyl-CoA reductase a
		ELOVL2	ELOVL fatty acid elongase 2
<b>Fatty acid elongation</b> (dre-miR-430c-3p, dre-miR-101a)	8.39 x 10 <sup>-5</sup>	HADHAA	Hydroxyacyl-CoA dehydrogenase trifunctional multienzyme complex subunit alpha a
		ELOVL4B	ELOVL fatty acid elongase 4b
		HADHAB	Hydroxyacyl-CoA dehydrogenase trifunctional multienzyme complex subunit alpha b
<b>Fatty acid degradation</b> (dre-miR-430c-3p, dre-miR-101a)	0.003	ECIL	Enoyl-CoA delta isomerase 1
		HADHAA	Hydroxyacyl-CoA dehydrogenase trifunctional multienzyme complex subunit alpha a
		ACSL3B	Acyl-CoA synthetase long chain family member 3b
		HADHAB	Hydroxyacyl-CoA dehydrogenase trifunctional multienzyme complex subunit alpha b
		ALDH7A1	Aldehyde dehydrogenase 7 family, member A1
<b>Fatty acid metabolism</b> (dre-miR-430c-3p, dre-miR-101a, dre-miR-15a-5p)	0.011	HADHAA	Hydroxyacyl-CoA dehydrogenase trifunctional multienzyme complex subunit alpha a
		ACSL3B	Acyl-CoA synthetase long chain family member 3b
		HADHAB	Hydroxyacyl-CoA dehydrogenase trifunctional multienzyme complex subunit alpha b
		TECRA	Trans-2,3-enoyl-CoA reductase a
<b>Purine metabolism</b> (dre-miR-144-3p, dre-miR-338)	0.013	NT5C2A	5,-nucleotidase, cytosolic IIa
		PAPSS1	3,-phosphoadenosine 5,-phosphosulfate synthase 1
		POLA1	Polymerase (DNA directed), alpha 1
		PNP6	Purine nucleoside phosphorylase 6
		NT5C1BA	5,-nucleotidase, cytosolic IB a
		GUK1A	Guanylate kinase 1a
		NT5C3A	5,-nucleotidase, cytosolic IIIA
		FHIT	Fragile histidine triad diadenosine triphosphatase
		POLR2G1	Polymerase (RNA) II (DNA directed) polypeptide G-like
		ENTPD8	Ectonucleoside triphosphate diphosphohydrolase 8
<b>Mucin type O-Glycan biosynthesis</b> (dre-miR-30e-5p, dre-miR-722, dre-miR-216a)	0.034	C1GALT1C1	C1GALT1-specific chaperone 1
		GALNT18B	N-acetylgalactosaminyltransferase 18b
		GALNT7	N-acetylgalactosaminyltransferase 7
		POC1B1	POC1 centriolar protein homolog B
		GALNT18B	N-acetylgalactosaminyltransferase 1
		GALNT2	N-acetylgalactosaminyltransferase 2

**Table 3-12: KEGG pathways: PYR relative INH (up-regulated miRNAs).**

KEGG pathways identified from up-regulated miRNAs (>+1.5-fold change), with an adjusted p-value <0.05.

KEGG pathway (associated miRNAs)	p-value	Gene symbol	Gene description
<b>Mucin type O-Glycan biosynthesis</b> (dre-miR-133b-3p, dre-miR-146a, dre-miR-19c-3p, dre-miR-133a-3p)	1.23 x 10 <sup>-6</sup>	WBSCR17	Polypeptide N-acetylgalactosaminyltransferase 17
		GALNT7	Polypeptide N-acetylgalactosaminyltransferase 7
		POC1B1	POC1 centriolar protein homolog B
<b>Metabolism of xenobiotics by cytochrome P450</b> (dre-miR-735-5p)	2.26 x 10 <sup>-4</sup>	MGST2	Microsomal glutathione S-transferase 2
<b>Steroid hormone biosynthesis</b> (dre-miR-212, dre-miR-132-3p, dre-miR-34c-3p)	0.001	CYP11A1	Cytochrome P450, family 11, subfamily A, polypeptide 2
		CYP19A1B	Cytochrome P450, family 19, subfamily A, polypeptide 1b
		CYP17A1	Cytochrome P450, family 17, subfamily A, polypeptide 1

**Table 3-13: KEGG pathways: PYR relative to INH (down-regulated miRNAs).**

KEGG pathways identified from down-regulated miRNAs (<-1.5-fold change), with an adjusted p-value <0.05.

KEGG pathway (associated miRNAs)	p-value	Gene symbol	Gene description
<b>Other glycan degradation</b> (dre-miR-205-3p, dre-miR-124-5p)	3.00 x 10 <sup>-4</sup>	GBA2	Glucosidase, beta 2
		NEU1	Neuraminidase 1
<b>Glycosaminoglycan biosynthesis - heparan sulfate / heparin</b> (dre-miR-200b-5p, dre-miR-200c-5p)	7.00 x 10 <sup>-4</sup>	EXT2	Exostosin glycosyltransferase 2
<b>ECM-receptor interaction</b> (dre-miR-205-3p, dre-let-7c-3p, dre-let-7d-3p)	8.80 x 10 <sup>-4</sup>	COL4A5	Collagen, type IV, alpha 5
		COL11A2	Collagen, type I, alpha 2
		ITGB4	Integrin, beta 4
		COL6A2	Collagen, type VI, alpha 2
		COL1A1A	Collagen, type I, alpha 1A
<b>Biosynthesis of unsaturated fatty acids</b> (dre-miR-96-3p, dre-miR-221-5p)	0.03	PTPLA	Protein tyrosine phosphatase-like, member A
		ELOV12	EVOVL fatty acid elongase 2
		ELOV15	EVOVL fatty acid elongase 5

**Table 3-14: KEGG pathways: TP relative to vehicle control.**

KEGG pathways identified using statistically significantly changed (adjusted p-value <0.05) miRNAs with a fold change >1.5.

### 3.3.3 MiRNA changes in specific cell populations:

In order to investigate the miRNA changes occurring in hepatocytes during DILI, larvae were exposed to 1.6  $\mu$ M TP or vehicle control for 6 or 24 hrs. Following digest of the larvae GFP positive and mCherry positive cells were collected by FACS. The transgenic larvae had GFP-tagged hepatocytes, with GFP tagged to liver fatty acid binding protein. Transgenic larvae also had mCherry tagged immune cells, either neutrophils, through tagging of the myeloid-specific peroxidase, or macrophages, through tagging of the macrophage-expressed gene 1. The percentage of live cells was 83-95% and the percentage of GFP positive cells was 2-7% (Figure 3-17 A & B). There was no significant difference in the percentage of live cells and GFP positive cells between the different groups. Median fluorescence intensity of the collected GFP cells was also calculated (Figure 3-17C). Median GFP fluorescence intensity declined with increased exposure time to TP, however, this decline was not significant.

RNA was extracted and quantified from the sorted cells and whole fish controls. The relative gene expression of dre-miR-122-5p, dre-miR-155, dre-miR-124-5p and dre-let-7c-3p was determined by qRT-PCR. The miRNAs dre-miR-124-5p and dre-let-7c-3p were chosen as they had greater than 2-fold changes in expression between treated and control conditions in the small RNA sequencing experiment (Table 3-7). In order to check that the cell populations collected were hepatocytes and immune cells, miRNAs highly expressed in these cell populations were quantified using qRT-PCR.

As previously described, miR-122 is highly specific for, and highly expressed in the liver, making up 70% of hepatocytes miRNA content [87]. The relative gene expression of miR-122 in whole fish, GFP and mCherry positive cells is shown in Figure 3-18A & Figure 3-19A. The relative gene expression of miR-122 was significantly higher in GFP positive cells compared to whole fish within both treatment groups at 6 hrs, (Control  $P=0.0002$ ; TP  $P=0.009$ ) (Figure 3-18A). This difference was demonstrated after 24 hrs exposure in the vehicle control group, ( $P=0.02$ ) (Figure 3-19A). Furthermore, the relative gene expression of miR-122 was significantly higher in GFP positive cells compared to mCherry positive cells within both treatment groups after 6 hrs exposure, (Control  $P<0.0001$ ; TP  $P=0.002$ ) (Figure 3-18A). This difference is again seen after 24 hrs exposure in the vehicle control group, ( $P=0.006$ ) (Figure 3-19A). Therefore, this indicates that the GFP positive cells are hepatocytes as they are

enriched in miR-122. The microRNA miR-155 was used to determine the presence of immune cells. MiR-155 is expressed at high levels in the human spleen and thymus and at lower levels in the liver, lung and kidney [189]. MiR-155 is specific for haemopoietic cells including B-cells, T-cells, monocytes and granulocytes [190] and is part of the primary macrophage response to different types of inflammatory mediators [191]. The relative gene expression of miR-155 is shown in Figure 3-18B & Figure 3-19B. The relative gene expression of miR-155 was significantly higher in mCherry positive cells compared to whole fish at 6 hrs in both treatment groups, (Control  $P=0.0001$ ; TP  $P=0.0004$ ) (Figure 3-18B). In addition, the relative gene expression of miR-155 was significantly higher in mCherry cells compared to GFP positive cells at 6 hrs in both treatment groups, (Control  $P<0.0001$ ; TP  $P=0.0001$ ) (Figure 3-18B). However, this was not demonstrated at 24 hrs (Figure 3-19B). This indicates that mCherry positive cells are immune cells as they are enriched with miR-155. Interestingly, the relative gene expression of miR-124-5p and let-7c-3p were significantly higher in mCherry positive cells compared to GFP positive cells, indicating these miRNAs are significantly enriched in immune cells compared to hepatocytes, (Figure 3-18 C & D) (Figure 3-19 C & D). Statistical analysis did not identify any significant differences between the TP-treated and vehicle controls, when grouped by whole fish or cell type. However, at 6 hrs there is a slight reduction in miR-122 expression in whole fish, hepatocytes and immune cells (Figure 3-18A). MiR-122 further decreases after 24 hrs exposure (Figure 3-19A). MiR-155 expression was slightly increased after exposure to TP, after both 6 and 24 hrs (Figure 3-18B & Figure 3-19B).

The fold change in miRNA expression between treated and vehicle control whole fish, GFP and mCherry positive cell, was then calculated. The fold changes in miRNA expression, after 6 hrs of exposure to TP (1.6  $\mu\text{M}$ ), calculated by qRT-PCR and miRNA-sequencing correlate for whole fish, (Figure 3-20A). Furthermore, the fold changes in miRNA expression correlate for GFP positive cells but not mCherry positive cells (Figure 3-20 B & C). This indicates that the changes seen in the sequencing are largely due to the changes in miRNA expression in hepatocytes.

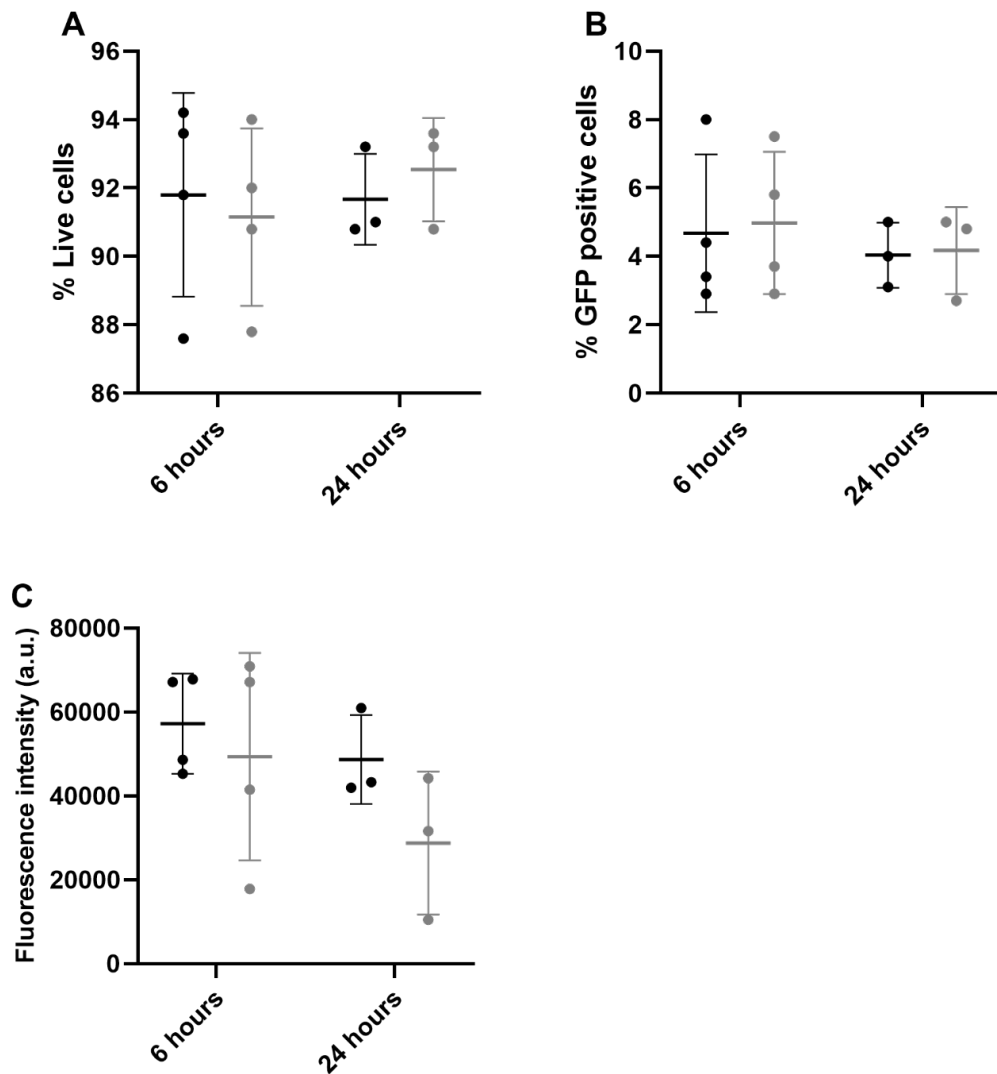


**Figure 3-17: FACS data analysis.**

(A) % Live cells; (B) % GFP positive cells; (C) Median GFP fluorescence intensity (a.u. = arbitrary units). Larvae exposed to vehicle control (black points) or 1.6 μM TP (grey points) for 6 or 24 hrs. Data shown as dot plots. Lines show mean and bars show standard deviation. Statistical significance was determined by two-way ANOVA (all comparisons were not significant).

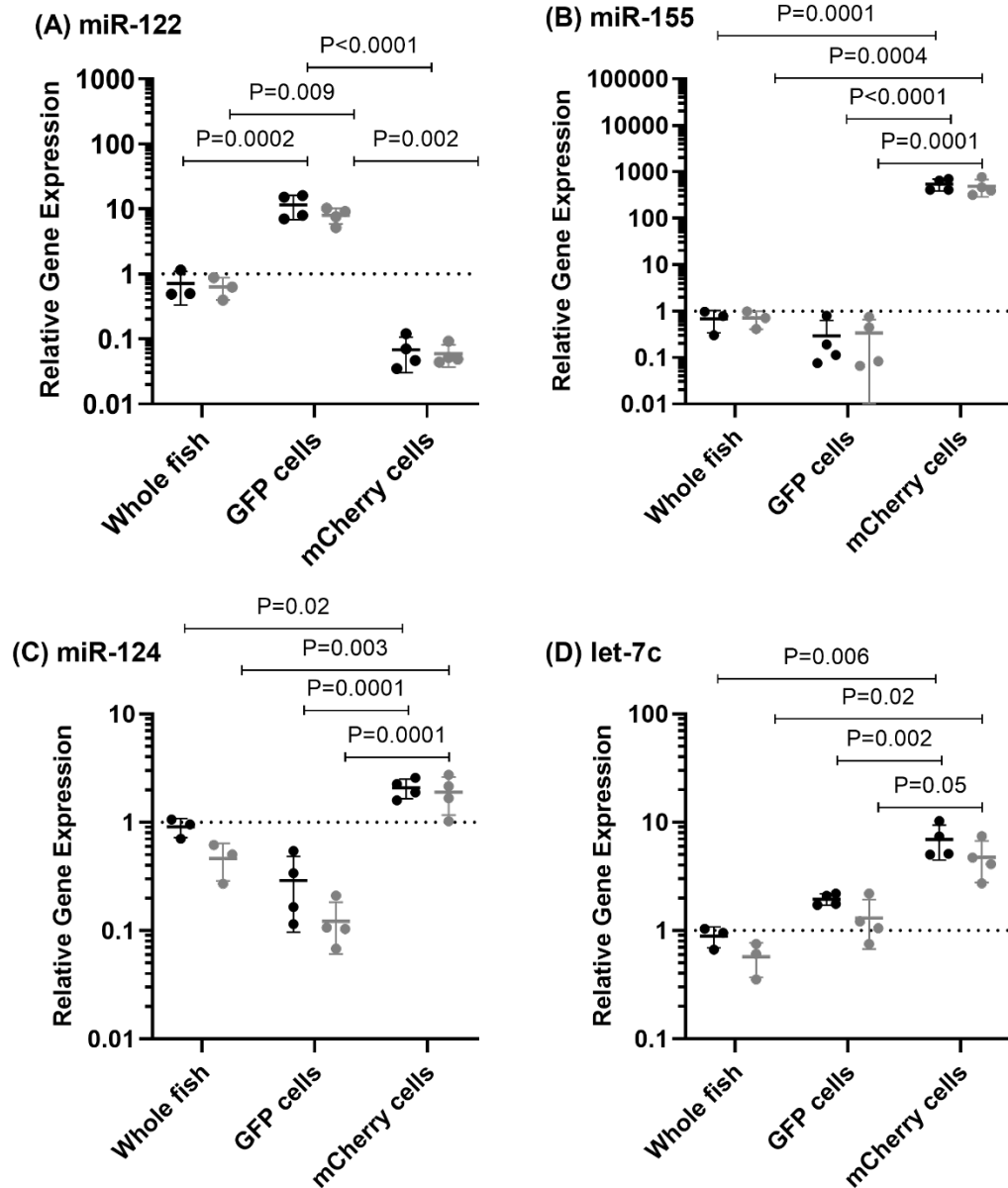


**Figure 3-18: Relative gene expression of miRNAs in TP-exposed larvae and cell populations after 6 hrs.**

Relative gene expression of; (A) miR-122; (B) miR-155; (C) miR-124-5p; (D) let-7c-3p in whole fish, GFP cells and mCherry cells exposed to vehicle control or TP (1.6  $\mu$ M) for 6 hrs. Data shown as dot plots. Black points show vehicle control and grey points show TP-treated experiments. Lines show mean and bars show standard deviation. Data normalised using the  $2^{-\Delta\Delta C_t}$  method, normalising the miRNA of interest to SNORD95 and subsequently to untreated whole fish control. Statistical significance was determined by two-way ANOVA with Sidak's multiple comparisons.



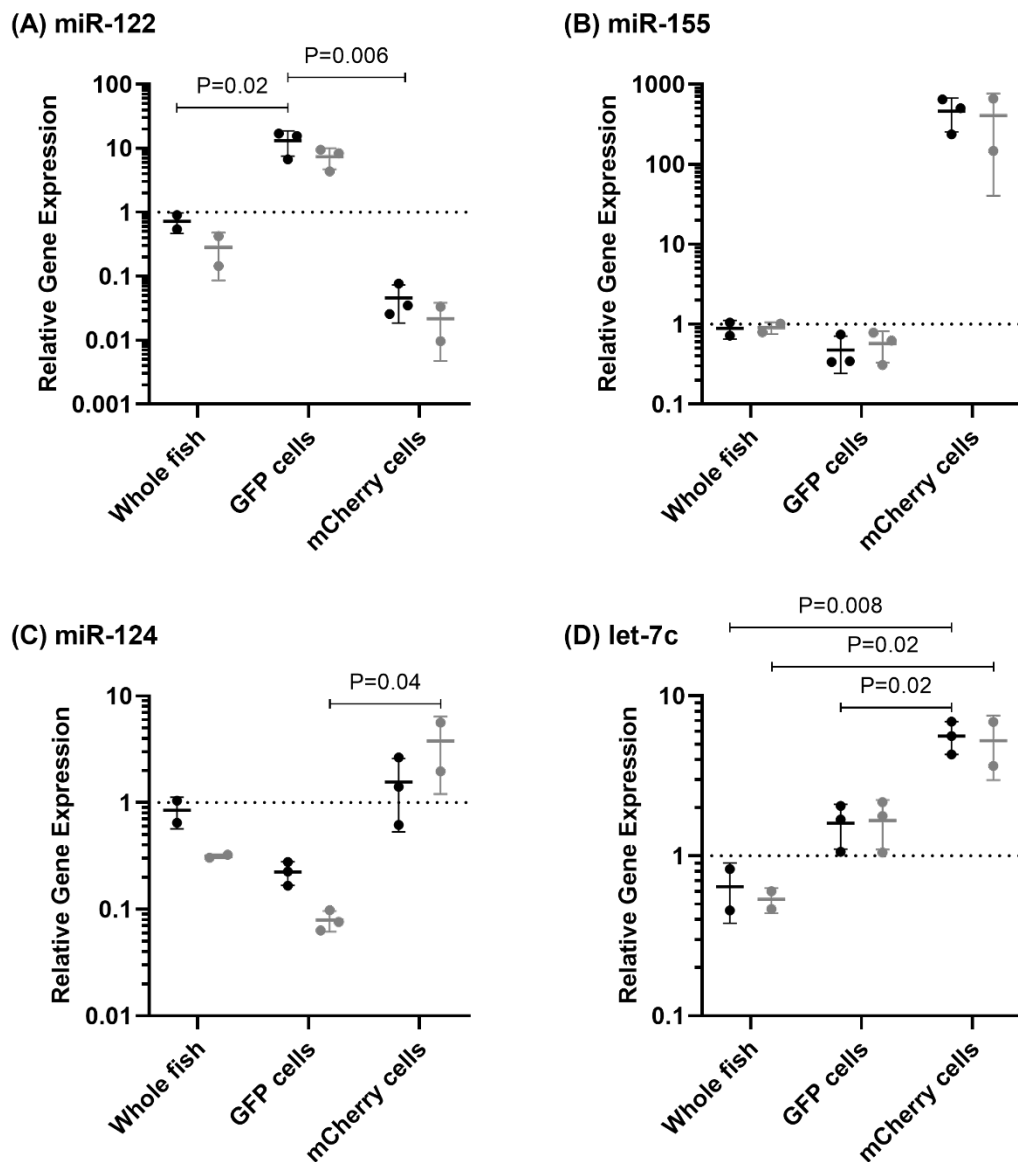


**Figure 3-19: Relative gene expression of miRNAs in TP-exposed larvae and cell populations after 24 hrs.**

Relative gene expression of; (A) miR-122; (B) miR-155; (C) miR-124-5p; (D) let-7c-3p in whole fish, GFP cells and mCherry cells exposed to vehicle control or TP (1.6  $\mu$ M) for 24 hrs. Data shown as dot plots. Black points show vehicle control and grey points show TP-treated experiments. Lines show mean and bars show standard deviation. Data normalised using the  $2^{-\Delta\Delta C_t}$  method, normalising the miRNA of interest to SNORD95 and subsequently to untreated whole fish control. Statistical significance was determined by two-way ANOVA with Sidak's multiple comparisons.

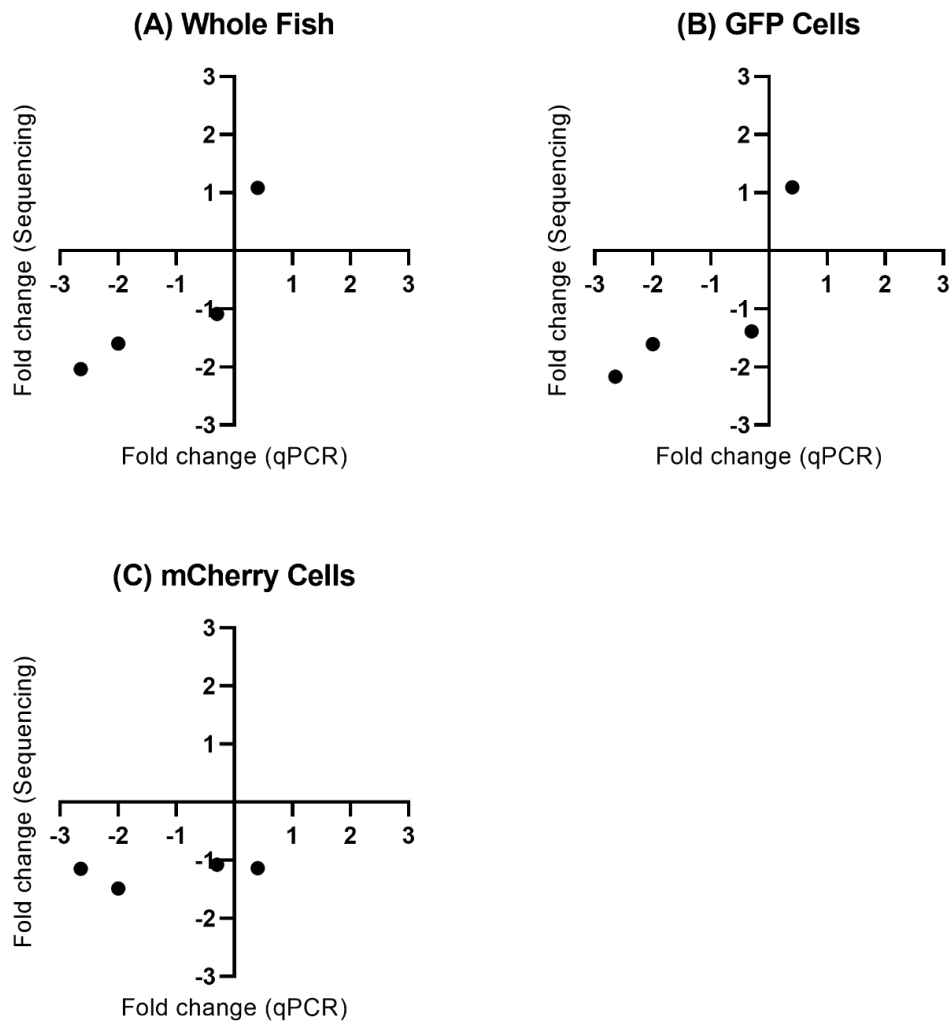


**Figure 3-20: Fold change in miRNA expression in whole fish small RNA sequencing vs qRT-PCR of whole fish and specific cell populations.**

Fold change in miRNA expression in larvae exposed to TP or vehicle control for 6 hrs. Fold change in miRNA expression was quantified using whole fish small RNA sequencing and qRT-PCR of whole fish and specific cell populations. (A) Whole Fish; (B) GFP positive cells; (C) mCherry positive cells. MiRNAs quantified; miR-122, miR-155, miR-124-5p & let-7c-3p.

## 3.3.4 Novel miRNA biomarkers of drug-induced liver injury:

## 3.3.4.1 Identification of novel miRNA biomarkers from small RNA sequencing:

Novel biomarkers of anti-TB and TP liver injury were identified from small RNA sequencing data. The miRNAs which exhibited a 2-fold or greater change in expression in each drug treatment group compared to their control were identified (Table 3-15 & Figure 3-21). In order to determine if these miRNAs can translate into humans their sequences were checked in miRbase. 16 miRNAs had no equivalent human miRNA in the miRbase database. Of the remaining miRNAs 15 had identical sequences to the equivalent human miRNA and the other 26 had a similar sequence, typically differing by 2-3 bases.

	TP vs vehicle control		INH vs Control		PYR vs Control		Identity
	FC	Adj P	FC	Adj P	FC	Adj P	
dre-miR-7146-5p	2.22	0.406	-1.03	0.924	-1.18	0.554	NM
dre-miR-133c-5p	2.07	0.126	-1.05	0.764	-1.25	<b>0.042</b>	NM
dre-miR-19d-5p	-7.84	<b>0.004</b>	-2.07	<b>9.22 x 10<sup>-7</sup></b>	-2.45	<b>1.61 x 10<sup>-9</sup></b>	NM
dre-miR-204-2-3p	-5.82	0.377	-1.48	0.178	-1.69	0.055	SIM
<b>dre-miR-205-3p</b>	-5.35	<b>3.11 x 10<sup>-24</sup></b>	-1.75	<b>4.90 x 10<sup>-7</sup></b>	-1.40	<b>0.010</b>	SIM
dre-miR-128-3-5p	-4.79	<b>3.11 x 10<sup>-24</sup></b>	-1.37	<b>0.003</b>	-1.05	0.614	SIM
dre-miR-92b-5p	-3.97	0.222	-2.31	<b>0.007</b>	-1.05	0.870	SIM
dre-miR-204-3-3p	-3.46	<b>0.007</b>	-1.85	<b>0.006</b>	-2.79	<b>1.24 x 10<sup>-8</sup></b>	NM
dre-miR-96-3p	-3.23	<b>5.28 x 10<sup>-22</sup></b>	-1.10	0.603	-1.04	0.819	SIM
dre-miR-128-5p	-2.81	<b>1.89 x 10<sup>-12</sup></b>	-1.15	0.286	-1.30	<b>0.006</b>	SIM
dre-miR-125b-3-3p	-2.57	<b>9.70 x 10<sup>-26</sup></b>	-1.17	0.284	-1.74	<b>1.22 x 10<sup>-5</sup></b>	SIM
dre-miR-25-5p	-2.55	<b>2.13 x 10<sup>-9</sup></b>	-2.48	<b>2.00 x 10<sup>-9</sup></b>	-2.10	<b>1.21 x 10<sup>-8</sup></b>	SIM
dre-miR-137-5p	-2.55	<b>1.69 x 10<sup>-4</sup></b>	-1.57	<b>5.98 x 10<sup>-8</sup></b>	-1.43	<b>1.63 x 10<sup>-4</sup></b>	SIM
dre-miR-18b-3p	-2.36	0.568	-1.60	0.444	-1.62	0.295	SIM
dre-miR-29b3-5p	-2.31	0.118	-1.05	0.868	-1.21	0.440	SIM
dre-miR-124-5p	-2.22	<b>1.38 x 10<sup>-12</sup></b>	-1.35	<b>1.92 x 10<sup>-8</sup></b>	-1.47	<b>2.19 x 10<sup>-18</sup></b>	ID
dre-miR-92a-5p	-2.20	<b>7.32 x 10<sup>-10</sup></b>	-1.18	0.323	1.20	<b>0.008</b>	SIM
dre-miR-338-5p	-2.06	<b>0.003</b>	-1.06	0.716	-1.17	0.127	SIM
dre-miR-125c-3p	-2.04	<b>0.032</b>	-1.21	0.138	-1.78	<b>2.18 x 10<sup>-6</sup></b>	SIM
dre-miR-200b-5p	-2.01	<b>0.022</b>	1.15	0.229	-1.01	0.910	SIM
dre-miR-2185-3p	1.00	1.00	5.86	0.464	1.00	1.00	NM
<b>dre-miR-132-3p</b>	1.16	0.0707	4.11	<b>2.71 x 10<sup>-115</sup></b>	1.45	<b>9.86 x 10<sup>-8</sup></b>	ID
dre-miR-738	1.08	0.826	3.76	0.051	1.28	0.697	NM
dre-miR-132-5p	1.02	0.954	3.58	<b>5.35 x 10<sup>-7</sup></b>	1.00	0.997	SIM
dre-miR-212-5p	-1.29	0.283	3.23	<b>7.04 x 10<sup>-87</sup></b>	1.27	<b>0.002</b>	ID
dre-miR-212	1.02	0.902	3.12	<b>1.41 x 10<sup>-40</sup></b>	-1.23	<b>0.050</b>	ID
dre-miR-212-3p	1.02	0.902	3.12	<b>1.41 x 10<sup>-40</sup></b>	-1.23	<b>0.050</b>	SIM
dre-miR-735-3p	-1.47	0.223	2.95	<b>1.66 x 10<sup>-8</sup></b>	1.38	0.135	NM
dre-miR-129-5p	1.17	0.181	2.64	<b>5.61 x 10<sup>-21</sup></b>	1.53	<b>2.56 x 10<sup>-18</sup></b>	SIM
<b>dre-miR-146a</b>	-1.26	0.472	2.31	<b>1.20 x 10<sup>-9</sup></b>	1.09	0.567	ID
<b>dre-miR-21</b>	1.02	0.858	2.25	<b>2.36 x 10<sup>-24</sup></b>	1.20	<b>0.004</b>	ID
dre-miR-735-5p	1.27	0.568	2.10	<b>0.002</b>	1.10	0.726	NM
dre-miR-31	1.19	0.581	2.08	<b>4.97 x 10<sup>-8</sup></b>	1.18	0.300	SIM
dre-miR-1788-3p	1.00	0.986	2.06	0.815	1.82	0.842	NM
dre-miR-7133-5p	1.00	1.00	2.01	0.607	1.83	0.631	NM
<b>dre-miR-193a-3p</b>	1.06	0.906	-6.59	0.499	-2.16	0.718	ID
dre-miR-202-3p	1.00	1.00	-3.56	0.603	-3.56	0.636	SIM
dre-miR-301b-3p	1.20	0.151	-2.58	0.183	1.73	0.314	SIM
dre-miR-2188-3p	-1.05	0.560	-2.20	<b>1.43 x 10<sup>-13</sup></b>	-1.53	<b>2.78 x 10<sup>-6</sup></b>	NM
dre-miR-736	1.29	0.473	1.36	0.877	3.58	0.242	NM
dre-miR-144-3p	1.13	0.509	1.20	0.699	3.39	<b>6.71 x 10<sup>-5</sup></b>	ID

	TP vs vehicle control		INH vs Control		PYR vs Control		Identity
	FC	Adj P	FC	Adj P	FC	Adj P	
dre-miR-430i-3p	1.39	0.849	2.00	0.242	2.51	0.050	NM
dre-miR-430a-3p	1.35	<b>9.93 x 10<sup>-4</sup></b>	1.85	<b>6.00 x 10<sup>-5</sup></b>	2.46	<b>2.14 x 10<sup>-17</sup></b>	NM
dre-miR-9-5p	1.09	0.285	1.72	<b>4.50 x 10<sup>-4</sup></b>	2.22	<b>2.66 x 10<sup>-26</sup></b>	ID
<b><u>dre-miR-133b-3p</u></b>	-1.09	0.380	-1.58	0.202	-3.68	<b>1.75 x 10<sup>-10</sup></b>	ID
dre-miR-133b-5p	-1.32	0.387	1.05	0.929	-2.68	0.157	NM
dre-miR-15a-3p	1.48	0.293	1.52	0.849	-2.68	0.721	SIM
dre-miR-1788-5p	1.11	0.933	-1.61	<b>0.011</b>	-2.50	<b>1.24 x 10<sup>-17</sup></b>	NM
<b><u>dre-miR-365</u></b>	-1.25	<b>0.009</b>	-1.56	<b>0.036</b>	-2.33	<b>3.62 x 10<sup>-9</sup></b>	ID
dre-miR-19d-3p	1.28	0.147	-1.62	<b>0.009</b>	-2.31	<b>1.42 x 10<sup>-17</sup></b>	SIM
dre-miR-129-3p	-1.07	0.670	1.28	0.489	-2.30	<b>2.67 x 10<sup>-5</sup></b>	ID
dre-miR-19c-3p	1.25	<b>0.004</b>	-1.34	0.160	-2.23	<b>5.09 x 10<sup>-15</sup></b>	SIM
dre-let-7c-3p	-1.69	<b>0.024</b>	-1.76	<b>1.24 x 10<sup>-5</sup></b>	-2.22	<b>3.69 x 10<sup>-12</sup></b>	ID
dre-let-7d-3p	-1.69	<b>0.024</b>	-1.76	<b>1.24 x 10<sup>-5</sup></b>	-2.22	<b>3.69 x 10<sup>-12</sup></b>	SIM
dre-miR-133a-2-5p	1.06	0.713	-1.92	<b>7.66 x 10<sup>-7</sup></b>	-2.20	<b>4.49 x 10<sup>-41</sup></b>	ID
dre-miR-133a-5p	1.06	0.713	-1.92	<b>7.66 x 10<sup>-7</sup></b>	-2.20	<b>4.49 x 10<sup>-41</sup></b>	ID
dre-miR-181d-3p	1.00	1.00	-1.59	0.856	-2.11	0.725	SIM

**Table 3-15: Novel miRNA biomarkers identified from small RNA sequencing.**

MiRNAs with a fold change of greater than 2-fold were identified from each comparison, TP vs vehicle control, INH vs control and PYR vs control. MiRNAs which have >2 fold upregulation are in green text. MiRNAs with >2 fold downregulation are in red text. MiRNAs with a fold change between -2 and +2 are in black text. Significantly adjusted P-values (<0.05) are shown in bold. MiRNAs which were translated into human ATDILI samples are highlighted in bold and underlined. (FC) Fold change; (Adj P) adjusted P-value; (NM) no match for miRNA in humans; (SIM) similar miRNA found in humans; (ID) identical miRNA sequence in humans.

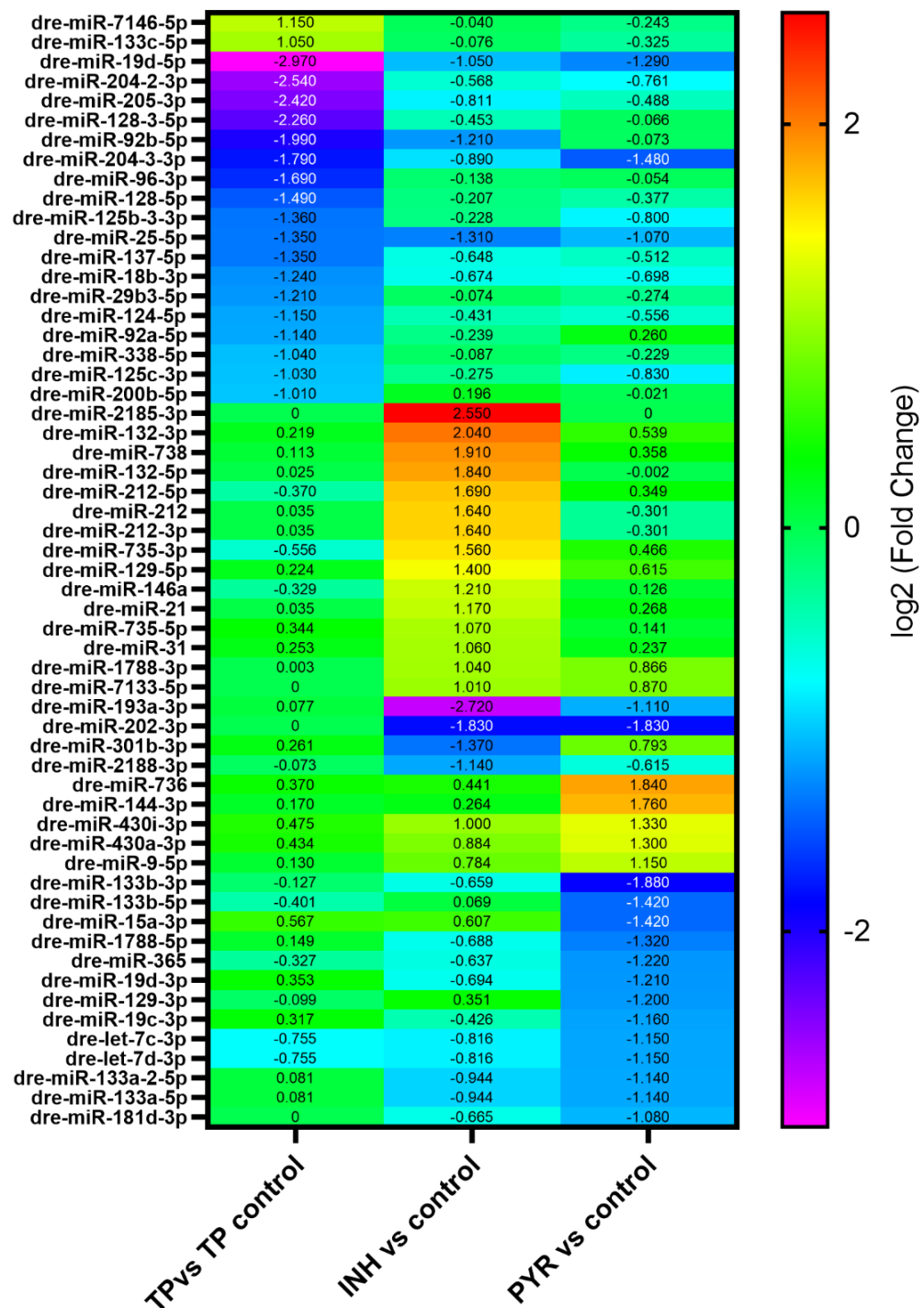


**Figure 3-21: Heatmap of novel miRNA biomarkers of DILI.**

MiRNAs with a fold change of greater than 2-fold were identified from each comparison, TP vs vehicle control, INH vs control and PYR vs control. Heatmap shows  $\log_2(\text{fold change})$  for miRNAs for each comparison.

#### 3.3.4.2 Translation of novel miRNA biomarkers of liver injury into humans:

Several of these identified biomarkers were taken forward and validated in human plasma samples, in ATDILI patients from the ALISTER study, as described in section 2.3.5. Both patients who developed ATDILI were undergoing treatment for latent TB with isoniazid alone. Isoniazid was determined as the probable cause of liver injury. The miRNAs chosen from the zebrafish larvae small RNA sequencing were miR-21 (2.25-fold up regulated in INH DILI), miR-146a (2.31-fold up regulated in INH DILI), miR-132-3p (4-fold up regulated in INH DILI), miR-133b-3p (2.68-fold down regulated in PYR DILI), miR-205-3p (5-fold down regulated in TP DILI), miR-365 (2.33-fold down regulated in PYR DILI) and miR-193a-3p (6.59-fold down regulated in INH DILI and 2.16-fold down regulated in PYR DILI) (Table 3-15). Two of the miRNAs, miR-133b-3p and miR-193a-3p, were below the limit of quantification in the human plasma samples. MiR-21 and miR-146a, which were demonstrated to rise in INH DILI in zebrafish, also increased in the two ALISTER patients who developed DILI caused by INH, (Figure 3-22 A & B). The other miRNAs quantified in the human samples demonstrated differing patterns of expression, and differed from the pattern seen in the zebrafish sequencing data (Figure 3-22 C & D). MiR-365 increased in both patients, rising with ALT, however, in the zebrafish sequencing data miR-365 is down-regulated across all three patterns of liver injury. MiR-132-3p rises with INH induced liver injury in the zebrafish sequencing data but does not rise in the plasma of the ATDILI patients. MiR-205-3p is substantially downregulated in the TP exposed larvae and slightly downregulated in larvae exposed to INH and PYR, however in the patient samples miR-205-3p rose in one patient and fell in the other.

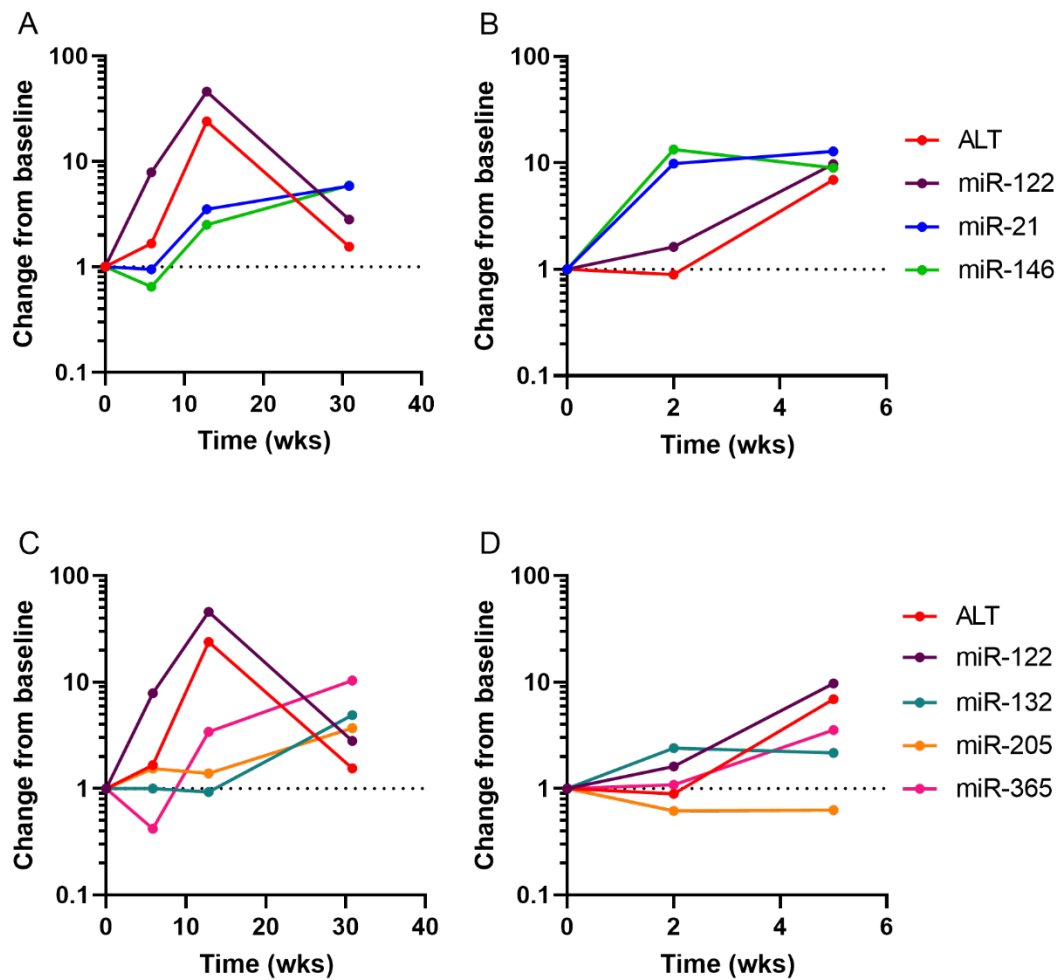


**Figure 3-22: Translation of novel miRNA biomarkers of DILI into human ATDILI samples.**

MiRNAs identified from the zebrafish small RNA sequencing experiment were quantified in human plasma samples from ATDILI patients in the ALISTER study. (A & C) Case 1; (B & D) Case 2. MiRNAs quantified were; miR-122, miR-21, miR-146a, miR-132-3p, miR-205-3p and miR-365. The change from baseline was determined for ALT (IU/L) and the different miRNAs. Time on treatment in weeks (wks).

### 3.4 Discussion:

#### 3.4.1 Main findings:

- The anti-TB drugs INH and PYR cause DILI in zebrafish larvae at mM concentrations.
- Small RNA sequencing identifies miRNA changes in DILI due to INH, PYR and TP. In ATDILI these changes are associated with microsomal enzymes in the liver. In TP-DILI miRNAs are largely down-regulated, fitting with the mechanism of action of TP.
- FACS can be used to sort hepatocytes and immune cells from transgenic larvae, and miRNA expression can be quantified in these cell populations. The miRNA changes identified in TP-DILI were demonstrated in hepatocytes but not immune cells.
- Zebrafish larvae DILI models can be used to identify novel biomarkers of liver injury. Two of these miRNAs, miR-146a and miR-21, increased with elevated ALT in patients with ATDILI.

#### 3.4.2 Isoniazid and pyrazinamide cause liver injury in zebrafish larvae:

INH and PYR induce dose- and time-dependent hepatotoxicity. Morphological abnormalities seen which are associated with DILI include the presence of oedema, yolk sac retention and swim bladder deficiency. These morphological changes in larvae exposed to INH and PYR have been identified in previously published work, with larvae exposed to INH and PYR exhibiting spinal curvature, yolk sac retention, lack of swim bladder, tail bending and shorter body lengths [49], [171]. Furthermore, in larvae exposed to PYR pericardial oedema and liver degeneration was also observed [49]. In this study, INH-exposed larvae demonstrated higher prevalence of these morphological abnormalities compared to PYR-exposed larvae. INH also caused developmental toxicity as demonstrated by curvature of the spine and a reduced larvae size, which was not seen in larvae exposed to PYR. Although zebrafish larvae movement was not measured in this study it was noted that larvae exposed to INH had reduced swimming speeds compared to controls. Reduced locomotor capacity has been identified in larvae exposed to INH in a previous study [171].

In this study, exposure of transgenic larvae to INH and PYR demonstrated a time-dependent reduction in liver size and fluorescence intensity. For larvae exposed to 10 mM INH liver area and liver fluorescence were significantly reduced after exposure for 24 hrs and for larvae exposed to 6 mM PYR a significant reduction was demonstrated after 48 hrs. Recent work



has also demonstrated a dose- and time-dependent reduction in liver size and fluorescence intensity in transgenic zebrafish lines with fluorescent protein (DsRed or eGFP) expression under the *fabp10a* promoter when exposed to INH or PYR [49], [148].

Liver histology demonstrated the formation of vacuoles and hepatocyte necrosis in larvae exposed to INH and PYR, with these features becoming more common with increasing periods of exposure. Previous work has demonstrated similar results, with the presence of loose cell-to-cell contact and large vacuoles in the hepatocytes of larvae exposed to INH [171] and PYR [49]. Histology of liver biopsies from patients with isoniazid-induced liver injury shows hepatocellular necrosis, either in foci or across several lobes of the liver, along with an inflammatory response [29]. The histology of INH-exposed larvae in this study demonstrated a similar pattern of hepatocellular liver injury to that seen in humans.

This study demonstrates that the liver-abundant microRNA miR-122 is reduced after anti-TB drug exposure, with a slight reduction after exposure to INH and significant reduction after exposure to PYR for 48 hrs. This fits with recent work that showed exposure of zebrafish larvae to 6 mM INH for 48 hrs led to a significant reduction in miR-122 concentration [173].

3.4.3 Changes in miRNA expression in anti-tuberculosis drug-induced liver injury are associated with the metabolism of drugs in the liver:

Small RNA sequencing of larvae exposed to INH and PYR enabled identification of changes in miRNA expression associated with DILI. Of all the miRNAs identified approximately 50% were up-regulated and 50% down-regulated after drug exposure. Similarly, for the significantly changed miRNAs with a fold change of >1.5 approximately 50% were up-regulated and 50% down-regulated. PYR exposed larvae had a higher number of significantly, >1.5 fold changed miRNAs compared to INH exposed larvae.

In INH exposed larvae, KEGG analysis identified the metabolism of xenobiotics by cytochrome P450 pathway. The miRNA dre-miR-735-5p was associated with microsomal glutathione S-transferase 2 (MGST2) and dre-miR-133a-5p was associated with microsomal glutathione S-transferase 3 (MGST3). Up-regulation of dre-miR-735-5p potentially leads to the down-regulation of MGST2 due to the mechanism of action of miRNAs. Similarly, the

down-regulation of dre-miR-133a-5p possibly leads to the up-regulation of MGST3. GSTs are phase II enzymes which catalyse the conjugation of glutathione to metabolites, resulting in their detoxification. The up-regulation of GSTs has been identified in mouse models following exposure to xenobiotics and during oxidative stress [192]. Furthermore, GSTs are known to play a role in INH metabolism. Previous work identified the up-regulation of GSTP2, a GST which is a member of the pi class, and also CYP3A, in larvae exposed to INH [171]. In addition, a reduction in glutathione content has also been demonstrated in larvae exposed to INH [173]. Pharmacogenomic data has identified polymorphisms in GST1 as a risk factor for ATDILI [55], [57]. Interestingly, in this study, the changes in miRNAs suggest that MGST2 is down-regulated and MGST3 is up-regulated. However, this study relies on predicted target data and therefore would require experimental validation.

In PYR exposed larvae KEGG analysis identified the metabolism of xenobiotics by cytochrome P450 pathway. This pathway was associated with the down-regulation of dre-miR-133a-5p, dre-miR-133a-5p and dre-miR-145-5p. Similar to INH exposed larvae, the genes associated with this pathway were MGST2 and MGST3. However, as both these genes are associated with down-regulated miRNAs it is likely that both MGST2 and MGST3 are up-regulated in PYR-induced DILI. GSTs have been identified to be up-regulated in the liver of rats exposed to pyrazinamide, with MGST3 shown to be approximately 2-fold up-regulated [50].

3.4.4 Changes in miRNA expression in anti-tuberculosis drug-induced liver injury are associated with further pathways:

There were several further pathways which were identified as being significantly altered in INH-induced liver injury. Pathways associated with up-regulated miRNAs, and therefore which are likely to be down-regulated, include ECM-receptor interaction, mucin type O-glycan biosynthesis, glycosphingolipid biosynthesis, steroid hormone biosynthesis and other types of O-glycan biosynthesis. Pathways associated with down-regulated miRNAs, and therefore which are likely to be up-regulated, include ECM-receptor interaction and tyrosine metabolism.

Several of the genes in the ECM-receptor interaction pathway were associated with both up-regulated and down-regulated miRNAs, including several collagen genes. Therefore, it is possible that the expression of these gene changes little in INH-induced liver injury as the effect of the differences in miRNA expression cancel each other out.

The up-regulation of dre-miR-146a and dre-miR-182-5p is associated the mucin type O-glycan biosynthesis pathway. The mucin type O-glycan biosynthesis pathway is a protein post-translation modification pathway, with O-glycosylation largely occurring in secreted proteins or mucins present on mucosal surfaces. The process is usually associated with development, host-environment interactions and disease pathologies. However, specific patterns of protein glycosylation have been identified in chronic liver diseases such as cirrhosis and hepatocellular carcinoma [193].

The up-regulation of dre-miR-132-3p and dre-miR-212 is associated with the steroid hormone biosynthesis pathway. The cytochrome P450 enzymes CYP19A1B and CYP17A1 were identified as potentially being down-regulated in INH-induced liver injury. Exposure to INH may affect the expression of these enzymes as they are localised to the liver. Previously published work has identified mechanisms of hepatotoxicity for both INH which include induction of oxidative stress, reduced antioxidant capacity, up-regulation of apoptosis and up-regulation of inflammatory cytokines [171], [173].

Several of the miRNAs identified by sequencing as having altered expression in this study following exposure to INH are associated with inflammation, including the up-regulation miR-146 and miR-29, along with down-regulation of let-7, miR-92b and miR-181a. This pattern of miRNA expression changes has been previously identified in zebrafish larvae infected with *Salmonella typhimurium* [194]. Further miRNA expression changes identified in INH exposed larvae by sequencing was the up-regulation of the miR-212 and miR-132. These miRNAs share a common seed sequence and have been associated with regulation of cardiomyocytes [195], brain vascular integrity [196] and memory [197] in mice. Isoniazid treatment in humans is associated with neuropathy, with the most common symptom being tingling in peripheral limbs such as the fingers. The up-regulation of miR-212 and miR-132 may be related to neurotoxicity rather than hepatotoxicity. Several other miRNAs which are

significantly down-regulated in INH exposed larvae are miR-19b and miR-17a. These miRNAs have been associated with cardiac development and function in zebrafish [198], [199].

There were several further pathways which were identified as being significantly altered in PYR-induced liver injury. Pathways associated with up-regulated miRNAs, and therefore which are likely to be down-regulated, include ECM-receptor interaction, mucin type O-glycan biosynthesis, biosynthesis of fatty acids, lysine degradation and valine, leucine and isoleucine degradation. Pathways associated with down-regulated miRNAs, and therefore which are likely to be up-regulated, include mucin type O-glycan biosynthesis.

The down-regulated miRNAs associated with mucin type O-glycan biosynthesis pathway identified the genes GALNT7 and POC1B1. Both these genes were also identified in the up-regulated miRNAs dataset, suggesting that the changes seen in miRNA expression may cancel out each other, resulting in no change in GALNT7 and POC1B1 gene expression.

Mechanisms of PYR hepatotoxicity in zebrafish larvae are less well characterised than for INH but there is evidence that PYR induces oxidative stress and the release of inflammatory cytokines, contributing to apoptosis and liver injury [49].

The validation of the association between significantly changed miRNAs identified in the small RNA sequencing experiment and specific genes and pathways is challenging due to the lack of experimental data. The genes and pathways identified in this study relied on a predicted dataset, assessing the zebrafish genome to identify potential binding sites for the miRNAs. Using the reverse search feature of the DIANA-miRPath software with an experimentally validated dataset (TarBase v7.0) did not generate any experimentally-validated miRNA targets which were associated with the KEGG pathways identified in this study. Earlier work has provided some evidence that the pathways identified in this study are likely to be altered in INH- and PYR-induced liver injury. However, the data linking miRNAs with these specific pathways is lacking.

Despite these limitations, the data collected in this study allows assessment of the miRNA changes seen in INH and PYR DILI. There are some similarities in the miRNA expression

changes identified in INH and PYR DILI. Furthermore, several of the same KEGG pathways and associated genes are the same. Although there are similarities, there are also differences in the patterns of miRNA changes seen, highlighting potentially different mechanisms of liver injury for INH and PYR. These differences may be attributed to the differential metabolism of these drugs in the liver.

These small RNA sequencing data provide an insight into the changes occurring in zebrafish larvae when exposed to INH and PYR. The miRNA changes can be associated with the pathways they affect, enabling a greater understanding of the mechanisms of DILI and potentially highlighting areas for therapeutic interventions to prevent the development of ATDILI.

#### 3.4.5 Triptolide-induced liver injury causes miRNA down-regulation:

Exposure of larvae to TP induces down-regulation of miRNA expression, with significantly changed miRNAs (adjusted  $P < 0.05$ ,  $FC > \pm 1.5$ ) only exhibiting down-regulation. This fits with TP's mechanism of action, that it covalently binds to a subunit of the transcription factor II human complex (TFIIH) resulting in inhibition of RNA polymerase II mediated transcription [181]. Furthermore, this fits with the RNA-sequencing data of the same RNA used for this study. RNA sequencing identified down-regulation of GO and KEGG terms associated with RNA transcription, and up-regulation of GO terms associated with protein synthesis [145].

In this study KEGG analysis of miRNAs altered in TP exposure identified the following pathways; glycan degradation, glycosaminoglycan biosynthesis, ECM receptor interaction and the biosynthesis of unsaturated fatty acids. Previous work, with the RNA sequencing data, identified the up-regulation of pathways involving the ribosome, cardiac muscle contraction, oxidative phosphorylation and steroid hormone biosynthesis, and the down-regulation of notch signalling pathways, progesterone-mediated oocyte maturation, ubiquitin mediated proteolysis and gap junction [145]. There appears to be limited similarity in the KEGG pathways identified from the RNA sequencing and small RNA sequencing data, however, this may be due to the limited data available on the interactions of miRNAs and genes in zebrafish. However, several of the miRNAs which were significantly down-regulated in TP-DILI are associated with cardiac function, including miR-128 [200] and miR-19d [199],

and cardiac muscle contraction was a KEGG pathway identified in the RNA sequencing dataset [145].

Previous work has identified that TP exposure leads to up-regulation of inflammation, including up-regulation of NOS2b, TNF- $\alpha$ , CCR2, IL-10, IL-1b and IL-6 [145]. However, none of the significantly differentially expressed miRNAs were associated with these genes or with inflammation pathways. This may be due to the limited data available on miRNAs, and their associated gene targets, in zebrafish.

3.4.6 FACS can be used to investigate miRNA changes specific to different cell populations:

This study demonstrated that GFP and mCherry positive cells from transgenic larvae can be isolated using FACS. The relative gene expression of miR-122 was higher in GFP positive cells compared to mCherry positive cells and whole larvae, indicating that these cells were hepatocytes. Similarly, for mCherry positive cells, the relative gene expression of miR-155 was higher in these cells than GFP positive cells and whole larvae. The isolation of cells from TP exposed larvae enabled quantification of changes in miRNA expression in hepatocytes and immune cells compared to the whole larvae. Correlation of the changes in these specific cell populations with small RNA sequencing of RNA extracted from whole fish demonstrated that the changes seen in the sequencing were likely due to changes in the liver. TP is known to be extensively metabolised, and to be present at much higher levels in the liver than other organs [201]. Therefore, it is not surprising that miRNA changes caused by TP-induced liver injury appear to predominantly occur in the hepatocytes of the zebrafish.

Modelling DILI in the context of a whole organism enables a more complete understanding of DILI within the complex physiology of a whole organism. However, the technique described in this chapter enables hepatocytes to be extracted from the whole organism following drug exposure. This gives the option to analyse changes specific to hepatocytes, including mRNA, miRNA and protein expression, whilst still investigating DILI in the context of a whole organism.

#### 3.4.7 Zebrafish larvae models of liver injury can be used to identify novel biomarkers of liver injury:

The small RNA sequencing work undertaken in this study enabled the identification of potential novel miRNA biomarkers of liver injury. Several of these miRNAs were quantified in ATDILI patient samples, with miR-146a and miR-21 increasing along with a rise in ALT. This demonstrates that zebrafish models of liver injury can be used for the identification of novel miRNA biomarkers. Previous work has found a link between both miR-146a and miR-21 and liver diseases. The miRNA miR-146a is associated with the innate immune system and negative regulation of inflammation [202], [203]. Furthermore, increases in circulating miR-146a have been linked to liver disease, hepatocellular carcinoma and HCV infection [204]. Rises in circulating miR-21 have been linked to liver fibrosis in a rat model of NASH [205]. In addition, miR-21 has been associated with chronic hepatitis and hepatocellular carcinoma in humans [206]. These miRNAs do not appear to exhibit a pattern of expression specific to liver injury caused by a particular drug. However, there may be other miRNAs which have a specificity to individual drugs, providing information on which drug in an anti-TB treatment regime may be the cause of the liver injury. The ability to identify the specific drug which is the cause of the liver injury would aid the management of TB patients, enabling the tailoring of drug regimes, reducing the risk of DILI reoccurring and increasing the likelihood of treatment completion.

#### 3.4.8 Limitations of this study:

There are several limitations to this study. Firstly, the quantity of each drug taken up by the zebrafish larvae is unknown. The uptake of drugs from solution is dependent on their physiochemical properties. Although there are methods to determine drug uptake by zebrafish larvae this was not included in this study. Further to drug uptake, drug metabolism in zebrafish larvae is not completely understood. Zebrafish larvae have demonstrated phase I and II metabolic reactions [132], along with similar cellular and physiological processes [131]. However, there is limited previous work on the metabolism of the drugs used in this study in zebrafish larvae. Therefore, key enzymes needed for the metabolism of TP, INH and PYR which are present in human drug metabolism pathways may be absent in zebrafish larvae.

Another component that may be missing in zebrafish larvae is the ability to generate an immune response to drugs and drug metabolites. Although zebrafish larvae have some components of an immune system there is limited evidence that they can model the full complexity of the human immune system. As a result, the mechanisms of liver injury seen in zebrafish larvae may not provide the complete picture of what occurs in humans. However, there is also evidence that both mice and rats exhibit a different immune response to anti-TB drugs to humans [30]. This highlights the limitations of using animal models to understand DILI.

A further limitation is that this work uses non-therapeutic concentrations of INH and PYR. Patients receive 5 mg/kg INH when undergoing standard TB treatment, giving a plasma concentration of approximately 2 mg/l or 15  $\mu$ M [163]. Similarly, for PYR, patients receive 15 mg/kg, generating a plasma concentration of 35 mg/l or 285  $\mu$ M [163]. Zebrafish larvae in this study were exposed to mM concentrations of these drugs as this concentration was required to generate reproducible liver injury. This limitation is linked to two further problems. Firstly, the quantity of the drug absorbed by the zebrafish larvae is not known, depending on the drug's physiochemical properties. It may be that the plasma concentration of the drug in zebrafish larvae is close to that observed in humans. Secondly, ATDILI is largely idiosyncratic in humans, thus, to induce reproducible DILI in zebrafish larvae a higher dose is required. Therefore, the mechanisms of DILI identified in this study in zebrafish larvae may not accurately reflect those found in humans.

This study has demonstrated that the anti-TB drugs INH and PYR can induce liver injury in a zebrafish larvae model. However, this was only possible as these drugs were soluble in water and could be absorbed by zebrafish larvae. Preliminary experiments with another TB drug rifampicin were limited due to rifampicin being insoluble in water and having limited solubility in other solvents. Dissolving rifampicin in DMSO led to high larvae mortality due to the volumes of DMSO which had to be used. Although zebrafish larvae have utility as models of DILI, especially due to the potential for high throughput experiments, the physiochemical properties of the test drugs need to be appropriate, being able to dissolve in water and absorbed by the larvae.



This work is further limited by the limited amount of data available on miRNAs, especially in zebrafish. MiRNAs are usually well conserved between species, with near identical sequences and similar expression patterns both temporally and spatially, thus suggesting they have analogous regulating behaviour [207]. However, in some instances, despite species having miRNAs with common sequence motifs their expression and biological processes they regulate can differ [207]. MiRNAs are not completely conserved between zebrafish and mammals. The fact that there is no direct match for some miRNAs between zebrafish and humans reduces the number of potential novel biomarkers which can be translated from these studies back into humans. In addition, the datasets available for miRNAs in zebrafish are limited to predicted gene targets and not experimentally validated targets. Therefore, the targets identified in the KEGG and GO analyses in this work may not be correct. Significant work is needed to validate predicted hits identified by this approach.

#### 3.4.9 Further work:

Further work could address some of the limitations of this work. Firstly, by quantifying the uptake of the drugs used in these studies by zebrafish larvae. Methods to quantify drug uptake include using radio-labelled compounds, liquid scintillation, radio high-performance liquid chromatography and lysing of embryos followed by liquid chromatography-tandem mass spectrometry [121]. An additional method would be to quantify the amount of drug administered to the larvae by injecting it directly into the yolk sac of the embryo [115].

A second limitation of this work which could be addressed is the limited understanding we have of the miRNA-mRNA interactions occurring. The targets identified in this study in the KEGG and GO analyses relied on predicted datasets, looking at the 3' UTR of genes and predicting whether specific miRNAs would bind to these regions. It is possible to validate whether these predicted miRNA-mRNA interactions are true with experiments using reporter systems, determining if the miRNA and mRNA co-express in the cell type of interest and through gain-of-function and loss-of-function experiments investigating the effect on the target protein or biological function [208]. In this study it would be interesting to determine if the predicted miRNAs bind and regulate GST2 and GST3 mRNAs.

This thesis demonstrated a method to isolate specific cell populations from zebrafish larvae. This method enables the identification of miRNA changes in specific cell populations to understand different cellular responses to DILI. Future work could assess the miRNA changes in hepatocytes and immune cells in ATDILI to further understand mechanisms of liver injury.

The zebrafish model of ATDILI in this thesis enabled the identification of novel miRNA biomarkers of DILI which could be translated back into human studies. Only a subset of the substantially changed miRNAs were validated in a limited number of human samples. Further work should investigate more of these identified miRNAs, assessing their potential as DILI biomarkers in more human samples with ATDILI. The cases of ATDILI included in this work were caused by isoniazid. Future work should include patient samples whose liver injury was caused by different anti-TB drugs. The miRNAs identified from the zebrafish model of ATDILI could be unique to ATDILI, therefore potentially able to determine the causative agent of liver injury when patients are being treated with multi-drug anti-TB regimens. The identification of unique signatures of miRNAs for specific patterns of liver injury would inform patient treatment and enable early adaptation of anti-TB treatment regimens to reduce the risk of ATDILI and enable patients to more easily complete treatment regimes.

#### 3.4.10 Summary:

In summary, the work in this study describes a zebrafish larvae model of ATDILI with the anti-TB drugs INH and PYR. DILI occurred with mM concentrations of the drugs, resulting in morphological changes, hepatocyte necrosis, a reduction in liver size and a fall in miR-122. Small RNA sequencing identified pathways which may be altered. In ATDILI microsomal GST enzymes were identified as being altered. Larvae exposed to TP exhibited miRNA down-regulation, fitting with TP's mechanism of action. The miRNA changes identified in small RNA sequencing of TP-exposed larvae were demonstrated to be due to miRNA changes in hepatocytes. Novel biomarkers of DILI were identified and quantified in human plasma samples from patients with ATDILI, with increases in the miRNAs miR-146a and miR-21 associated with an elevation in ALT.

## 4 Development of a novel diagnostic test for miR-122

## 4.1 Introduction:

### 4.1.1 Background:

The current gold standard for diagnosing DILI is the biomarker ALT. However, ALT has limitations to its use as described previously. The novel biomarker miR-122 has shown promise as a biomarker of liver injury, being both diagnostic and prognostic for outcomes of paracetamol-induced liver injury. However, current diagnostics for miRNAs are time-consuming and require complex and expensive laboratory facilities. Therefore, there is a real need for a point of care diagnostic test for miR-122.

Toehold switches are a novel technology which enable the detection of a specific sequence. A toehold switch consists of a hairpin loop containing a sequestered ribosome binding site, with a repressed gene. In the presence of the sequence of interest, there is complementary sequence binding, unwinding of the hairpin loop and expression of the previously repressed gene, generating a quantifiable output. The first toehold switch in this study designed to quantify miR-122 was toehold switch 1 (THS1). This toehold switch was based on one of the forward-engineered toehold switches designed by Green, Pardee and colleagues [157]. The sequence of the toehold switch was adapted so that the binding region in the 5' toehold end was complementary to miR-122, the trigger for the toehold switch. The sequence of THS1 is shown in Figure 4-1, along with a schematic of the toehold switch structure. THS1 consists of a miR-122 binding region and a hairpin loop, containing the RBS and start codon, a linker and a repressed gene. The miR-122 binding region forms the 5' toehold domain as well as extending into the lower stem of the hairpin loop by 6 bases. Binding of miR-122 to the toehold domain leads to the unwinding of the lower region of the hairpin loop. Above the lower stem containing the miR-122 binding site sits a bulge of three bases which forms as it is non-complementary to the AUG start codon in the downstream section of the hairpin stem. Within the loop of the hairpin is sequestered the RBS, which is inaccessible when the hairpin loop structure is present. In the presence of miR-122, the hairpin loop unwinds enabling binding of a ribosome to the RBS. Ribosome binding initiates translation of the previously repressed gene, generating a measurable output.

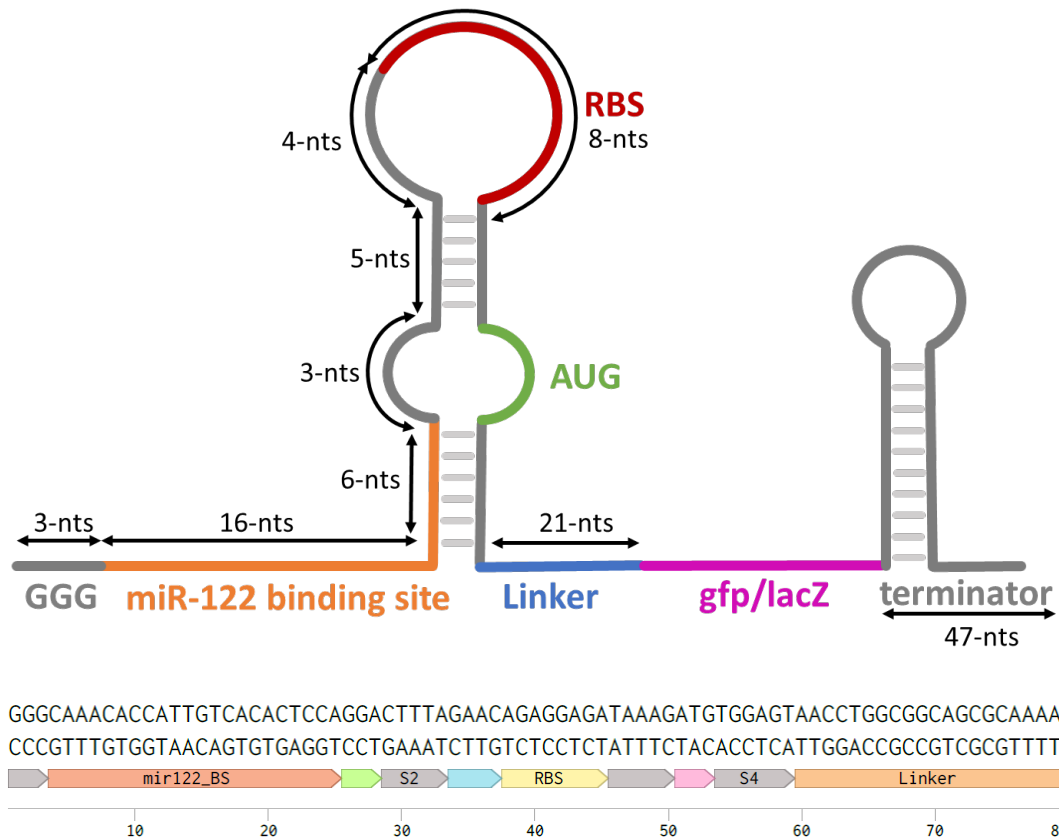


**Figure 4-1: Schematic for toehold switch 1.**

Upper section describes the structure of toehold switch 1. Lower section describes the sequence of the toehold switch. (RBS) ribosome binding site; (AUG) start codon; (nts) nucleotides.

The outputs chosen for this system were the genes *gfp* and *lacZ*. Green fluorescent protein (GFP) was chosen as it is an easy output to use, not requiring any additional substrates. GFP is encoded by a ~750 bp gene, making it easy to clone into constructs, and generates a protein of 238 amino acids, 26.9 kDa. GFP's major excitation peak is at 395 nm, with an emission peak of 509 nm and so can be easily measured in a plate reader. The second output used was the *lacZ* gene which encodes a  $\beta$ -galactosidase, a glycoside hydrolase enzyme which catalyses the hydrolysis of  $\beta$ -galactosides into monosaccharides through the breaking of a glycosidic bond. There are several substrates which can be used with  $\beta$ -galactosidase, however, for this study chlorophenol-red- $\beta$ -D-galactopyranoside (CPRG) was used. CPRG is a yellow substrate which, when cleaved by  $\beta$ -galactosidase, produces chlorophenol-red, a purple/red substrate.  $\beta$ -galactosidase was chosen as it provides a colorimetric output which

can be quantified in a plate reader or other handheld reader and can also be quantified by eye when used in a paper-based diagnostic.

From the initial switch (THS1) a panel of switches were then designed to understand how changes to the structure of the switch alters sensitivity and specificity (Table 4-1). Features which could impact on the behaviour of the switch included; the stability of the switch, the accessibility of the RBS, and the accessibility of the miR-122 binding site.

Firstly, the stability of the switch was adjusted by altering the length of the stem of the hairpin. The stability of the switch alone depends on the binding in the stem regions, both in the upper and lower stem. Altering the length of either the upper or lower stem regions should affect the stability of the toehold switch, both alone, and how easily it unwinds in the presence of miR-122. Therefore, THS2 and THS3 were designed with increased lower stem lengths of 3 and 6 bases respectively. In addition, THS4 was designed with upper stem which is increased by 3 bases.

Secondly, the accessibility of the RBS, which determines the rate of translation of the reporter gene, was changed, either through altering the size of the loop within the hairpin, or through altering the secondary structures which form upon miR-122 binding. A series of toehold switches were developed with differing loop sizes. Switches with reduced loop size are THS5a, THS5b and TH6. Switches with increased loop sizes are TH5, THS5d, THS5e, THS5f, THS5g and TH5h. The THS5s were adapted from loops used by Green and colleagues [157]. The accessibility of the RBS was changed through altering the secondary structures which form upon miR-122 binding. One way in which this was achieved was through the addition of a refolding domain, as in THS7. Upon miR-122 binding, the newly exposed sequence of the switch should refold, generating a new secondary structure. This secondary structure should weaken the secondary structure around the RBS, resulting in unwinding of the structure, binding of the ribosome and translation. Again, this adaptation is described by Green and colleagues [157]. The second way the secondary structures formed were altered was through changing bases found at the bottom of the unwound loop. THS10 has a weakly binding base (A or T) at the bottom of the unwound loop, resulting in a weaker secondary

structure. This should lead to the ribosome being able to more easily unwind the secondary structure present and translate the reporter gene.

Thirdly, the accessibility of the miR-122 binding site was altered by altering the sequence which is complementary to miR-122. Due to the short length of microRNAs the entire length of miR-122 binds to THS1, with 16 bases in the 5' toehold domain and 6 bases in the lower stem region. Two of the new panel of switches have altered miR-122 binding sites. THS8 has a reduced miR-122 binding site, with bases removed from the lower stem. THS9 has a shifted miR-122 binding site, with 3 bases of the miR-122 binding site shifted into the lower stem, therefore, becoming less accessible for binding with trigger miR-122 and reducing the length of the 5' toehold region.

#### 4.1.2 Aims:

The hypothesis of this chapter was that the novel toehold switch system can be used to detect miR-122.

1. Design and assemble a panel of novel toehold switches for miR-122 with a fluorescent output
2. Investigate the sensitivity and specificity of the panel of toehold switches with fluorescent output
3. Assemble the toehold switches for miR-122 with a colorimetric output
4. Investigate the sensitivity of the toehold switches with a colorimetric output

Switch	Design alteration	Feature	Sequence
THS1	Initial design	n/a	CAAACACCATTGTCACACTCCAGGACTTTAGAAC AGAGGAGATAAAGATGTGGAGT
THS2	Increased lower stem (addition of 3 bases)	Stability of switch	CAAACACCATTGTCACACTCCA <u>CAC</u> GGACTTTAG AACAGAGGAGATAAAGATG <u>GTG</u> TGGAGT
THS3	Increased lower stem (addition of 6 bases)	Stability of switch	CAAACACCATTGTCACACTCCA <u>TGTCAC</u> GGACTT TAGAACAGAGGAGATAAAGATG <u>GTGACA</u> TGGA GT
THS4	Increased upper stem (addition of 3 bases)	Stability of switch	CAAACACCATTGTCACACTCCAGGACTTTA <u>GCCG</u> AACAGAGGAGA <u>GGCT</u> AAAGATGTGGAGT
THS5	Increased loop size (by 4 bases)	Access to RBS	CAAACACCATTGTCACACTCCAGGACTTTA <u>GAA</u> <u>GGAACAGAGGAGATAAAGATGTGGAGTT</u>
THS5a	Reduced loop size (by 4 bases)	Access to RBS	CAAACACCATTGTCACACTCCAGGACTTTA <sup>^</sup> AGA GGAGATAAAGATGTGGAGT
THS5b	Reduced loop size (by 1 bases)	Access to RBS	CAAACACCATTGTCACACTCCAGGACTTTA <sup>^</sup> AAAC AGAGGAGATAAAGATGTGGAGT
THS5d	Increased loop size (by 3 bases)	Access to RBS	CAAACACCATTGTCACACTCCAGGACTTTA <u>CAAG</u> AACAGAGGAGATAAAGATGTGGAGT
THS5e	Increased loop size (by 6 bases)	Access to RBS	CAAACACCATTGTCACACTCCAGGACTTTA <u>AGAC</u> <u>AA</u> GAAACAGAGGAGATAAAGATGTGGAGT
THS5f	Increased loop size (by 9 bases)	Access to RBS	CAAACACCATTGTCACACTCCAGGACTTTA <u>ACAA</u> <u>GACAA</u> GAAACAGAGGAGATAAAGATGTGGAGT
THS5g	Increased loop size (by 12 bases)	Access to RBS	CAAACACCATTGTCACACTCCAGGACTTTA <u>CGAA</u> <u>CAAGACAA</u> GAAACAGAGGAGATAAAGATGTGGA GT
THS5h	Increased loop size (by 15 bases)	Access to RBS	CAAACACCATTGTCACACTCCAGGACTTTA <u>GAAC</u> <u>GAACAAGACAA</u> GAAACAGAGGAGATAAAGATGT GGAGT
THS6	Reduced loop size (by 4 bases)	Access to RBS	CAAACACCATTGTCACACTCCAGGACTTTA <sup>^</sup> GAG AGGAGATAAAGATGTGGAGT
THS7	Refold domain	Access to RBS	CAAACACCATTGTCAC <u>ACTCCAGGT</u> GGACTTTA GAACAGAGGAGATAAAGATG <u>ACCTGGAGTTTT</u> <u>CCAGGT</u>
THS8	Reduced length of lower stem with reduced miR-122 complementarity region	Accessibility of miR-122 binding	CAAACACCATTGTCACACT <sup>^</sup> GGACTTTAGAACA GAGGAGATAAAGATGAGT CAAACACCATTGTCACACTCCAGGACTTTAGAAC AGAGGAGATAAAGATGTGGAGT
THS9	Increased lower stem with miR-122 sequence	Accessibility of miR-122 binding	CAAACACCATTGTCACACTCCAGGACTTTAGAAC AGAGGAGATAAAGATGTGGAGT <u>GTG</u>
THS10	Weak base at base of unwound RBS loop	Access to RBS	CAAACACCATTGTCACACTCCAGGACTTTAGAAC AGAGGAGATAAAATGTGGAGT

**Table 4-1: Panel of toehold switches.**

*Detailing the structural changes made to the switches along with the anticipated effect. Sequences shown from after the initial GGG linker at the upstream end of the switch. Additions to each switch in comparison to THS1 shown in red underlined. Removal of bases from the switch detailed by ^ at the location the bases were removed.*



## 4.2 Materials and methods:

The materials and methods section is split into four broad sections. Section 4.2.1 describes the different methods used to assemble the different toehold switches. The techniques and materials used for these assembly processes are described in sections 4.2.3 and 4.2.2 respectively. The methods used to test the switches are described in section 4.2.4.

### 4.2.1 Toehold switch assembly overview:

Due to the different design features of each switch several different methods were used to construct the switches. The methods used for each switch are overviewed in Table 4-2 and Figure 4-2. Following construction of the GFP switches and initial testing which confirmed they worked, the *gfp* reporter gene was converted to a *lacZ* gene to provide a colorimetric output, however this was undertaken only for a subset of switches. Details of each assembly method, circular polymerase extension cloning (CPEC), mutagenic primers and pJET cloning vector, are described in the following sections.

Switch	GFP Assembly Method	LacZ Assembly Method
<b>THS1</b>	THS1 sequence ordered and assembled into pSB1K3 using CPEC	pJET cloning vector
<b>THS2</b>	Oligonucleotide THS sequences annealed and assembled into pSB1K3 using CPEC	pJET cloning vector
<b>THS7</b>	Oligonucleotide THS sequences annealed and assembled into pSB1K3 using CPEC	pJET cloning vector
<b>THS10</b>	Oligonucleotide THS sequences annealed and assembled into pSB1K3 using CPEC	n/a
<b>THS5s</b>	Mutagenic primers	Mutagenic primers (THS5b & 5h only)
<b>THS9</b>	Mutagenic primers	Mutagenic primers

**Table 4-2: Overview of the different techniques used for the assembly of each switch.**

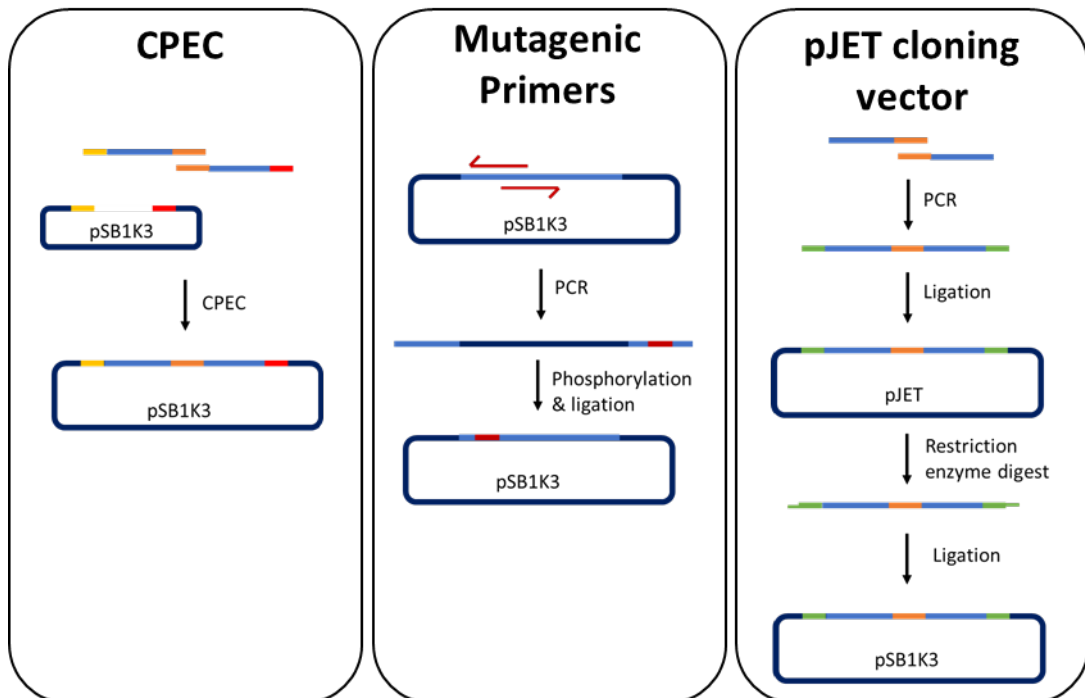


**Figure 4-2: Schematic of the different assembly techniques used for the assembly of the toehold switches into plasmid backbones.**

**Circular DNA polymerase extension cloning (CPEC):** DNA fragments required for construct were generated with overlaps at either end of at least 20 bp by PCR. pSB1K3 was amplified and overlap regions added at either end of the sequence. The DNA fragments containing the toehold switch and reporter gene were combined with the plasmid backbone pSB1K3 using a polymerase in the CPEC reaction. **Mutagenic primers:** Primers containing the required sequence changes were used to generate a linear product. The resulting linear product was phosphorylated and ligated to generate a complete plasmid containing the new switch sequence. **pJET cloning vector:** DNA fragments required for construct were generated with an overlap of 21 bp by PCR. The 2 DNA fragments were combined, and restriction enzyme sites added to either end using PCR. The resulting blunt-ended PCR product was ligated into the pJET cloning vector and transformed into *E. coli* Top10 cells. Following colony screening the insert was cut out with *EcoRI* and *PstI* to generate a sticky-ended product. The sticky-ended DNA product was then ligated into pSB1K3.

For all assemblies Phusion PCR (section 4.2.2.1) was used to generate and amplify the DNA fragments and plasmid backbone pSB1K3 used. The primer sequences for the reactions described in the following sections can be found in Appendix 4.i. For all assemblies, the resulting plasmid constructs were transformed into *E. coli* Top10 cells and plated on LB agar containing appropriate antibiotics (sections 4.2.2.4 & 4.2.2.6). To confirm the presence of the correct sized inserts colony PCR (section 4.2.2.7) was undertaken. All plasmids containing the correct size insert were sequenced to check the sequence was correct (section 4.2.2.8). Plasmids containing the correct sequence were extracted and stored at -20 °C (section 4.2.2.6) and glycerol stocks were made and stored at -80 °C (section 4.2.2.9).

#### 4.2.1.1 Circular polymerase extension cloning:

Circular DNA polymerase extension cloning (CPEC) is designed for the cloning of complex genes. The technique relies on the presence of overlaps of at least 20 base pairs at the ends of the fragments, which are to be assembled together or into a plasmid backbone. The polymerase present in the reaction mixture joins overlapping DNA fragments together into a plasmid. The protocol used for the CPEC assembly is based on work by Quan and Tian [209].

To assemble fragment(s) into a backbone using CPEC, purified linearized backbone fragments along with switch and reporter gene DNA fragments were combined with the other components of the CPEC reaction mixture (Table 4-3). Phusion polymerase (Thermo Fisher Scientific, Loughborough, UK) was used for the reaction. The resulting reaction mixture was then placed in a thermocycler (Table 4-4). The CPEC assembly method was used to generate THS1-gfp@1K3, THS2-gfp@1K3, THS7-gfp@1K3 and THS10-gfp@1K3.

Component of reaction mixture	Volume (µl)
Linearized vector backbone	(up to 100 ng)
Other assembly pieces	(equimolar to backbone)
5x HF Phusion Reaction Buffer (Thermo Fisher Scientific, Loughborough, UK)	5.0
dNTPs (10mM) (Thermo Fisher Scientific, Loughborough, UK)	1.0
DMSO	0.75
Phusion Polymerase (2U/µl) (Thermo Fisher Scientific, Loughborough, UK)	0.5
RNase free water	(up to 25 µl)

**Table 4-3: CPEC reaction mixture components.**

Cycle	Time (sec)	Temperature (°C)	Cycles
Initial denaturation	30	98	1
Denaturation	10	98	15
Annealing	30	Dependent on the melting temperature of the overlap of the fragments/backbone	15
Extension	=length (kb) x 15	72	15
Final extension	600	72	1
Hold	-	4	-

**Table 4-4: CPEC reaction cycling conditions.**

To assemble the first toehold switch, THS1, the THS1-gfp sequence was ordered from (Invitrogen, Thermo Fisher Scientific). The THS1-gfp sequence was amplified using the primers THS\_PT7\_fwd and THS\_tT7\_rev. The plasmid backbone, pSB1K3 was amplified using the primers PT7\_XE\_fwd and tT7\_SP\_rev. Gel purified DNA fragments were assembled using CPEC to generate THS1-gfp@1K3. After CPEC assembly the construct was transformed into *E. coli* Top10 cells and screened for the correct sequence (sections 4.2.2.4 - 4.2.2.9).

Following the assembly of THS1-gfp@1K3, this construct was used as the template DNA to help create the panel of switches. For the assembly of THS2-gfp@1K3, THS7-gfp@1K3 and THS10-gfp@1K3 CPEC was used to assemble 3 fragments, the THS-linker, linker-gfp and pSB1K3 backbone. Firstly, oligonucleotide primers (THS2 & 10 (Sigma-Aldrich, Gillingham, UK); THS7 (Integrated DNA Technologies, Leuven, Belgium)) containing the different THS sequences were annealed together. The sequences of the oligonucleotides are shown in Appendix 4.ii. Briefly, 5 µl of the forward and 5 µl of the reverse oligonucleotide and 90 µl of RNase-free water were incubated at 95° for 5 min and then cooled to room temperature over 1 hour. Secondly, the linker-gfp fragment was generated using the primers linker\_gfp\_fwd and THS\_tT7\_rev. The plasmid backbone pSB1K3 was amplified using the primers PT7\_XE\_fwd and tT7\_SP\_rev. CPEC was used to assemble the annealed THS oligonucleotides, linker-gfp fragment and pSB1K3 plasmid backbone. Following assembly, the constructs were transformed into *E. coli* Top10 cells and screened for the correct sequence (sections 4.2.2.4 - 4.2.2.9).

#### 4.2.1.2 Mutagenic primers:

The second method used to generate toehold switch constructs was to use mutagenic primers to introduce changes to the sequence of the switch in specific regions. For the construction of the different THS5 switches and THS9 switches mutagenic primers were designed which introduced the required sequence changes, using THS1-gfp@1K3 as a template. Similarly, the same primers were used to generate the following *lacZ* switches, THS5b-lacZ@1K3, THS5h-lacZ@1K3 and THS9-lacZ@1K3, using THS1-lacZ@1K3 as the template DNA.

PCR was performed with the mutagenic primers to generate linear PCR products containing the required sequence changes. For the THS5s, different forward primers for each switch were used with THS5\_rev primer, primer sequences shown in Appendix 4.iii. For THS9 2 different reverse primers were tried, primer sequences shown in Appendix 4.iii.

Gel purified linear PCR products were phosphorylated with T4 polynucleotide kinase (New England BioLabs, Hitchin, UK) and then ligated with T4 ligase (New England BioLabs, Hitchin, UK) following the manufacturer's instructions. Briefly, 4 µl of purified PCR product, 1 µl T4 polynucleotide kinase, 1 µl of FastDigest buffer and 4 µl of RNase-free water were incubated for 30 min at 37 °C. Then, 1 µl T4 ligase, 1 µl FastDigest buffer and 8 µl RNase-free water were added and the reaction incubated at room temperature for a further hour.

After the circularisation of the linear PCR product a DpnI enzyme (Life Technologies, Glasgow, UK) digest was used to remove any remaining template DNA. DpnI only digests methylated DpnI restriction enzyme cut sites, therefore it will digest template DNA which is methylated from being inside a bacterial cell. Reactions were set up according to the manufacturer's instructions, consisting of up to 1 µg DNA, 2 µl of 10x FastDigest buffer, 1 µl restriction digest enzyme and RNase-free water up to 20 µl. Following removal of the template DNA the constructs were transformed into *E. coli* Top10 cells and screened for the correct sequence (sections 4.2.2.4 - 4.2.2.9).

#### 4.2.1.3 pJET cloning vector:

Using CPEC DNA assembly proved to be too difficult for larger DNA fragments, as the *lacZ* gene is 3.1 kb long compared to the *gfp* gene which is approximately 800 bases. Therefore, the pJET cloning vector system (Fisher Scientific, Loughborough, UK) was used instead. The pJET cloning vector contains a lethal restriction enzyme which is disrupted by ligation of an insert into the cloning site. pJET is a linearized blunt-ended cloning vector able to receive inserts which have been generated by PCR.

The following technique using the pJET cloning vector was used to assemble THS1-lacZ@1K3, THS2-lacZ@1K3 and THS7-lacZ@1K3. Firstly, separate DNA fragments, with an overlapping linker region were generated using PCR. These fragments were THS-linker, using the primers THS\_PT7\_fwd and linker\_THS\_rev, and linker-lacZ using the primers linker\_lacZ\_fwd and tT7\_lacZ\_rev. The resulting products were gel purified. A second PCR reaction was then used to combine the two fragments, THS-linker and linker-lacZ, and to add EcoRI and PstI restriction enzyme sites at either end of the product. This was possible due to a 21-base overlap between the THS-linker and linker-lacZ fragment. The primers used for this reaction were EcoRI\_THS\_fwd and PstI\_tT7\_rev. The resulting products were gel purified. This blunt-ended PCR product was then ligated into pJET following the manufacturer's instructions. Briefly, 1 µl of pJET vector, 0.15 pM linear PCR product, 2 µl 2x reaction buffer, 1 µl T4 ligase and RNase free water were combined to a total volume of 20 µl. This reaction mixture was then incubated for 30 min at room temperature. The resulting ligation mix was then directly transformed into *E. coli* Top10 cells and colonies were colony screened for the presence of a correctly sized insert (section 4.2.2.7). The correctly sized insert was determined by gel electrophoresis. DNA was extracted, gel purified, and DNA concentration checked on the NanoDrop spectrophotometer (Thermo Fisher Scientific, Perth, UK).

A sticky-ended plasmid backbone pSB1K3, capable of receiving the newly generated sticky-ended insert, was generated by double digestion by EcoRI (Life Technologies, Glasgow, UK) and PstI (Life Technologies, Glasgow, UK). For the restriction enzyme digest of pSB1K3 the reaction was set up according to the manufacturer's instructions, consisting of up to 1 µg DNA, 2 µl of 10x FastDigest buffer, 1 µl PstI enzyme, 1 µl EcoRI enzyme and RNase-free water

up to 20  $\mu$ l. The reaction mixture was then incubated at 37 °C for 30 min, followed by 85 °C for 5 min.

The sticky-ended insert and backbone were ligated in the following ligation mix, consisting of 100 ng pSB1K3 plasmid backbone, >2:1 molar ratio of the linear sticky-ended insert, 2  $\mu$ l 10x reaction buffer, 1  $\mu$ l T4 ligase and RNase-free water up to 20  $\mu$ l. The resulting reaction mixture was incubated at room temperature for 30 min. Following assembly, the constructs were transformed into *E. coli* Top10 cells and screened for the correct sequence (sections 4.2.2.4 - 4.2.2.9).

An adapted version of the technique described above was used to construct PT7-lacZ@1K3, used as a positive control for the lacZ cell-free reaction solution tests. In the first step a single DNA fragment, containing the *lacZ* gene under the PT7 promoter, was generated using the primers PT7\_lacZ\_fwd and tT7\_lacZ\_rev. Restriction enzyme sites were then added in the second PCR step, using the primers EcoRI\_THS\_fwd and PstI\_tT7\_rev as described above. Following from this the technique was the same as for the THS-lacZ@1K3 constructs.

#### 4.2.2 Molecular biology and microbiology techniques:

The protocols used to generate each toehold switch and assemble into its plasmid backbone are described in (sections 4.2.1.1 - 4.2.1.3). However, the individual techniques used for these protocols are described in the following sections.

##### 4.2.2.1 Phusion PCR:

The high-fidelity Phusion polymerase (Thermo Fisher Scientific, Perth, UK) was used for the amplification of DNA fragments for the construction of plasmid constructs and for the amplification of DNA used to test the switches in cell-free reaction solutions. The reaction mix was made up as described in Table 4-5 and the cycling conditions as described in Table 4-6. Primer sequences used for reactions, and their melting temperatures are described in Appendix 4.i.

Component of reaction mixture	Volume ( $\mu$ l)
5x Phusion HF Buffer (Thermo Fisher Scientific, Perth, UK)	4.0
10 mM dNTPs (Thermo Fisher Scientific, Perth, UK)	0.4
Forward Primer (10 $\mu$ M) (Metabion, Planegg, Germany)	1.0
Reverse Primer (10 $\mu$ M) (Metabion, Planegg, Germany)	1.0
Template DNA	(up to 1 ng)
Phusion DNA Polymerase (Thermo Fisher Scientific, Perth, UK)	0.2
RNase-free water	(up to 20 $\mu$ l)

**Table 4-5: Phusion PCR reaction mixture components.**

Cycle	Time (sec)	Temperature ( $^{\circ}$ C)	Cycles
<b>Initial denaturation</b>	30	98	1
<b>Denaturation</b>	10	98	35
<b>Annealing</b>	30	Dependent on the melting temperature of the primers	35
<b>Extension</b>	=length (kb) x 30	72	35
<b>Final extension</b>	600	72	1
<b>Hold</b>	-	4	-

**Table 4-6: Phusion PCR cycling conditions.**

#### 4.2.2.2 Gel analysis:

The size of PCR products or restriction enzyme digests was analysed by gel electrophoresis. Agarose gels were made from 1% agarose, consisting of 100 ml TBE, 1 g agarose (Thistle Scientific Ltd, Glasgow, UK) and 10  $\mu$ l SybrSafe (Life Technologies, Glasgow, UK).

#### 4.2.2.3 Gel and PCR purification of DNA:

PCR products or excised gel bands were purified with the Wizard SV Gel and PCR clean-up system (Promega Corporation, Southampton, UK) following the manufacturer's instructions. For PCR products an equal volume of the membrane binding solution was added to the PCR product prior to transfer to the SV minicolumn. For gel products, the required DNA band was extracted from the gel, membrane binding solution (10  $\mu$ l per 10 mg gel) was added and the mixture was heated at 50-60  $^{\circ}$ C until the gel slice had dissolved. The resulting mix was then added to the SV minicolumn and the column was spun at 13,000 rpm for 1 min. The column was then washed twice with the Membrane Wash solution (700  $\mu$ l then 500  $\mu$ l) and the column dried by centrifugation (1 min then 5 min at 13,000 rpm). 30  $\mu$ l RNase-free water was then added to the minicolumn and the DNA collected. DNA was frozen at -20 $^{\circ}$ C until use.



#### 4.2.2.4 Transformation procedure:

Once plasmid constructs were assembled, as described in detail in section 4.2.1, they were transformed into *E. coli* Top 10 cells. For transformations plasmid constructs were added to 100  $\mu$ l *E. coli* Top 10 cells. The mixture was then incubated on ice for 30 min before a heatshock at 42 °C for 65 sec. Cells were then placed on ice for 3 min before the addition of LB up to a total volume of 500  $\mu$ l. Cells were then incubated at 37 °C for approximately 1 hour. 100  $\mu$ l of the cells were plated onto LB agar plates containing appropriate antibiotics.

#### 4.2.2.5 *E. coli* Top10 cells:

*E. coli* Top10 cells were used as the host organism for all plasmid constructs. *E. coli* Top10 cells and this protocol were a gift from Xinyi Wang. *E. coli* Top10 cells were generated using the following procedure. *E. coli* Top10 cells from a colony were placed in 5 ml of LB in a 15 ml reaction vessel and left overnight in a shaking incubator (200 rpm, 37 °C). 0.5 ml of the overnight culture was used to inoculate 200 ml LB in a 500 ml conical flask and left in a shaking incubator (200 rpm, 37 °C). Bacterial  $OD_{600}$  was measured at periodic intervals until optical density reached 0.3 - 0.4. The culture was then transferred to pre-frozen 50 ml falcon tubes and left on ice for 20 min. Cells were collected at 4,000 rpm, 8 min, 0 °C. The pelleted cells were resuspended in 10 ml cold 50 mM  $CaCl_2$ . Cells were then centrifuged at 4,000 rpm, 8 min, 0 °C and resuspended again in 10 ml 50 mM  $CaCl_2$ . Once resuspended, the cells were left on ice for 30 min before centrifuging at 4,000 rpm, 6 min, 0 °C. The pellet was then resuspended finally in 1 ml cold 50mM  $CaCl_2$  and 15 % glycerol and left on ice for 2 hrs. The cell solution was then aliquoted into tubes and frozen at -80 °C.

#### 4.2.2.6 Miniprep of plasmid DNA:

The QIAprep Miniprep Spin Kit (Qiagen, Venlo, Netherlands) was used for plasmid minipreps. A single colony was picked and placed in 5 ml LB broth overnight in a 15 ml reaction vessel. Bacterial cells were pelleted at 8,000 rpm for 4 min. The bacterial pellet was resuspended in 250  $\mu$ l buffer P1 and transferred to a 1.5 ml tube. 250  $\mu$ l buffer P2 was then added, followed by 350  $\mu$ l buffer N3. The solution was centrifuged at 13,000 rpm for 10 min and 800  $\mu$ l of supernatant transferred to the spin column. The spin column was centrifuged at 13,000 rpm for 1 min and flow-through discarded. The column was then washed with 750  $\mu$ l buffer PE, centrifuged at 13,000 rpm for 1 min and flow-through discarded. The column was

transferred to a new 1.5 ml tube, 50  $\mu$ l RNase-free water added, and DNA collected by centrifugation at 13,000 rpm for 1 min. Plasmid DNA was frozen at -20°C until use.

#### 4.2.2.7 Colony screening:

GoTaq polymerase (Promega Corporation, Southampton, UK) was used for colony screening to determine the presence of correct size inserts in the plasmid constructs. A single bacterial colony was touched with a pipette tip and cells transferred to 100  $\mu$ l RNase-free water and this was used as the template DNA for the reaction. The reaction mix was assembled according to the manufacturer's instructions (Table 4-7). A two-step cycling protocol was used (Table 4-8). Following the PCR reaction products were analysed on a gel to determine the size of the PCR product.

Component of reaction mixture	Volume ( $\mu$ l)
5x GoTaq Reaction Buffer (Promega Corporation, Southampton, UK)	4.0
dNTPs	0.4
Forward Primer (10 $\mu$ M) (Metabion, Planegg, Germany)	2.0
Reverse Primer (10 $\mu$ M) (Metabion, Planegg, Germany)	2.0
Template DNA	0.4
GoTaq Polymerase (Promega Corporation, Southampton, UK)	0.1
RNase-free water	11.1

**Table 4-7: GoTaq PCR reaction mixture components.**

Cycle	Time (sec)	Temperature (°C)	Cycles
<b>Initial denaturation</b>	120	95	1
<b>Denaturation</b>		95	25
<b>Annealing</b>		Dependent on the melting temperature of the primers	25
<b>Extension</b>	= length (1kb) x 60	72	25
<b>Final extension</b>	300	72	1
<b>Hold</b>	-	4	-

**Table 4-8: GoTaq PCR cycling conditions.**

#### 4.2.2.8 Sequencing:

To determine the presence of correct sequences within plasmid constructs, minipreped plasmids were sent for sequencing at MRC PPU Sequencing, Dundee. Sequences were aligned with the correct sequence in Benchling software, (2016, <https://benchling.com>).

#### 4.2.2.9 Glycerol stocks:

Glycerol stocks of bacteria were made up by adding 0.5 ml overnight culture in LB to 0.5 ml 50% glycerol. Once mixed glycerol stocks were stored at -80 °C.

#### 4.2.3 Materials:

##### 4.2.3.1 Antibiotic stock solutions:

50 mg/ml ampicillin and kanamycin stock solutions were made by dissolving ampicillin (Sigma-Aldrich, Gillingham, UK) or kanamycin (Sigma-Aldrich, Gillingham, UK) in RNase-free water. The antibiotic stocks solutions were then filter sterilised, aliquoted and stored frozen at -20 °C.

##### 4.2.3.2 Chlorophenol red-beta-D-galactopyranoside solution:

Chlorophenol red-beta-D-galactopyranoside (CPRG) (Sigma-Aldrich, Gillingham, UK) was made into stock solutions of 6 mg/ml in RNase-free water. The stock solutions were then aliquoted and stored at -20 °C.

##### 4.2.3.3 LB agar and LB broth:

LB agar (Fisher Scientific, Loughborough, UK) and LB broth (Fisher Scientific, Loughborough, UK) were made up according to the manufacturer's instructions. For LB agar and broth containing antibiotics, antibiotics were diluted 1000-fold from stock solutions to give a final concentration of 50 µg/ml.

##### 4.2.3.4 MicroRNA solutions:

MiRNAs (Metabion, Planegg, Germany) were dissolved in RNase-free water, aliquoted and stored at -80 °C. MiRNA solutions were diluted in RNase-free water prior to use in cell-free reaction solutions.

##### 4.2.3.5 Plasmids:

The plasmid backbone pSB1K3 was used for the assembly of all the toehold switch constructs. pSB1K3 is a high-copy plasmid containing the kanamycin resistance gene. Toehold switch inserts were inserted between the BioBrick sites. The PT7-30gfpt@3K3 plasmid, which expresses GFP under the t7 promoter was used as a positive control for the

experiments using the GFP switches. The r30-lacZ-B15@3K3 plasmid was used to generate the lacZ switches. The  $\phi$ 1A3 plasmid was used as a negative control for both GFP and lacZ switch tests. All plasmid sequences used in this work were a gift from Xinyi Wang.

#### 4.2.3.6 Primers:

Primers (Metabion, Planegg, Germany) were dissolved in RNase-free water to generate stock solutions of 100  $\mu$ M and stored at -20 °C. When used for PCR reactions primers were diluted to 10  $\mu$ M. The primers used in the assemblies are detailed in Appendix 4.i.

#### 4.2.4 Testing of the switches:

##### 4.2.4.1 GFP switches - cell-free reaction solutions:

The commercially available Pt7 expression system, PURExpress in vitro protein synthesis kit (New England BioLabs, Hitchin, UK), was used for the cell-free reaction solution experiments. The system is assembled from ribosomes and 35 purified *E. coli* bacterial proteins, which provide all the necessary components for in vitro transcription and translation. Cell-free reaction solutions were assembled for each reaction at 4 °C according to the manufacturer's instructions (Table 4-9) and then immediately incubated at 37 °C for the duration of the experiment.

Component of reaction mixture	Volume ( $\mu$ l)
Cell-free reaction solution A (New England BioLabs, Hitchin, UK)	2.0
Cell-free reaction solution B (New England BioLabs, Hitchin, UK)	1.5
RNase inhibitor (New England BioLabs, Hitchin, UK)	0.1
DNA (THS constructs generated by PCR)	1.0
MiRNA (Metabion, Planegg, Germany)/RNase-free water	0.4

**Table 4-9: Cell-free reaction solution components for GFP switch tests.**

*Volumes shown for single 5  $\mu$ l reaction.*

Once assembled, 5  $\mu$ l of the reaction mix was placed in a 384 well plate, covered with 15  $\mu$ l of mineral oil (to prevent evaporation) and then incubated for 12 hrs at 37 °C in a plate reader (POLARstar, Optima, BMG Labtech, Aylesbury, UK) with readings taken every 5 min. The plate reader measured an excitation frequency of 395 nm and emission frequency of 509 nm. For all GFP switch experiments the positive control used was PT7-30gft@3K3 and the negative control was an empty 1A3 plasmid ( $\phi$ 1A3). Controls were at the same

concentration as linear DNA constructs. Details for each experiment, including DNA concentration, miRNA concentrations and number of replicates are provided in the results sections.

#### 4.2.4.2 GFP switches - analysis:

To adjust for autofluorescence of the cell-free reaction solution the background signal was subtracted from each well using the negative control ( $\phi$ 1A3) reaction for that experiment. The minimum value of each well was then adjusted to zero. Data was smoothed using a 3-point average at each data point. Fluorescence intensity reached a maximum for most experiments after 2.5 hrs; therefore, this is the time point which data for background subtracted fluorescence and fold induction is shown. Fold induction calculations were done by dividing the 3-point average at 2.5 hrs by the corresponding uninduced wells of the same switch. An average was then taken for the replicates of each condition and standard deviation calculated. The time course data for each experiment can be found in Appendix 4.v-vii, with the mean of three replicates (unless otherwise stated) and the standard error of the mean. For the initial panel test of all the switches, the statistical significance of the difference between background subtracted fluorescence of the switches was determined using a t-test for each switch. For the other tests of the switches, the statistical significance of the difference between background subtracted fluorescence of the switches was determined using a one-way ANOVA and Dunnett's multiple tests between non-induced and induced switches. Statistical analyses were performed using Graphpad Prism (GraphPad Software, La Jolla, California). A P-value of  $<0.05$  was considered significant.

#### 4.2.4.3 LacZ switches - cell free reaction solutions:

Cell-free reaction solutions were assembled for each reaction at 4 °C according to the manufacturer's instructions (Table 4-10) and then immediately incubated at 37 °C for the duration of the experiment.

Component of reaction mixture	Volume ( $\mu$ l)
Cell-free reaction solution A (New England BioLabs, Hitchin, UK)	2.0
Cell-free reaction solution B (New England BioLabs, Hitchin, UK)	1.5
RNase inhibitor (New England BioLabs, Hitchin, UK)	0.1
CPRG (6 mg/ml) (Sigma-Aldrich, Gillingham, UK)	0.5
DNA (THS constructs generated by PCR)	0.5
microRNA (Metabion, Planegg, Germany)/RNase-free water	0.4

**Table 4-10: Cell-free reaction solution components for lacZ switch tests.**

Volumes shown for single 5  $\mu$ l reaction.

Once assembled, 5  $\mu$ l of the reaction mix was placed in a 384 well plate, covered with 10  $\mu$ l of mineral oil (to prevent evaporation) and then incubated for 12 hrs at 37 °C in a plate reader (CLARIOstar, Optima, BMG Labtech, Aylesbury, UK) with readings taken every 5 min. The plate reader measured absorbance at 575 nm. For all *lacZ* switch experiments the positive control used was PT7-lacZ@1K3 and the negative control used was an empty 1A3 plasmid ( $\phi$ 1A3). Controls were at the same concentration as linear DNA constructs. Details for each experiment, including DNA concentration, miRNA concentrations and number of replicates are provided in the results sections.

For the paper-based tests, blotting paper was washed with either ethanol, methanol or isopropanol to remove impurities. The positive control PT7-lacZ@1K3, cell-free reaction solution and pieces of the washed paper were incubated overnight at 37°C.

#### 4.2.4.4 LacZ switches - analysis:

To adjust for slow degradation of CPRG in reactions, data was normalised using the negative control reaction ( $\phi$ 1A3). The absorbance measurement of the negative control ( $\phi$ 1A3) was subtracted from each reaction for that experiment. The minimum value of each well was then adjusted to zero. Data was smoothed using a 3-point average for each time point. Absorbance at 575 nm demonstrated different kinetics to the GFP production in previous experiments. Therefore, two different timepoints are described in the results section. Data shows the background subtracted absorbance at 575 nm. Fold induction calculations were done by dividing the 3-point average at 1 or 2.5 hour(s) by the corresponding uninduced wells of the same switch. An average was then taken for the replicates of each condition and standard deviation calculated. The time course data for each experiment can be found in

Appendix 4.viii, data shows an average of three experiments and the standard error of the mean. The statistical significance of the difference between background subtracted absorbance of the switches was determined using a one-way ANOVA and Dunnett's multiple tests between non-induced and induced switches. Statistical analyses were performed using GraphPad Prism (GraphPad Software, La Jolla, California). A P-value of  $<0.05$  was considered significant.

### 4.3 Results:

#### 4.3.1 NUPACK assessment of switches:

Prior to assembling all the switches developed, the structures were analysed to assess the structure of the switches and the complexes formed when switches were combined with miR-122. The NUPACK web application software [210] was used to generate switch structures in the presence and absence of miR-122 showing the minimum free energy (MFE) structures at 37 °C. Diagrams showing the MFE structures of the switches in the presence and absence of miR-122 at 37 °C can be found in Appendix 4.iv, and the free energy is shown in Table 4-11.

NUPACK assessment of switches enables initial assessment of the switch functionality. Firstly, the diagrams of the switch structure indicate whether miR-122 can bind to its binding site on the switch and whether any loops that form would inhibit miR-122 binding. For all switches there is a single loop structure present in the miR-122 binding site, however, this cannot be avoided, as the switch design is limited to the length and sequence of miR-122. Secondly, the diagrams of the switch structures demonstrate the length and base pairing of the stem region and so indicate the ease of which miR-122 binding should unwind the stem. Furthermore, the complex that forms when miR-122 binds can be assessed, indicating how accessible the RBS is when miR-122 is bound and whether any other inhibitory loop structures are likely to form.

The free energy of a secondary structure is an indicator of the stability of an RNA sequence or RNA complex. The more negative the free energy, the more stable a structure is. For the switches alone, the minimum free energy is higher than for switch-miR-122 complexes indicating that the switch-miR-122 complex is more stable. For most switches, in the absence of miR-122, their free energy is approximately -18 kcal/mol. However, for THS2, THS3, THS4, THS7 and THS9 their free energy is lower, indicating that these switches are more stable.



Switch	Without miR-122 (kcal/mol)	With miR-122 (kcal/mol)	Difference (kcal/mol)
THS1	-18.40	-44.78	26.38
THS2	-24.40	-46.58	22.18
THS3	-29.40	-51.48	22.08
THS4	-27.00	-53.38	26.38
THS5	-18.10	-44.48	26.38
THS5a	-18.10	-44.88	26.78
THS5b	-17.80	-44.88	27.08
THS5d	-17.30	-47.68	30.38
THS5e	-17.30	-44.38	27.08
THS5f	-17.10	-44.18	27.08
THS5g	-16.80	-46.68	29.88
THS5h	-17.50	-43.88	26.38
THS6	-18.70	-45.08	26.38
THS7	-27.60	-54.88	27.28
THS8	-11.40	-37.28	25.88
THS9	-24.30	-45.98	21.68
THS10	-16.70	-43.18	26.48

**Table 4-11: Free energy of switches in the presence and absence of miR-122 at 37 °C .**

*Free energy of switches as determined by the NUPACK software, [210].*

After assessing the results of the NUPACK analysis several switches were deemed unsuitable for use. Firstly, THS3 and THS4 have extended stems, which when bound to miR-122 generated a complex where the RBS is still sequestered in a large and stable hairpin loop. Unwinding of this loop is not energetically favourable and so the reporter gene would likely remain untranslated after binding by miR-122. Secondly, THS6 has a reduced loop size where the RBS is, making binding of the ribosome more difficult and therefore unlikely to occur. The final switch, which was excluded from further analysis was THS8. THS8 contains a reduced miR-122 binding site along with a reduced stem length. Although miR-122 can still bind to the 5' toehold domain, the reduced miR-122 binding sequence makes it more likely to be leaky, and to generate output in the absence of miR-122.

#### 4.3.2 GFP switches:

##### 4.3.2.1 Optimisation of test conditions:

In order to determine the optimum volume of cell-free reaction mixture and mineral oil to use an initial test was undertaken with the positive control, PT7-30gfp@3K3 (Figure 4-3A). Fluorescence produced was highest for 10  $\mu$ l of cell-free reaction solution alone, however, after 12 hrs incubation there was some evaporation on the film of the plate cover. There was not a large difference between the fluorescence produced by 10  $\mu$ l and 5  $\mu$ l of cell-free reaction solution with the addition of mineral oil. Therefore, in order to conserve cell-free reaction solution, an expensive reagent, 5  $\mu$ l of cell-free reaction solution was used for future experiments.

In order to determine the optimal concentration of the linear DNA switch construct to use, a test was undertaken with 33, 3.3 and 0.33 nM DNA, concentrations taken from work by Pardee and colleagues [158], (Figure 4-3 B & C). As maximum fluorescence was typically achieved by 2.5 hrs for all switches this was the endpoint used. 3.3 nM linear DNA switch with 500 nM miR-122 gave the highest level of fluorescence (Figure 4-3B). The highest fold induction was seen for 0.33 nM of linear DNA switch with 500 nM miR-122 (Figure 4-3C). Although 3.3 nM THS1 DNA demonstrated the greatest fluorescence intensity, a greater fold induction was seen with 0.33 nM of THS1 DNA. Therefore, further testing used 0.33 nM of linear toehold switch DNA construct. In addition, a substantial increase in fold induction was only observed upon the addition of 500 nM miR-122, therefore this was the concentration used for the first test with the entire panel of switches.

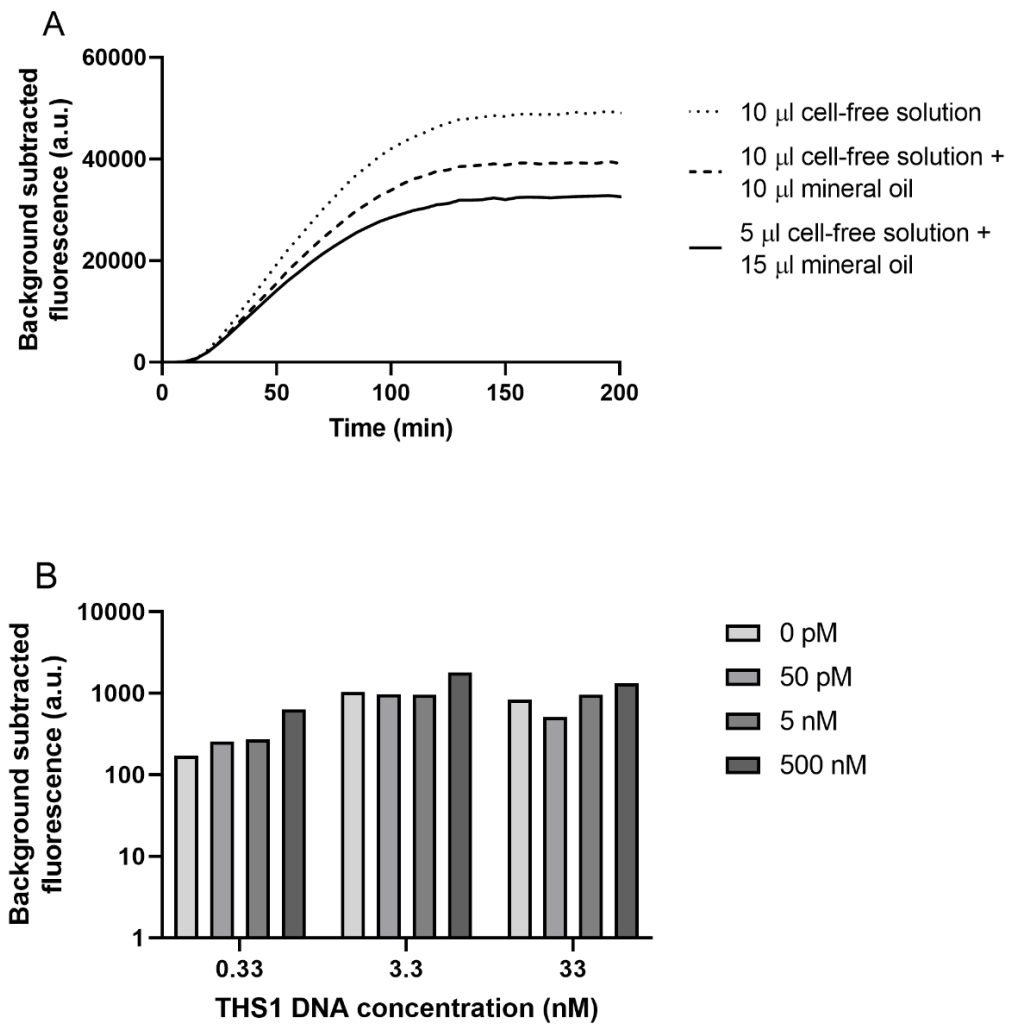


**Figure 4-3: Optimisation of conditions for GFP switch tests.**

Optimisation of cell-free reaction solution and mineral oil volumes for testing of the switches. (A) The positive control (PT7-30gfpt@3K3) was incubated alone and with mineral oil ( $n=1$ ). Background subtracted fluorescence (arbitrary units) shown. (B & C) THS1 DNA of varying concentrations (0.33, 3.3 & 33 nM) were added to cell-free reaction solutions in the presence of 0 pM, 5 pM, 5 nM & 500 nM miR-122, ( $n=1$ ). (B) Background subtracted fluorescence; (C) Fold induction.

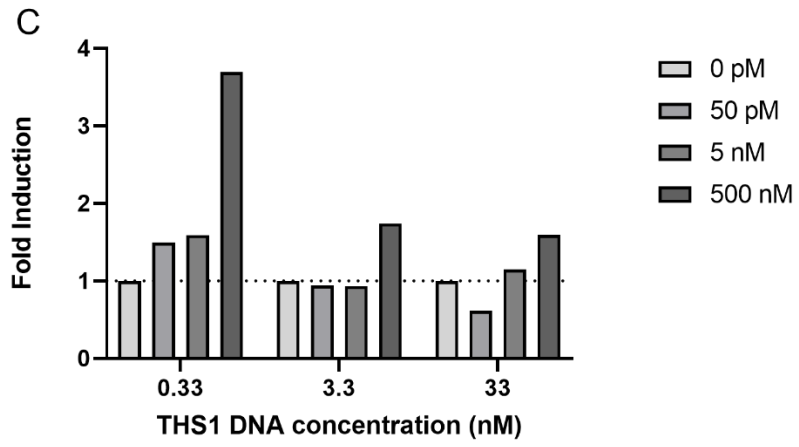
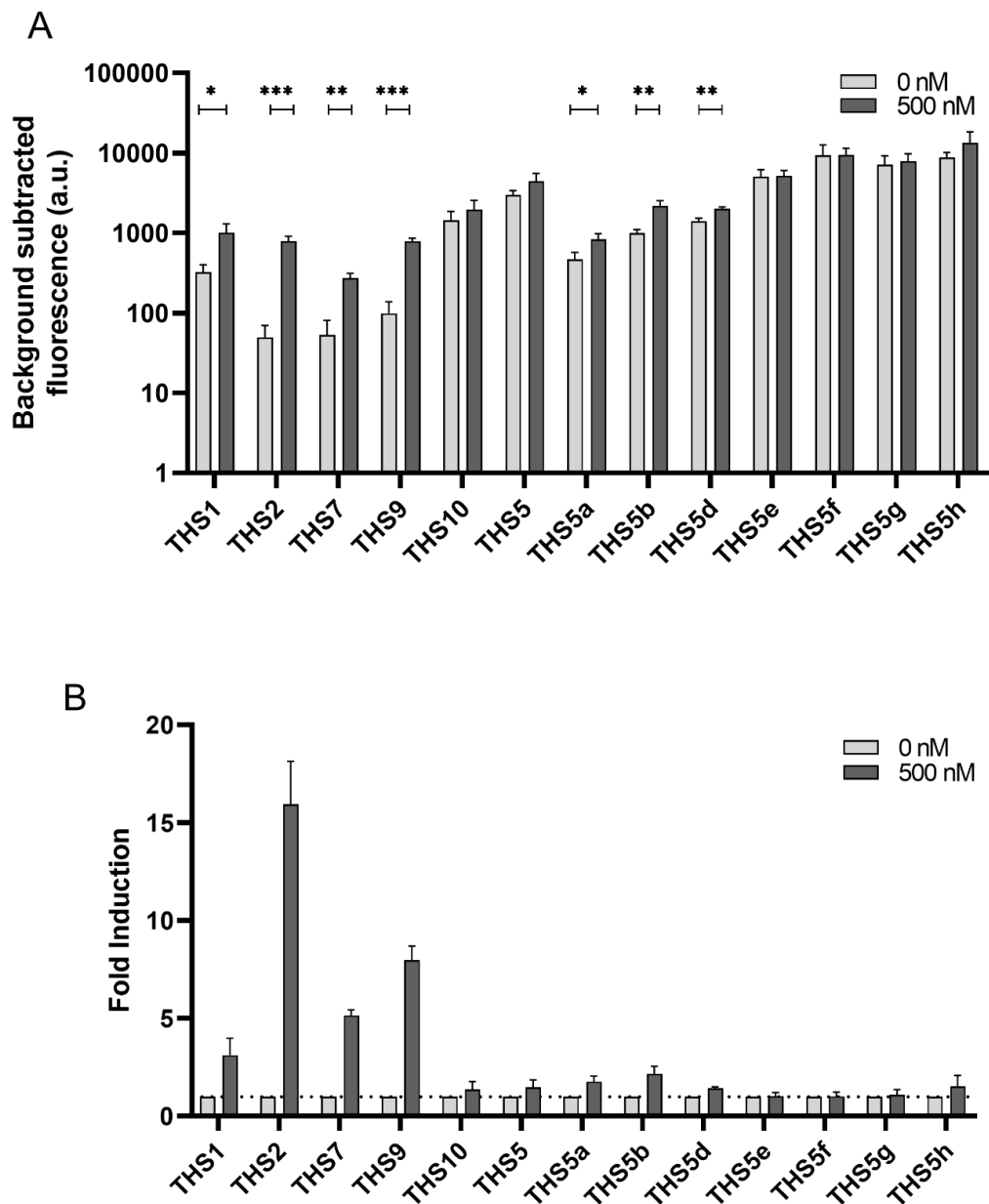


Figure 4-3: (cont.)

#### 4.3.2.2 Sensitivity:

After identifying the optimal conditions for testing the switches the complete panel of switches was tested with 500 nM miR-122, or uninduced (0 nM) (Figure 4-4). The time course data for these experiments can be found in Appendix 4.v. Fluorescence expression was highly variable between the different switches (Figure 4-4A). The highest levels of fluorescence expression were seen in THS5f, THS5g and TH5h, with the lowest levels of fluorescence expression for THS2, THS7 and THS9. There was a significant increase in the fluorescence produced by switches THS1, THS2, THS7, THS9, THS5a, THS5b and THS5d when induced with 500 nM miR-122 compared to uninduced switches (0 nM). The fold induction of the switches was calculated by the ratio of the induced switches compared to uninduced switches (Figure 4-4B). The greatest fold induction was seen for THS2 with a 16-fold increase in fluorescence when exposed to 500 nM miR-122 compared to the uninduced switch. Switches with a fold induction of greater than two included THS1, THS2, THS7, THS9 and THS5b.

A subset of switches from the complete panel were selected for further investigation. This subset included switches with a fold induction greater than two. In addition, THS10 and THS5h were included as they both produced high levels of fluorescence. These switches were tested with miR-122 concentrations of 5, 50 & 500 nM, as well as uninduced controls (0 nM), (Figure 4-5). For THS1, THS2, THS7, THS9 and THS5b with increasing concentrations of miR-122 an increase in fluorescence was seen (Figure 4-5A). However, there were only significant differences in fluorescence for THS1, THS2, THS7, THS9 when induced with 500 nM, and not at lower concentrations of miR-122. THS5b demonstrated a significant increase in fluorescence expression when induced with 50 nM miR-122, however, this was associated with a limited increase in fold induction of the switch. Both THS10 and THS5h did not demonstrate a dose-response to increasing concentration of miR-122, with higher fluorescence expression when induced with 5 nM than 500 nM miR-122. THS1, THS2, THS7, THS9 and THS5b had a fold induction greater than two for 50 nM miR-122 (Figure 4-5B). Fold induction was limited for switches induced with 5 nM miR-122.



**Figure 4-4: Test of panel of switches.**

The complete panel of switches was tested with 0 nM & 500 nM miR-122. (A) Background subtracted fluorescence (arbitrary units); (B) Fold induction. DNA concentration of switches = 330 pM. Bar chart shows data at 2.5 hrs,  $n=3$ . Bars show mean and error bars standard deviation. Statistical significance of the difference between 0 and 500 nM fluorescence was determined with a *t*-test for each switch. Statistical significance ( $P > 0.05 = ns$ ;  $P < 0.05 = *$ ;  $P < 0.01 = **$ ;  $P < 0.001 = ***$ ;  $P < 0.0001 = ****$ ).

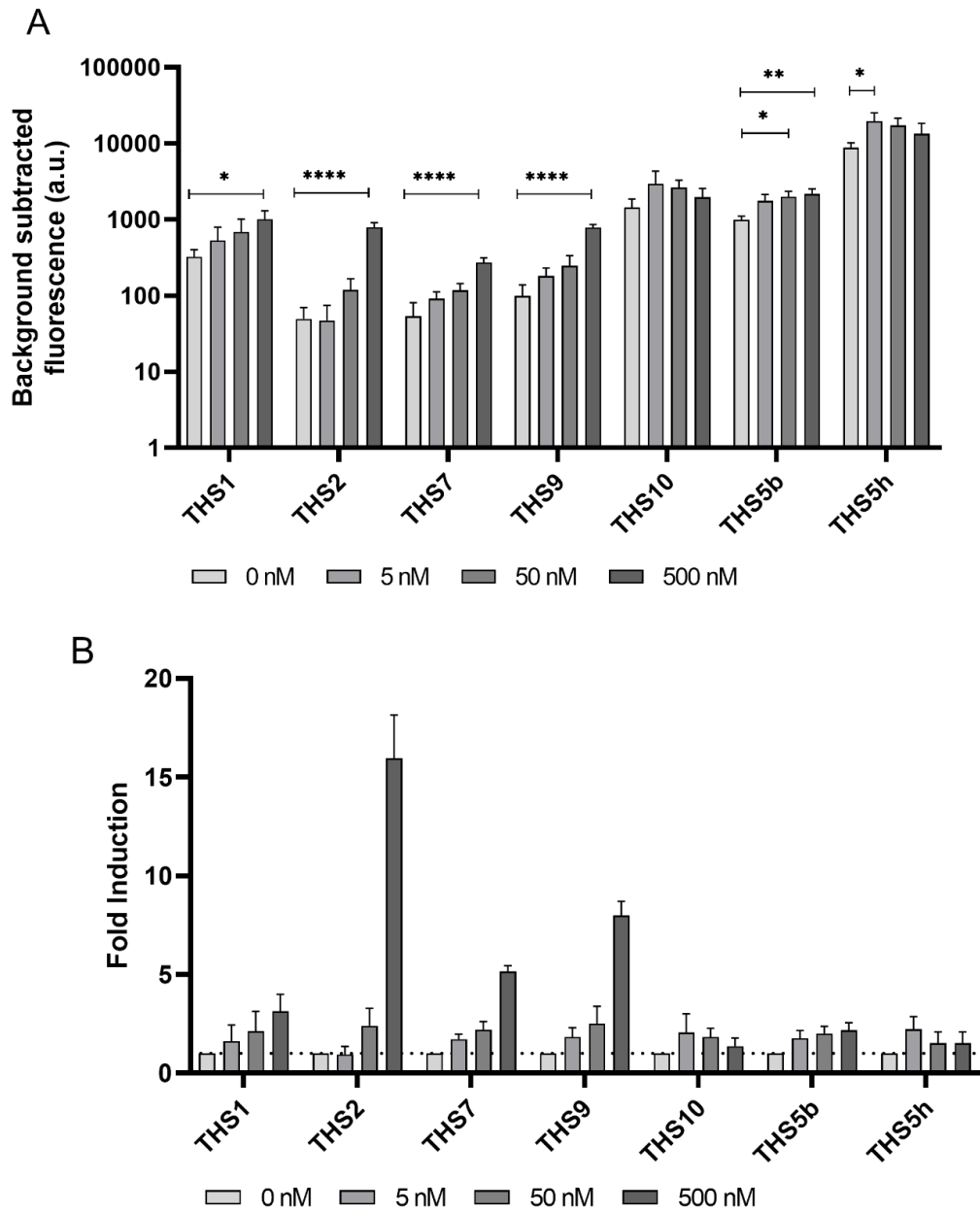


**Figure 4-5: Sensitivity test of a subset of switches.**

A subset of the panel of switches were tested with 0, 5, 50 & 500 nM miR-122. (A) Background subtracted fluorescence (arbitrary units); (B) Fold induction. DNA concentration of switches = 330 pM. Bar graphs show data at 2.5 hrs,  $n=3$ . Bars show mean and error bars standard deviation. Statistical significance of the difference in fluorescence was determined using a one-way ANOVA for each switch with Dunnett's multiple comparison tests between 0 nM and other miR-122 concentrations. Statistical significance ( $P > 0.05 = ns$ ;  $P < 0.05 = *$ ;  $P < 0.01 = **$ ;  $P < 0.001 = ***$ ;  $P < 0.0001 = ****$ ).

## 4.3.2.3 Specificity:

In order to test the specificity of the switches two miRNA were tested, miR-39 and miR-3591. MiR-39 is a *C. elegans* microRNA which is used as a spike-in control in the Qiagen serum/plasma RNA extraction kit. MiR-3591 is a human microRNA with high sequence similarity to miR-122 (Table 4-12). A subset of the panel of switches was tested with 500 nM of miR-122, miR-39 and miR-3591 as well as uninduced control (Figure 4-6), time-course data shown in (Appendix 4.vi). THS1, THS2, THS7 and THS9 demonstrated a higher fluorescence expression for miR-122 than for switches induced with miR-39 or miR-3591, or uninduced switches (Figure 4-6A). This increase in fluorescence was significant for THS2, THS7 and THS9. For these switches, the expression of fluorescence when induced with miR-39 and miR-3591 was of a similar level to uninduced switches. Furthermore, these switches had a fold induction of approximately one for both miR-39 and miR-3591 (Figure 4-6B). THS5b and THS5h had similar fluorescence production when uninduced, and induced with miR-122, miR-39 and miR-3591, indicating these switches are not specific for miR-122.

MicroRNA	Sequence	Length
hsa-mir-122-5p	uggagugugacaaugguguuug	22
cel-miR-39-3p	ucaccggguguaaaucagcuug	22
hsa-miR-3591-5p	uuuagugugauaauggcguuuga	23

**Table 4-12: MicroRNA sequences of miR-122, miR-39 and miR-3591.**



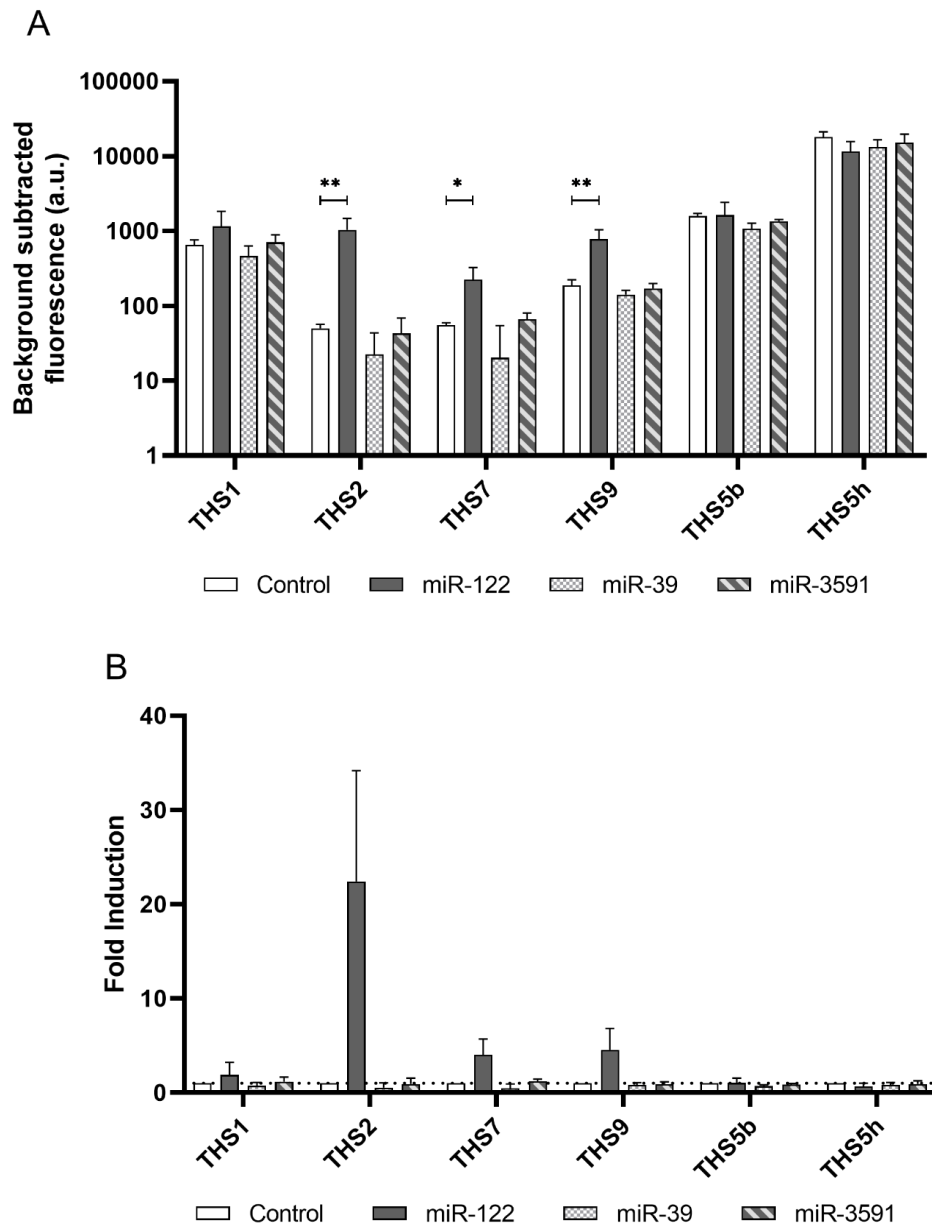


**Figure 4-6: Specificity test of switches.**

A subset of the panel of switches was tested with H<sub>2</sub>O (control), 500 nM miR-122, 500 nM miR-39 or 500 nM miR-3591. (A) Background subtracted fluorescence (arbitrary units); (B) Fold induction. DNA concentration of switches = 330 pM. Bar graphs show data at 2.5 hrs, n=3. Bars show mean and error bars standard deviation. Statistical significance of the difference in background subtracted fluorescence was determined using a one-way ANOVA for each switch with Dunnett's multiple comparison tests between control and miRNAs. Statistical significance ( $P > 0.05 = ns$ ;  $P < 0.05 = *$ ;  $P < 0.01 = **$ ).

#### 4.3.2.4 Further optimisation of test conditions:

The switch tests so far had used DNA constructs at 330 pM, a concentration determined to work well by the initial test of THS1, and as used by Pardee and colleagues [156]. However, altering the DNA concentration of the DNA constructs added to the cell-free reaction solution could affect the fold induction of the switches, and furthermore could affect the individual switches differently. The cell-free reaction solution is a finite resource, with two processes occurring which use up resources. Firstly, the DNA construct is transcribed into mRNA, containing the toehold switch and reporter gene. This mRNA transcript is then bound to by the miR-122 inducer, resulting in the translation of the *gfp* reporter gene into a protein. Both transcription and translation consume resources from the cell-free reaction solution. Adding more DNA to the cell-free system should in theory lead to the production of more mRNA transcript, leading to less resources being available to produce the reporter protein. Therefore, increasing the DNA concentration of the THS construct should lead to an increased sensitivity of the system, whilst keeping the leakiness of the system low. On the other hand, reducing the DNA concentration of the construct should in theory result in reduced leakiness of the switches.

Therefore, THS1, THS5b and THS5h were tested with reduced DNA concentration, at 33 pM rather than 330 pM. In addition, THS1, THS2, THS7, THS9 and THS10 were tested with 3300 pM DNA. The background fluorescence data is shown in Figure 4-7, the fold induction data is shown in Figure 4-8 and the time-course data can be found in Appendix 4.vii for these experiments. The general trends identified were that increasing the DNA concentration increased fluorescence production. Furthermore, lower DNA concentrations had a higher fold induction. THS5b and THS5h produced much higher levels of fluorescence than the other switches in the panel, however, they had a low fold induction. Reducing the concentration of the DNA construct reduced the levels of fluorescence produced. Furthermore, reducing the concentration of the DNA construct led to an improvement in fold induction, with an increase from 3 to 4.5 for THS1, and from 2 to 3.5 for THS5b. For THS1, THS2, THS7, THS9 and THS10 increasing the DNA concentration did not lead to an increase in fold induction, nor in sensitivity, for any of the switches tested. However, the increase in DNA concentration did lead to a slight increase in fluorescence production for all the switches.

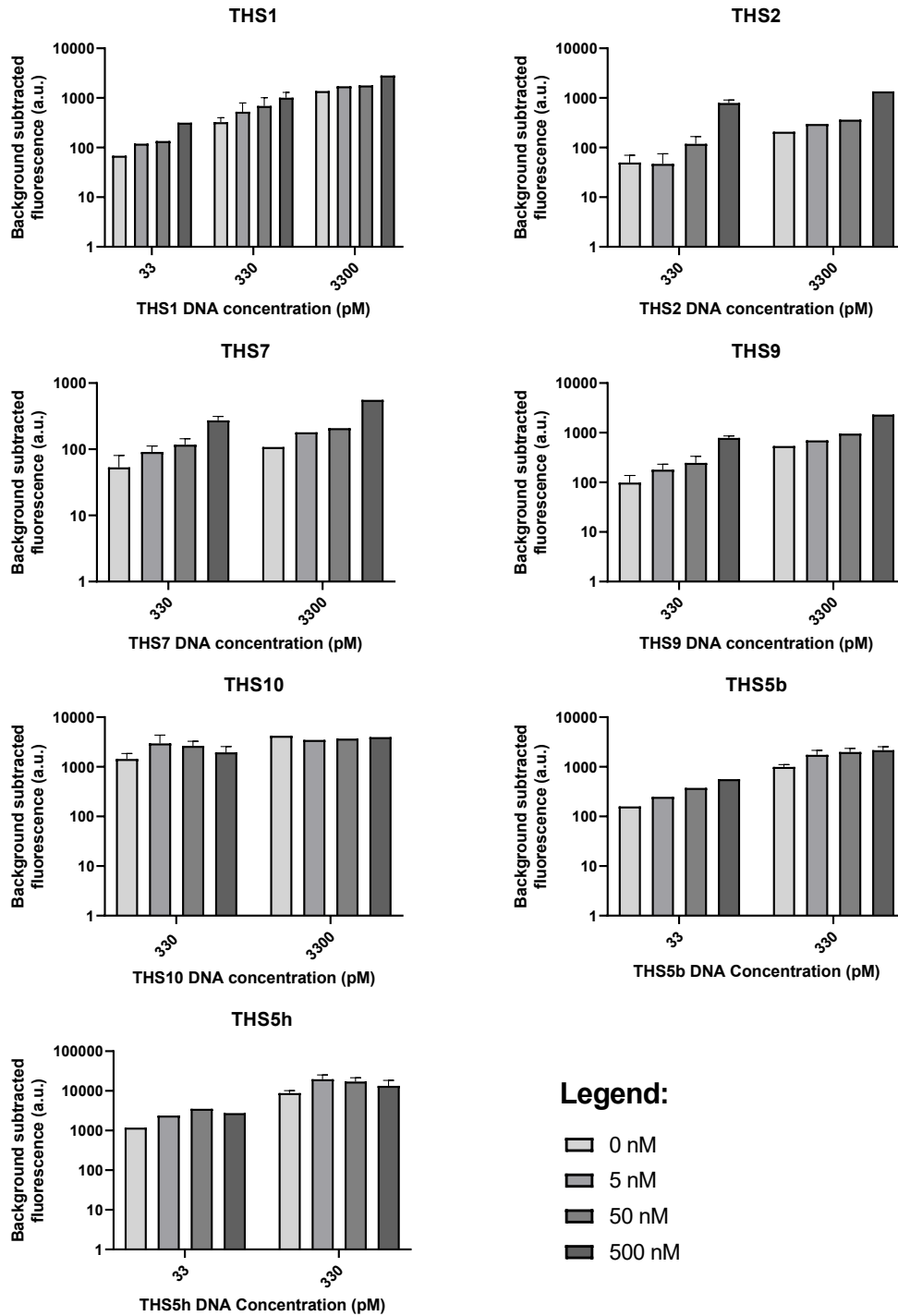


**Figure 4-7: Test of switches using different DNA concentrations: Fluorescence.**

Graphs show background subtracted fluorescence (arbitrary units). Different switch DNA concentrations used described on the graphs. Concentrations of miR-122 used were 0, 5, 50 & 500 nM. Bar graphs show data at 2.5 hrs. For THS DNA concentrations of 330 pM three replicates were taken from the previous sensitivity experiment, error bars show standard deviation. For DNA concentrations of 33 & 3300 pM a single replicate was done.

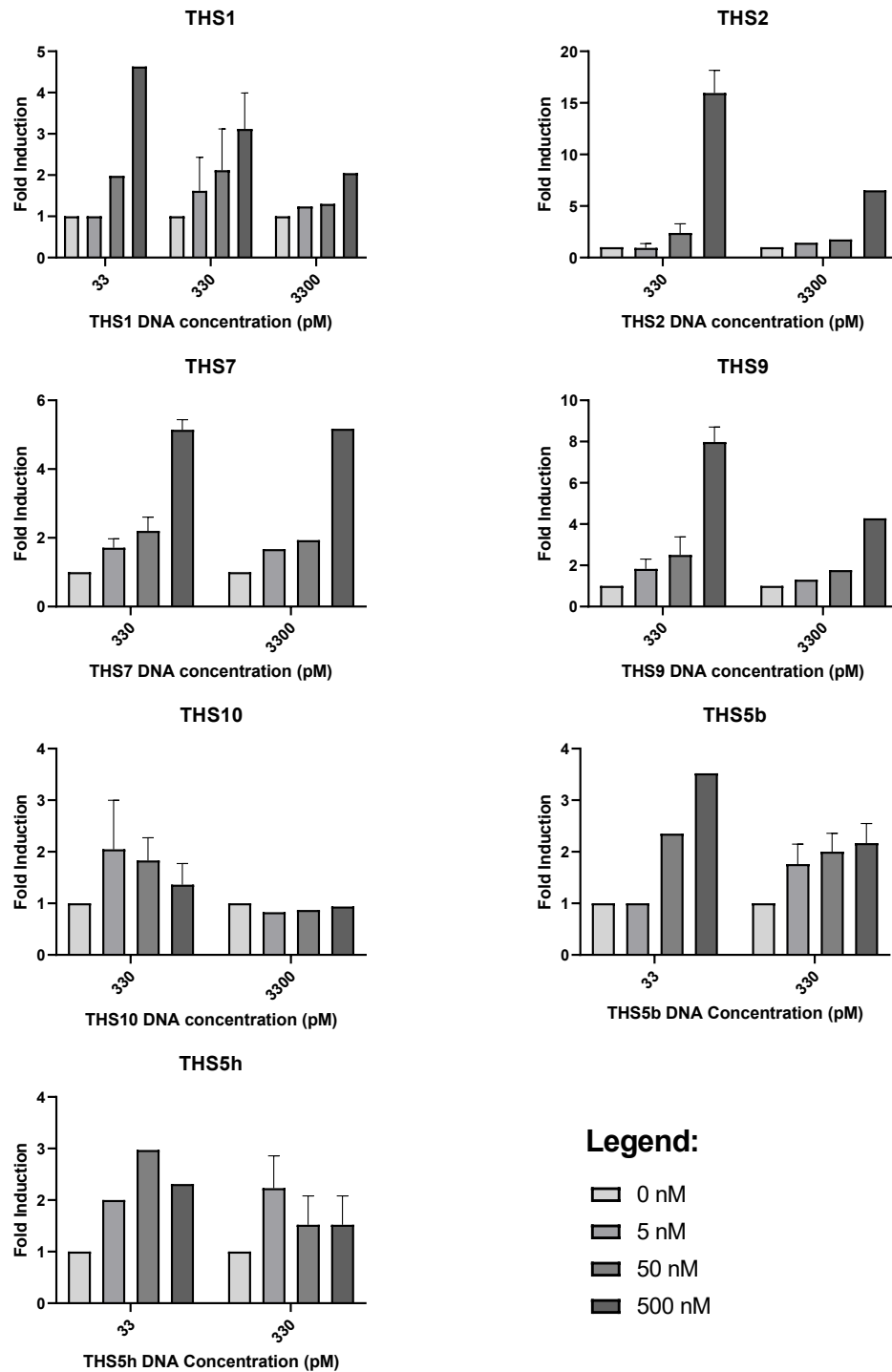


**Figure 4-8: Test of switches using different DNA concentrations: Fold induction.**

Graphs show fold induction. Different switch DNA concentrations used described on the graphs. Concentrations of miR-122 used were 0, 5, 50 & 500 nM. Bar graphs show data at 2.5 hrs. For THS DNA concentrations of 330 pM three replicates were taken from the previous sensitivity experiment, error bars show standard deviation. For DNA concentrations of 33 & 3300 pM a single replicate was done.

### 4.3.3 LacZ switches:

#### 4.3.3.1 Sensitivity:

After testing the GFP switches a subset of switches was taken forward, with the *gfp* gene replaced by the *lacZ* gene to create a colorimetric output. The toehold switches THS1, THS2, THS7 and THS9 were tested with 50, 100 and 500 nM miR-122, along with uninduced controls. The time course data for these experiments can be found in Appendix 4.viii. Due to the saturation of the plate reader by 3.3 nM THS1 and THS9 the concentration of the DNA construct was reduced from 3.3 nM to 0.33 nM to investigate whether this would prevent saturation. Absorbance is shown at two different timepoints, 1 hour (Figure 4-9A) and 2.5 hrs (Figure 4-10A). Fold induction was calculated at the two time points, 1 hour (Figure 4-9B) and 2.5 hrs (Figure 4-10B).

3.3 nM THS1 demonstrates near saturation at 1 hour and saturation at 2.5 hrs. The fold induction for this switch at 1 hour is approximately 2 for 100 and 500 nM miR-122, however, the variation seen is high. For 0.33 nM THS1, at 1 hour the absorbance shown for the different concentrations of miR-122 and uninduced switches was similar and at 2.5 hrs saturation was again seen. 3.3 nM THS9 demonstrated a dose-response relationship between miR-122 concentration and absorbance at 1 hour, however, at 2.5 hrs saturation is reached. Reducing the DNA construct concentration to 0.33 nM reduced the absorbance measured. Furthermore, at 2.5 hrs, for 0.33 nM THS9 a dose-response to increasing miR-122 concentrations is identified. As a result, there is an approximately 1.5-fold induction in absorbance when 0.33 nM THS9 is induced with 500 nM miR-122. Both THS2 and THS7 demonstrated smaller increases in absorbance, thus not saturating the plate reader. After 1 hour THS2 demonstrated a marginal fold induction with 500 nM miR-122. After 2.5 hrs both THS2 and THS7 had a greater than 1.5-fold induction with 500 nM miR-122.

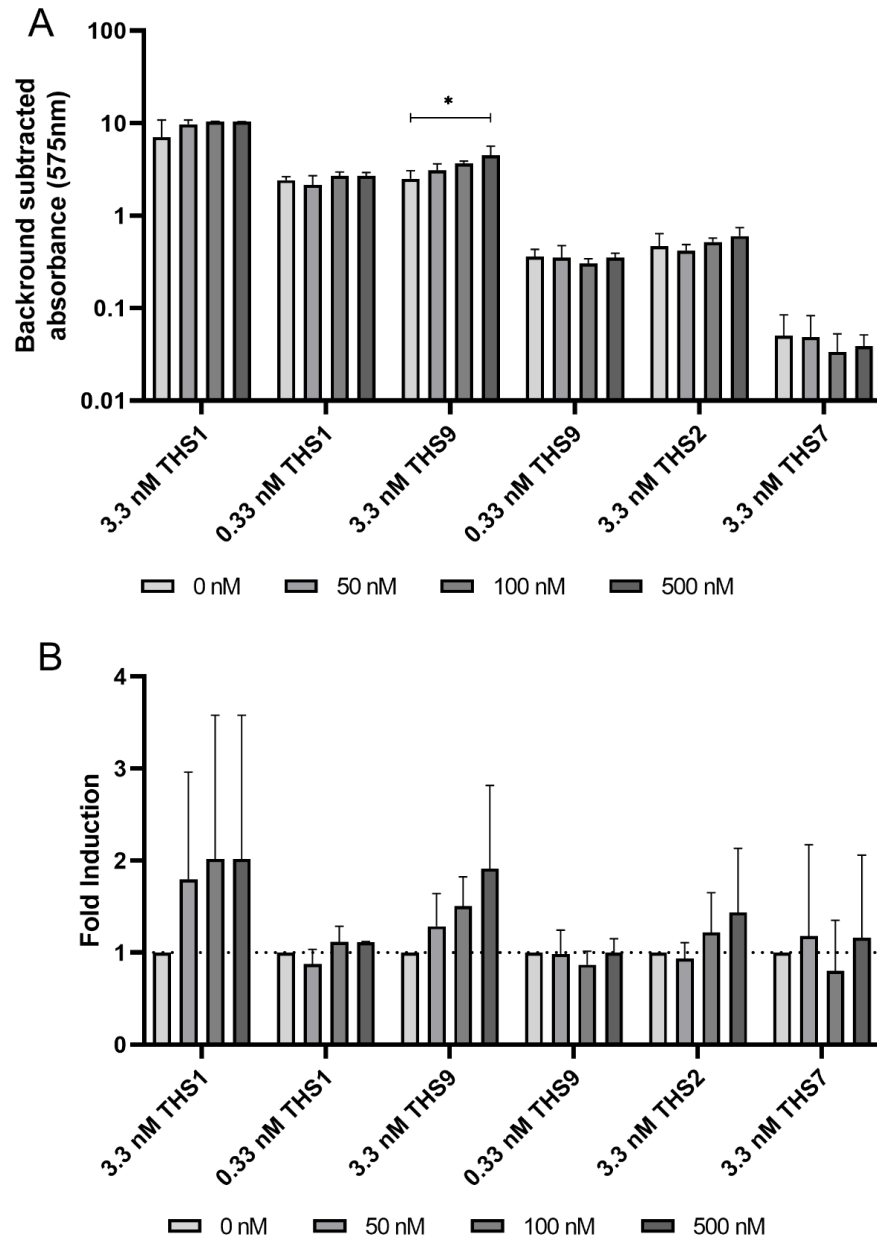


**Figure 4-9: Test of lacZ switches: 1 hour.**

Test of lacZ switches after incubation for 1 hour. (A) Background subtracted absorbance (575 nm); (B) Fold induction. DNA concentrations of switches described in graphs. Concentrations of miR-122; 0, 50, 100 & 500 nM. Bars show mean and error bars standard deviation, n=3. Statistical significance of the difference in background subtracted absorbance was determined using a one-way ANOVA for each switch with Dunnett's multiple comparison tests between 0 nM and other miR-122 concentrations. Statistical significance ( $P > 0.05 = ns$ ;  $P < 0.05 = *$ ).

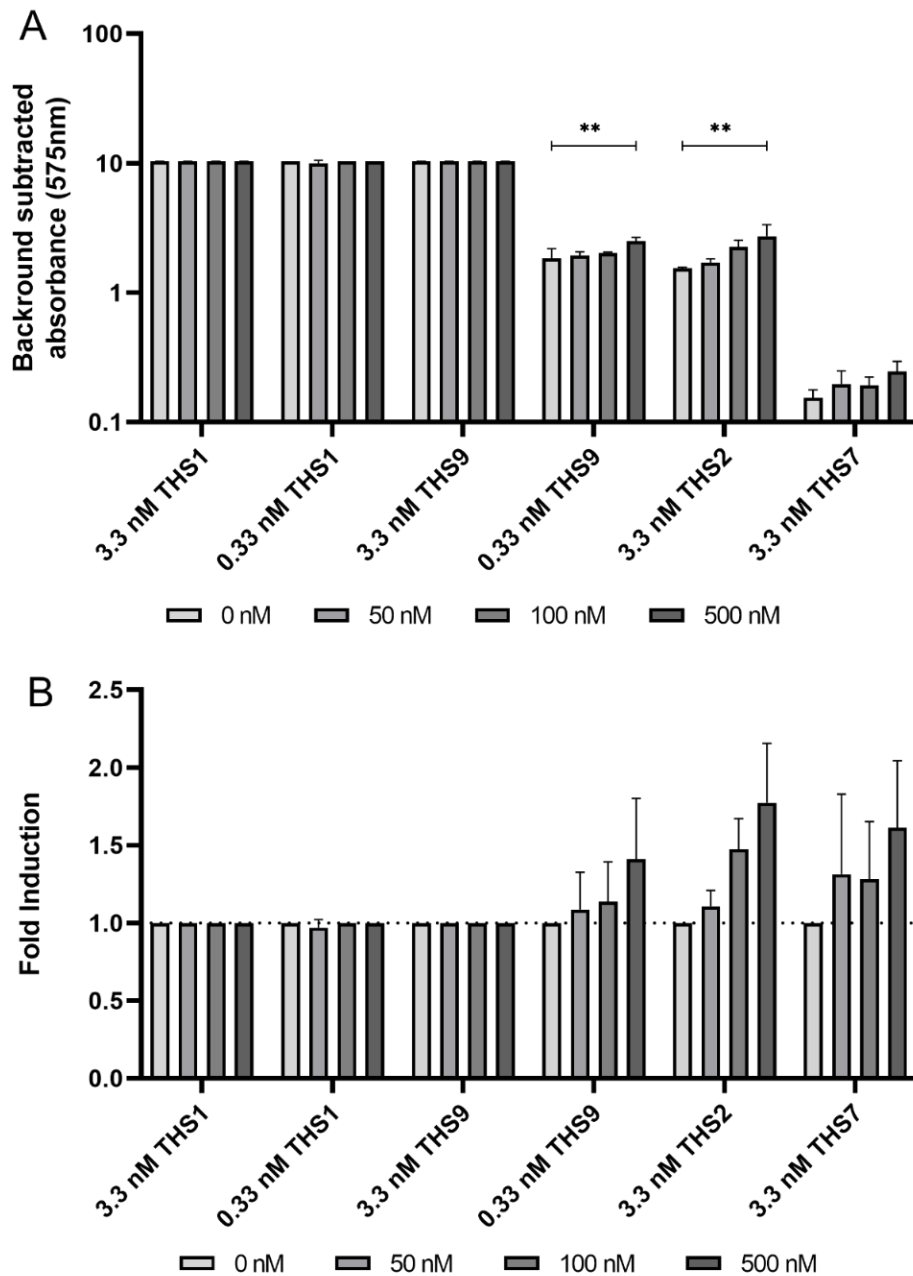


**Figure 4-10: Test of lacZ switches: 2.5 hrs.**

Test of lacZ switches after incubation for 2.5 hrs. (A) Background subtracted absorbance (575 nm); (B) Fold induction. DNA concentrations of switches described in graphs. Concentrations of miR-122; 0, 50, 100 & 500 nM. Bars show mean and error bars standard deviation,  $n=3$ . Statistical significance of the difference in background subtracted absorbance was determined using a one-way ANOVA for each switch with Dunnett's multiple comparison tests between 0 nM and other miR-122 concentrations. Statistical significance ( $P > 0.05 = ns$ ;  $P < 0.05 = *$ ;  $P < 0.01 = **$ ).

## 4.3.3.2 Paper test of lacZ positive control:

An initial test of the positive control PT7-lacZ@1K3 on paper indicated that something present in the paper was inhibiting the reaction. Therefore, blotting paper was washed with either ethanol, methanol or isopropanol. Pieces of washed paper were incubated with the positive control PT7-lacZ@1K3 and cell-free reaction solution (Figure 4-11). Despite washing, the reaction in the presence of paper remained inhibited.



**Figure 4-11: Paper test with lacZ positive control.**

*Test of the positive control when incubated with paper pieces washed with either (a) ethanol, (b) methanol, (c) isopropanol, or (d) no paper control.*



#### 4.4 Discussion:

##### 4.4.1 Main findings:

- Several of the GFP switches developed in this project demonstrated a relationship between miR-122 concentration and the level of fluorescence produced, with a fold induction greater than two for 5 nM miR-122.
- The GFP switches THS1, THS2, THS7 and THS9 demonstrated specificity for miR-122 with limited induction in the presence of miR-39 and miR-3591.
- Some of the *lacZ* switches had a relationship between absorbance and miR-122 concentration. *LacZ* switches showed different kinetics to the GFP switches.

##### 4.4.2 Toehold switches can detect miRNAs:

This work is some of the earliest work to demonstrate that toehold switches can be used to detect miRNAs. Work on toehold switches began in 2014, with the development of the idea of toehold switches by Green and colleagues [157], and the development of paper-based synthetic networks by Pardee and colleagues [156]. Recent work has described toehold switches to a range of targets, however, most of this work was limited to RNA and DNA targets, with only one recently published paper describing a toehold switch for a miRNA target [161]. The previously developed toehold switch could detect exogenous and endogenous miR-155 and miR-21 in mammalian cells, with switches demonstrating sensitivity to the nanomolar range, high specificity and a fold induction of approximately two [161].

The work described in this chapter demonstrates that toehold switches can be used to detect the liver injury biomarker miR-122. The GFP toehold switches developed demonstrated variable sensitivity and specificity to miR-122, with several switches demonstrating a fold induction of greater than two for 50 nM miR-122. The *lacZ* switches demonstrated different kinetics along with a more limited ability to detect lower concentrations of miR-122.

##### 4.4.3 GFP and *lacZ* switches exhibit different reaction kinetics:

Testing switches with both a GFP and  $\beta$ -galactosidase output has identified a difference in reaction kinetics between the two outputs. The GFP switches all had an initial rise in GFP

production, eventually leading to a plateau at approximately 2.5 hrs for all switches. The height of plateau reached differed between the GFP switches, with a 10-fold higher level of fluorescence reached with some switches compared to others. The *lacZ* switches demonstrated different reaction kinetics, with THS1 and THS9 saturating the reading capabilities of the plate reader. THS2 and TH7 exhibited different kinetics, with absorbance rising more slowly and not reaching the same plateau that the other switches did. The increase in absorbance was more rapid than the generation of fluorescence seen for the GFP switches. This is likely since the *lacZ* switches produce a  $\beta$ -galactosidase enzyme capable of converting many substrate molecules to generate the change in absorbance. However, the GFP switches rely on the continued production of GFP to cause the level of fluorescence to rise.

#### 4.4.4 Structural changes to toehold switches impact their functionality:

One aspect of this project was to investigate the effect different structural changes have on switch behaviour. As described in section 4.1.1, the panel of switches designed, assembled and tested had alterations designed to affect switch stability, access of the ribosome to the RBS and the accessibility of the miR-122 binding site. This panel of switches was then tested to assess how alterations in the switch sequence impacted the output, sensitivity and specificity.

One of the main issues common across all switches was leakiness, with some switches having a nearly equal production of GFP or  $\beta$ -galactosidase in the absence of miR-122. One of the toehold switch modifications which had the greatest impact on leakiness was the increase in loop size in the THS5s. With an increased loop size comes an increased accessibility of the RBS, and so binding of miR-122 is not required for the ribosome to bind and for GFP or  $\beta$ -galactosidase production to occur. The switches with a loop size of 8-15 nucleotides demonstrated a significant increase in fluorescence production in the presence of 500 nM miR-122 compared to uninduced switches. Switches with a loop size of greater than 15 bases had similar fluorescence production in the presence and absence of miR-122. Previous work on Zika virus switches used a switch with a loop of 11 nucleotides after identifying leakiness in switches with a loop size of 18 nucleotides [158].

A further design modification which aimed to combat the problem of leakiness was the increased lower stem length of THS2. The aim of this modification was to increase the stability of the toehold switch. Although THS2 has a lower output than THS1 it is the least leaky switch, with the lowest production of fluorescence in the absence of miR-122. As a result, THS2 has the highest fold induction of all the switches, showing an approximately 15-fold increase in the presence of 500 nM miR-122. One of the limitations of THS2 however is its limited induction in the presence of lower concentrations of miR-122, with a fold induction of approximately 1 for 5 nM miR-122. The *lacZ* THS2 appeared the most promising of the *lacZ* switches tested, demonstrating a dose-response to miR-122 concentrations and a fold induction of greater than 1.5 in the presence of 500 nM miR-122. The stability of THS2 prevents leakiness at higher concentrations of miR-122 but results in lower concentrations of miR-122 being unable to activate the switch.

The addition of a refolding domain to THS7 was designed to alter the accessibility of the RBS, generating a weaker secondary structure, which is more easily unwound and bound to by a ribosome. THS7 demonstrated a low fluorescence output but a fold induction of greater than 5-fold for 500 nM miR-122, along with fold induction greater than one for 5 nM miR-122. Similarly, the *lacZ* switch for THS7 has a low output. Although the *lacZ* THS7 switch demonstrated a dose-response to miR-122 concentrations, the low output limits the use of this switch. The low output makes identifying a significant colour change on paper-based system challenging, thus limiting its use.

A further switch modification aimed to alter the accessibility of the RBS was included in THS10. THS10 was altered to include a weak base at the bottom of the unwound RBS loop, making the miR-122-switch complex more unstable, leading to easier binding of a ribosome. THS10 had a slightly higher GFP output than THS1. However, THS10 produced a low fold induction in response to miR-122, and surprisingly lower concentrations of miR-122 had a greater fold induction than higher concentrations.

The final alteration in switch structure was the shift of the miR-122 binding site in THS9. THS9 had a reduced toehold domain and more of the miR-122 binding sequence sequestered in the stem of the hairpin loop. Shifting the miR-122 binding site reduces its

accessibility. Despite the reduction in the length of the toehold domain THS9 demonstrated the second-best fold induction in the presence of 500 nM miR-122, with a fold induction of greater than one for 5 nM miR-122. Furthermore, THS9 had good specificity for miR-122. Of the *lacZ* switches developed THS9 showed some promise, with a limited fold induction after 2.5 hrs in the absence of miR-122. However, given the similarities in absorbance between the induced and uninduced switches differentiating on a paper-based test would be challenging.

The structural changes designed in the switches explain some of the reasons why GFP and  $\beta$ -galactosidase production differ. After testing both the GFP and *lacZ* switches, the two best structural modifications appear to be those included in THS2 and THS9, an increased lower stem length and a shifted miR-122 binding site.

#### 4.4.5 Limitations:

The toehold switch system developed for this PhD project has limited sensitivity, meaning that it currently cannot identify clinical levels of miR-122, even in DILI. This limitation is not uncommon across other toehold switch systems with many relying on amplification methods prior to quantification using the toehold switch system. One of the most commonly used methods to amplify RNA for diagnostic systems is by nucleic-acid sequence-based amplification (NASBA). The main advantage of NASBA, and the reason why it is included in diagnostic assays, is that it works at isothermal conditions, usually at a constant temperature of 41 °C. NASBA uses 2 primers specific to the RNA template, along with a reverse transcriptase, which replicate the RNA present in the sample in a cyclical process. The addition of an amplification step for miR-122 prior to quantification by the toehold switch system could overcome the limited sensitivity. However, the inclusion of extra steps in the process increases the time of the assay and its cost. Furthermore, designing the primers for NASBA is challenging, and with the limited sequence of miR-122, of 22 nucleotides, may not be possible to achieve.

A further limitation of the *lacZ* system used in this project is the speed of production of the output. For the switches which did not saturate (0.33 nM THS9, 3.3 nM THS2 and 3.3 nM THS7), the reaction took longer to reach a plateau than the GFP switches. This is likely due

to the GFP being a smaller protein than  $\beta$ -galactosidase. Longer periods of time are required for the synthesis and folding of the  $\beta$ -galactosidase. In addition, more of the resources of the cell-free reaction solution are consumed in this process. To overcome this problem a novel approach has been developed,  $\alpha$ -complementation, by Ma and colleagues [159]. This technique works by splitting the  $\beta$ -galactosidase protein into 2 fragments,  $\alpha$  and  $\omega$ . The lacZ  $\alpha$ -peptide (lacZ $\alpha$ ) consists of the first 50-59 residues (6% of complete lacZ) from the N terminus of lacZ and the  $\omega$ -peptide (lacZ $\omega$ ) consists of the remaining  $\sim$ 970 residues. In the toehold switch system Ma and colleagues proposed that lacZ $\alpha$  could be the output of the system and the lacZ $\omega$  peptide would be present as a pre-synthesised component already present on the paper. The production of lacZ $\alpha$  would enable complementation with lacZ $\omega$ , producing the fully assembled and active enzyme product  $\beta$ -galactosidase. This method has been demonstrated to reduce the time to detection of the paper-based assay by 23 min, or 41%, compared to experiments using the full-length lacZ as the output [159].

#### 4.4.6 Further work:

Further work should look to address some of the limitations of the current switches. Firstly, additional novel toehold switch structures could be designed and tested. These could include switches which combine the features of THS2 and THS9. THS2 and THS9 had the best fold induction of all the switches, therefore a combination of these features may further improve the functionality of the switch. In addition to combining features already investigated in this study, further modifications could be investigated. Previous work has utilised bioinformatics algorithms to determine possible optimal toehold switch sequences [157]. This approach may yield switches with improved sensitivity and specificity.

In order to determine the diagnostic power of these novel toehold switches, they should be tested with clinical samples from healthy volunteers and patients with DILI. This would demonstrate whether the toehold switch system was sensitive and specific enough to diagnose the presence of DILI. Serum or plasma sample from patients will contain a wide variety of miRNAs. Therefore, a switch which was not sufficiently specific for miR-122 could become activated from the binding of other miRNA species. The specificity experiment in this study demonstrated that some of the switches are specific for miR-122 over miR-39 and

miR-3591. However, it is possible that other miRNAs not tested in this work may activate the switches.

However, despite further modifications to the toehold switch structure it may not be possible to reach the level of sensitivity required for the identification of DILI in clinical samples. Therefore, the inclusion of an amplification step may be required. Recent work has utilised various approaches to amplify target sequences including NASBA [158], [160] and synbodies [159]. The addition of an amplification step may enable detection of clinical levels of miR-122.

A further potential issue with quantifying miR-122 from clinical samples is the different forms that miRNA exists in when extracellular. MiRNAs exist either in vesicles or associated with proteins [84], [85]. This limits the accessibility of the miRNA and may prevent miRNA binding to the toehold switch. Previous work has quantified endogenously expressed miRNAs within a cell [161] suggesting that protein binding does not inhibit miRNA binding. However, there is no evidence that toehold switches can bind to extracellular miRNAs, which may be encapsulated in vesicles or bound to proteins. Further work should investigate whether this is an issue in clinical samples. Although an RNA extraction step may provide an answer to this issue.

In order to be useful as a point of care test, the toehold system needs to fulfil several criteria, being rapid, easy to use and not require complex laboratory facilities. Therefore, a paper-based system should be used, combining a toehold switch with a colorimetric output and utilising a freeze-dried cell-free system on paper. Work in this thesis found that the reaction was inhibited on paper, despite washing of the paper prior to use. Recent work by Pardee and colleagues have demonstrated that a *lacZ* output combined with a freeze-dried cell-free system on paper can provide a visual output for Zika virus detection which can be read by eye [158]. Further work on the toehold switch system for miR-122 should develop a paper-based system, determining its diagnostic utility.

#### 4.4.7 Summary:

This work has developed an initial panel of toehold switch designs, which are able to detect miR-122 and have specificity in the presence of different miRNAs. Furthermore, this work has demonstrated that GFP and  $\beta$ -galactosidase can provide quantitative outputs for this novel system. The toehold switches developed have limitations including sensitivity and speed of output. Further work should focus on improving the functionality of the system and testing it with clinical samples.

## 5 Conclusions



### 5.1 Summary of findings:

The studies presented in this thesis have three broad aims, firstly to assess the potential of miR-122 and K18 as biomarkers of ATDILI, secondly to develop a model of ATDILI in zebrafish in order to assess miRNA changes, and thirdly, to develop a novel toehold switch system capable of detecting miR-122.

Chapter 2 of this thesis describes the circulating concentration of miR-122 and K18 in healthy volunteers and patients receiving treatment for mycobacterial infections. There was no significant difference in miR-122 and K18 across healthy volunteers and patients with mycobacterial infections, indicating that infection itself does not affect miR-122 and K18. Upon starting treatment there was no change in miR-122 and K18 in the absence of DILI. Patients with elevations in ALT also experienced elevations in miR-122 and K18. Furthermore, in two cases of ATDILI both miR-122 and K18 were elevated with peak ALT, suggesting these biomarkers have potential in the diagnosis of ATDILI. Most of the previous work on miR-122 and K18 has focussed on the specific issue of paracetamol overdose induced liver injury. This study contributes to the field of knowledge on these biomarkers, primarily demonstrating that infection itself doesn't affect miR-122 and K18.

The third chapter of this thesis demonstrated that the anti-TB drugs INH and PYR cause DILI in zebrafish larvae. INH and PYR induced morphological changes, a reduction in liver size and hepatocyte vacuolation and necrosis. MiRNA changes identified in anti-TB DILI were associated with the microsomal enzymes GST2 and GST3. Novel miRNA biomarkers of DILI were identified and two of them, miR-146a and miR-21, rose with ALT in ATDILI patient samples. A TP model of DILI was further investigated with the down regulation of miRNA in TP-DILI fitting with the mechanism of action of TP, inhibition of RNA synthesis [181]. These changes in miRNA expression were shown to be occurring in hepatocyte cells and not immune cells.

Chapter 4 describes the development of a novel toehold switch system as a diagnostic test for miR-122. The toehold switches were designed with fluorescent and colorimetric outputs. Several of the toehold switches demonstrated sensitivity to miR-122 down to 5 nM. Furthermore, several of the switches had a high specificity. This is the first toehold switch

system designed to quantify a circulating miRNA biomarker of disease, demonstrating a potential new approach to point of care detection of miRNAs.

## 5.2 The possible role of miR-122 in liver injury beyond acting as a biomarker:

MiR-122 is highly expressed in, and highly specific for, the liver, with little to no expression in other tissues [87]. In addition, miR-122 plays a role in hepatocyte differentiation and liver development, maintaining the phenotype of adult hepatocytes through the suppression of non-liver genes [78]. Furthermore, miR-122 has a role in lipid metabolism, cholesterol accumulation and fatty acid metabolism [89]. However, miRNAs are also known to act as signalling molecules, functioning in an autocrine, paracrine and endocrine manner [83]. Although much is known about the production and mechanism of action of miR-122, there is still a limited understanding of whether it plays a specific role in signalling in liver injury.

Research has identified that the release of hepatocyte-derived exosome from stressed cells may act as a signal, initiating early immune responses in DILI [211]. Hepatocyte-derived exosomes contain functional genomic material, such as mRNAs and miRNAs, and including miR-122 [211]. In a mouse model of ethanol-induced liver injury, miR-122 transferred via exosomes inhibited the heme oxygenase (HO-1) pathway, which plays a role in reducing superoxide and other reactive oxygen species [212]. In addition, miR-122 also sensitized to lipopolysaccharide (LPS) stimulation, and increased levels of pro-inflammatory cytokines in monocytes and macrophages [212]. Circulating miR-122 was also identified as being transported to mouse lungs and taken up by alveolar macrophages [213]. Inflammatory responses were activated by miR-122 through binding of the Toll-like receptor 7 (TLR7) [213]. Recent work has demonstrated that miR-122 can be transferred from the liver to the kidney in acute liver injury, resulting in the regulation of kidney CYP enzymes [214]. It has been hypothesised that miR-122, and possibly other miRNAs, have the potential to mediate resistance to drug toxicity in the kidney, helping to prevent multi-organ failure in liver injury [214]. Further work should identify the organs within the body which miR-122 is transferred to, and what signalling role miR-122 has. The pathways which miR-122 regulates in these organs, and the effect of liver injury should be assessed. In addition, future work should assess the potential for therapeutic interventions in these pathways to limit the impact of DILI on a patient.

### 5.3 The expanding field of biomarkers of drug-induced liver injury:

The field of miRNAs as biomarkers of disease is rapidly expanding. In some diseases one miRNA biomarker may be sufficient to determine a disease state, for example, miR-122 in DILI. However, in other diseases a panel of miRNAs is required for diagnostic accuracy. MiRNAs are expressed throughout the body and are present in a wide range of biological samples including urine, peripheral blood, saliva and cerebrospinal fluid [77]. The accessibility and stability of miRNAs makes them ideal biomarkers. Furthermore, miRNA quantification can be carried out using Next-Generation Sequencing, real-time PCR and microarrays, rapidly providing a wealth of data. The use of miRNA biomarkers can provide an assessment of a patient's disease state, potentially enabling earlier diagnosis and the use of more personalised treatment. However, in order to translate miRNA biomarkers into clinical practice several steps must be first achieved. The methodology for miRNA quantification must be standardised, including miRNA extraction, storage conditions for samples and normalisation procedures [82]. In addition, large scale studies are needed to gather data on miRNA levels along with clinical and demographic data from patients, as well as healthy controls [82].

The work in Chapter 2 of this thesis begins the process of determining the utility of miR-122 and K18 as biomarkers of ATDILI. However, further work is needed to determine the diagnostic and prognostic capability of these biomarkers. An ideal study would recruit a sample size of 120 participants per patient group of interest, enabling the determination of a reference interval through the 5<sup>th</sup> and 95<sup>th</sup> percentile of the dataset [170]. Patient groups of interest include different ethnic groups such as Caucasian, and Asian and African, where TB is more common. Further patient subgroups should assess the effect of mycobacterial disease on the biomarkers, including healthy volunteers and patients with active TB and those with latent disease, as in the ALISTER study. The SAEFRIF study enabled assessment of the effect of HIV infection on the circulating concentration of miR-122 and K18. Determining whether HIV infection affects miR-122 and K18 in the absence of DILI is important in disentangling any variations seen in biomarker concentrations. However, there are potentially other comorbidities which may influence the circulating concentration of these biomarkers and this should be considered in the study design. In addition to determining the

reference intervals for different populations, a study including a larger number of participants should include more patients who develop ATDILI. The sample size calculation for the ALISTER study suggests that a sample size of 10 patients with ATDILI, with 10 matched controls, is enough to determine whether the biomarkers diagnose ATDILI.

Mir-122 was a focus of this thesis, however, there are other biomarkers which have been identified in DILI. Further work should also determine the diagnostic and prognostic capability of these other previously identified biomarkers of DILI [75]. These biomarkers can give different insights into the physiological processes occurring in liver injury and an understanding of the mechanisms behind liver injury. Several biomarkers assessed by Church and colleagues are associated with cell injury and death, including arginase-1, liver fatty acid protein 1, glutathione S-transferase  $\alpha$ , keratin-18, sorbitol dehydrogenase and glutamate dehydrogenase [75]. Other biomarkers are associated with inflammation, such as macrophage colony-stimulating factor receptor and osteopontin, or with regeneration, such as leukocyte cell-derived chemotaxin and alpha-fetoprotein [75]. A greater understanding of changes in biomarker levels in ATDILI would provide information on the possible mechanisms and pathways involved in ATDILI. Furthermore, one or several of these biomarkers may be a better biomarker for different types of liver injury. This may depend on the mechanism and pathways involved in different types of drug-induced liver injury.

In addition to assessing the potential diagnostic and prognostic capabilities of already identified biomarkers, there are potentially novel biomarkers of DILI which have yet to be identified. These biomarkers may be specific to individual drugs. In ATDILI, an understanding of which specific TB drug is the causative agent of DILI would enable tailored patient treatment. Identification of potential new biomarkers of ATDILI may be possible from models of liver injury, such as the zebrafish model of ATDILI developed in this thesis.

#### 5.4 Point of care tests are needed for biomarkers of drug-induced liver injury:

Future work should also develop point of care tests for miR-122 and K18 which can be used in acute care, at the bedside of patients, in clinical research and resource poor settings. Point of care tests are particularly needed for ATDILI due to the greater burden of ATDILI in developing countries. Previous work has demonstrated that miR-122 can be quantified in

fingerprick blood samples [215], limiting the need for blood handling. The toehold switch system described in this thesis demonstrates one way of quantifying miR-122, however, there are limitations to the utility of the switch in its current form. Recent work has demonstrated that miR-122 can be quantified directly from serum, accurately diagnosing liver injury [154]. Further work should focus on testing and implementing this diagnostic test into clinical practice, potentially alongside studies determining reference intervals. Although there has been substantial progress in the development of a point of care test for miR-122, there is currently no point of care test for K18. This limits the potential utility of K18 as a biomarker of ATDILI. However, the process for the quantification of K18 relies on a simple ELISA, compared to the multi-step process needed for miR-122 quantification.

### 5.5 MiRNAs can be used as therapeutics:

MiRNA expression changes have been identified in a broad range of diseases including cancer, and cardiovascular, autoimmune and neurodegenerative disease [82]. Targeting these miRNAs expression changes has been a recent focus of this field, with the development of miRNA mimics which lead to overexpression of the target, and miRNA repressors which silence transcript function [216]. Currently there are no miRNA drug candidates which have entered the market, however, several clinical trials are investigating the safety and efficacy of these compounds [216]. An example of a miRNA repressor is the drug miravirsen designed to prevent hepatitis C viral replication. Miravirsen is a locked nucleic acid-modified antisense oligonucleotide to miR-122 which been demonstrated to inhibit viral replication and prevent disease [217]. Miravirsen binds and sequesters miR-122, preventing it from stabilising HCV and thus inhibiting viral replication [217].

MiRNA therapeutics may also be able to play a role in patients with drug resistant disease. Deregulated miRNA expression is associated with drug resistance in cancer, epilepsy, MDR TB and insulin sensitivity [216]. There is limited understanding on how miRNAs are involved in the specific mechanisms of drug resistance. However, evidence suggests that the ATP-binding cassette (ABC) transporter family of proteins that activate drug resistance are regulated by miRNAs. Early work indicates that the co-administration of standard treatment alongside a select miRNA may help limit drug resistance [216].

An understanding of the miRNA expression changes and their associated targets in DILI has the potential to aid in the development of therapeutics. Targeting the altered pathways in which result in liver injury through therapeutics could prevent the development of liver injury and enable patients to complete anti-TB treatment without side-effects. Therapeutics which work by influencing miRNAs are an interesting and rapidly growing field with potential to aid not only in DILI prevention but also across other diseases.

#### 5.6 Bioinformatics approaches for miRNA research:

The growing wealth of data in the field of miRNAs has led to a growing number of miRNA databases and algorithms able to predict miRNA regulatory targets. For example, the TargetScan algorithm was used in this thesis to predict miRNA gene targets based on seed regions that are critical for binding to mRNAs. In addition, there are databases containing experimentally supported interactions. The linking of these databases with further platforms allows the identification of potential pathways and disease states associated with specific miRNAs. The expansion of these databases to include more data and additional model organisms has the potential to streamline clinical research, with the identification of novel biomarkers and therapeutic targets using bioinformatics approaches prior to validation in *in vitro* and *in vivo* models. This field of research is continually expanding, with the creation of new analysis tools and addition of further data to databases. Currently, there is a wealth of data available for humans and mice, however, the databases for zebrafish miRNAs are more limited. This limits analyses of data which can be carried out on zebrafish models. Future work should build on these databases, providing more data for zebrafish and experimentally validating identified targets and pathways. In this thesis, zebrafish larvae were used as a model organism of DILI and pathways associated with miRNA expression changes were identified. Further work should validate these pathways by determining whether the miRNAs bind to the identified gene targets. In addition, potential therapeutics for these pathways should be investigated to determine whether up- or down-regulating miRNA expression could prevent liver injury developing.

#### 5.7 Zebrafish larvae have substantial benefits as models of liver injury:

Zebrafish larvae have several advantages over other model organisms, being easy and economical to maintain, their short generation time, external fertilisation and the large

numbers of eggs produced per mating. Furthermore, as zebrafish larvae are transparent and develop externally they are ideal to study the development of organs. Despite the obvious differences between mammals and fish, many of the components necessary for hepatogenesis have been conserved. Studying liver development in zebrafish larvae has unique advantages over mammals. In mammals the liver is an early haematopoietic organ, therefore mutations in the liver will cause anaemia and frequent early lethality [126]. In addition, in the mammalian system, liver development occurs in intrauterine, making the embryonic liver inaccessible [126]. However, zebrafish larvae, develop externally and are sustained for the early stages of development by their yolk sac. Forward and reverse genetic approaches are possible in zebrafish larvae. Forward genetic screens allows the identification of gene essential for a process of interest by identifying embryonic mutants that are defective in that process [130]. Reverse genetic approaches, where a specific gene is targeted, are possible through the use of antisense morpholino oligonucleotides which are used to generate gene knock-down in embryos [130]. These genetic approaches have informed research on liver diseases. For example, a genetic screen for hepatomegaly in zebrafish with mutations in gene essential for embryonic development identified 3 mutants with phenotypes resembling different liver diseases, thus identifying 3 genes associated with liver disease [218]. Further work should focus on understanding more fully the molecular pathways involved in liver disease in zebrafish larvae.

A further advantage of using zebrafish as model organisms is the easy of creating transgenic larvae. The creation of transgenic zebrafish larvae is easy, rapid and inexpensive. The generation of transgenic zebrafish with fluorescent transgenes allows visualisation of gene expression in a spatial and temporal manner. Furthermore, crossing transgenic lines will generate multi-labelled zebrafish. In this thesis the transgenic zebrafish lines used enabled visualisation of liver injury. Combining transgenic larvae with technology capable of following fluorescence changes over time would allow a more detailed understanding of the changes in liver structure during liver injury. Furthermore, the addition of further fluorescent tags would allow assessment of other cell types during liver injury.

The zebrafish model of ATDILI developed in this thesis demonstrates the potential for zebrafish larvae as models of DILI, providing evidence of liver toxicity following exposure to

anti-TB medication. Zebrafish have been widely used as models of toxicity, however, recently, they are being more widely utilised as high-throughput screening tools. For example, the ZeGlobalTox assay which assesses cardio-, neuro- and hepatotoxicity organ effects within the same organism [117]. Developing standardised assay systems using zebrafish larvae has the potential to aid in the screening of new drug targets. Furthermore, the use of zebrafish aligns with the 3R's principle, as well as reducing experimental time and cost during drug discovery. Future work should focus on the development of these assays.

#### 5.8 Zebrafish have the ability to regenerate tissues:

The liver differs from many organs as it has the ability to regenerate following liver injury through the differentiation of hepatocytes or progenitor cells [219]. Under normal conditions hepatocytes are quiescent, however, when the liver is damaged they can be stimulated to grow and generate new liver mass [219]. Despite this, the level of liver injury can overwhelm the liver's regenerative capacity, leading to liver failure. Currently, the only treatment for liver failure is liver transplantation. Harnessing the potential of liver regeneration, through promoting hepatocyte regrowth, could provide an alternative treatment for liver failure. Zebrafish have a robust regenerative capacity, unlike mammals. Zebrafish larvae are able to regenerate tissues including the fin, spinal cord, retina, and heart [220]. Regeneration of the heart has been a particular area of interest, with research indicating that zebrafish are capable of regenerating heart tissue following different forms of injury, with pre-existing cardiomyocytes proliferating to regenerate tissue, and the surrounding tissues including, endocardium, epicardium, and inflammatory cells playing an important role [221]. Zebrafish have been a particular focus of regenerative medicine due to their ability to regenerate a broad range of tissues. Work has focussed on manipulating mammalian cells so that they are more like zebrafish cells, and are capable of repairing or replacing damaged organs [219]. The use of zebrafish larvae in regenerative medicine had many advantages, as larvae are cheap and quick to develop, they develop a fully functioning liver at 5 dpf, and transgenic larvae offer a wide range of opportunities to assess how different cell populations contribute to liver regeneration [219]. Future work should investigate the mechanisms involved in liver regeneration in zebrafish larvae and determining how these pathways can be manipulated in humans so as to aid in liver regeneration.



### 5.9 Conclusion:

Circulating miRNAs are being developed as biomarkers of disease and are an important field of research. This thesis has demonstrated the potential of the novel biomarkers miR-122 and K18 to diagnose ATDILI and should support future work on these biomarkers in the context of ATDILI. Furthermore, the work described in this thesis shows the utility of zebrafish larvae models of liver injury in identifying pathways changed in liver injury and potential novel miRNA biomarkers which can be translated into humans. Advances in the field of synthetic biology provide new approaches to tackle developing point of care diagnostics for miRNAs.

## Appendix

Chapter 2 Appendices:

i RUCAM causality assessment:

RUCAM Causality Assessment						
Drug: _____		Initial ALT: _____	Initial Alk P: _____	R ratio = $\frac{[ALT/ULN] \div [Alk P/ULN]}{[Alk P/ULN]}$ = _____		
The R ratio determines whether the injury is hepatocellular (R > 5.0), cholestatic (R < 2.0), or mixed (R = 2.0 – 5.0)						
Hepatocellular Type			Cholestatic or Mixed Type		Assessment	
1. Time to onset						
	Initial Treatment	Subsequent Treatment	Initial Treatment	Subsequent Treatment	Score (check one only)	
o From the beginning of the drug:	5 – 90 days < 5 or > 90 days	1 – 15 days > 15 days	5 – 90 days < 5 or > 90 days	1 – 90 days > 90 days	<input type="checkbox"/> +2 <input type="checkbox"/> +1	
o From cessation of the drug:	≤ 15 days	≤ 15 days	≤ 30 days	≤ 30 days	<input type="checkbox"/> +1	
<b>Note:</b> If reaction begins before starting the medication or >15 days after stopping (hepatocellular), or >30 days after stopping (cholestatic), the injury should be considered unrelated and the RUCAM cannot be calculated.						
2. Course						
	Change in ALT between peak value and ULN		Change in Alk P (or total bilirubin) between peak value and ULN		Score (check one only)	
After stopping the drug:						
• Highly suggestive	Decrease ≥ 50% within 8 days		Not applicable		<input type="checkbox"/> +3	
• Suggestive	Decrease ≥ 50% within 30 days		Decrease ≥ 50% within 180 days		<input type="checkbox"/> +2	
• Compatible	Not applicable		Decrease < 50% within 180 days		<input type="checkbox"/> +1	
• Inconclusive	No information or decrease ≥ 50% after 30 days		Persistence or increase or no information		<input type="checkbox"/> 0	
• Against the role of the drug	Decrease < 50% after 30 days OR Recurrent increase		Not applicable		<input type="checkbox"/> -2	
o If the drug is continued:	All situations		All situations		<input type="checkbox"/> 0	
• Inconclusive	All situations		All situations		<input type="checkbox"/> 0	
3. Risk Factors:						
Ethanol		Ethanol or Pregnancy (either)		Score (check one for each)		
o Alcohol or Pregnancy	Presence Absence	Presence Absence	Presence Absence	<input type="checkbox"/> +1 <input type="checkbox"/> 0		
o Age	Age of the patient ≥ 55 years Age of the patient < 55 years	Age of the patient ≥ 55 years Age of the patient < 55 years	Age of the patient ≥ 55 years Age of the patient < 55 years	<input type="checkbox"/> +1 <input type="checkbox"/> 0		

<b>4. Concomitant drug(s):</b>		Score (check one only)
<input type="radio"/>	None or no information or concomitant drug with incompatible time to onset	<input type="checkbox"/> 0
<input type="radio"/>	Concomitant drug with suggestive or compatible time to onset	<input type="checkbox"/> -1
<input type="radio"/>	Concomitant drug known to be hepatotoxic with a suggestive time to onset	<input type="checkbox"/> -2
<input type="radio"/>	Concomitant drug with clear evidence for its role (positive rechallenge or clear link to injury and typical signature)	<input type="checkbox"/> -3
<b>5. Exclusion of other causes of liver injury:</b>		Score (check one only)
<b>Group I (6 causes):</b>	<input type="radio"/> All causes in Group I and II ruled out <input type="radio"/> The 6 causes of Group I ruled out <input type="radio"/> Five or 4 causes of Group I ruled out <input type="radio"/> Less than 4 causes of Group I ruled out <input type="radio"/> Non drug cause highly probable	<input type="checkbox"/> +2 <input type="checkbox"/> +1 <input type="checkbox"/> 0 <input type="checkbox"/> -2 <input type="checkbox"/> -3
<b>Group II (2 categories of causes):</b>	<input type="radio"/> Acute viral hepatitis due to HAV (IgM anti-HAV), or HBV (HBsAg and/or IgM anti-HBc), or HCV (anti HCV and/or HCV RNA with appropriate clinical history) <input type="radio"/> Biliary obstruction (By imaging) <input type="radio"/> Alcoholism (History of excessive intake and AST/ALT $\geq$ 2) <input type="radio"/> Recent history of hypotension, shock or ischemia (within 2 weeks of onset)	
<b>Group III (2 categories of causes):</b>	<input type="radio"/> Complications of underlying disease(s) such as autoimmune hepatitis, sepsis, chronic hepatitis B or C, primary biliary cirrhosis or sclerosing cholangitis; or <input type="radio"/> Clinical features or serologic and virologic tests indicating acute CMV, EBV, or HSV.	
<b>6. Previous information on hepatotoxicity of the drug:</b>		Score (check one only)
<input type="radio"/>	Reaction labeled in the product characteristics	<input type="checkbox"/> +2
<input type="radio"/>	Reaction published but unlabeled	<input type="checkbox"/> +1
<input type="radio"/>	Reaction unknown	<input type="checkbox"/> 0
<b>7. Response to readministration:</b>		Score (check one only)
<input type="radio"/>	Positive	<input type="checkbox"/> +3
<input type="radio"/>	Compatible	<input type="checkbox"/> +1
<input type="radio"/>	Negative	<input type="checkbox"/> -2
<input type="radio"/>	Not done or not interpretable	<input type="checkbox"/> 0
<b>TOTAL (add the checked figures)</b>		

Abbreviations used: ALT, alanine aminotransferase; Alk P, alkaline phosphatase; ULN, upper limit of the normal range of values  
 Modified from: Danan G and Benichou C. *J Clin Epidemiol* 1993; 46: 1323-30.

ii ALISTER: Protocol:



## PROTOCOL

### Study Title - Assessing Antibiotic

### Induced Liver Injury for Stratification of Tuberculosis Patients

### - (ALISTER study)

#### Protocol authors:

- Sarah Stedman (UoE, PhD Student)
- Till Bachmann (UoE DIPM, 1<sup>st</sup> PhD supervisor)
- James Dear (UoE CVS, 2<sup>nd</sup> PhD supervisor)
- Adam Hill (NHS Lothian)

#### Abbreviations used:

- ALT – alanine aminotransferase
- ATDILI – Anti-tuberculosis drug-induced liver injury
- DILI – Drug-induced liver injury
- EIS – Electrochemical impedance spectroscopy
- HMGB1 – high mobility group box 1
- K18 – keratin 18
- RIE – Royal Infirmary Edinburgh
- TB - Tuberculosis
- ULN – Upper limit of normal
- WGH –Western General Hospital

#### Introduction:

A panel of highly sensitive circulating biomarkers for acute liver injury have been identified and demonstrated to identify liver injury on first presentation to hospital before standard

tests are elevated in patients with paracetamol overdose. Furthermore, some of this panel can identify which patients will develop clinically important liver failure once liver injury has started.

We wish to test these biomarkers in patients with active and latent tuberculosis to see if they can be used to stratify patients undertaking anti-tuberculosis drug therapy. Anti-tuberculosis drug induced liver injury is the most frequent side-effect of anti-tuberculosis therapy, affecting 2-5% of tuberculosis patients seen at the Royal Infirmary Edinburgh and hindering their effective treatment. The biomarkers we will use in this study have the potential to be translated into use in a point of care assay, so as to rapidly benefit patients. Our long term aim is to develop a commercial diagnostic test, able to be used at point of care, to rapidly detect liver injury from whole blood fingerprick samples.

Patients will be recruited from the TB out-patient clinic and in-patient wards at the Royal Infirmary Edinburgh and Western General Hospital. Blood samples will be taken every time the patient visits the clinic and also retrieved from the biochemistry lab. The biomarkers in the blood samples will be analysed to determine if they rise in patients who develop liver injury.

This clinical study is being funded by the Medical Research Council and University of Edinburgh as part of a doctoral training grant.

### **Rationale of study:**

To improve patient stratification, we have developed a panel of novel circulating liver specific and mechanistic biomarkers that report early acute liver injury. Such biomarkers are needed as current early biomarkers of liver injury lack sensitivity and specificity. Our biomarkers either have enhanced liver specificity (microRNA-122 – miR-122) or provide mechanistic insights (keratin-18 (K18) - apoptosis and necrosis, and high mobility group box 1 (HMGB1) - necrosis and inflammation).

In humans, we started the process of qualification in paracetamol overdose-induced hepatotoxicity, the commonest cause of drug-induced liver injury (DILI) in Europe and North

America. In the emergency department miR-122, HMGB1 and K18 accurately detect DILI soon after overdose, at a time when established markers such as serum alanine transaminase activity (ALT) are normal. A key step in our translational pathway is to qualify these biomarkers in multiple clinical scenarios where patient care would be improved by early diagnosis or exclusion of liver injury.

The European Medicines Agency and the US Food and Drug Administration (FDA) have provided letters of support for the continued development of these markers. A key question now is: do the markers retain their efficacy in the presence of infection?

Currently, antituberculosis drug-induced liver injury (ATDILI) is the most frequent side-effect of anti-tuberculosis therapy and this hinders the effective treatment of TB, as it means that treatment regimens are not completed. The tuberculosis (TB) clinic at the Royal Infirmary Edinburgh (RIE) sees 60-90 new cases of active TB every year, as well as 150-200 new cases of latent TB and 20 new cases of environmental TB. 2-5% of these patients develop ATDILI.

At present, the risk of ATDILI means that monitoring of liver function is required, with levels of ALT measured monthly. If levels of ALT rise to 2-5x the upper limit of normal levels (ULN) and the patient is unwell the frequency of monitoring is increased to biweekly monitoring. Antibiotic therapy is only changed if levels of ALT remain greater than 3xULN, the patient continues to display symptoms and there is a positive causality assessment that the anti-tuberculosis drugs are causing ATDILI.

This project will recruit patients taking antituberculosis drugs and determine the diagnostic and prognostic value of three biomarkers, miR-122, HMGB1 and K18, in relation to liver injury as a result of anti-tuberculosis therapy. In the long term we aim to link these biomarkers with electrochemical impedance spectroscopy (EIS) to develop a rapid point of care test to both diagnose and predict the outcome of ATDILI. A rapid point of care test for ATDILI has the potential to guide anti-tuberculosis therapy, reduce the number of people with ATDILI, and enable more patients to finish treatment regimens.

### **Objectives and endpoints:**

This 'proof of concept' study will determine whether a panel of biomarkers are elevated in tuberculosis patients who develop ATDILI.

**Novel biomarkers:** microRNA, HMGB1, keratin 18

**End-point:** ATDILI - as defined by DILI expert working group (Aithal et al. 2011)

**Primary research questions:**

Q1: Can the biomarkers accurately identify patients with anti-tuberculosis drug induced liver injury in latent tuberculosis?

Q2: Can the biomarkers accurately identify patients with anti-tuberculosis drug induced liver injury in active tuberculosis?

This will be determined by a nested case control design. Patients with ATDILI (cases) will be age, sex and treatment matched with patients who have not developed ATDILI (controls). The difference in biomarkers from baseline (pre or at starting TB medication) to time of established DILI will be compared with controls.

It is important that latent and active TB are considered separately as some members of the biomarker panel report inflammation. This may affect their performance in patients with active inflammation due to active TB.

**Secondary questions:**

Q3: Determine if the biomarkers can be used as prognostic biomarkers for predicting the need to halt medication in latent tuberculosis patients?

Q4: Determine if the biomarkers can be used as prognostic biomarkers for predicting the need to halt medication in active tuberculosis patients?

These two questions will analyse samples and determine if clinically significant DILI (defined as resulting in medication change) can be accurately predicted. This is in comparison with standard markers, and will involve calculation of sensitivity, specificity, positive and negative predictive values as per our published work.



Q5: Determine if fingerprick capillary blood measurement can replace venous sampling.

The markers that have efficacy in Q1-4 will be measured in the fingerprick samples. We will determine if the biomarkers can be detected from fingerprick samples using electrochemical impedance spectroscopy. Measurement of biomarkers in finger prick capillary blood using electrochemical impedance spectroscopy would allow near patient testing.

### **Study design:**

**Location:** TB out-patient clinics and in-patient wards.

**Number of visits:** Patients typically visit the TB clinic for appointments pre-treatment, at 2 weeks, 8 weeks, 4 months and 6 months, if they are on a typical 6 month treatment programme. The total number of visits a patient makes to the TB clinic will depend on the length of treatment and whether they experience any issues with their treatment. We aim to collect samples from participants at every visit to the TB clinic so as to follow changes in biomarker levels over time.

### **Procedures involved:**

- Eligible patients will be identified from clinic lists each week or by the clinical staff at out-patient clinics and in-patient wards.
  - A broad recruitment approach will be taken to recruit all eligible patients with a high likelihood of starting TB treatment or already on treatment.
  - Some eligible patients may not have a definitive diagnosis of TB at time of recruitment due to the long time taken to culture Mycobacterium and the requirement for sufficient positive Mycobacterium cultures. Not all patients with latent TB undergo treatment. Some patients may start TB treatment before a definitive diagnosis.
  - For those patients recruited who do not start TB treatment basic data will be retained, along with any collected blood samples, but further patient progress will not be monitored, and no further blood samples will be collected.

- In addition, clinical staff may identify eligible patients at the sites who are starting TB treatment, but who are not at the TB clinic, and inform research staff who will recruit them to the study. This is due to some TB patients being started on treatment by the TB nurses at other times than the dedicated clinics.
- The patient will be given information – Patient Information Sheet, Data Protection Information Sheet and Patient Consent Form
- If they consent, three copies of the completed consent form will be made, one of which should be placed in the patient records, one given to the patient and the other should be safely stored in the site file
- Then, demographic information and blood results will be recorded, and additional blood samples will be taken at every visit to the TB clinic (NEW RESEARCH SAMPLE).
- Samples will be processed as per our established biomarker SOP.
- Samples will be transported to the University of Edinburgh for analysis
- The research specific samples will be both a venous sample taken at the time of routine clinical venepuncture and an additional finger prick capillary blood sample (as taken by diabetic patients to check their blood sugar).
- Patient progress will be monitored remotely through the review of electronic medical records.
- Patients with abnormal blood results may be further monitored at their GPs. If required, additional blood samples (NEW RESEARCH SAMPLE) taken at the GPs may be requested and used in our analysis.
- We will ask the patient's GP to take one extra 9mL serum sample when routine blood sampling is taking place. This will be communicated by letter and we will telephone the patient's GP to communicate the clinical need for blood sampling and ask for an extra research blood tube. For patients at the RIE the extra tube will be sent for 'virology storage' and we have already arranged for the laboratory to process and freeze these samples for this study. We will send the patient's GP a partially completed request form for virology storage.
- For sites other than RIE anonymised samples and patient data will be sent to the University of Edinburgh.

**Sample SOP collection and storage:**

- Collect blood samples in 9.0ml serum and plasma tubes
- Label sample with study ID, patient unique ID number and date
- Leave the samples to stand at room temperature for 20-30 minutes
- Centrifuge the blood sample at 2600g for 20 minutes (Separating the blood into an upper serum/plasma layer and lower RBC layer)
- Without disturbing the lower layer, transfer all the serum/plasma to a sterile container (approximately 5ml of serum/plasma should be obtained)
- Prepare 0.5ml aliquots in cryovials
- Samples collected at sites other than RIE will be stored and then transported to the University of Edinburgh for analysis
- Store samples in -80°C freezers in QMRI or Chancellors Building

Fingerprick samples stored in -80°C freezers in QMRI or Chancellors Building.

Samples will be stored in a linked anonymised form, with each patient assigned a 4 digit code and the link between the code and patient stored on NHS or University of Edinburgh password protected computer system. For samples and data outside of RIE, anonymised samples and data will be sent to the University of Edinburgh for analysis.

**Storage and use of personal data:**

- With patient consent the research team will extract relevant clinical and demographic data from the patient's medical notes.
- Paper copies of the anonymised patient data and consent forms are kept in a locked drawer in a locked office.
- Patient identifiable data that links blood sample to patient is on a secure NHS server space.
- With consent, the research team will record data from patient's records and this will be kept secure. All identifiable data will be removed when the data is entered into a database for the study.
- The data will be analysed by the research team and no one else. These data will be fully anonymised.

- For sites other than RIE, anonymised patient data will be sent to the University of Edinburgh.

**Study population:**

**Patient cohort:** Primary cohort - TB out-patient clinics at the different sites. Additional patients recruited from in-patients wards.

**Number of participants:** Total sample size – 200 participants. We aim to recruit 15 patients/month over one year.

**Inclusion criterion:** adults, aged 16-85, receiving treatment with anti-tuberculosis drugs (including individuals tested positive for Mycobacterium tuberculosis and Nontuberculosis Mycobacterium). Capacity to consent.

**Exclusion criteria:** patients unable to give informed consent or who refuse, HIV positive patients.

**Identification of participants:** Clinical staff will identify new patients starting TB treatment, and liaise with research staff so they can collect the relevant data and samples.

**Consenting process:** Patients will first be approached by the clinical team who manage patients at the sites. The patient will be approached for consent by an individual who has completed Good Clinical Practice (GCP) training and who has undergone specific training (research staff). The patient will be given the patient information sheet, data protection information sheet and consent form. They will be allowed time to assimilate the information and to ask any questions. We appreciate that 24 hrs is the recommended time for patients to consider whether to take part in a clinical study however in this setting of a short hospital appointment/admission this is too long to be possible. If the patient does not wish to consent, then no further action is required. If the patient is willing to consent then written informed consent will be taken using the consent form. Three copies of the completed consent form will be made, one of which should be placed in the patient records, one given to the patient and the other should be safely stored in the site file.

**Analysis of data:**

**Type of study:** Nested case control

**Sample analysis:**

MicroRNA will be quantified by PCR, HMGB1 and molecular forms of K18 by ELISA, as described in our published papers (Antoine et al. 2013, Antoine et al. 2012, Vliegenthart et al. 2015). Later work will also use electrochemical impedance spectroscopy (EIS) to quantify microRNA, HMGB1 and K18 (Lisdat and Schafer 2008, Ciani et al. 2012). All analysis will be performed blinded to clinical data.

**Sample size calculation:**

We aim to recruit 15 patients a month over 3 years, giving a total sample size of around 540 patients. Out of those 540 patients, 2-5% of them will develop liver injury. The patients who develop liver injury are our cases, and will be compared to control patients, who have also been taking anti-tuberculosis drugs but have not developed liver injury.

For the primary data analysis of this clinical study a total of 40 patients (10 case and 10 control for separate latent TB and active TB groups) will be needed.

Using fold-change from baseline data generates a predicted study size of 20 patients (10 DILI, 10 control), as calculated below.

Based on our Journal of Hepatology paper (Antoine et al. 2012), the baseline circulating concentration of K18 was 170U/L and the concentration with DILI was 34,000U/L. This 200 fold increase had a standard deviation of 150 across subjects.

Therefore, with a 2 sided-significance level, 0.8 power, 20 patients (10 cases and 10 controls) are required for each group, active and latent TB.

**Interpretation of results:**

Primary research questions

Q1: Can the biomarkers accurately identify patients with anti-tuberculosis drug induced liver injury in latent tuberculosis?

Q2: Can the biomarkers accurately identify patients with anti-tuberculosis drug induced liver injury in active tuberculosis?

It is important that latent and active TB are considered separately as some members of the biomarker panel report inflammation. This may affect their performance in patients with active inflammation.

Analysis will be determined by a case control design. Patients with ATDILI will be age, sex and treatment matched with at least 10 patients who have not developed ATDILI. The difference in biomarkers from baseline (pre or at starting TB medication) to time of established DILI will be compared with controls.

Secondary questions:

Q3: Determine if the biomarkers can be used as prognostic biomarkers for predicting the need to halt medication in latent tuberculosis patients?

Q4: Determine if the biomarkers can be used as prognostic biomarkers for predicting the need to halt medication in active tuberculosis patients?

These two questions will analyse samples that pre-date the diagnosis of DILI and determine if DILI can be accurately predicted. This is in comparison with standard markers, and will involve calculation of sensitivity, specificity, positive and negative predictive values as per our published work (Antoine et al. 2013, Antoine et al. 2012).

Q5: Determine if fingerprick capillary blood measurement can replace venous sampling.

The markers that have efficacy in Q1-4 will be measured in the fingerprick samples. We will determine if the biomarkers can be detected from fingerprick samples using electrochemical impedance spectroscopy. Measurement of biomarkers in finger prick capillary blood using electrochemical impedance spectroscopy would allow near patient testing. Our long term aim is to further develop the electrochemical impedance spectroscopy biosensing platform to detect biomarkers of liver injury from whole blood fingerprick samples, so as to develop a rapid point of care diagnostic test for liver injury.

**References:**

- Aithal, G. P., P. B. Watkins, R. J. Andrade, D. Larrey, M. Molokhia, H. Takikawa, C. M. Hunt, R. A. Wilke, M. Avigan, N. Kaplowitz, E. Bjornsson & A. K. Daly (2011) Case definition and phenotype standardization in drug-induced liver injury. *Clin Pharmacol Ther*, 89, 806-15.
- Antoine, D. J., J. W. Dear, P. S. Lewis, V. Platt, J. Coyle, M. Masson, R. H. Thanacoody, A. J. Gray, D. J. Webb, J. G. Moggs, D. N. Bateman, C. E. Goldring & B. K. Park (2013) Mechanistic biomarkers provide early and sensitive detection of acetaminophen-induced acute liver injury at first presentation to hospital. *Hepatology*, 58, 777-87.
- Antoine, D. J., R. E. Jenkins, J. W. Dear, D. P. Williams, M. R. McGill, M. R. Sharpe, D. G. Craig, K. J. Simpson, H. Jaeschke & B. K. Park (2012) Molecular forms of HMGB1 and keratin-18 as mechanistic biomarkers for mode of cell death and prognosis during clinical acetaminophen hepatotoxicity. *J Hepatol*, 56, 1070-9.
- Ciani, I., H. Schulze, D. K. Corrigan, G. Henihan, G. Giraud, J. G. Terry, A. J. Walton, R. Pethig, P. Ghazal, J. Crain, C. J. Campbell, T. T. Bachmann & A. R. Mount (2012) Development of immunosensors for direct detection of three wound infection biomarkers at point of care using electrochemical impedance spectroscopy. *Biosens Bioelectron*, 31, 413-8.
- Lisdat, F. & D. Schafer (2008) The use of electrochemical impedance spectroscopy for biosensing. *Anal Bioanal Chem*, 391, 1555-67.
- Vliegenthart, A. D., J. M. Shaffer, J. I. Clarke, L. E. Peeters, A. Caporali, D. N. Bateman, D. M. Wood, P. I. Dargan, D. G. Craig, J. K. Moore, A. I. Thompson, N. C. Henderson, D. J. Webb, J. Sharkey, D. J. Antoine, B. K. Park, M. A. Bailey, E. Lader, K. J. Simpson & J. W. Dear (2015) Comprehensive microRNA profiling in acetaminophen toxicity identifies novel circulating biomarkers for human liver and kidney injury. *Sci Rep*, 5, 15501.

iii ALISTER: Patient Information Sheet:



**Participant Information Sheet  
Assessing Antibiotic Induced  
Liver Injury for Stratification of  
Patients**



**(ALISTER study)**

**Principal Investigator – Dr James Dear**

**You are being invited to take part in a research study. Before you decide whether or not to agree, it is important for you to understand why the research is being done and what it will involve. Please take time to read the following information carefully. Talk to others about the study if you wish. Contact us if there is anything that is not clear or if you would like more information. Take time to decide whether or not you wish to take part.**

This study is being undertaken by a student for the purpose of a PhD project.

**What is the purpose of the study?**

We are developing a new blood test that promises to identify those people who have developed liver damage as a result of taking antibiotics. We wish to collect a blood sample from you today and when you return at future clinics. This will enable us to further develop our blood test and identify people at risk of developing liver damage.

**Why have I been asked to take part?**

You are being asked to take part as you may have an infection. This infection may be treated with antibiotics. Some antibiotics have a small risk of causing liver damage, as your health professional will discuss with you if you are treated with antibiotics. We would like to ask you to take part because we are trying to find a way to better identify people at risk of liver problems with these antibiotics.

**Do I have to take part?**

No, it is up to you to decide whether or not to take part. If you do decide to take part you will be given this information sheet to keep and be asked to sign a consent form. If you decide to take part you are still free to withdraw at any time and without giving a reason. Deciding not to take part or withdrawing from the study will not affect the healthcare that you receive, or your legal rights.

**What will happen if I take part?**

We would like to take a blood sample now and also when you return at future clinics. This will be done by standard blood taking procedure, taking about 2 teaspoons of



blood, and also by pricking your finger (like when a diabetic measures their sugar levels). If possible our blood sample will be obtained when you are having blood taken as part of your routine care. Otherwise we will take separate samples whilst you are at the clinic. If you are monitored at your GPs during the time of your treatment to check how your liver is functioning we will ask them to collect an additional blood sample for this study.

We will record some simple information about you such as age, sex, symptoms and routine blood test results. This information will be kept secure within the NHS. Your information will be linked to the blood sample by a four digit number so it will not be possible for anyone to identify you from the other study participants.

Our new blood tests measure the levels of specific biological molecules (proteins and nucleic acids) in the blood. Samples collected will be transported to the University of Edinburgh for analysis. This study will create a bank of samples that we can use to develop our new tests for liver damage. The samples will be carefully stored in a freezer for a maximum of 10 years and, with appropriate ethical approval, these samples may be shared with other clinical, academic and commercial researchers in the UK and worldwide.

#### **What are the possible benefits of taking part?**

There are no direct benefits to you from taking part in this study, but the results from this study might inform the future health care of other people. The results of this study may be used for the future commercial development of a new test. Your participation in this study will not entitle you to benefit financially from the company developing the product, treatment or test.

#### **What are the possible disadvantages and risks of taking part?**

The only disadvantage is you will have extra blood taken. We will take great care that the blood sample cannot be identified.

#### **What if there is a problem?**

If you have a concern about any aspect of this study please contact Dr James Dear who will do his best to answer your questions.

In the unlikely event that something goes wrong and you are harmed during the research and this is due to someone's negligence then you may have grounds for a legal action for compensation against NHS Lothian but you may have to pay your legal costs. The normal National Health Service complaints mechanisms will still be available to you (if appropriate).

If you wish to make a complaint about the study please contact:

Patient Experience Team  
Waverley Gate  
2 - 4 Waterloo Place  
Edinburgh

EH1 3EG  
Tel: 0131 536 3370  
feedback@nhslothian.scot.nhs.uk

**What happens when the study is finished?**

At the end of the research, with your permission, we will store your anonymous blood samples for a maximum of 10 years. This will allow other researchers in our field the chance to benefit by using these samples.

**Will my taking part in the study be kept confidential?**

All the information we collect during the course of the research will be kept confidential and there are strict laws which safeguard your privacy at every stage. All identifiable records (for example your hospital number) will be kept exclusively within the NHS and will be protected by a password. Any information that leaves the NHS system will be anonymised so you cannot be identified. Anonymised patient data will be sent to the University of Edinburgh.

With your consent we will inform your GP that you are taking part.

To ensure that the study is being run correctly, we will ask your consent for responsible representatives from the Sponsor and NHS Institution to access your records and data collected during the study, where it is relevant. The Sponsor is responsible for overall management of the study and providing insurance and indemnity.

**What will happen to the results of the study?**

The study will be written up in medical publications and shared with other doctors at national and international meetings. If you are interested we will share our results with you.

**Who is organising the research and why?**

This study is being organised/sponsored by the University of Edinburgh and NHS Lothian.

**Who has reviewed the study?**

All research in the NHS is looked at by an independent group of people, called a Research Ethics Committee (REC). A favourable ethical opinion has been obtained from the West of Scotland REC. NHS management approval has also been obtained.

**If you have any further questions about the study please contact Dr James Dear on 0131 242 9214 or email: [james.dear@ed.ac.uk](mailto:james.dear@ed.ac.uk)**

**If you would like to discuss this study with someone independent of the study please contact:**

**Dr Neeraj Dhaun**

**[Bean.Dhaun@ed.ac.uk](mailto:Bean.Dhaun@ed.ac.uk)**

**0131 242 6786**

Thank you for taking the time to read this information sheet.

iv ALISTER: Patient Consent Form:



# CONSENT FORM



## Assessing Antibiotic Induced Liver Injury for Stratification of Patients - (ALISTER study)

**Participant ID:**

**Person taking consent:**

**Please initial box**

1. I confirm that I have read and understand the information sheet (version 4.0, dated – 17/01/2019 and the Data Protection Sheet version 1.0 dated 16/01/2018) for the above study and have had the opportunity to consider the information and ask questions.
2. I understand that my participation is voluntary and that I am free to withdraw at any time, without giving any reason, without medical care or legal rights being affected.
3. I understand that data collected during the study may be looked at by individuals from the Sponsor (University of Edinburgh and NHS Lothian), from the NHS organisation or other authorities, where it is relevant to my taking part in this research. I give permission for these individuals to have access to my data collected in this study.
4. I understand that the results of this study may be used for future commercial development of products/tests/treatments and I will not benefit financially from this.
5. I agree to my anonymous data/tissue being sent to the University of Edinburgh and I agree to my anonymous data/tissue being stored for 10 years and used for future ethically approved studies, including clinical, academic and commercial studies in UK and abroad.
6. I agree to my General Practitioner being informed of participation in this study
7. I agree to take part in the above study

\_\_\_\_\_  
Name of Participant

\_\_\_\_\_  
Date

\_\_\_\_\_  
Signature

\_\_\_\_\_  
Name of Person taking consent

\_\_\_\_\_  
Date

\_\_\_\_\_  
Signature

v ALISTER: GP Letter:



Royal Infirmary of Edinburgh  
EDINBURGH

EH16 4SA  
DATE

General Practitioner name  
Medical Centre name  
Address line 1  
Address line 2/postcode

**Assessing Antibiotic Induced Liver Injury for Stratification of Patients - (ALISTER study)**

Dear Dr.

I write with reference to your patient, \_\_\_\_\_. As you will know, he/she has visited the TB clinic at the Royal Infirmary Edinburgh and may be undergoing treatment with anti-tuberculosis drugs. They have given consent to take part in a research study into a new diagnostic blood test. This involves the collection of blood samples whilst at the TB clinic. If your patient needs their liver function monitoring at your GP surgery, we would request that an additional blood sample (9ml, serum) is collected and then sent on to the Virology lab at the Royal Infirmary Edinburgh. We will telephone you to discuss this further if indicated. Study blood samples will then be analysed to measure levels of new biomarkers of liver damage. Consent has been obtained to inform you of their participation. This study is being conducted under sponsorship of the University of Edinburgh.

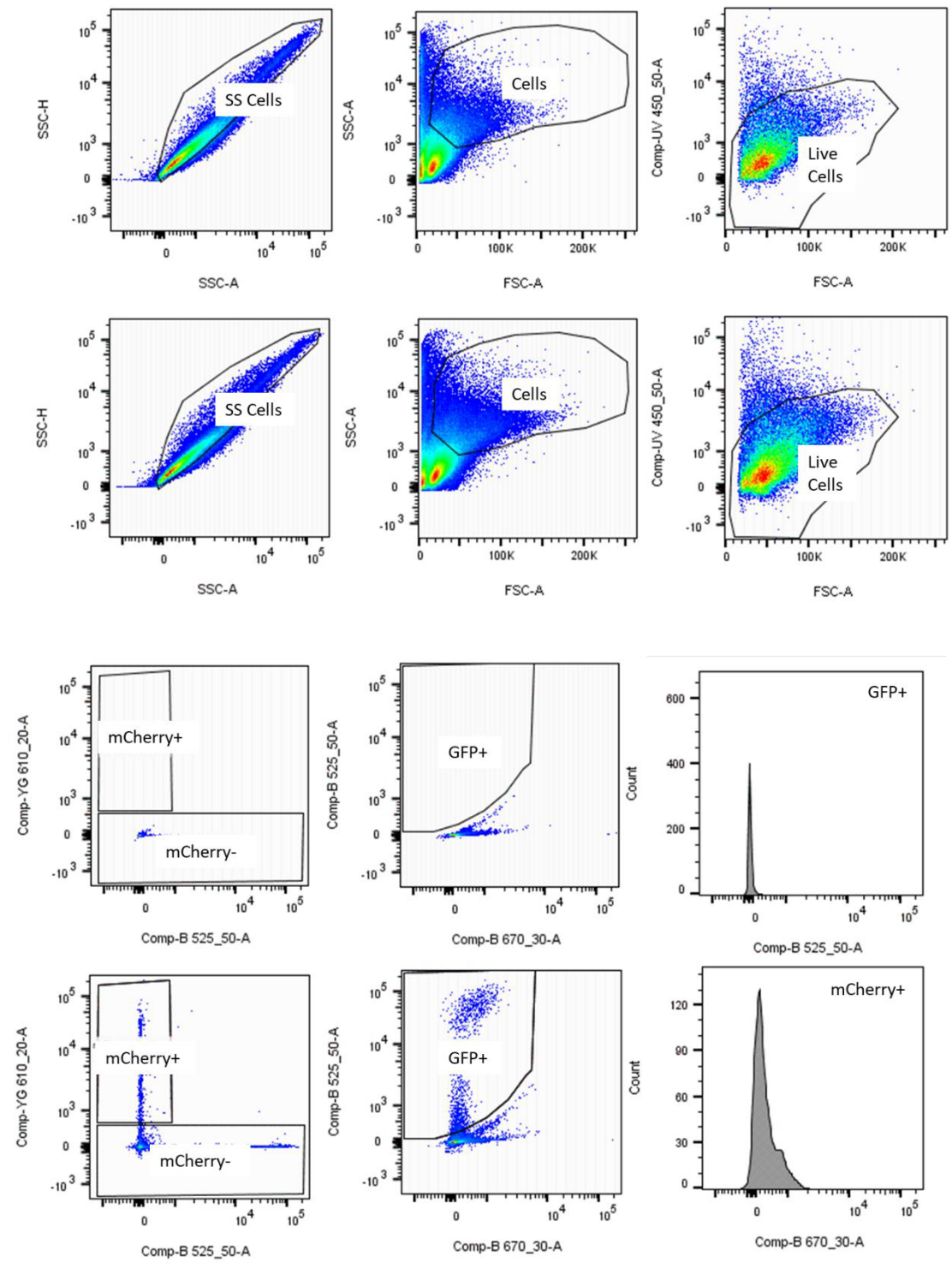
**Please find attached a copy of the patient information sheet for this study.**

If you have any questions about the study, please do not hesitate to contact me.

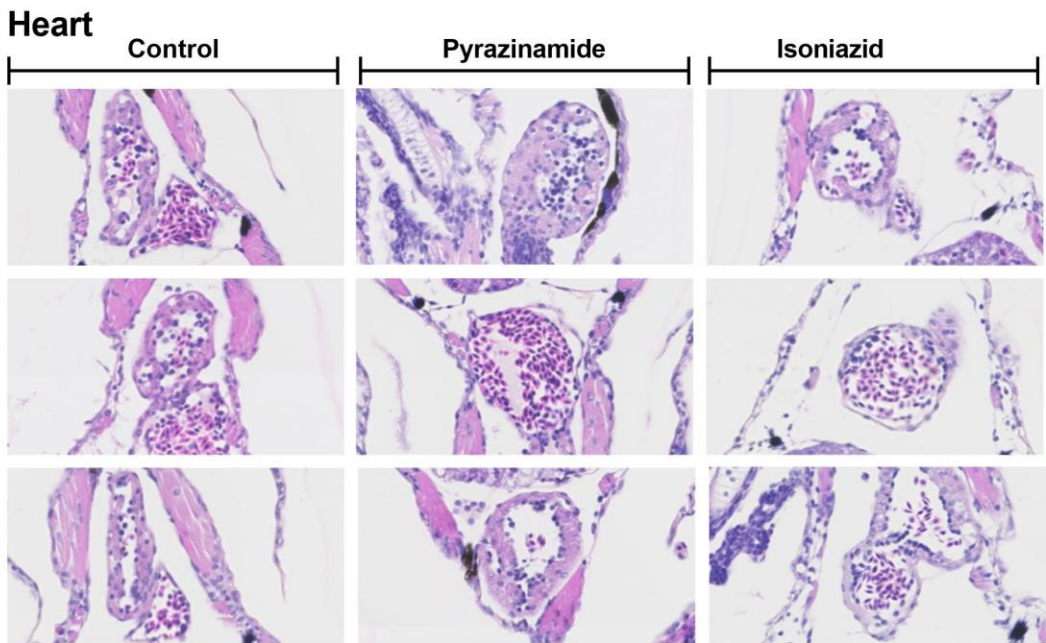
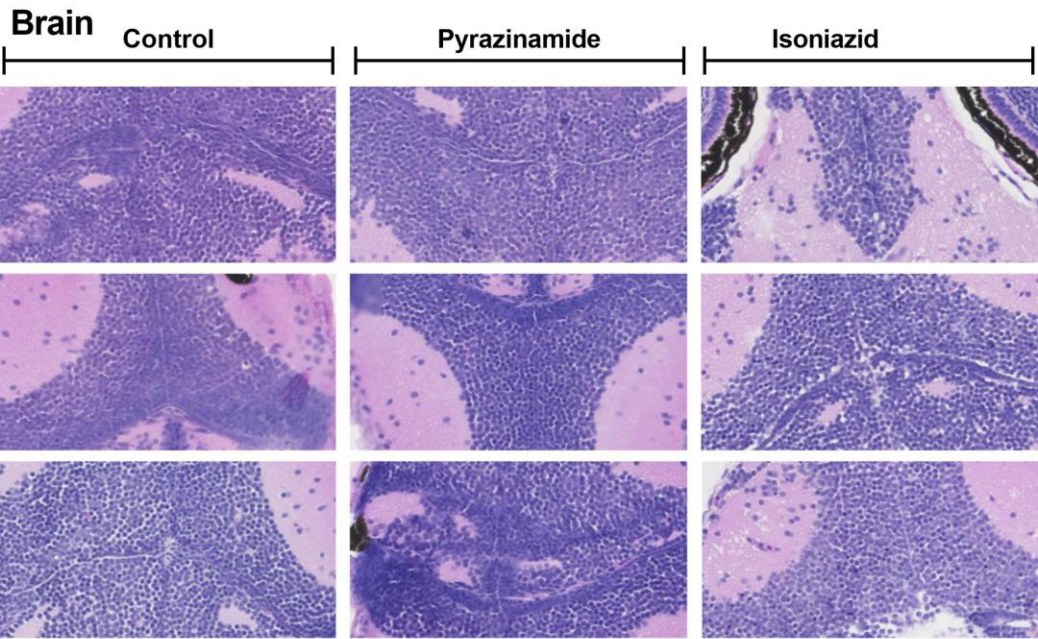
Yours sincerely  
Dr James Dear  
Consultant Clinical Pharmacologist

Chapter 3 Appendices:

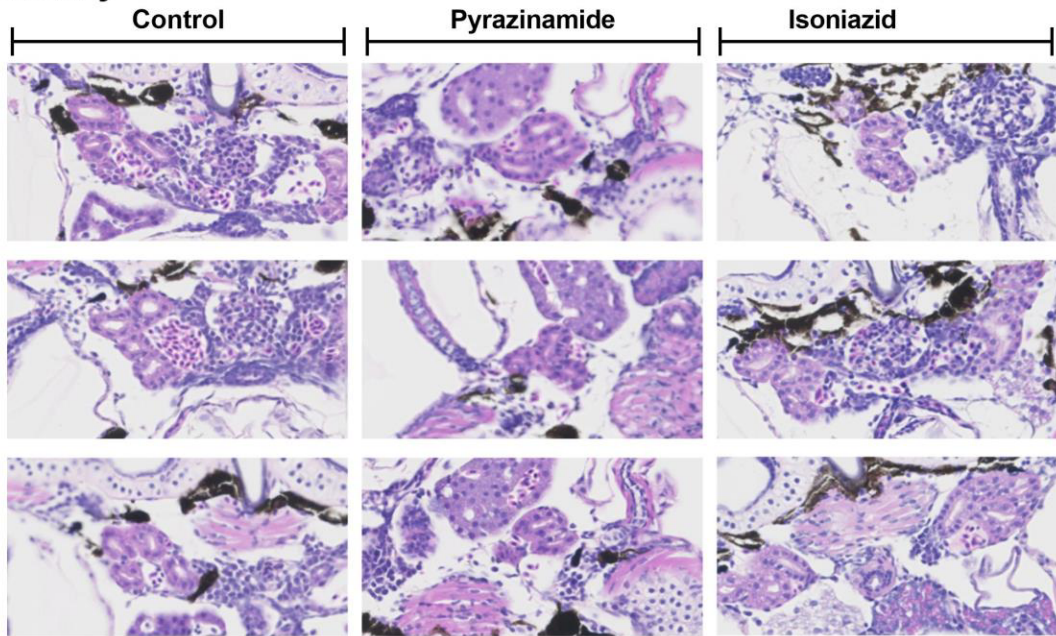
i FACS gating strategy:



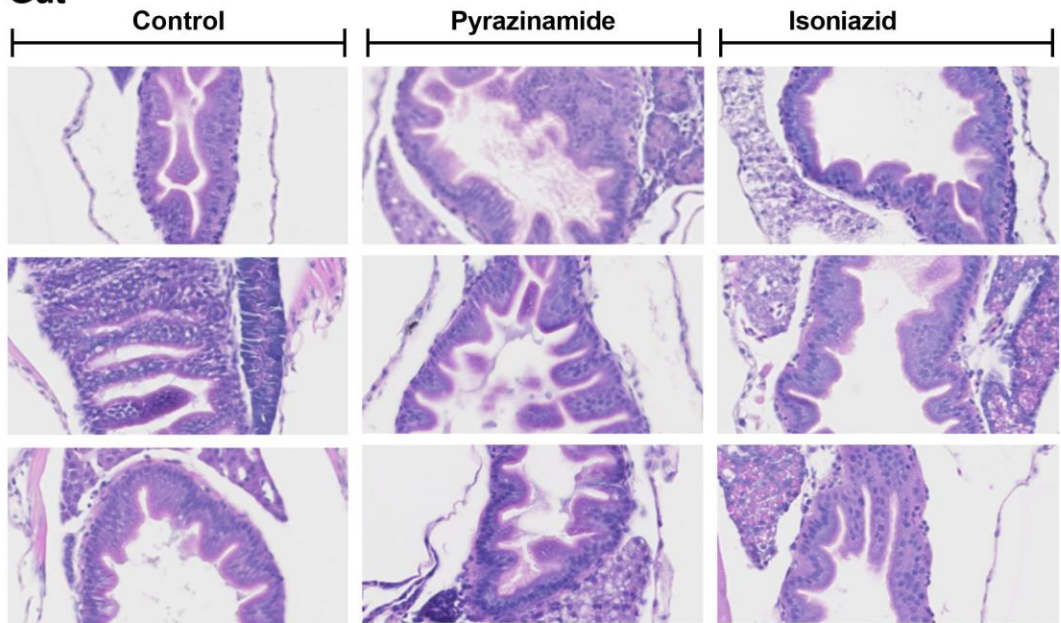
ii Histology of other organs:



**Kidney**



**Gut**



## iii Data normalisation for qRT-PCR:

There were 2 candidate miRNAs for use as a normaliser, either SNORD95 or U6. Significant correlation was seen for both SNORD95 and U6 when plotted against the number of cells collected by FACS. However, when comparing the RNA extracted from whole fish, SNORD95 Ct values were lower with higher RNA concentrations. Whereas, for U6, correlation between RNA concentration and U6 Ct value was less.

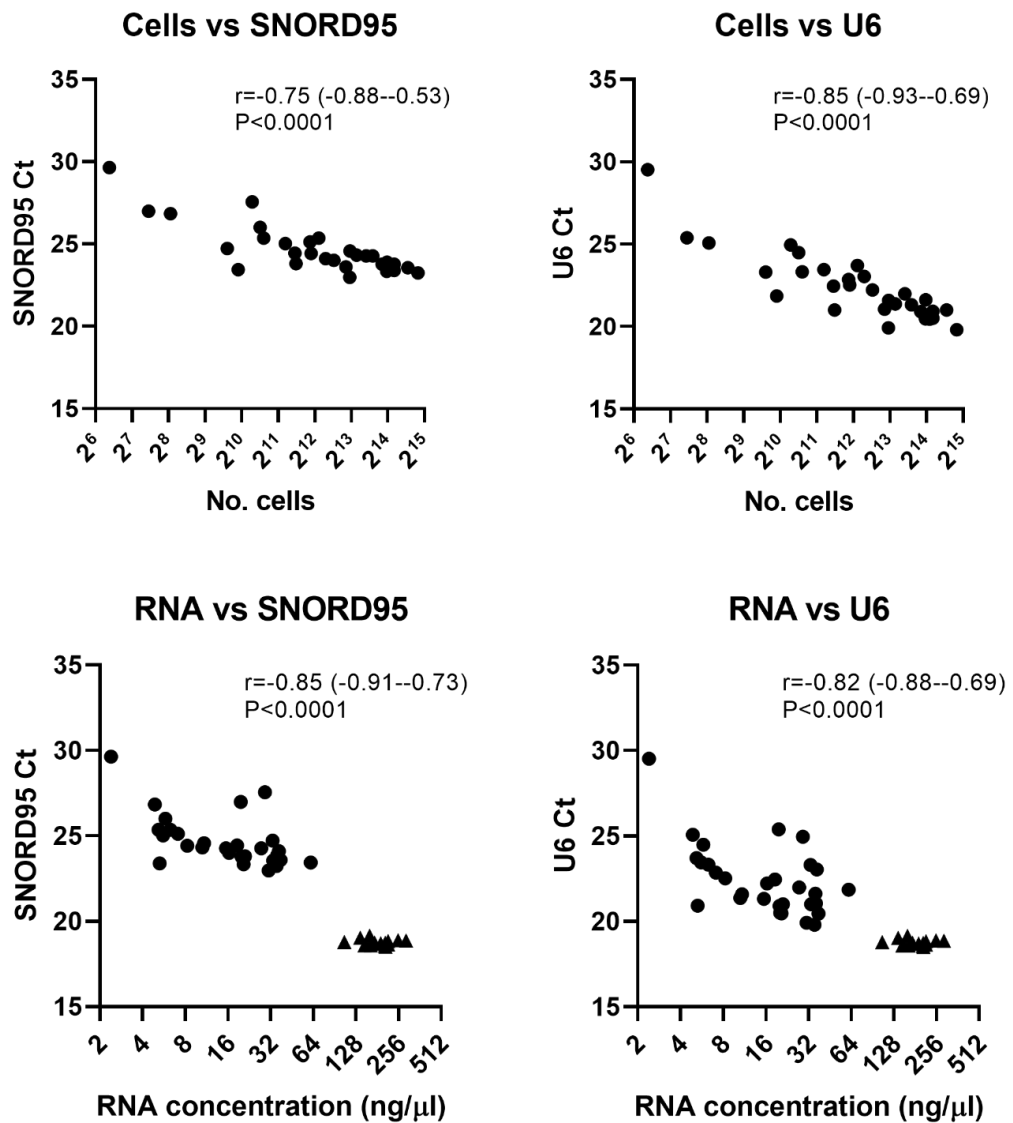


**Figure:** qRT-PCR data normalisation, comparing Ct values of SNORD95 and U6 with the number of cells collected via FACS and RNA concentration. Significance of correlation was



*calculated with Spearman's rank correlation coefficient. Circles = FACS collected cells, triangles = whole fish RNA.*

iv GO analysis: Isoniazid relative to control (up-regulated miRNAs):

GO Category	p-value	Number of genes	Number of miRNAs
molecular_function	$<1 \times 10^{-325}$	95	12
biological_process	$<1 \times 10^{-325}$	105	13
protein binding	$<1 \times 10^{-325}$	345	14
cellular_component	$<1 \times 10^{-325}$	167	15
lipopolysaccharide biosynthetic process	0.0009	17	2
phosphotransferase activity, alcohol group as acceptor	0.074	18	2
extracellular matrix structural constituent	0.401	10	1
collagen trimer	0.894	10	1
S-adenosylmethionine cycle	>0.999	1	1
negative regulation of growth rate	>0.999	1	1
cellular response to methanol	>0.999	1	1
optic nerve formation	>0.999	1	1

v GO analysis: Isoniazid relative to control (down-regulated miRNAs):

GO Category	p-value	Number of genes	Number of miRNAs
molecular_function	$<1 \times 10^{-325}$	113	18
biological_process	$<1 \times 10^{-325}$	115	19
protein binding	$<1 \times 10^{-325}$	367	20
cellular_component	$<1 \times 10^{-325}$	171	21
aflatoxin B1 metabolic process	>0.999	1	2
embryonic retina morphogenesis in camera-type eye	>0.999	1	1
midbrain development	>0.999	1	1
skeletal muscle fiber development	>0.999	1	1
mitochondrial proton-transporting ATP synthase complex, coupling factor F(o)	>0.999	1	1
atrial cardiac muscle tissue development	>0.999	1	1
phosphogluconate dehydrogenase (decarboxylating) activity	>0.999	1	1
pentose-phosphate shunt	>0.999	1	1
catecholamine metabolic process	>0.999	1	1
O-methyltransferase activity	>0.999	1	1
procollagen-lysine 5-dioxygenase activity	>0.999	1	1
hydrogen ion transmembrane transporter activity	>0.999	1	1
ATP synthesis coupled proton transport	>0.999	1	1
catechol O-methyltransferase activity	>0.999	1	1
proline racemase activity	>0.999	1	1
fin development	>0.999	1	1
fin morphogenesis	>0.999	1	1
neurotransmitter catabolic process	>0.999	1	1
proton-transporting ATP synthase activity, rotational mechanism	>0.999	1	1

vi GO analysis: Pyrazinamide relative to control (up-regulated miRNAs):

GO Category	p-value	Number of genes	Number of miRNAs
molecular_function	$<1 \times 10^{-325}$	352	33
biological_process	$<1 \times 10^{-325}$	936	33
protein binding	$<1 \times 10^{-325}$	520	33
cellular_component	$<1 \times 10^{-325}$	362	33
extracellular matrix structural constituent	0.902	10	2
glomerular visceral epithelial cell fate commitment	>0.999	2	3
pronephric glomerulus development	>0.999	2	3
pronephric duct development	>0.999	2	3
collagen trimer	>0.999	10	2
atrioventricular valve development	>0.999	2	3
fin regeneration	>0.999	11	1
angioblast cell migration involved in selective angioblast sprouting	>0.999	1	1
hemi-methylated DNA-binding	>0.999	2	1
iron ion homeostasis	>0.999	2	1
nucleate erythrocyte development	>0.999	2	2

## vii GO analysis: Pyrazinamide relative to control (down-regulated miRNAs):

GO Category	p-value	Number of genes	Number of miRNAs
molecular_function	<1 x 10 <sup>-325</sup>	169	30
biological_process	<1 x 10 <sup>-325</sup>	173	30
protein binding	<1 x 10 <sup>-325</sup>	512	32
cellular_component	<1 x 10 <sup>-325</sup>	257	33
pseudouridine synthesis	>0.999	1	1
atrial cardiac muscle tissue development	>0.999	1	1
sevenless binding	>0.999	1	1
eukaryotic translation initiation factor 3 complex	>0.999	1	1
catecholamine metabolic process	>0.999	1	1
O-methyltransferase activity	>0.999	1	1
procollagen-lysine 5-dioxygenase activity	>0.999	1	1
pyridoxal kinase activity	>0.999	1	1
pyridoxal 5'-phosphate salvage	>0.999	1	1
RNA modification	>0.999	1	1
pseudouridine synthase activity	>0.999	1	1
catechol O-methyltransferase activity	>0.999	1	1
aspartate N-acetyltransferase activity	>0.999	1	1
midbrain development	>0.999	1	1
translation initiation factor binding	>0.999	1	1
fin development	>0.999	1	1
fin morphogenesis	>0.999	1	1
swimming	>0.999	1	1
neurotransmitter catabolic process	>0.999	1	1
Wnt signaling pathway involved in digestive tract morphogenesis	>0.999	1	1
skeletal muscle fiber development	>0.999	1	1
embryonic retina morphogenesis in camera-type eye	>0.999	1	1
regulation of synaptic transmission, glycinergic	>0.999	1	1
non-canonical Wnt signaling pathway involved in heart development	>0.999	1	1
cellular response to cold	>0.999	1	1
cellular response to prostaglandin stimulus	>0.999	1	1
aflatoxin B1 metabolic process	>0.999	1	2

viii GO analysis: Pyrazinamide relative to isoniazid (up-regulated miRNAs):

GO Category	p-value	#genes	#miRNAs
biological_process	$<1 \times 10^{-325}$	316	18
molecular_function	$<1 \times 10^{-325}$	835	18
protein binding	$<1 \times 10^{-325}$	464	18
cellular_component	$<1 \times 10^{-325}$	324	18
fin regeneration	>0.999	11	1
hemi-methylated DNA-binding	>0.999	2	1
nucleate erythrocyte development	>0.999	2	1

ix GO analysis: Pyrazinamide relative to isoniazid (down-regulated miRNAs):

GO Category	p-value	#genes	#miRNAs
biological_process	$<1 \times 10^{-325}$	97	18
molecular_function	$<1 \times 10^{-325}$	96	19
protein binding	$<1 \times 10^{-325}$	302	20
cellular_component	$<1 \times 10^{-325}$	153	21
lipopolysaccharide biosynthetic process	0.031104	17	2
phosphotransferase activity, alcohol group as acceptor	0.466756	18	2
epiboly involved in gastrulation with mouth forming second	>0.999	1	1
anatomical structure homeostasis	>0.999	1	1
purinergic nucleotide receptor activity	>0.999	1	1
extracellular ATP-gated cation channel activity	>0.999	1	1
sevenless binding	>0.999	1	1
establishment of endothelial blood-brain barrier	>0.999	1	1
optic nerve formation	>0.999	1	1
purinergic nucleotide receptor signaling pathway	>0.999	1	1
swimming	>0.999	1	1
posterior lateral line development	>0.999	1	1
regulation of synaptic transmission, glycinergic	>0.999	1	1
protein localization to adherens junction	>0.999	1	1

x GO analysis: Triptolide relative to vehicle control:

GO Category	p-value	Number of genes	Number of miRNAs
molecular_function	$<1 \times 10^{-325}$	68	16
biological_process	$<1 \times 10^{-325}$	63	17
protein binding	$<1 \times 10^{-325}$	240	21
cellular_component	$<1 \times 10^{-325}$	112	21
primitive erythrocyte differentiation	0.999	1	2
response to biotic stimulus	>0.999	1	2
phosphogluconate dehydrogenase (decarboxylating) activity	>0.999	1	1
mitochondrial proton-transporting ATP synthase complex, coupling factor F(o)	>0.999	1	1
pseudouridine synthesis	>0.999	1	1
purinergic nucleotide receptor activity	>0.999	1	1
extracellular ATP-gated cation channel activity	>0.999	1	1
eukaryotic translation initiation factor 3 complex	>0.999	1	1
pentose-phosphate shunt	>0.999	1	1
catecholamine metabolic process	>0.999	1	1
O-methyltransferase activity	>0.999	1	1
procollagen-lysine 5-dioxygenase activity	>0.999	1	1
RNA modification	>0.999	1	1
pseudouridine synthase activity	>0.999	1	1
hydrogen ion transmembrane transporter activity	>0.999	1	1
ATP synthesis coupled proton transport	>0.999	1	1
catechol O-methyltransferase activity	>0.999	1	1
fatty acid elongation, unsaturated fatty acid	>0.999	1	1
hemoglobin metabolic process	>0.999	2	1
neural plate anterior/posterior regionalization	>0.999	1	1
midbrain development	>0.999	1	1
translation initiation factor binding	>0.999	1	1
fin development	>0.999	1	1
fin morphogenesis	>0.999	1	1
angioblast cell migration involved in selective angioblast sprouting	>0.999	1	1
purinergic nucleotide receptor signaling pathway	>0.999	1	1
neurotransmitter catabolic process	>0.999	1	1
proton-transporting ATP synthase activity, rotational mechanism	>0.999	1	1
skeletal muscle fiber development	>0.999	1	1
hatching gland development	>0.999	1	1
embryonic retina morphogenesis in camera-type eye	>0.999	1	1

## Chapter 4 Appendices:

## i Primer Sequences:

PCR product	Tm (°C)	Extension time (sec)	Primer	Sequence	Length (bases)
<b>THS1-gfp</b>	62.1	27	THS_PT7_fwd	AATTCTAATACGACTCACTATAGGGAG	27
			THS_tT7_rev	CAAAAAACCCCTCAAGACCC	20
<b>pSB1K3</b>	71.7	68	tT7_SP_fwd	GGGTCTTGAGGGGTTTTTGTACTAGTAGCGGCCGCTGCAG	41
			PT7_XE_rev	TAGTGAGTCGTATTAGAATCTCTAGAAGCGGCCGCAATTC	42
<b>Linker-gfp</b>	64.7	24	linker_gfp_fwd	ACCTGGCGGCAGCGCAAAAGCGTAAAGGAGAAGAACTTTTC	41
			THS_tT7_rev	CAAAAAACCCCTCAAGACCC	20
<b>THS-linker</b>	62.5	10	THS_PT7_fwd	AATTCTAATACGACTCACTATAGGGAG	27
			linker_THS_rev	CTTTTGCGCTGCCGCCAG	18
<b>Linker-LacZ</b>	60.3	93	linker_lacZ_fwd	AACCTGGCGGCAGCGCAAAAGaccatgattacggattcactg	42
			tT7_lacZ_rev	AAGACCCGTTTAGAGGCCCCAAAGGGTTATGCTAttatTTTTgacaccagaccaac	56
<b>Full insert with restriction enzyme sites (pJET)</b>	67	103	EcoRI_THS_fwd	CCAgaattcAATTCTAATACGACTCACTATAG	32
			PstI_tT7_rev	GCCTCTAAACGGGTCTTGAGGGGTTTTTgctgcagTAT	39
<b>PT7-LacZ-tT7</b>	58.3	93	PT7_LacZ_FWD	CTAATACGACTCACTATAGGAGAAGGatgaccatgattacggattc	47
			tT7_LacZ_REV	AAGACCCGTTTAGAGGCCCCAAAGGGTTATGCTAttatTTTTgacaccagaccaac	56
<b>Screening primers</b>	60.0	Product dependent	VF2	TGCCACCTGACGTCTAAGAA	20
			VR	ATTACCGCCTTTGAGTGAGC	20

## ii Oligonucleotide sequences for THS2, 7 &amp; 10:

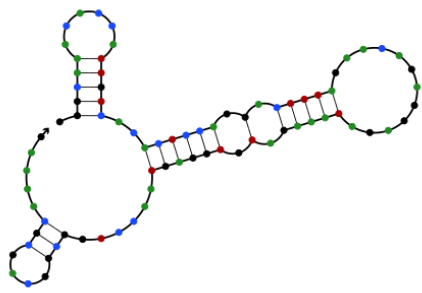
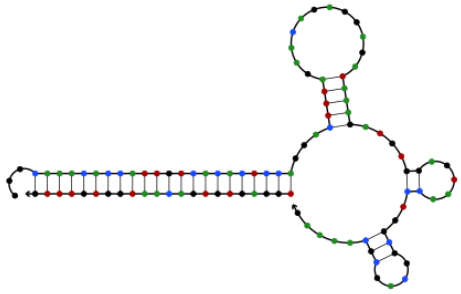
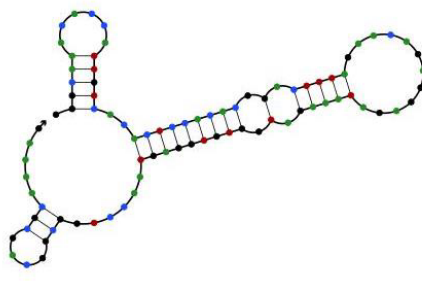
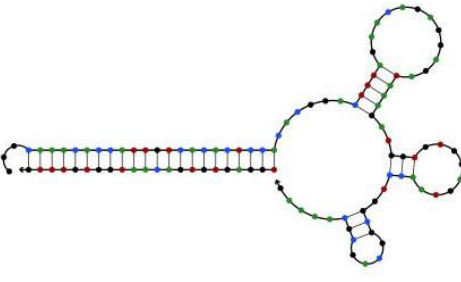
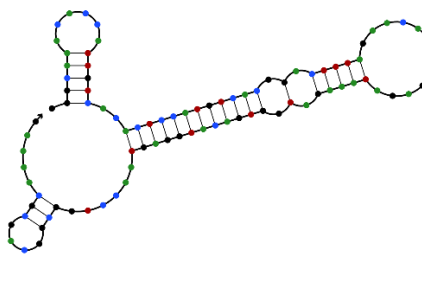
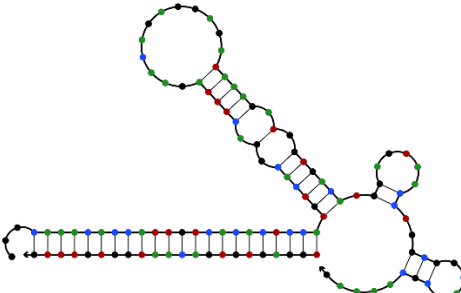
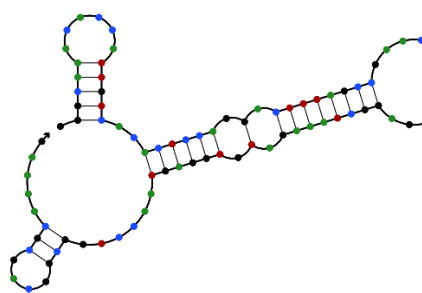
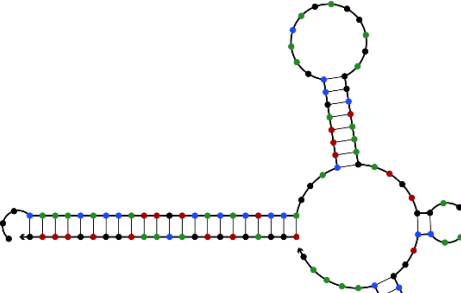
<b>Product</b>	<b>Oligonucleotide</b>	<b>Sequence</b>	<b>Length (bases)</b>
<b>THS2</b>	THS2_fwd	AATTCTAATACGACTCACTATAGGGAGAAGGGG GCAAACACCATTGTCACACTCCACACGGACTTTA GAACAGAGGAGATAAAGATGGTGTGGAGTAAC CTGGCGGCAGCGCAAAG	117
	THS2_rev	CTTTTGCCTGCGCCAGGTTACTCCACACCATC TTTATCTCCTCTGTTCTAAAGTCCGTGTGGAGTGT GACAATGGTGTGGCCCCCTTCTCCCTATAGTGA GTCGTATTAGAATT	117
<b>THS10</b>	THS10_fwd	AATTCTAATACGACTCACTATAGGGAGAAGGGG GCAAACACCATTGTCACACTCCAGGATTTAGAAC AGAGGAGATAAAATGTGGAGTAACCTGGCGGC AGCGCAAAG	109
	THS10_rev	CTTTTGCCTGCGCCAGGTTACTCCACATTTTAT CTCCTCTGTTCTAAATCCTGGAGTGTGACAATGG TGTTTGGCCCCCTTCTCCCTATAGTGAATCGTATTA GAATT	109
<b>THS7</b>	THS7_fwd	AATTCTAATACGACTCACTATAGGGAGAAGGGG GCAAACACCATTGTCACACTCCAGGTGGACTTTA GAACAGAGGAGATAAAGATGACCTGGAGTTTTTC CAGGTAACCTGGCGGCAGCGCAAAG	126
	THS7_rev	CTTTTGCCTGCGCCAGGTTACCTGGAAAACCTC CAGGTCATCTTTATCTCCTCTGTTCTAAAGTCCAC CTGGAGTGTGACAATGGTGTGGCCCCCTTCTCC CTATAGTGAATCGTATTAGAATT	126

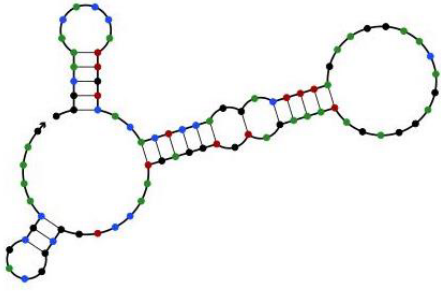
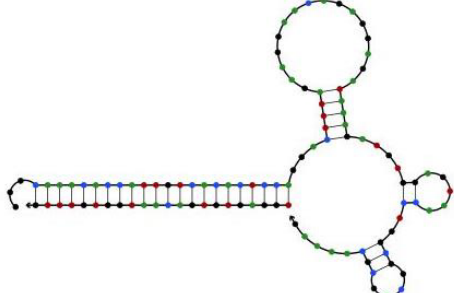
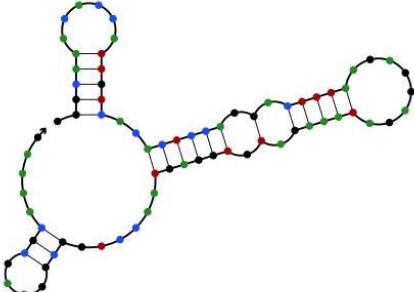
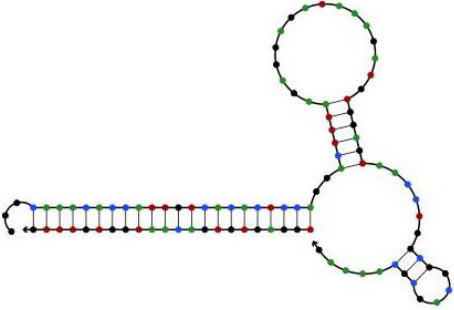
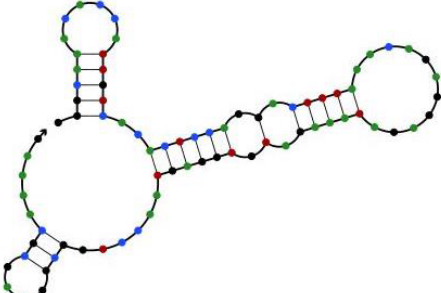
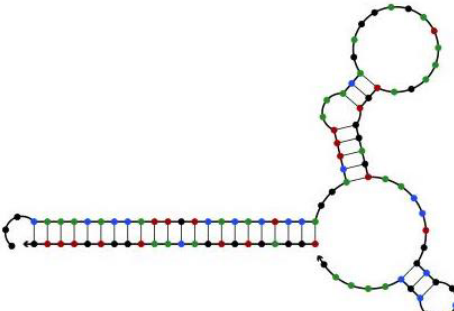
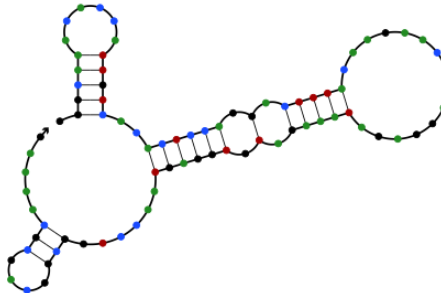
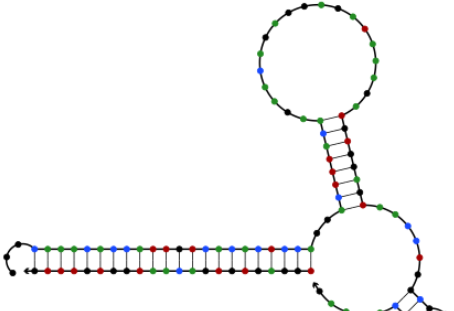
## iii Primer sequences for THS5 and THS9:

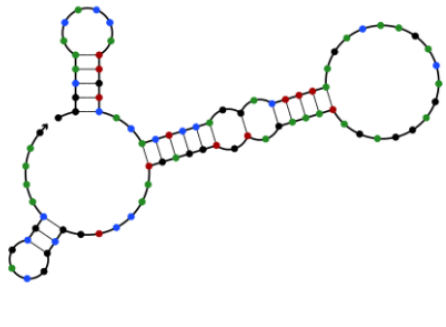
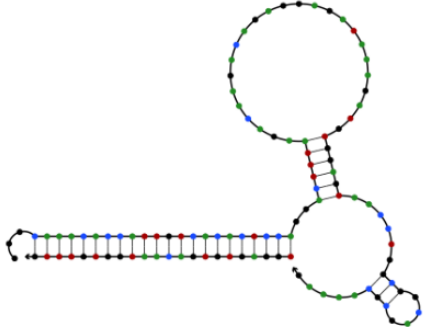
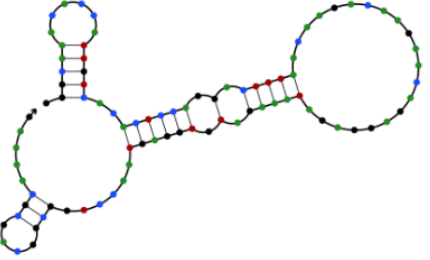
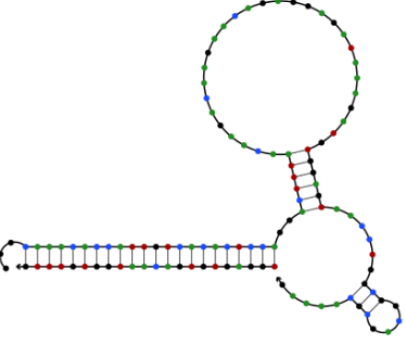
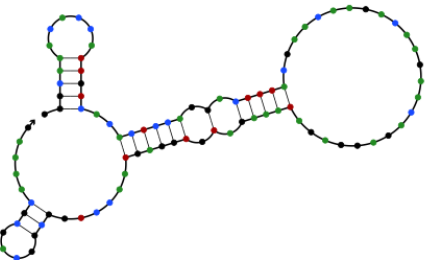
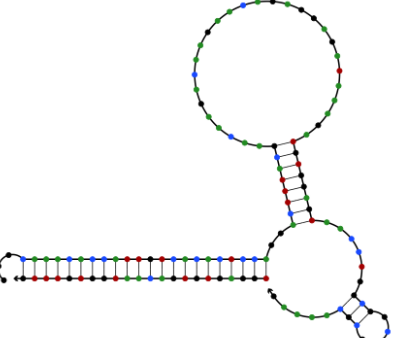
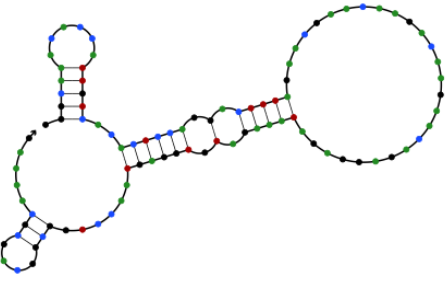
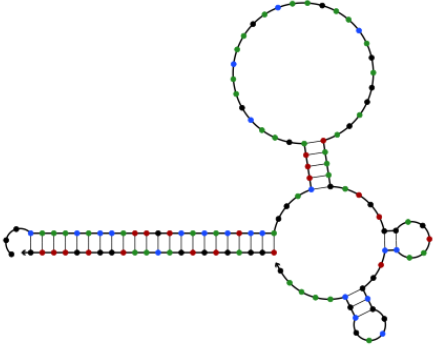
PCR product	T <sub>m</sub> (°C)	Extension time (sec)	Primer	Sequence	Length (bases)
THS5	57.6	90	THS5_fwd	GAAGGAACAGAGGAGATAAAGATG	24
THS5a			THS5a_fwd	AGAGGAGATAAAGATGTGG	19
THS5b			THS5b_fwd	AACAGAGGAGATAAAGATG	19
THS5d			THS5d_fwd	CAAGAACAGAGGAGATAAAGATG	23
THS5e			THS5e_fwd	AGACAAGACAGAGGAGATAAAGATG	25
THS5f			THS5f_fwd	ACAAGACAAGAACAGAGGAGATAAAGATG	29
THS5g			THS5g_fwd	CGAACAAGACAAGAACAGAGGAGATAAAGATG	32
THS5h			THS5h_fwd	GAACGAACAAGACAAGAACAGAGGAGATAAAGATG	35
THS5s			THS5_rev	TAAAGTCCTGGAGTGTGAC	19
THS9	67.5	90	THS9_fwd	AACCTGGCGGCAGCGCAAAG	21
			THS9_rev	CACACTCCACATCTTTATCTCCTCTGTTTC	29
			THS9-2_rev	TGTCACACTCCACATCTTTATCTCCTCTGTTTC	32

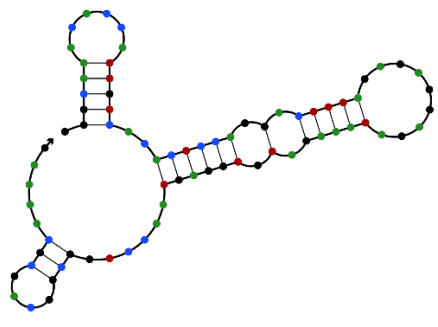
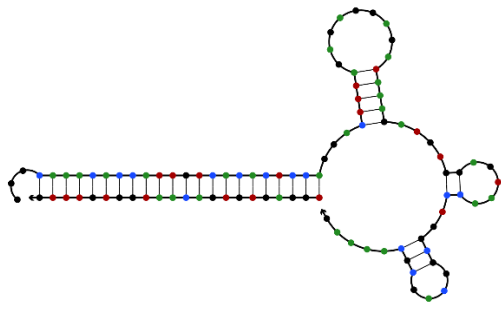
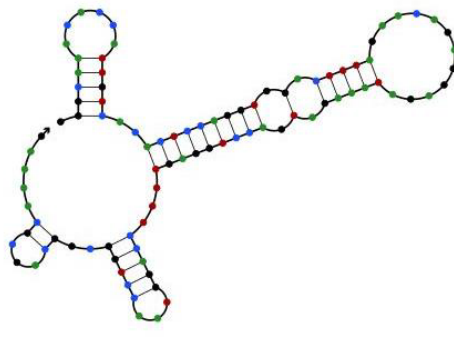
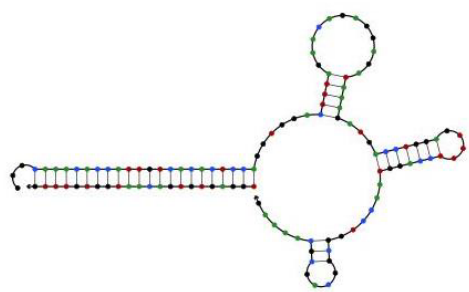
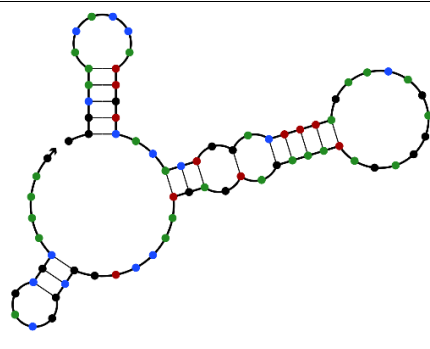
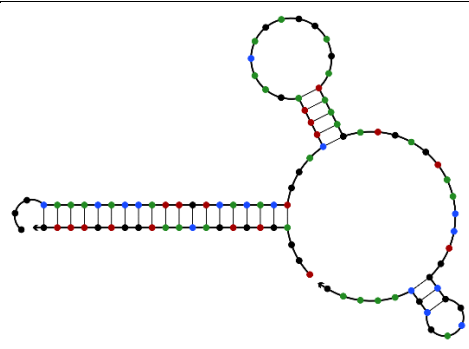
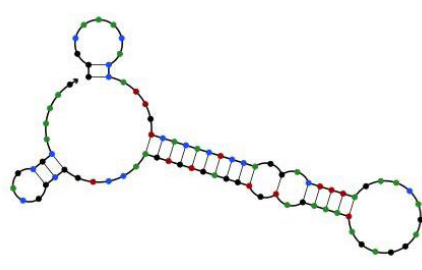
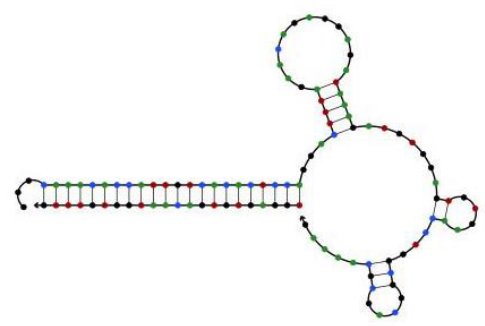


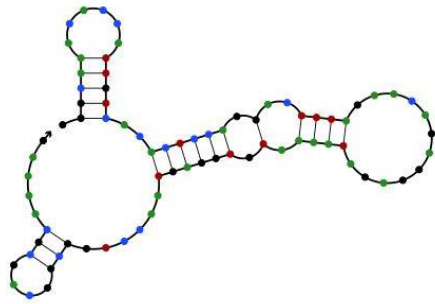
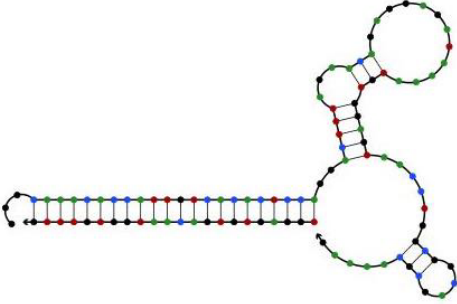
iv Toehold switch diagrams:

	Switch alone	Switch with miR-122
THS1		
THS2		
THS3		
THS4		

	Switch alone	Switch with miR-122
THS5		
THS5a		
THS5b		
THS5d		

	Switch alone	Switch with miR-122
THS5e		
THS5f		
THS5g		
THS5h		

	Switch alone	Switch with miR-122
THS6		
THS7		
THS8		
THS9		

	Switch alone	Switch with miR-122
THS10	 The diagram shows the secondary structure of THS10 RNA alone. It features a large central loop on the left, connected by a stem to a smaller loop on the right. Several other smaller loops and stems are distributed throughout the structure, with nucleotides represented by colored dots (black, red, blue, green).	 The diagram shows the secondary structure of THS10 RNA in the presence of miR-122. The structure is significantly altered, with a long, straight stem extending to the left from the main body of the RNA. The right side of the structure remains similar to the 'Switch alone' condition, but the overall conformation is different due to the binding of miR-122.

v GFP switches time course data: Sensitivity:

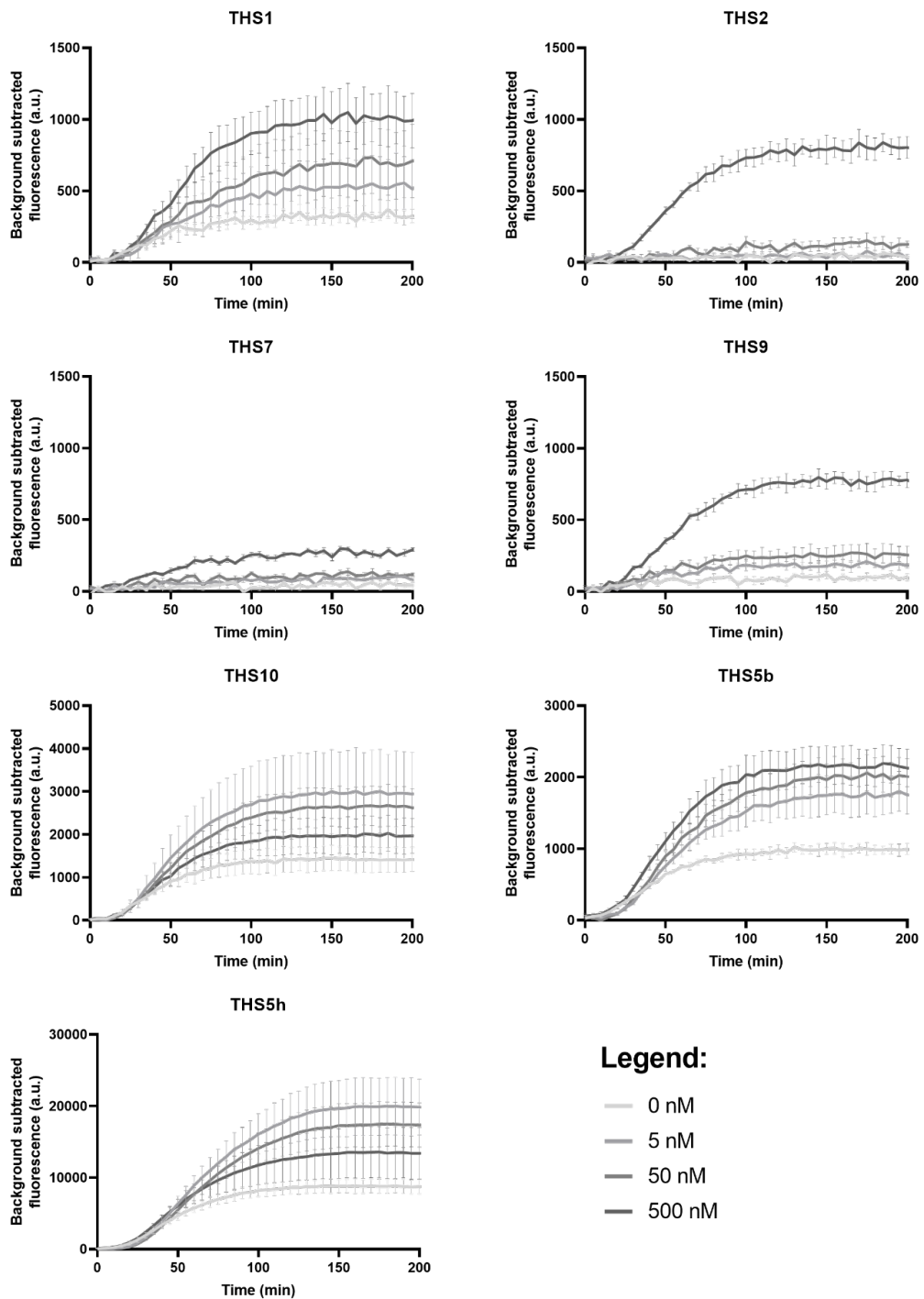


**Figure: Time course data from sensitivity test of switches.**

Data shows background subtracted fluorescence over time (min). Switches were used with 0, 5, 50 & 500 nM miR-122. Graphs show mean and error bars standard deviation of the mean.  $N=3$ .

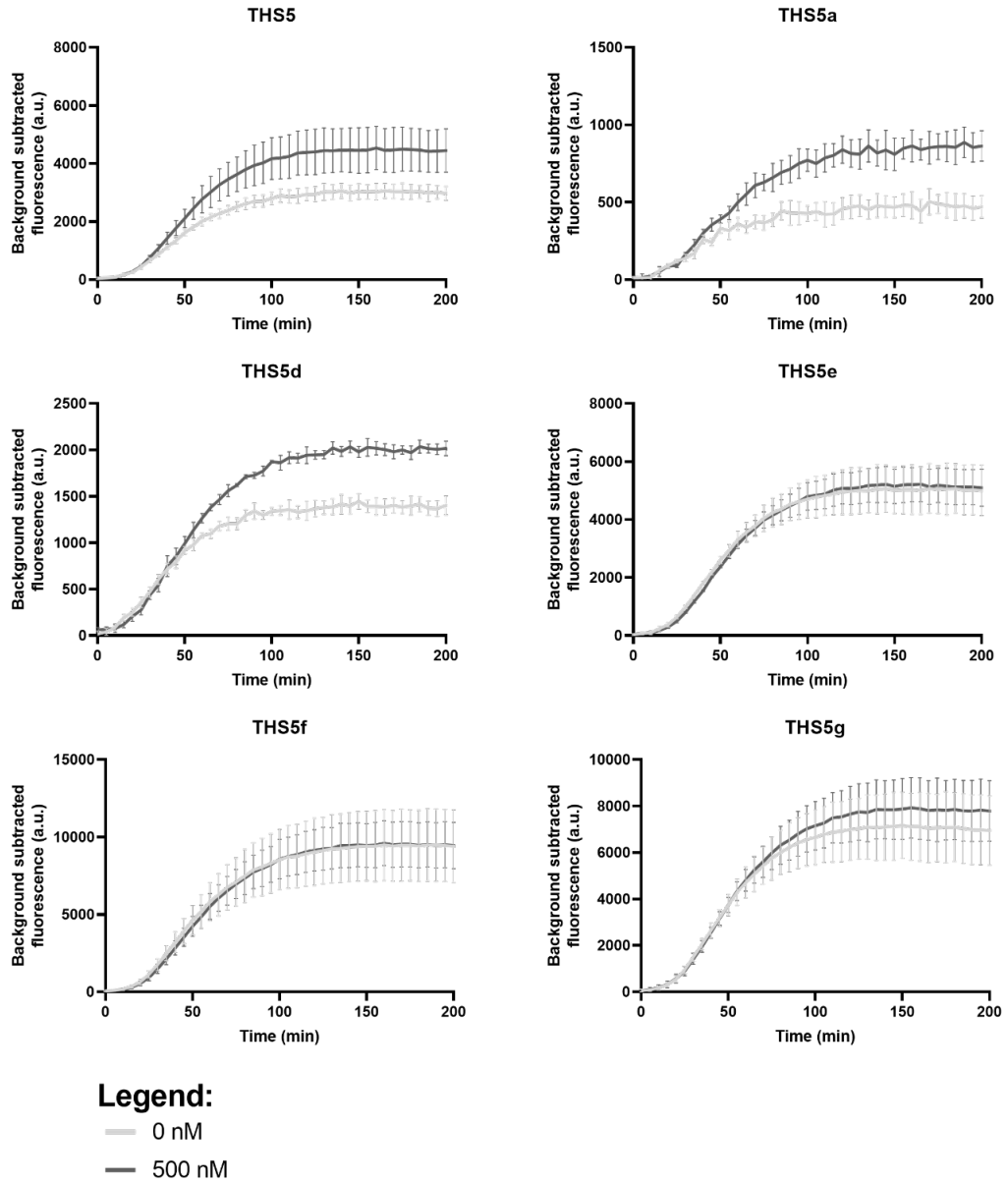


**Figure: Time course data from sensitivity test of switches.**

Data shows background subtracted fluorescence over time (min). Switches were used with 0, & 500 nM miR-122. Graphs show mean and error bars standard deviation of the mean. N=3.

vi GFP switches time course data: Specificity:

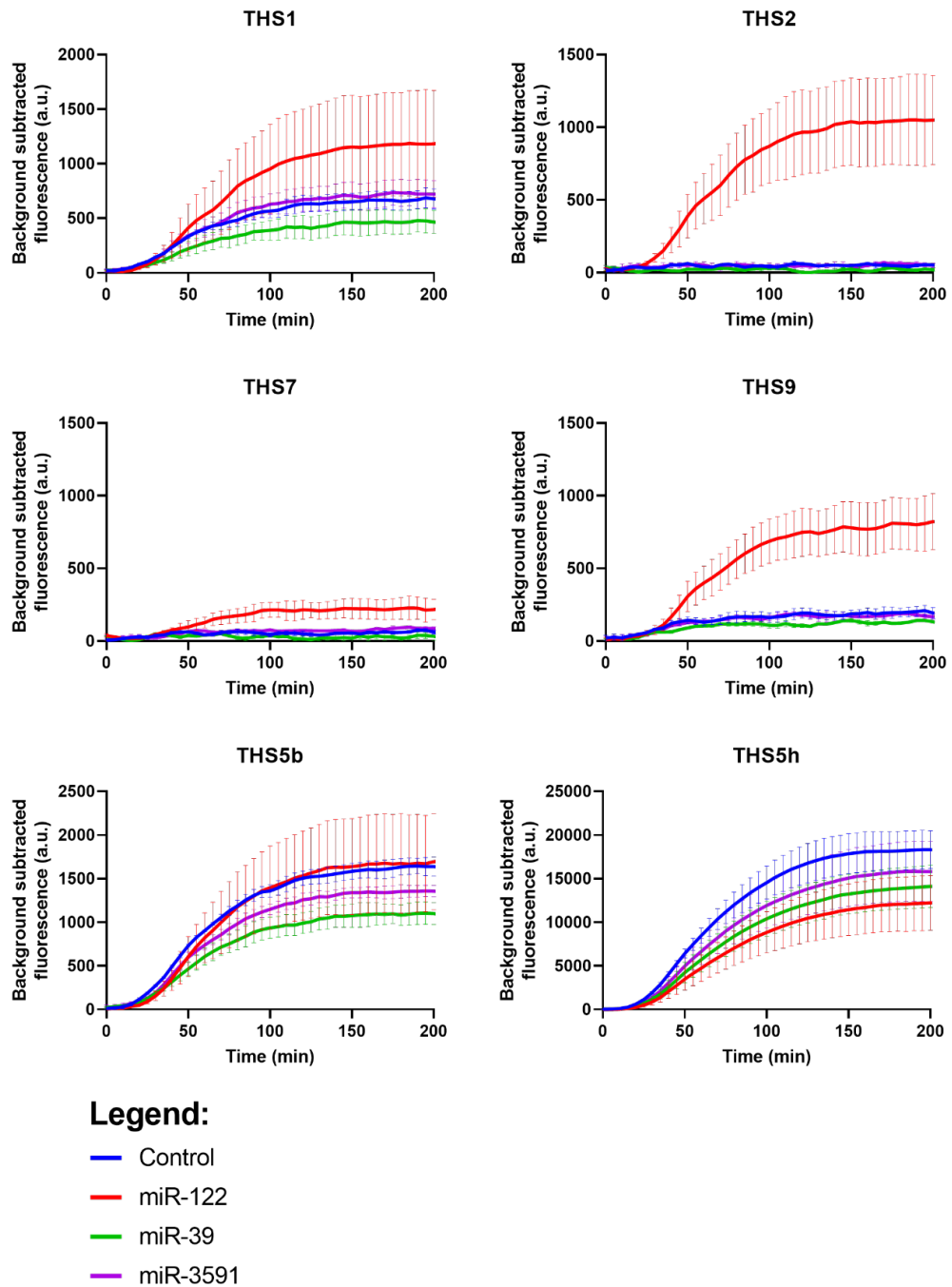


**Figure: Time course data from specificity test of switches.**

Data shows background subtracted fluorescence over time (min). Switches were used with water (control), 500 nM miR-122, miR-39 & miR-3591. Graphs show mean and error bars standard deviation of the mean. N=3.



vii GFP switches time course data: Further optimisation:

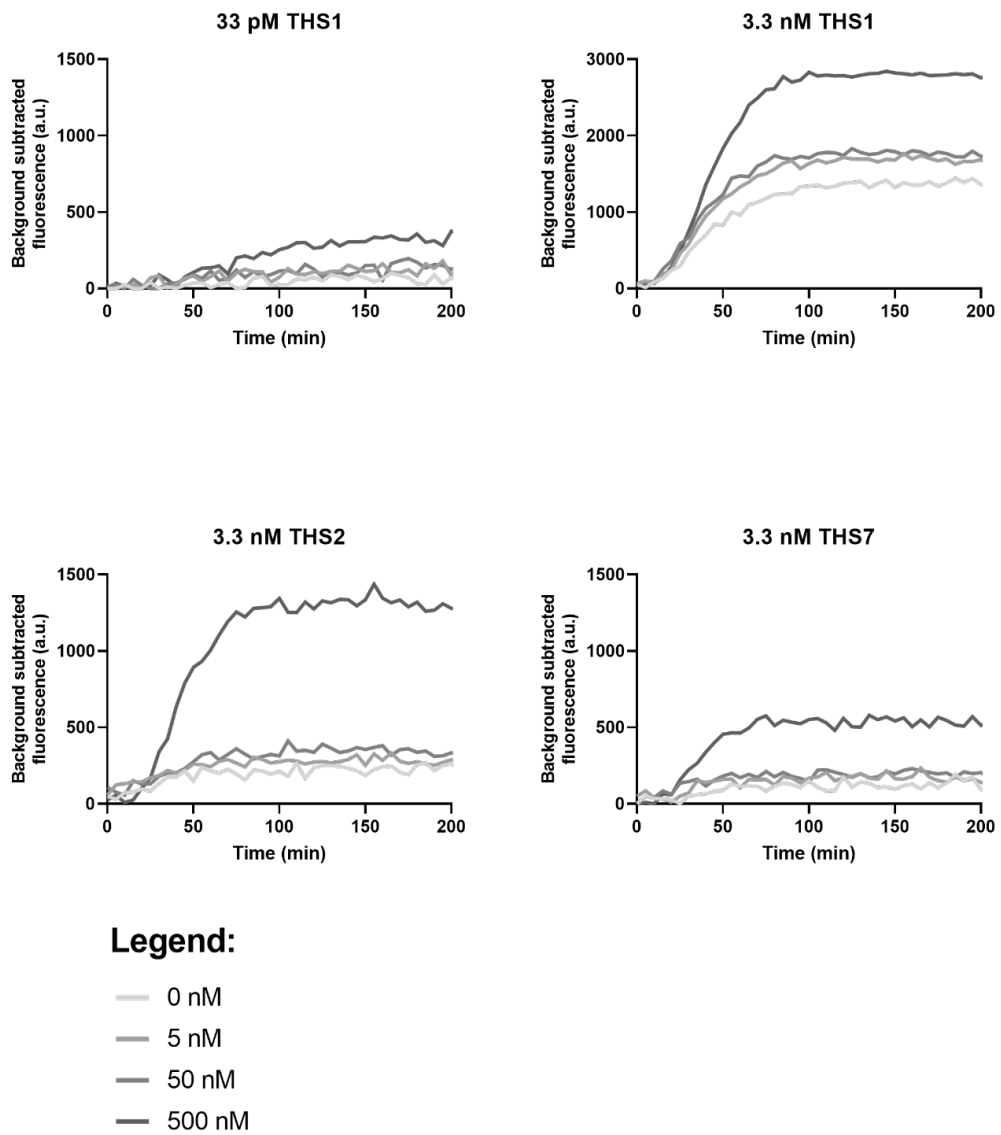


**Figure: Time course data from further optimisation tests of switches.**

Data shows background subtracted fluorescence over time (min). DNA concentration of switches described in figures, with 0, 5, 50 & 500 nM miR-122. N=1.

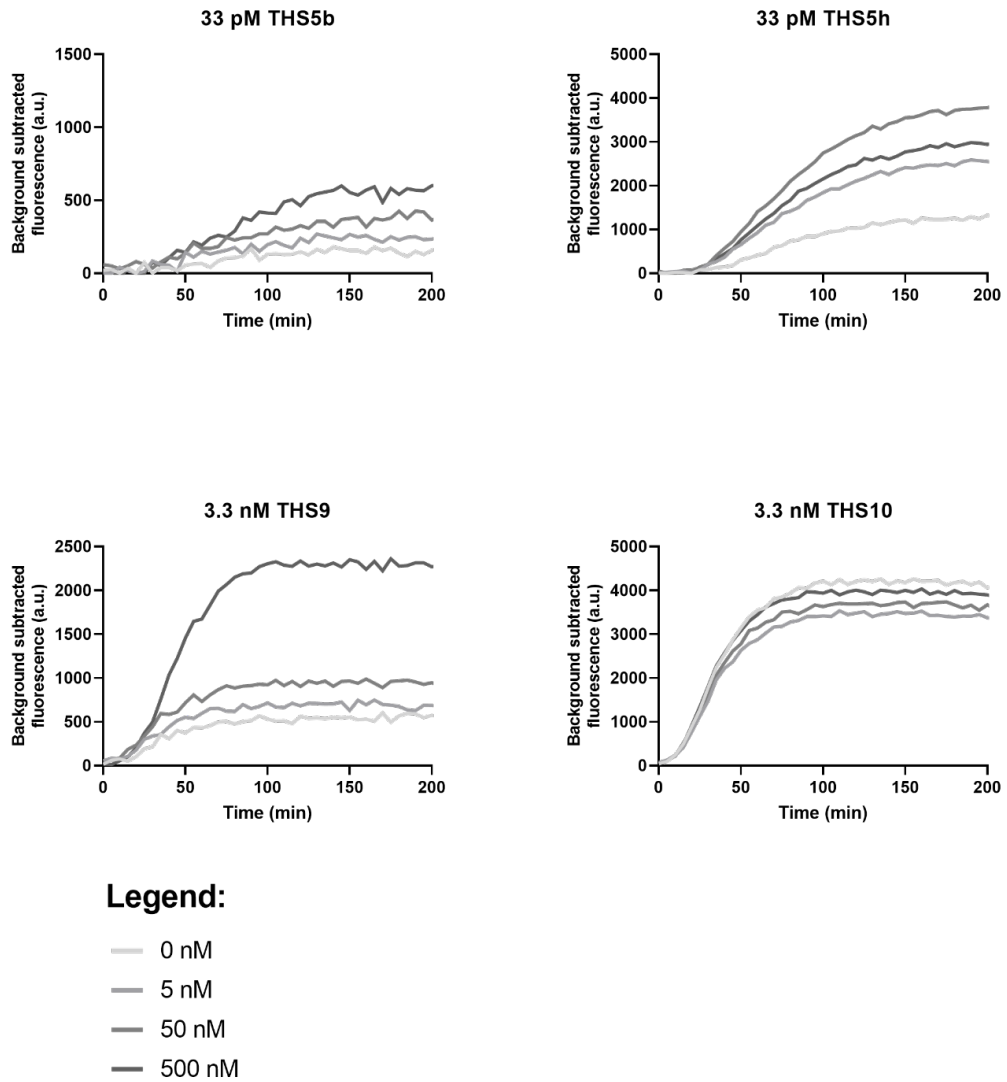


**Figure: Time course data from further optimisation tests of switches.**

Data shows background subtracted fluorescence over time (min). DNA concentration of switches described in figures, with 0, 5, 50 & 500 nM miR-122. N=1.

viii LacZ switches time course data:

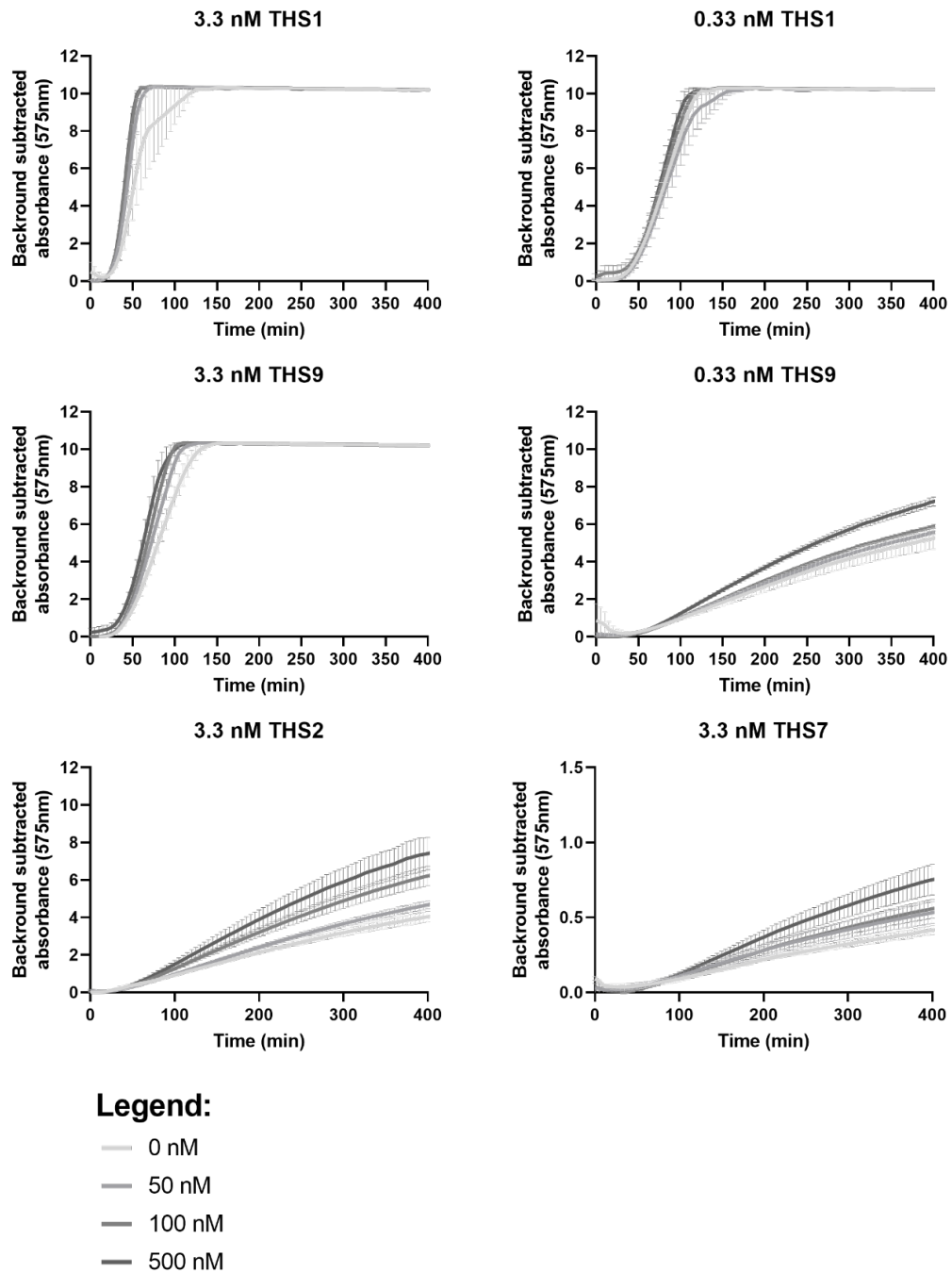


**Figure: Test of *lacZ* switches.**

Background subtracted absorbance (575 nm) over time (min). DNA concentrations used described in graph titles. Concentrations of miR-122 used 0, 50, 100 & 500 nM. Graph show mean and error bars show standard error of the mean.  $N=3$ .

## Bibliography

- [1] W. M. Lee, "Drug-induced acute liver failure," *Clin. Liver Dis.*, vol. 17, no. 4, pp. 575–586, 2013, doi: 10.1016/j.cld.2013.07.001.
- [2] W. Bernal, G. Auzinger, A. Dhawan, and J. Wendon, "Acute liver failure," *Lancet*, vol. 376, no. 9736, pp. 190–201, 2010, doi: 10.1016/S0140-6736(10)60274-7.
- [3] A. Iorga, L. Dara, and N. Kaplowitz, "Drug-induced liver injury: Cascade of events leading to cell death, apoptosis or necrosis," *Int. J. Mol. Sci.*, vol. 18, no. 5, 2017, doi: 10.3390/ijms18051018.
- [4] E. S. Björnsson, O. M. Bergmann, H. K. Björnsson, R. B. Kvaran, and S. Olafsson, "Incidence, presentation, and outcomes in patients with drug-induced liver injury in the general population of iceland," *Gastroenterology*, vol. 144, no. 7, pp. 1419–1425.e3, 2013, doi: 10.1053/j.gastro.2013.02.006.
- [5] P. B. Watkins, P. J. Seligman, J. S. Pears, M. I. Avigan, and J. R. Senior, "Using controlled clinical trials to learn more about acute drug-induced liver injury," *Hepatology*, vol. 48, no. 5, pp. 1680–1689, 2008, doi: 10.1002/hep.22633.
- [6] N. Chalasani *et al.*, "Features and outcomes of 899 patients with drug-induced liver injury: The DILIN prospective study," *Gastroenterology*, vol. 148, no. 7, pp. 1340–1352.e7, 2015, doi: 10.1053/j.gastro.2015.03.006.
- [7] W. Abera, W. Cheneke, and G. Abebe, "Incidence of antituberculosis-drug-induced hepatotoxicity and associated risk factors among tuberculosis patients in Dawro Zone, South Ethiopia: A cohort study," *Int. J. Mycobacteriology*, vol. 5, no. 1, pp. 14–20, 2016, doi: 10.1016/j.ijmyco.2015.10.002.
- [8] N. Kaplowitz, *Drug-induced liver injury: Introduction and overview*, Third Edit. Elsevier Inc., 2013.
- [9] K. T. Suk and D. J. Kim, "Drug-induced liver injury: present and future.," *Clin. Mol. Hepatol.*, vol. 18, no. 3, pp. 249–57, Sep. 2012, doi: 10.3350/cmh.2012.18.3.249.
- [10] R. Ramachandran and S. Kakar, "Histological patterns in drug-induced liver disease," *J. Clin. Pathol.*, vol. 62, no. 6, pp. 481–492, 2009, doi: 10.1136/jcp.2008.058248.
- [11] D. E. Kleiner, *Histopathological evaluation of drug-induced liver disease*, Third Edit. Elsevier Inc., 2013.
- [12] World Health Organization, "Global Health Estimates 2016: Deaths by Cause, Age,

- Sex, by Country and by Region, 2000-2016. Geneva, World Health Organization; 2018.," 2018. [Online]. Available: <https://www.who.int/news-room/fact-sheets/detail/the-top-10-causes-of-death>.
- [13] World Health Organization (WHO), "WHO TB Report," *WHO Libr. Cat. Data World*, 2019.
- [14] World Health Organization (WHO), "Guidelines for treatment of drug-susceptible tuberculosis and patient care," 2017. doi: 10.1586/17476348.1.1.85.
- [15] World Health Organization (WHO), "Latent tuberculosis infection: updated and consolidated guidelines for programmatic management.," 2018. doi: 10.1056/NEJMcp021045.
- [16] World Health Organisation (WHO), "Progress report on HIV, viral hepatitis and sexually transmitted infections 2019: Accountability for the global health sector strategies, 2016–2021," *Who*, pp. 2016–2021, 2019.
- [17] G. Doitsh *et al.*, "Pyroptosis drives CD4 T-cell depletion," *Nature*, vol. 505, no. 7484, pp. 509–514, 2014, doi: 10.1038/nature12940.Pyroptosis.
- [18] H. Garg, J. Mohl, and A. Joshi, "HIV-1 induced bystander apoptosis," *Viruses*, vol. 4, no. 11, pp. 3020–3043, 2012, doi: 10.3390/v4113020.
- [19] H. Getahun, C. Gunneberg, R. Granich, and P. Nunn, "HIV Infection–Associated Tuberculosis: The Epidemiology and the Response," *Clin. Infect. Dis.*, vol. 50, no. s3, pp. S201–S207, 2010, doi: 10.1086/651492.
- [20] E. L. Corbett *et al.*, "The Growing Burden of Tuberculosis," *Arch. Intern. Med.*, vol. 163, no. 9, p. 1009, 2003, doi: 10.1001/archinte.163.9.1009.
- [21] S. K. Sharma, A. Mohan, and T. Kadiravan, "HIV-TB co-infection: Epidemiology, diagnosis & management," *Indian J. Med. Res.*, vol. 121, no. 4, pp. 550–567, 2005.
- [22] K. R. Collins, M. E. Quiñones-mateu, Z. Toossi, and E. J. Arts, "Impact of Tuberculosis on HIV-1 Replication , Diversity , and Disease Progression," pp. 165–176, 2002.
- [23] D. Wilkinson, S. B. Squire, and P. Garner, "Effect of preventive treatment for tuberculosis in adults infected with HIV: Systematic review of randomised placebo controlled trials," *Br. Med. J.*, vol. 317, no. 7159, pp. 625–629, 1998, doi: 10.1136/bmj.317.7159.625.
- [24] S. C. Piscitelli and K. D. Gallicano, "Interactions Among Drugs for HIV and Opportunistic Infections," *N. Engl. J. Med.*, vol. 344, no. 13, pp. 984–996, 2001, doi:

- 10.1056/NEJM200103293441307.
- [25] C. S. Haworth *et al.*, *British Thoracic Society guidelines for the management of nontuberculous mycobacterial pulmonary disease (NTM-PD)*, vol. 72, no. Grade D. 2017.
- [26] D. E. Griffith *et al.*, "An official ATS/IDSA statement: Diagnosis, treatment, and prevention of nontuberculous mycobacterial diseases," *Am. J. Respir. Crit. Care Med.*, vol. 175, no. 4, pp. 367–416, 2007, doi: 10.1164/rccm.200604-571ST.
- [27] H. M. Hassan, H. L. Guo, B. A. Yousef, Z. Luyong, and J. Zhenzhou, "Hepatotoxicity mechanisms of isoniazid: A mini-review," *J. Appl. Toxicol.*, vol. 35, no. 12, pp. 1427–1432, Dec. 2015, doi: 10.1002/jat.3175.
- [28] I. Metushi, J. Uetrecht, and E. Phillips, "Mechanism of isoniazid-induced hepatotoxicity: Then and now," *Br. J. Clin. Pharmacol.*, vol. 81, no. 6, pp. 1030–1036, Jun. 2016, doi: 10.1111/bcp.12885.
- [29] M. Black, J. R. Mitchell, H. J. Zimmerman, K. G. Ishak, and G. R. Epler, "Isoniazid associated hepatitis in 114 patients," *Gastroenterology*, vol. 69, no. 2, pp. 289–302, 1975, doi: 10.1016/s0016-5085(19)32568-5.
- [30] I. G. Metushi and J. Uetrecht, "Isoniazid-induced liver injury and immune response in mice," *J. Immunotoxicol.*, vol. 11, no. 4, pp. 383–392, 2014, doi: 10.3109/1547691X.2013.860644.
- [31] I. G. Metushi, T. Nakagawa, and J. Uetrecht, "Direct oxidation and covalent binding of isoniazid to rodent liver and human hepatic microsomes: Humans are more like mice than rats," *Chem. Res. Toxicol.*, vol. 25, no. 11, pp. 2567–2576, 2012, doi: 10.1021/tx300341r.
- [32] C. E. Schwab and H. Tuschl, "In vitro studies on the toxicity of isoniazid in different cell lines," *Hum. Exp. Toxicol.*, vol. 22, no. 11, pp. 607–615, 2003, doi: 10.1191/0960327103ht401oa.
- [33] Y. Chen *et al.*, "Isoniazid suppresses antioxidant response element activities and impairs adipogenesis in mouse and human preadipocytes," *Toxicol. Appl. Pharmacol.*, vol. 273, no. 3, pp. 435–441, 2013, doi: 10.1016/j.taap.2013.10.005.
- [34] R. J. Warrington, K. S. Tse, B. A. Gorski, R. Schwenk, and A. H. Sehon, "Evaluation of isoniazid-associated hepatitis by immunological tests," *Clin. Exp. Immunol.*, vol. 32, no. 1, pp. 97–104, Apr. 1978.
- [35] I. G. Metushi, C. Sanders, W. M. Acute Liver Study Group, W. M. Lee, and J. Uetrecht,

- “Detection of anti-isoniazid and anti-cytochrome P450 antibodies in patients with isoniazid-induced liver failure,” *Hepatology*, vol. 59, no. 3, pp. 1084–93, Mar. 2014, doi: 10.1002/hep.26564.
- [36] P. A. Aristoff, G. A. Garcia, P. D. Kirchhoff, and H. D. Hollis Showalter, “Rifamycins - Obstacles and opportunities,” *Tuberculosis*, vol. 90, no. 2, pp. 94–118, 2010, doi: 10.1016/j.tube.2010.02.001.
- [37] M. I. Prince, A. D. Burt, and D. E. J. Jones, “Hepatitis and liver dysfunction with rifampicin therapy for pruritus in primary biliary cirrhosis,” *Gut*, vol. 50, no. 3, pp. 436–439, 2002, doi: 10.1136/gut.50.3.436.
- [38] J. A. Byrne, S. S. Strautnieks, G. MieliVergani, C. F. Higgins, K. J. Linton, and R. J. Thompson, “The human bile salt export pump: Characterization of substrate specificity and identification of inhibitors,” *Gastroenterology*, vol. 123, no. 5, pp. 1649–1658, 2002, doi: 10.1053/gast.2002.36591.
- [39] N. Mohan, J. Kumar, A. Chakrawarty, and P. Ranjan, “Comprehensive review of anti-tubercular treatment induced liver injury,” *Int. J. Basic Clin. Pharmacol.*, vol. 4, no. 3, pp. 397–403, Jan. 2015, doi: 10.18203/2319-2003.ijbcp20150030.
- [40] O. Burk *et al.*, “The induction of cytochrome P450 3A5 (CYP3A5) in the human liver and intestine is mediated by the xenobiotic sensors pregnane X receptor (PXR) and constitutively activated receptor (CAR),” *J. Biol. Chem.*, vol. 279, no. 37, pp. 38379–38385, 2004, doi: 10.1074/jbc.M404949200.
- [41] A. Nannelli, V. Chirulli, V. Longo, and P. G. Gervasi, “Expression and induction by rifampicin of CAR- and PXR-regulated CYP2B and CYP3A in liver, kidney and airways of pig,” *Toxicology*, vol. 252, no. 1–3, pp. 105–112, 2008, doi: 10.1016/j.tox.2008.08.004.
- [42] H. M. J. Nijland *et al.*, “Rifampicin Reduces Plasma Concentrations of Moxifloxacin in Patients with Tuberculosis,” *Clin. Infect. Dis.*, vol. 45, no. 8, pp. 1001–1007, 2007, doi: 10.1086/521894.
- [43] D. J. Girling, “The hepatic toxicity of antituberculosis regimens containing isoniazid, rifampicin and pyrazinamide,” *Tubercle*, vol. 59, no. 1, pp. 13–32, Sep. 1977, doi: 10.1016/0041-3879(77)90022-8.
- [44] J. G. Pasipanodya and T. Gumbo, “Clinical and toxicodynamic evidence that high-dose pyrazinamide is not more hepatotoxic than the low doses currently used,”

- Antimicrob. Agents Chemother.*, vol. 54, no. 7, pp. 2847–2854, 2010, doi: 10.1128/AAC.01567-09.
- [45] A. Medinger, “Death associated with rifampin and pyrazinamide 2-month treatment of latent mycobacterium tuberculosis,” *Chest*, vol. 121, no. 5, pp. 1710–1712, 2002, doi: 10.1378/chest.121.5.1710.
- [46] D. Pessayre, D. Larrey, and J. P. Benhamou, “Pyrazinamide Fulminant Hepatitis: an Old Hepatotoxin Strikes Again,” *Lancet*, vol. 318, no. 8254, pp. 1056–1057, 1981, doi: 10.1016/S0140-6736(81)91262-9.
- [47] T. Y. Shih, C. Y. Pai, P. Yang, W. L. Chang, N. C. Wang, and O. Y. P. Hu, “A novel mechanism underlies the hepatotoxicity of pyrazinamide,” *Antimicrob. Agents Chemother.*, vol. 57, no. 4, pp. 1685–1690, 2013, doi: 10.1128/AAC.01866-12.
- [48] A. Rawat *et al.*, “Metabolomics approach discriminates toxicity index of pyrazinamide and its metabolic products, pyrazinoic acid and 5-hydroxy pyrazinoic acid,” *Hum. Exp. Toxicol.*, vol. 37, no. 4, pp. 373–389, 2018, doi: 10.1177/0960327117705426.
- [49] Y. Zhang *et al.*, “Liver fatty acid binding protein deficiency provokes oxidative stress, inflammation, and apoptosis-mediated hepatotoxicity induced by pyrazinamide in zebrafish larvae,” *Antimicrob. Agents Chemother.*, vol. 60, no. 12, pp. 7347–7356, 2016, doi: 10.1128/AAC.01693-16.
- [50] Y. Zhang *et al.*, “Gene expression profiling reveals potential key pathways involved in pyrazinamide-mediated hepatotoxicity in Wistar rats,” *J. Appl. Toxicol.*, vol. 33, no. 8, pp. 807–819, 2013, doi: 10.1002/jat.2736.
- [51] J. Bertino and D. Fish, “The safety profile of the fluoroquinolones,” *Clin. Ther.*, vol. 22, no. 7, pp. 798–817, 2000, doi: 10.1016/S0149-2918(00)80053-3.
- [52] J. J. Saukkonen *et al.*, “An official ATS statement: Hepatotoxicity of antituberculosis therapy,” *Am. J. Respir. Crit. Care Med.*, vol. 174, no. 8, pp. 935–952, 2006, doi: 10.1164/rccm.200510-1666ST.
- [53] R. Chen, J. Wang, Y. Zhang, S. Tang, and S. Zhan, “Key factors of susceptibility to anti-tuberculosis drug-induced hepatotoxicity,” *Arch. Toxicol.*, vol. 89, no. 6, pp. 883–897, 2015, doi: 10.1007/s00204-015-1473-1.
- [54] A. Tostmann *et al.*, “Isoniazid and its toxic metabolite hydrazine induce in vitro pyrazinamide toxicity,” *Int. J. Antimicrob. Agents*, vol. 31, no. 6, pp. 577–580, 2008, doi: 10.1016/j.ijantimicag.2008.01.022.



- [55] V. Ramappa and G. P. Aithal, "Hepatotoxicity Related to Anti-tuberculosis Drugs: Mechanisms and Management," *J. Clin. Exp. Hepatol.*, vol. 3, no. 1, pp. 37–49, 2013, doi: 10.1016/j.jceh.2012.12.001.
- [56] W. W. Yew and C. C. Leung, "Antituberculosis drugs and hepatotoxicity," *Respirology*, vol. 11, no. 6, pp. 699–707, 2006, doi: 10.1111/j.1400-1843.2006.00941.x.
- [57] D. A. Perwitasari, J. Atthobari, and B. Wilffert, "Pharmacogenetics of isoniazid-induced hepatotoxicity," *Drug Metab. Rev.*, vol. 47, no. 2, pp. 222–228, May 2015, doi: 10.3109/03602532.2014.984070.
- [58] Y. S. Huang, "Recent progress in genetic variation and risk of antituberculosis drug-induced liver injury," *J. Chinese Med. Assoc.*, vol. 77, no. 4, pp. 169–173, 2014, doi: 10.1016/j.jcma.2014.01.010.
- [59] G. P. Aithal *et al.*, "Case definition and phenotype standardization in drug-induced liver injury," *Clin. Pharmacol. Ther.*, vol. 89, no. 6, pp. 806–815, 2011, doi: 10.1038/clpt.2011.58.
- [60] R. P. Cusack, L. Chawke, D. J. O'Brien, B. O'Connor, and T. M. O'Connor, "Predictors of hepatotoxicity among patients treated with antituberculous medication," *Qjm*, p. hcw160, 2016, doi: 10.1093/qjmed/hcw160.
- [61] National Institute for Health and Care Excellence (NICE), "Tuberculosis: Prevention, diagnosis, management and service organisation," 2016. doi: 10.1016/S1473-3099(14)70966-1.
- [62] L. P. Ormerod, H. J. Milburn, S. Gillespie, J. Ledingham, and D. Rampton, "BTS recommendations for assessing risk and for managing Mycobacterium tuberculosis infection and disease in patients due to start anti-TNF- $\alpha$  treatment," *Thorax*, vol. 60, no. 10, pp. 800–805, 2005, doi: 10.1136/thx.2005.046797.
- [63] Bethesda (MD): National Institute of Diabetes and Digestive and Kidney Diseases, "LiverTox: Clinical and Research Information on Drug-Induced Liver Injury [Internet] Roussel Uclaf Causality Assessment Method (RUCAM) in Drug Induced Liver Injury.," [Online], 2017, [Online]. Available: <https://livertox.nih.gov/rucam.html>.
- [64] J. R. Senior, "Alanine Aminotransferase: A Clinical and Regulatory Tool for Detecting Liver Injury—Past, Present, and Future," *Clin. Pharmacol. Ther.*, vol. 92, no. 3, pp. 332–339, Sep. 2012, doi: 10.1038/clpt.2012.108.
- [65] J. Pettersson *et al.*, "Muscular exercise can cause highly pathological liver function

- tests in healthy men.," *Br. J. Clin. Pharmacol.*, vol. 65, no. 2, pp. 253–9, Feb. 2008, doi: 10.1111/j.1365-2125.2007.03001.x.
- [66] J. S. LaDue and F. Wroblewski, "The Significance of the Serum Glutamic Oxalacetic Transaminase Activity Following Acute Myocardial Infarction," *Circulation*, vol. 11, no. 6, pp. 871–877, Jun. 1955, doi: 10.1161/01.CIR.11.6.871.
- [67] N. Sattar *et al.*, "Elevated alanine aminotransferase predicts new-onset type 2 diabetes independently of classical risk factors, metabolic syndrome, and C-reactive protein in the west of Scotland coronary prevention study.," *Diabetes*, vol. 53, no. 11, pp. 2855–60, Nov. 2004, doi: 10.2337/diabetes.53.11.2855.
- [68] A. J. G. Hanley *et al.*, "Elevations in markers of liver injury and risk of type 2 diabetes: the insulin resistance atherosclerosis study.," *Diabetes*, vol. 53, no. 10, pp. 2623–32, Oct. 2004, doi: 10.2337/diabetes.53.10.2623.
- [69] P. Thulin *et al.*, "PPAR $\alpha$  regulates the hepatotoxic biomarker alanine aminotransferase (ALT1) gene expression in human hepatocytes," *Toxicol. Appl. Pharmacol.*, vol. 231, no. 1, pp. 1–9, Aug. 2008, doi: 10.1016/J.TAAP.2008.03.007.
- [70] D. J. Antoine and J. W. Dear, "How to treat paracetamol overdose and when to do it," *Expert Rev. Clin. Pharmacol.*, vol. 9, no. 5, pp. 633–635, 2016, doi: 10.1586/17512433.2016.1154786.
- [71] A. D. B. Vliegenthart, D. J. Antoine, and J. W. Dear, "Target biomarker profile for the clinical management of paracetamol overdose," *Br. J. Clin. Pharmacol.*, vol. 80, no. 3, pp. 351–362, 2015, doi: 10.1111/bcp.12699.
- [72] A. M. Larson *et al.*, "Acetaminophen-induced acute liver failure: Results of a United States multicenter, prospective study," *Hepatology*, vol. 42, no. 6, pp. 1364–1372, 2005, doi: 10.1002/hep.20948.
- [73] J. A. Hinson, D. W. Roberts, and L. P. James, *Mechanisms of Acetaminophen-Induced Liver Necrosis*, vol. 196, no. 196. 2010.
- [74] J. W. Dear *et al.*, "Risk stratification after paracetamol overdose using mechanistic biomarkers: results from two prospective cohort studies," *Lancet Gastroenterol. Hepatol.*, vol. 3, no. 2, pp. 104–113, 2018, doi: 10.1016/S2468-1253(17)30266-2.
- [75] R. J. Church *et al.*, "Candidate biomarkers for the diagnosis and prognosis of drug-induced liver injury: An international collaborative effort.," *Hepatology*, vol. 00, no. 00, pp. 1–14, 2018, doi: 10.1002/hep.29802.

- [76] R. C. Lee, R. L. Feinbaum, and V. Ambros, "The *C. elegans* Heterochronic Gene *lin-4* Encodes Small RNAs with Antisense Complementarity to *lin-14* Rosalind," *Cell Press*, vol. 75, no. 5, pp. 843–854, 1993, doi: 10.1103/PhysRevLett.99.179704.
- [77] J. O'Brien, H. Hayder, Y. Zayed, and C. Peng, "Overview of MicroRNA Biogenesis, Mechanisms of Actions, and Circulation," *Front. Endocrinol. (Lausanne)*, vol. 9, p. 402, Aug. 2018, doi: 10.3389/fendo.2018.00402.
- [78] M. Girard, E. Jacquemin, A. Munnich, S. Lyonnet, and A. Henrion-Caude, "miR-122, a paradigm for the role of microRNAs in the liver," *J. Hepatol.*, vol. 48, no. 4, pp. 648–656, Apr. 2008, doi: 10.1016/J.JHEP.2008.01.019.
- [79] S. Lin and R. I. Gregory, "MicroRNA biogenesis pathways in cancer," *Nat. Rev. Cancer*, vol. 15, no. 6, pp. 321–333, Jun. 2015, doi: 10.1038/nrc3932.
- [80] X. Lai and J. Vera, "Encyclopedia of Systems Biology," *Encycl. Syst. Biol.*, no. October 2020, 2013, doi: 10.1007/978-1-4419-9863-7.
- [81] V. Ambros *et al.*, "A uniform system for microRNA annotation," pp. 277–279, 2003, doi: 10.1261/rna.2183803.One.
- [82] M. I. Almeida, R. M. Reis, and G. A. Calin, "MicroRNA history: Discovery, recent applications, and next frontiers," *Mutat. Res. - Fundam. Mol. Mech. Mutagen.*, vol. 717, no. 1–2, pp. 1–8, 2011, doi: 10.1016/j.mrfmmm.2011.03.009.
- [83] H. Iftikhar and G. E. Carney, "Evidence and potential in vivo functions for biofluid miRNAs: From expression profiling to functional testing: Potential roles of extracellular miRNAs as indicators of physiological change and as agents of intercellular information exchange," *BioEssays*, vol. 38, no. 4, pp. 367–378, 2016, doi: 10.1002/bies.201500130.
- [84] A. Gallo, M. Tandon, I. Alevizos, and G. G. Illei, "The majority of microRNAs detectable in serum and saliva is concentrated in exosomes," *PLoS One*, vol. 7, no. 3, pp. 1–5, 2012, doi: 10.1371/journal.pone.0030679.
- [85] J. D. Arroyo *et al.*, "Argonaute2 complexes carry a population of circulating microRNAs independent of vesicles in human plasma," *Proc. Natl. Acad. Sci. U. S. A.*, vol. 108, no. 12, pp. 5003–5008, 2011, doi: 10.1073/pnas.1019055108.
- [86] X. Chen *et al.*, "Characterization of microRNAs in serum: A novel class of biomarkers for diagnosis of cancer and other diseases," *Cell Res.*, vol. 18, no. 10, pp. 997–1006, 2008, doi: 10.1038/cr.2008.282.

- [87] T.-H. Su *et al.*, "Serum microRNA-122 level correlates with virologic responses to pegylated interferon therapy in chronic hepatitis C.," *Proc. Natl. Acad. Sci. U. S. A.*, vol. 110, no. 19, pp. 7844–9, May 2013, doi: 10.1073/pnas.1306138110.
- [88] A. P. Lewis and C. L. Jopling, "Regulation and biological function of the liver-specific miR - 122," *Biochem. Soc. Trans.*, vol. 38, no. 6, pp. 1553–1557, 2010, doi: 10.1042/bst0381553.
- [89] J. Hu, Y. Xu, J. Hao, S. Wang, C. Li, and S. Meng, "MiR-122 in hepatic function and liver diseases," *Protein Cell*, vol. 3, no. 5, pp. 364–371, 2012, doi: 10.1007/s13238-012-2036-3.
- [90] K. Wang *et al.*, "Circulating microRNAs, potential biomarkers for drug-induced liver injury," *Proc. Natl. Acad. Sci.*, vol. 106, no. 11, pp. 4402–4407, 2009, doi: 10.1073/pnas.0813371106.
- [91] S. Starckx *et al.*, "Evaluation of miR-122 and Other Biomarkers in Distinct Acute Liver Injury in Rats," *Toxicol. Pathol.*, vol. 41, no. 5, pp. 795–804, 2013, doi: 10.1177/0192623312464436.
- [92] A. D. B. Vliegenthart *et al.*, "Retro-Orbital Blood Acquisition Facilitates Circulating microRNA Measurement in Zebrafish with Paracetamol Hepatotoxicity," *Zebrafish*, vol. 11, no. 3, pp. 219–226, 2014, doi: 10.1089/zeb.2013.0912.
- [93] Y. Choi, H. P. Dienes, and K. Krawczynski, "Kinetics of miR-122 Expression in the Liver during Acute HCV Infection," *PLoS One*, vol. 8, no. 10, pp. 1–7, 2013, doi: 10.1371/journal.pone.0076501.
- [94] W. Oosthuyzen *et al.*, "Sensitivity and specificity of microRNA-122 for liver disease in dogs," *J. Vet. Intern. Med.*, no. January, pp. 1–8, 2018, doi: 10.1111/jvim.15250.
- [95] P. J. Starkey Lewis *et al.*, "Circulating microRNAs as potential markers of human drug-induced liver injury," *Hepatology*, vol. 54, no. 5, pp. 1767–1776, 2011, doi: 10.1002/hep.24538.
- [96] V. Bihrer *et al.*, "Serum mir-122 as a biomarker of necroinflammation in patients with chronic hepatitis C virus infection," *Am. J. Gastroenterol.*, vol. 106, no. 9, pp. 1663–1669, 2011, doi: 10.1038/ajg.2011.161.
- [97] J. C. McCrae, N. Sharkey, D. J. Webb, A. D. B. Vliegenthart, and J. W. Dear, "Ethanol consumption produces a small increase in circulating miR-122 in healthy individuals," *Clin. Toxicol.*, vol. 54, no. 1, pp. 53–55, Jan. 2016, doi:

10.3109/15563650.2015.1112015.

- [98] A. D. B. Vliegenthart *et al.*, “Comprehensive microRNA profiling in acetaminophen toxicity identifies novel circulating biomarkers for human liver and kidney injury,” *Sci. Rep.*, vol. 5, no. 1, p. 15501, 2015, doi: 10.1038/srep15501.
- [99] D. J. Antoine *et al.*, “Mechanistic biomarkers provide early and sensitive detection of acetaminophen-induced acute liver injury at first presentation to hospital,” *Hepatology*, vol. 58, no. 2, pp. 777–787, 2013, doi: 10.1002/hep.26294.
- [100] Food and Drug Administration Centre for Drug Evaluation and Research, “Letter of Support for Drug-Induced Drug-Induced Liver Injury (DILI) Biomarker(s),” 2016. <https://www.fda.gov/downloads/Drugs/DevelopmentApprovalProcess/UCM517355.pdf> (accessed Oct. 08, 2018).
- [101] European Medicines Agency, “Letter of support for drug-induced liver injury (DILI) biomarker,” 2016. [https://www.ema.europa.eu/documents/other/letter-support-drug-induced-liver-injury-dili-biomarker\\_en.pdf](https://www.ema.europa.eu/documents/other/letter-support-drug-induced-liver-injury-dili-biomarker_en.pdf) (accessed Oct. 08, 2018).
- [102] P. Thulin *et al.*, “Keratin-18 and microRNA-122 complement alanine aminotransferase as novel safety biomarkers for drug-induced liver injury in two human cohorts,” *Liver Int.*, vol. 34, no. 3, pp. 367–378, 2014, doi: 10.1111/liv.12322.
- [103] D. Adebayo, R. P. Mookerjee, and R. Jalan, “Mechanistic biomarkers in acute liver injury: Are we there yet?,” *J. Hepatol.*, vol. 56, no. 5, pp. 1003–1005, 2012, doi: 10.1016/j.jhep.2012.01.017.
- [104] C. Caulín, G. S. Salvesen, and R. G. Oshima, “Caspase cleavage of keratin 18 and reorganization of intermediate filaments during epithelial cell apoptosis,” *J. Cell Biol.*, vol. 138, no. 6, pp. 1379–1394, 1997, doi: 10.1083/jcb.138.6.1379.
- [105] A. Eguchi, A. Wree, and A. E. Feldstein, “Biomarkers of liver cell death,” *Hepatology*, vol. 60, no. 5, pp. 1063–1074, 2014, doi: 10.1016/j.jhep.2013.12.026.
- [106] M. P. G. Leers *et al.*, “Immunocytochemical detection and mapping of a cytokeratin 18 neo- epitope exposed during early apoptosis,” *J. Pathol.*, vol. 187, no. 5, pp. 567–572, 1999, doi: 10.1002/(SICI)1096-9896(199904)187:5<567::AID-PATH288>3.0.CO;2-J.
- [107] B. Schutte *et al.*, “Keratin 8/18 breakdown and reorganization during apoptosis,” *Exp. Cell Res.*, vol. 297, no. 1, pp. 11–26, 2004, doi: 10.1016/j.yexcr.2004.02.019.
- [108] D. J. Antoine *et al.*, “High-mobility group box-1 protein and keratin-18, circulating

- serum proteins informative of acetaminophen-induced necrosis and apoptosis in vivo," *Toxicol. Sci.*, vol. 112, no. 2, pp. 521–531, 2009, doi: 10.1093/toxsci/kfp235.
- [109] J. Cummings *et al.*, "Preclinical evaluation of M30 and M65 ELISAs as biomarkers of drug induced tumor cell death and antitumor activity," *Mol. Cancer Ther.*, vol. 7, no. 3, pp. 455–463, 2008, doi: 10.1158/1535-7163.MCT-07-2136.
- [110] A. Wieckowska, N. N. Zein, L. M. Yerian, A. R. Lopez, A. J. McCullough, and A. E. Feldstein, "In vivo assessment of liver cell apoptosis as a novel biomarker of disease severity in nonalcoholic fatty liver disease," *Hepatology*, vol. 44, no. 1, pp. 27–33, 2006, doi: 10.1002/hep.21223.
- [111] H. Bantel *et al.*, "Detection of apoptotic caspase activation in sera from patients with chronic HCV infection is associated with fibrotic liver injury," *Hepatology*, vol. 40, no. 5, pp. 1078–1087, 2004, doi: 10.1002/hep.20411.
- [112] D. J. Antoine *et al.*, "Molecular forms of HMGB1 and keratin-18 as mechanistic biomarkers for mode of cell death and prognosis during clinical acetaminophen hepatotoxicity," *Hepatology*, vol. 56, no. 5, pp. 1070–1079, 2012, doi: 10.1016/j.jhep.2011.12.019.Molecular.
- [113] V. Y. Soldatow, E. L. Lecluyse, L. G. Griffith, and I. Rusyn, "In vitro models for liver toxicity testing.," *Toxicol. Res. (Camb).*, vol. 2, no. 1, pp. 23–39, Jan. 2013, doi: 10.1039/C2TX20051A.
- [114] G. J. Lieschke and P. D. Currie, "Animal models of human disease: Zebrafish swim into view," *Nat. Rev. Genet.*, vol. 8, no. 5, pp. 353–367, 2007, doi: 10.1038/nrg2091.
- [115] P. McGrath and C. Q. Li, "Zebrafish: a predictive model for assessing drug-induced toxicity," *Drug Discov. Today*, vol. 13, no. 9–10, pp. 394–401, 2008, doi: 10.1016/j.drudis.2008.03.002.
- [116] T. P. Barros, W. K. Alderton, H. M. Reynolds, A. G. Roach, and S. Berghmans, "Zebrafish: An emerging technology for in vivo pharmacological assessment to identify potential safety liabilities in early drug discovery," *Br. J. Pharmacol.*, vol. 154, no. 7, pp. 1400–1413, 2008, doi: 10.1038/bjp.2008.249.
- [117] C. Cornet *et al.*, "ZeGlobalTox: An innovative approach to address organ drug toxicity using zebrafish," *Int. J. Mol. Sci.*, vol. 18, no. 4, 2017, doi: 10.3390/ijms18040864.
- [118] M. Westerfield, *The Zebrafish Book: A Guide for the Laboratory Use of Zebrafish (Danio Rerio)*. Eugene, USA: University of Oregon Press., 2007.

- [119] K. Howe *et al.*, "The zebrafish reference genome sequence and its relationship to the human genome," *Nature*, vol. 496, no. 7446, pp. 498–503, Apr. 2013, doi: 10.1038/nature12111.
- [120] S. Berghmans *et al.*, "Zebrafish based assays for the assessment of cardiac, visual and gut function — potential safety screens for early drug discovery," *J. Pharmacol. Toxicol. Methods*, vol. 58, no. 1, pp. 59–68, Jul. 2008, doi: 10.1016/J.VASCN.2008.05.130.
- [121] H. Diekmann and A. Hill, "ADMETox in zebrafish," *Drug Discov. Today Dis. Model.*, vol. 10, no. 1, pp. e31–e35, Mar. 2013, doi: 10.1016/J.DDMOD.2012.02.005.
- [122] J. V Goldstone *et al.*, "Identification and developmental expression of the full complement of Cytochrome P450 genes in Zebrafish," *BMC Genomics*, vol. 11, no. 1, p. 643, Nov. 2010, doi: 10.1186/1471-2164-11-643.
- [123] H. Ando *et al.*, "Daily rhythms of P-glycoprotein expression in mice," *Chronobiol. Int.*, vol. 22, no. 4, pp. 655–665, 2005, doi: 10.1080/07420520500180231.
- [124] J. M. Murtha, W. Qi, and E. T. Keller, "Hematologic and serum biochemical values for zebrafish (*Danio rerio*)," *Comp. Med.*, vol. 53, no. 1, pp. 37–41, 2003.
- [125] T. E. North *et al.*, "PGE2-regulated wnt signaling and N-acetylcysteine are synergistically hepatoprotective in zebrafish acetaminophen injury.," *Proc. Natl. Acad. Sci. U. S. A.*, vol. 107, no. 40, pp. 17315–20, Oct. 2010, doi: 10.1073/pnas.1008209107.
- [126] T. Tao and J. Peng, "Liver development in zebrafish (*Danio rerio*)," *J. Genet. Genomics*, vol. 36, no. 6, pp. 325–334, Jun. 2009, doi: 10.1016/S1673-8527(08)60121-6.
- [127] J. H. He *et al.*, "A zebrafish phenotypic assay for assessing drug-induced hepatotoxicity," *J. Pharmacol. Toxicol. Methods*, vol. 67, no. 1, pp. 25–32, 2013, doi: 10.1016/j.vascn.2012.10.003.
- [128] R. Zhao and S. A. Duncan, "Embryonic development of the liver," *Hepatology*, vol. 41, no. 5, pp. 956–967, 2005, doi: 10.1002/hep.20691.
- [129] A. D. B. Vliegenthart, C. S. Tucker, J. Del Pozo, and J. W. Dear, "Zebrafish as model organisms for studying drug-induced liver injury," *Br. J. Clin. Pharmacol.*, vol. 78, no. 6, pp. 1217–1227, 2014, doi: 10.1111/bcp.12408.
- [130] J. Chu and K. C. Sadler, "A New School in Liver Development: Lessons from Zebrafish," *Hepatology*, vol. 50, no. 5, p. 1656, Nov. 2009, doi: 10.1002/HEP.23157.

- [131] A. L. Menke, J. M. Spitsbergen, A. P. M. Wolterbeek, and R. A. Woutersen, "Normal Anatomy and Histology of the Adult Zebrafish," *Toxicol. Pathol.*, vol. 39, no. 5, pp. 759–775, Aug. 2011, doi: 10.1177/0192623311409597.
- [132] W. Alderton *et al.*, "Accumulation and metabolism of drugs and CYP probe substrates in zebrafish larvae," *Xenobiotica*, vol. 40, no. 8, pp. 547–557, 2010, doi: 10.3109/00498254.2010.493960.
- [133] S. Brox, B. Seiwert, N. Haase, E. Küster, and T. Reemtsma, "Metabolism of clofibrac acid in zebrafish embryos (*Danio rerio*) as determined by liquid chromatography–high resolution–mass spectrometry," *Comp. Biochem. Physiol. Part C Toxicol. Pharmacol.*, vol. 185–186, pp. 20–28, Jul. 2016, doi: 10.1016/J.CBPC.2016.02.007.
- [134] H. T. Chng, H. Kiat Ho, C. W. Yap, S. H. Lam, and E. C. Y. Chan, "An Investigation of the Bioactivation Potential and Metabolism of Zebrafish versus Human," *J. Biomol. Screen.*, vol. 17, no. 7, pp. 974–986, Mar. 2012, doi: <https://doi.org/10.1177/1087057112447305>.
- [135] C. Xu, C. Y.-T. Li, and A.-N. T. Kong, "Induction of phase I, II and III drug metabolism/transport by xenobiotics," *Arch. Pharm. Res.*, vol. 28, no. 3, pp. 249–268, Mar. 2005, doi: 10.1007/BF02977789.
- [136] H. S. Jones, H. T. Trollope, T. H. Hutchinson, G. H. Panter, and J. K. Chipman, "Metabolism of ibuprofen in zebrafish larvae," *Xenobiotica*, vol. 42, no. 11, pp. 1069–1075, 2012, doi: 10.3109/00498254.2012.684410.
- [137] K. Jemnitz, Z. Veres, K. Monostory, L. Kóbori, and L. Vereczkey, "Interspecies differences in acetaminophen sensitivity of human, rat, and mouse primary hepatocytes," *Toxicol. Vitro.*, vol. 22, no. 4, pp. 961–967, Jun. 2008, doi: 10.1016/J.TIV.2008.02.001.
- [138] J. E. Laine, S. Auriola, M. Pasanen, and R. O. Juvonen, "Acetaminophen bioactivation by human cytochrome P450 enzymes and animal microsomes," *Xenobiotica*, vol. 39, no. 1, pp. 11–21, 2009, doi: 10.1080/00498250802512830.
- [139] J. Berman, K. Hsu, and A. T. Look, "Zebrafish as a model organism for blood diseases," *Br. J. Haematol.*, vol. 123, no. 4, pp. 568–576, Nov. 2003, doi: 10.1046/j.1365-2141.2003.04682.x.
- [140] B. Bajoghli, "Evolution and function of chemokine receptors in the immune system of lower vertebrates," *Eur. J. Immunol.*, vol. 43, no. 7, pp. 1686–1692, Jul. 2013, doi:



- 10.1002/eji.201343557.
- [141] C. Ju and T. Reilly, "Role of immune reactions in drug-induced liver injury (DILI)," *Drug Metab. Rev.*, vol. 44, no. 1, pp. 107–115, 2012, doi: 10.3109/03602532.2011.645579.
- [142] S. C. Li, W. C. Chan, L. Y. Hu, C. H. Lai, C. N. Hsu, and W. chang Lin, "Identification of homologous microRNAs in 56 animal genomes," *Genomics*, vol. 96, no. 1, pp. 1–9, 2010, doi: 10.1016/j.ygeno.2010.03.009.
- [143] miRBase, "hsa-miR-122," 2020, 2020. [http://www.mirbase.org/cgi-bin/mirna\\_entry.pl?acc=MI0000442](http://www.mirbase.org/cgi-bin/mirna_entry.pl?acc=MI0000442) (accessed Jun. 15, 2020).
- [144] E. Wienholds *et al.*, "MicroRNA Expression in Zebrafish Embryonic Development," *Science (80-. )*, vol. 309, no. 5732, pp. 310 LP – 311, Jul. 2005, doi: 10.1126/science.1114519.
- [145] A. D. B. Vliegthart *et al.*, "Characterization of triptolide-induced hepatotoxicity by imaging and transcriptomics in a novel zebrafish model," *Toxicol. Sci.*, vol. 159, no. 2, pp. 380–391, 2017, doi: 10.1093/toxsci/kfx144.
- [146] A. Hill, N. Mesens, M. Steemans, J. J. Xu, and M. D. Aleo, "Comparisons between in vitro whole cell imaging and in vivo zebrafish-based approaches for identifying potential human hepatotoxicants earlier in pharmaceutical development," *Drug Metab. Rev.*, vol. 44, no. 1, pp. 127–140, 2012, doi: 10.3109/03602532.2011.645578.
- [147] S. Nadanaciva, M. D. Aleo, C. J. Strock, D. B. Stedman, H. Wang, and Y. Will, "Toxicity assessments of nonsteroidal anti-inflammatory drugs in isolated mitochondria, rat hepatocytes, and zebrafish show good concordance across chemical classes," *Toxicol. Appl. Pharmacol.*, vol. 272, no. 2, pp. 272–280, Oct. 2013, doi: 10.1016/J.TAAP.2013.06.019.
- [148] X. Zhang, C. Li, and Z. Gong, "Development of a convenient in vivo hepatotoxin assay using a transgenic zebrafish line with liver-specific dsred expression," *PLoS One*, vol. 9, no. 3, p. e91874, 2014, doi: 10.1371/journal.pone.0091874.
- [149] N. A. Sabaliauskas *et al.*, "High-throughput zebrafish histology," *Methods*, vol. 39, no. 3, pp. 246–254, Jul. 2006, doi: 10.1016/J.YMETH.2006.03.001.
- [150] N. Mesens *et al.*, "Are zebrafish larvae suitable for assessing the hepatotoxicity potential of drug candidates?," *J. Appl. Toxicol.*, vol. 35, no. 9, pp. 1017–1029, 2015, doi: 10.1002/jat.3091.
- [151] A. A. Amali *et al.*, "Thioacetamide induced liver damage in zebrafish embryo as a

- disease model for steatohepatitis," *J. Biomed. Sci.*, vol. 13, no. 2, pp. 225–232, 2006, doi: 10.1007/s11373-005-9055-5.
- [152] M. J. Passeri, A. Cinaroglu, C. Gao, and K. C. Sadler, "Hepatic steatosis in response to acute alcohol exposure in zebrafish requires sterol regulatory element binding protein activation," *Hepatology*, vol. 49, no. 2, pp. 443–452, 2009, doi: 10.1002/hep.22667.
- [153] V. P. Dave *et al.*, "MicroRNA amplification and detection technologies: opportunities and challenges for point of care diagnostics," *Lab. Investig.*, vol. 99, no. 4, pp. 452–469, 2019, doi: 10.1038/s41374-018-0143-3.
- [154] B. López-Longarela *et al.*, "Direct Detection of miR-122 in Hepatotoxicity Using Dynamic Chemical Labeling Overcomes Stability and isomiR Challenges," *Anal. Chem.*, vol. 92, no. 4, pp. 3388–3395, Feb. 2020, doi: 10.1021/acs.analchem.9b05449.
- [155] D. M. Rissin *et al.*, "Polymerase-free measurement of microRNA-122 with single base specificity using single molecule arrays: Detection of drug-induced liver injury," *PLoS One*, vol. 12, no. 7, pp. 1–15, 2017, doi: 10.1371/journal.pone.0179669.
- [156] K. Pardee *et al.*, "Paper-based synthetic gene networks," *Cell*, vol. 159, no. 4, pp. 940–954, 2014, doi: 10.1016/j.cell.2014.10.004.
- [157] A. A. Green, P. A. Silver, J. J. Collins, and P. Yin, "Toehold switches: De-novo-designed regulators of gene expression," *Cell*, vol. 159, no. 4, pp. 925–939, 2014, doi: 10.1016/j.cell.2014.10.002.
- [158] K. Pardee *et al.*, "Rapid, Low-Cost Detection of Zika Virus Using Programmable Biomolecular Components," *Cell*, vol. 165, no. 5, pp. 1255–1266, 2016, doi: 10.1016/j.cell.2016.04.059.
- [159] D. Ma, L. Shen, K. Wu, C. W. Diehnelt, and A. A. Green, "Low-cost detection of norovirus using paper-based cell-free systems and synbody-based viral enrichment.," *Synth. Biol. (Oxford, England)*, vol. 3, no. 1, p. ysy018, 2018, doi: 10.1093/synbio/ysy018.
- [160] M. K. Takahashi *et al.*, "A low-cost paper-based synthetic biology platform for analyzing gut microbiota and host biomarkers," *Nat. Commun.*, vol. 9, no. 1, p. 3347, 2018, doi: 10.1038/s41467-018-05864-4.
- [161] S. Wang, N. J. Emery, and A. P. Liu, "A Novel Synthetic Toehold Switch for MicroRNA

- Detection in Mammalian Cells,” *ACS Synth. Biol.*, vol. 8, no. 5, pp. 1079–1088, May 2019, doi: 10.1021/acssynbio.8b00530.
- [162] J. S. Park *et al.*, “Serum levels of antituberculosis drugs and their effect on tuberculosis treatment outcome,” *Antimicrob. Agents Chemother.*, vol. 60, no. 1, pp. 92–98, 2016, doi: 10.1128/AAC.00693-15.
- [163] E. Burhan *et al.*, “Isoniazid, rifampin, and pyrazinamide plasma concentrations in relation to treatment response in Indonesian pulmonary tuberculosis patients,” *Antimicrob. Agents Chemother.*, vol. 57, no. 8, pp. 3614–3619, 2013, doi: 10.1128/AAC.02468-12.
- [164] M. J. Boeree *et al.*, “A dose-ranging trial to optimize the dose of rifampin in the treatment of tuberculosis,” *Am. J. Respir. Crit. Care Med.*, vol. 191, no. 9, pp. 1058–1065, 2015, doi: 10.1164/rccm.201407-1264OC.
- [165] C. A. Peloquin *et al.*, “Pharmacokinetic evidence from the HIRIF Trial to support increased doses of rifampin for tuberculosis,” *Antimicrob. Agents Chemother.*, vol. 61, no. 8, pp. 1–6, 2017, doi: 10.1128/AAC.00038-17.
- [166] C. Schutz *et al.*, “Burden of antituberculosis and antiretroviral drug-induced liver injury at a secondary hospital in South Africa,” *South African Med. J.*, vol. 102, no. 6, pp. 506–511, 2012, doi: 10.7196/samj.5650.
- [167] R. Nabisere *et al.*, “Pharmacokinetics, Safety/tolerability, and Efficacy of high-dose Rifampicin in tuberculosis-HIV co-infected patients on efavirenz- or dolutegravir-based antiretroviral therapy: Study protocol for an open-label, phase II clinical trial (SAEFRIF),” *Trials*, vol. 21, no. 1, pp. 1–9, 2020, doi: 10.1186/s13063-020-4132-7.
- [168] F. Balzano *et al.*, “MiRNA stability in frozen plasma samples,” *Molecules*, vol. 20, no. 10, pp. 19030–19040, 2015, doi: 10.3390/molecules201019030.
- [169] R. G. Shaughnessy, D. Farrell, K. Riepema, D. Bakker, and S. V. Gordon, “Analysis of biobanked serum from a mycobacterium avium subsp paratuberculosis bovine infection model confirms the remarkable stability of circulating miRNA profiles and defines a bovine serum miRNA repertoire,” *PLoS One*, vol. 10, no. 12, pp. 1–22, 2015, doi: 10.1371/journal.pone.0145089.
- [170] H. E. Solberg, “International Federation of Clinical Chemistry (IFCC), Scientific Committee, Clinical Section, Expert Panel on Theory of Reference Values, and International Committee for Standardization in Haematology (ICSH), Standing

- Committee on Reference Values. Appro," *J. Clin. Chem. Clin. Biochem.*, vol. 25, no. 5, pp. 337–342, 1987.
- [171] Y. Zou *et al.*, "Oxidative stress-mediated developmental toxicity induced by isoniazide in zebrafish embryos and larvae," *J. Appl. Toxicol.*, vol. 37, no. 7, pp. 842–852, 2017, doi: 10.1002/jat.3432.
- [172] Y. Zhang *et al.*, "Hepatotoxicity Induced by Isoniazid-Lipopolysaccharide through Endoplasmic Reticulum Stress, Autophagy, and Apoptosis Pathways in Zebrafish.," *Antimicrob. Agents Chemother.*, vol. 63, no. 5, pp. e01639-18, May 2019, doi: 10.1128/AAC.01639-18.
- [173] Z. Jia *et al.*, "Mechanism of isoniazid-induced hepatotoxicity in zebrafish larvae: Activation of ROS-mediated ERS, apoptosis and the Nrf2 pathway," *Chemosphere*, vol. 227, pp. 541–550, Jul. 2019, doi: 10.1016/J.CHEMOSPHERE.2019.04.026.
- [174] C. Der Hsiao *et al.*, "A rapid assessment for predicting drug-induced hepatotoxicity using zebrafish," *J. Pharmacol. Toxicol. Methods*, vol. 84, pp. 102–110, 2017, doi: 10.1016/j.vascn.2016.12.002.
- [175] S. M. Kupchan, W. A. Court, R. G. Dailey, C. J. Gilmore, and R. F. Bryan, "Triptolide and triptidiolide, novel antileukemic diterpenoid triepoxides from *Tripterygium wilfordii*," *J. Am. Chem. Soc.*, vol. 94, no. 20, pp. 7194–5, Oct. 1972, Accessed: Jan. 08, 2019. [Online]. Available: <http://www.ncbi.nlm.nih.gov/pubmed/5072337>.
- [176] B. J. Chen, "Triptolide, A Novel Immunosuppressive and Anti-Inflammatory Agent Purified from a Chinese Herb *Tripterygium Wilfordii* Hook F," *Leuk. Lymphoma*, vol. 42, no. 3, pp. 253–265, Jan. 2001, doi: 10.3109/10428190109064582.
- [177] Q. Liu, "Triptolide and its expanding multiple pharmacological functions," *Int. Immunopharmacol.*, vol. 11, no. 3, pp. 377–383, Mar. 2011, doi: 10.1016/J.INTIMP.2011.01.012.
- [178] Y. Zheng, W.-J. Zhang, and X.-M. Wang, "Triptolide with Potential Medicinal Value for Diseases of the Central Nervous System," *CNS Neurosci. Ther.*, vol. 19, no. 2, pp. 76–82, Feb. 2013, doi: 10.1111/cns.12039.
- [179] S. Ziaei and R. Halaby, "Immunosuppressive, anti-inflammatory and anti-cancer properties of triptolide: A mini review.," *Avicenna J. phytomedicine*, vol. 6, no. 2, pp. 149–64, 2016, Accessed: Jan. 08, 2019. [Online]. Available: <http://www.ncbi.nlm.nih.gov/pubmed/27222828>.

- [180] S. M. Attia, "Deleterious effects of reactive metabolites.," *Oxid. Med. Cell. Longev.*, vol. 3, no. 4, pp. 238–53, 2010, doi: 10.4161/oxim.3.4.13246.
- [181] D. V Titov *et al.*, "XPB, a subunit of TFIIH, is a target of the natural product triptolide.," *Nat. Chem. Biol.*, vol. 7, no. 3, pp. 182–8, Mar. 2011, doi: 10.1038/nchembio.522.
- [182] J. Yao, L. Zhang, X. Zhao, L. Hu, and Z. Jiang, "Simultaneous Determination of Triptolide, Wilforlide A and Triptonide in Human Plasma by High-Performance Liquid Chromatography-Electrospray Ionization Mass Spectrometry," *Biol. Pharm. Bull.*, vol. 29, no. 7, pp. 1483–1486, 2006, doi: 10.1248/bpb.29.1483.
- [183] J. H. He *et al.*, "A zebrafish phenotypic assay for assessing drug-induced hepatotoxicity," *J. Pharmacol. Toxicol. Methods*, vol. 67, no. 1, pp. 25–32, 2013, doi: 10.1016/j.vascn.2012.10.003.
- [184] M. R. Friedländer, S. D. MacKowiak, N. Li, W. Chen, and N. Rajewsky, "MiRDeep2 accurately identifies known and hundreds of novel microRNA genes in seven animal clades," *Nucleic Acids Res.*, vol. 40, no. 1, pp. 37–52, 2012, doi: 10.1093/nar/gkr688.
- [185] I. S. Vlachos *et al.*, "DIANA-miRPath v3.0: Deciphering microRNA function with experimental support," *Nucleic Acids Res.*, vol. 43, no. W1, pp. W460–W466, 2015, doi: 10.1093/nar/gkv403.
- [186] D. Karagkouni *et al.*, "DIANA-TarBase v8: a decade-long collection of experimentally supported miRNA–gene interactions," *Nucleic Acids Res.*, vol. 46, no. D1, pp. D239–D245, Jan. 2018, doi: 10.1093/nar/gkx1141.
- [187] M. Manoli and W. Driever, "Fluorescence-activated cell sorting (FACS) of fluorescently tagged cells from zebrafish larvae for RNA isolation.," *Cold Spring Harb. Protoc.*, vol. 2012, no. 8, p. pdb.prot069633, Aug. 2012, doi: 10.1101/pdb.prot069633.
- [188] V. E. Gallardo and M. Behra, "Fluorescent activated cell sorting (FACS) combined with gene expression microarrays for transcription enrichment profiling of zebrafish lateral line cells.," *Methods*, vol. 62, no. 3, pp. 226–31, Aug. 2013, doi: 10.1016/j.ymeth.2013.06.005.
- [189] W. Tam, "Identification and characterization of human BIC, a gene on chromosome 21 that encodes a noncoding RNA," *Gene*, vol. 274, no. 1–2, pp. 157–167, Aug. 2001, doi: 10.1016/S0378-1119(01)00612-6.
- [190] T. S. Elton, H. Selemon, S. M. Elton, and N. L. Parinandi, "Regulation of the MIR155

- host gene in physiological and pathological processes," *Gene*, vol. 532, no. 1, pp. 1–12, Dec. 2013, doi: 10.1016/J.GENE.2012.12.009.
- [191] R. M. O'Connell, K. D. Taganov, M. P. Boldin, G. Cheng, and D. Baltimore, "MicroRNA-155 is induced during the macrophage inflammatory response," *Proc. Natl. Acad. Sci. U. S. A.*, vol. 104, no. 5, pp. 1604–9, Jan. 2007, doi: 10.1073/pnas.0610731104.
- [192] L. G. Higgins and J. D. Hayes, "Mechanisms of induction of cytosolic and microsomal glutathione transferase (GST) genes by xenobiotics and pro-inflammatory agents," *Drug Metab. Rev.*, vol. 43, no. 2, pp. 92–137, 2011, doi: 10.3109/03602532.2011.567391.
- [193] B. Blomme, C. Van Steenkiste, N. Callewaert, and H. Van Vlierberghe, "Alteration of protein glycosylation in liver diseases," *J. Hepatol.*, vol. 50, no. 3, pp. 592–603, 2009, doi: 10.1016/j.jhep.2008.12.010.
- [194] A. Ordas *et al.*, "MicroRNA-146 function in the innate immune transcriptome response of zebrafish embryos to *Salmonella typhimurium* infection," *BMC Genomics*, vol. 14, no. 1, p. 696, 2013, doi: 10.1186/1471-2164-14-696.
- [195] A. Ucar *et al.*, "The miRNA-212/132 family regulates both cardiac hypertrophy and cardiomyocyte autophagy," *Nat. Commun.*, vol. 3, 2012, doi: 10.1038/ncomms2090.
- [196] B. Xu *et al.*, "Neurons secrete MIR-132-containing exosomes to regulate brain vascular integrity," *Cell Res.*, vol. 27, no. 7, pp. 882–897, 2017, doi: 10.1038/cr.2017.62.
- [197] K. F. Hansen *et al.*, "Targeted deletion of miR-132/-212 impairs memory and alters the hippocampal transcriptome," *Learn. Mem.*, vol. 23, no. 2, pp. 61–71, 2016, doi: 10.1101/lm.039578.115.
- [198] M. Li *et al.*, "Overexpression of miR-19b impairs cardiac development in zebrafish by targeting *ctnnb1*," *Cell. Physiol. Biochem.*, vol. 33, no. 6, pp. 1988–2002, 2014, doi: 10.1159/000362975.
- [199] A. Benz *et al.*, "MIR-19b Regulates Ventricular Action Potential Duration in Zebrafish," *Sci. Rep.*, vol. 6, no. April, pp. 1–11, 2016, doi: 10.1038/srep36033.
- [200] V. P. Yin, A. Lepilina, A. Smith, and K. D. Poss, "Regulation of zebrafish heart regeneration by miR-133," *Dev. Biol.*, vol. 365, no. 2, pp. 319–327, 2012, doi: 10.1016/j.ydbio.2012.02.018.
- [201] M. Xue *et al.*, "Comparison of toxicokinetic and tissue distribution of triptolide-

- loaded solid lipid nanoparticles vs free triptolide in rats,” *Eur. J. Pharm. Sci.*, vol. 47, no. 4, pp. 713–717, 2012, doi: 10.1016/j.ejps.2012.05.012.
- [202] K. D. Taganov, M. P. Boldin, K. J. Chang, and D. Baltimore, “NF- $\kappa$ B-dependent induction of microRNA miR-146, an inhibitor targeted to signaling proteins of innate immune responses,” *Proc. Natl. Acad. Sci. U. S. A.*, vol. 103, no. 33, pp. 12481–12486, 2006, doi: 10.1073/pnas.0605298103.
- [203] Y. Chen, Z. Zeng, X. Shen, Z. Wu, Y. Dong, and J. C. H. Cheng, “MicroRNA-146a-5p negatively regulates pro-inflammatory cytokine secretion and cell activation in lipopolysaccharide stimulated human hepatic stellate cells through inhibition of toll-like receptor 4 signaling pathways,” *Int. J. Mol. Sci.*, vol. 17, no. 7, pp. 1–13, 2016, doi: 10.3390/ijms17071076.
- [204] S. Bandiera *et al.*, “Hepatitis C Virus-Induced Upregulation of MicroRNA miR-146a-5p in Hepatocytes Promotes Viral Infection and Deregulates Metabolic Pathways Associated with Liver Disease Pathogenesis,” *J. Virol.*, vol. 90, no. 14, pp. 6387–6400, 2016, doi: 10.1128/jvi.00619-16.
- [205] A. Takeuchi-Yorimoto *et al.*, “MicroRNA-21 is associated with fibrosis in a rat model of nonalcoholic steatohepatitis and serves as a plasma biomarker for fibrotic liver disease,” *Toxicol. Lett.*, vol. 258, pp. 159–167, 2016, doi: 10.1016/j.toxlet.2016.06.012.
- [206] J. Xu *et al.*, “Circulating MicroRNAs, miR-21, miR-122, and miR-223, in patients with hepatocellular carcinoma or chronic hepatitis,” *Mol. Carcinog.*, vol. 50, no. 2, pp. 136–142, 2011, doi: 10.1002/mc.20712.
- [207] C. T. Lee, T. Risom, and W. M. Strauss, “Evolutionary conservation of microRNA regulatory circuits: An examination of microRNA gene complexity and conserved microRNA-target interactions through metazoan phylogeny,” *DNA Cell Biol.*, vol. 26, no. 4, pp. 209–218, 2007, doi: 10.1089/dna.2006.0545.
- [208] D. E. Kuhn, M. M. Martin, D. S. Feldman, A. V. Terry, G. J. Nuovo, and T. S. Elton, “Experimental validation of miRNA targets,” *Methods*, vol. 44, no. 1, pp. 47–54, 2008, doi: 10.1016/j.ymeth.2007.09.005.
- [209] J. Quan and J. Tian, “Circular polymerase extension cloning for high-throughput cloning of complex and combinatorial DNA libraries,” *Nat. Protoc.*, vol. 6, no. 2, pp. 242–251, Feb. 2011, doi: 10.1038/nprot.2010.181.

- [210] S. Fias, S. Van Damme, and P. Bultinck, "Multidimensionality of delocalization indices and nucleus independent chemical shifts in polycyclic aromatic hydrocarbons," ... *Comput. Chem.*, vol. 29, pp. 358–366, 2008, doi: 10.1002/jcc.
- [211] N. S. Holman, M. Mosedale, K. K. Wolf, E. L. LeCluyse, and P. B. Watkins, "Subtoxic alterations in hepatocyte-derived exosomes: An early step in drug-induced liver injury?," *Toxicol. Sci.*, vol. 151, no. 2, pp. 365–375, 2016, doi: 10.1093/toxsci/kfw047.
- [212] F. Momen-Heravi, S. Bala, K. Kodys, and G. Szabo, "Exosomes derived from alcohol-treated hepatocytes horizontally transfer liver specific miRNA-122 and sensitize monocytes to LPS," *Sci. Rep.*, vol. 5, no. May, pp. 1–16, 2015, doi: 10.1038/srep09991.
- [213] Y. Wang *et al.*, "Injured liver-released miRNA-122 elicits acute pulmonary inflammation via activating alveolar macrophage TLR7 signaling pathway," *Proc. Natl. Acad. Sci. U. S. A.*, vol. 116, no. 13, pp. 6162–6171, 2019, doi: 10.1073/pnas.1814139116.
- [214] O. Matthews *et al.*, "Transfer of hepatocellular microRNA regulates cytochrome P450 2E1 in renal tubular cells," *EBioMedicine*, vol. 62, 2020, doi: 10.1016/j.ebiom.2020.103092.
- [215] A. D. B. Vliegenthart, C. Berends, C. M. J. Potter, M. Kersaudy-Kerhoas, and J. W. Dear, "MicroRNA-122 can be measured in capillary blood which facilitates point-of-care testing for drug-induced liver injury.," *Br. J. Clin. Pharmacol.*, vol. 83, no. 9, pp. 2027–2033, Sep. 2017, doi: 10.1111/bcp.13282.
- [216] J. Hanna, G. S. Hossain, and J. Kocerha, "The potential for microRNA therapeutics and clinical research," *Front. Genet.*, vol. 10, no. MAY, 2019, doi: 10.3389/fgene.2019.00478.
- [217] H. L. A. Janssen *et al.*, "Treatment of HCV infection by targeting microRNA," *N. Engl. J. Med.*, vol. 368, no. 18, pp. 1685–1694, 2013, doi: 10.1056/NEJMoa1209026.
- [218] K. C. Sadler, A. Amsterdam, C. Soroka, J. Boyer, and N. Hopkins, "A genetic screen in zebrafish identifies the mutants vps18, nf2 and foie gras as models of liver disease," *Development*, vol. 132, no. 15, pp. 3561–3572, 2005, doi: 10.1242/dev.01918.
- [219] S. Wang, S. R. Miller, E. A. Ober, and K. C. Sadler, "Making it new again: Insight into liver development, regeneration, and disease from zebrafish research," *Curr Top Dev Biol.*, vol. 124, no. 3, pp. 161–195, 2017.
- [220] R. J. Major and K. D. Poss, "Zebrafish heart regeneration as a model for cardiac tissue



repair,” *Drug Discov. Today Dis. Model.*, vol. 4, no. 4, pp. 219–225, 2007, doi: 10.1016/j.ddmod.2007.09.002.

- [221] J. M. González-Rosa, C. E. Burns, and C. G. Burns, “Zebrafish heart regeneration: 15 years of discoveries,” *Regeneration*, vol. 4, no. 3, pp. 105–123, 2017, doi: 10.1002/reg2.83.